ORGANIZED STRUCTURES IN THE TURBULENT BOUNDARY LAYER

Andrew S. W. Thomas, B.E. (Hons)

University of Adelaide

Department of Mechanical Engineering

Thesis Submitted for the Degree of
Doctor of Philosophy

September, 1977

ABSTRACT

Experimental evidence is presented which supports the concept that the turbulent boundary layer is dominated by an organized large structure, and that the occurrence of an observed small scale flow near the wall, probably related to bursts and sweeps, can be attributed directly to the presence of this structure.

The evidence is in the form of long time averaged correlations and conditional ensemble averages of short time correlations between the signals from a flush mounted hot film shear stress gauge and those from a rake of hot wire elements spaced across the boundary layer in both the normal and transverse directions. The correlations have a spatial and temporal extent well in excess of typical wall scales and indicate the presence of a large structure with a character not unlike that of the turbulent spot that has been observed during transition. The experiments show it to be inclined to the wall at an angle of about 18° which is in remarkable agreement with recent flow visualization studies. In the spanwise direction, it gives rise to an unusual feature of twin maxima in the velocity correlations and these result, evidently, from the sides of the structure lying oblique to the mean flow direction.

As this structure passes over the wall, there is a characteristic small scale response of that region, and the turbulent bursts and sweeps are probably part of this process. The response is perceived as intense high frequency shear stress fluctuations and a novel technique was developed to correlate between the existence of these fluctuations and the corresponding low frequency or large scale fluctuations. The results of this work have indicated that for the wall shear stress, there is a definite phase relation between the two

scales of motion with the intense small scale disturbances occurring mostly when the shear stress is high. For the velocity signals occurring over the remainder of the layer, the same technique has indicated that the large structure may be characterized by steep positive velocity gradients on its rear or upstream surface.

By detecting these gradients in an unbiased manner, ensemble averaged time histories of both the streamwise and normal components of velocity have been generated and used to create a streamline pattern of the large structure. This pattern shows a large rotating structure with the dominant feature being a strong outflow along the rear of the structure. In this region very large contributions to Reynolds stress have been observed to occur.

The velocity gradients of this region also generate wall pressure fluctuations whose ensemble averaged time histories have been determined. Although a careful interpretation is required, these time histories are the same as might be expected from the measured velocity time histories if there is dominance of turbulence-mean shear interaction. It is suggested from this work that the wall pressure signature of the large structure, as measured at a fixed point, is characterized mainly by a steep fall of pressure in time. Such features have been identified in the signals and tracked downstream over distances in excess of 2δ at a convection velocity of $0.67U_o$.

The pressure data were examined in some detail in order to clarify the mechanism responsible for the apparent generation of bursts and sweeps by the large structure. It appears however that the pressure field of the large structure has neither sufficient amplitude nor the correct character to play the role in this mechanism that has been suggested by others.

For this reason an alternative concept based upon a rotational instability has been proposed in which a Taylor-Görtler mechanism near the wall gives rise to the well documented streaks of longitudinal vorticity in that region. The stretching of this vorticity then gives rise to the small scale turbulent bursts which are, in turn, followed by sweep motions as the vorticity is swept back toward the wall. Experimental evidence to support this concept lies in the finding that, in a frame of reference moving with the large structure, small scale shear stress fluctuations are associated with a flow near the wall whose streamlines are in opposition to the mean vorticity. An opposition of this kind is a necessary condition for such an instability to occur.

TABLE OF CONTENTS

Page No.

APPENDICES

STATEMENT OF ORIGINALITY

The material reported in this thesis is original work and does not contain work that has been accepted for the award of a degree or diploma at any other University. To the best of the author's knowledge and belief, this thesis contains no material previously published or written by another person, except when due reference is made in the text of the thesis.

Andrew S. W. Thomas

September, 1977

ACKNOWLEDGEMENTS

The work leading to this thesis was undertaken in the Mechanical Engineering Department of the University of Adelaide, South Australia, under the aegis of Professor R. E. Luxton.

The author would like to thank Dr. M. K. Bull for his supervision and encouragement throughout the project and for allowing considerable freedom in the choice of experiments that were undertaken.

To Dr. G. L. Brown the author is also particularly indebted for many useful discussions and ideas throughout the work and also for guidance in the preparation of this thesis.

Likewise Professor R. E. Luxton and Dr. C. J. Abell provided some stimulating discussions during the latter part of the research program, and these were greatly appreciated.

Mr. G. Osborne displayed considerable skill in manufacturing the pressure transducers and without his help that part of the work could not have been undertaken. The author appreciated his efforts and those of other members of the workshop staff, in particular Mr. P. E. Walker, Mr. D. Kerr and Mr. H. Bode.

Finally, the author expresses his gratitude to Barbara for displaying considerable patience and understanding throughout the more difficult times of this project.

LIST OF COMMONLY USED SYMBOLS

A, B	Constants in Coles law of the wall.
d	Transducer diameter.
δ, δ^*	Boundary layer thickness and displacement thickness.
f	Frequency in cycles per second.
k	Wave-number.
κ	Thermal diffusivity.
L_a, L_e	Actual and effective streamwise length of a hot film.
ν	Kinematic viscosity.
p'	Rms wall pressure.
$\phi(\omega)$	Power spectral density value.
q(t)	Any fluctuating turbulent quantity.
$q_{sh}(t)$	The smoothed rectified high frequency component of q(t).
q'	Rms value of q(t).
R_{xy}	Correlation value $x(t) \cdot y(t + \tau) / x'y'$.
R	Generalized correlation value.
t	The variable time.
T_{av}	Averaging time used with short time correlations.
τ	Correlation time delay value.
$\overline{\tau}_w$, τ_w	Mean and fluctuating component of wall shear.
θ	Boundary layer momentum thickness.
u	Streamwise fluctuating component of velocity.
U_c	Convection velocity.
U_o	Free stream velocity.
U_τ	Skin friction velocity = $\sqrt{\overline{\tau}_w/\rho}$.
U_m	Local mean velocity.
v	Normal fluctuating component of velocity.
W	Width of hot film in the spanwise direction.
x,y,z	Coordinates of streamwise, normal and spanwise directions.

1. INTRODUCTION

Considerable time has passed since Osborne Reynolds first formulated the problem of turbulence and yet the majority of the experimental studies on boundary layer turbulence, for example, have been performed only in the last two or three decades. This can be attributed to the development in this period of sophisticated anemometry techniques and, more recently, to the advent of low cost digital data processing. However, despite the wealth of statistical data in the form of spectral and correlation measurements that is now available, the detailed features of the structure of boundary layer turbulence still remain hidden.

In practical terms the turbulent boundary layer is of great importance because of its frequent occurrence in aerodynamics and hydrodynamics and other fields of engineering and science. The flat plate, zero pressure gradient turbulent boundary is a basic turbulent flow and the simplest turbulent boundary layer flow to study. The simplicity is however very deceptive for in reality it may well be one of the most complex basic turbulent flows because of the two significant scales in the motion. There is the large scale motion with velocity and length scales of U_o and δ, and the viscous scales near the wall with scales U_τ and ν/U_τ. It is, however, because the boundary layer is of such practical significance and because it is such a well defined basic turbulent flow that it has been studied exhaustively. To review all the available literature here is neither appropriate nor necessary. The reader is referred to Willmarth (1975a) for an excellent review of the present knowledge of turbulent boundary layer structure and to Reynolds (1976) for a review of some of the boundary layer prediction methods. In what follows only some of

the more important results that have emerged from various experimental studies and which are relevant to the work will be discussed.

Perhaps the most significant finding of recent years in boundary layer work and indeed in turbulence research in general is the discovery that organized motions exist within the flow. These have been highlighted by flow visualization studies and a dramatic example can be seen in the photographs of Brown and Roshko (1974) of the turbulent mixing layer. The flow is dominated by a very large and highly organized structure which controls the dynamics of the flow. In the boundary layer, because of the three dimensionality and the two scales of motion, the organized motions that have been identified are considerably more complex than for the plane mixing layer. These motions in the boundary layer may be divided into two categories and although these are discussed separately it will become apparent that there is some relation between the two.

(i) The first is the organized small scale structure that is known to exist near the wall and which has been reported in the flow visualization studies carried out at Stanford (Kline, Reynolds, Schraub and Rundstadler, 1967, Kim, Kline and Reynolds, 1971, Offen and Kline, 1973) and at Ohio (Corino and Brodkey, 1969, Nychas, Hershey and Brodkey, 1973).

(ii) The second is the organized large structure that is known to exist on a scale of the boundary layer thickness and which has been extensively studied by Kovasznay et al (1970) and others using conditional sampling and averaging techniques.

With reference first to the organized small scale structures, which are more usually known as the burst-sweep cycle of events, there is evidently a cyclic phenomenon present which is characterized by

the appearance near the wall of alternate regions of high and low speed fluid. The sequence of events from that time is well described by Kim et al (1971) and, following their description, one of these low speed "streaks" sometimes lifts slowly away from the wall during its passage downstream and then turns more sharply away from the wall. Because of the momentum deficiency this gives rise to a point of inflexion in the instantaneous velocity profile. Downstream of this inflexional zone oscillatory motions have been observed which result predominantly from a streamwise vortex which grows in extent but whose growth is terminated by random chaotic small scale motions which Kim et al refer to as "breakup". Although the terminology is different, the cycle of events described by Corino and Brodkey (1969) is very similar and they have found that the ejection or bursting phase ended with a "sweep" of high speed fluid carrying away the retarded fluid that remained from the ejection process.

Following Corino and Brodkey (1969), Kim et al (1971), Grass (1971) and Lu and Willmarth (1973) it appears that these events are associated with very large contributions to the Reynolds stress and turbulence production. On this evidence alone it is clear that they play an important role in the dynamics of the turbulence process.

The occurrence of bursts and sweeps at a given point is repeated in time and it appears that the mean period between bursts is the same as the mean period between sweeps (Lu and Willmarth 1973). Although queried by Meek (1972) it also appears that these periods scale on outer flow variables (Lu and Willmarth, 1973, Rao, Narasimha and Badri Narayanan, 1971) so that the outer flow appears in some sense to be controlling the flow at the wall.

The experiments of Offen and Kline (1973) attempted to shed more light on this interaction and the cyclical regeneration of

bursts. They have suggested that the vortex within a burst or lifted wall streak can impose an adverse pressure gradient on the wall which may stimulate the lift up of a new wall streak. In this way the process is regenerative but the outer layer influence is not clear; it is perhaps only playing a passive role. Willmarth (1975a) has proposed a similar model for the cyclical occurrence of bursts in which pressure provides a link between the outer flow and the wall flow. He has appreciated the advantage of viewing events in a convected frame of reference and in his model the initiation of a burst is caused by the convected massaging action of the pressure field of a large scale structure on the low speed sublayer fluid. Unlike the model of Offen and Kline however, Willmarth proposes a large scale effect in which the large structure or large scale vorticity arises from the previous bursts so that in this way the wall events are controlled by outer layer structures and are also regenerative.

The flow visualization studies of Nychas et al (1973) have shown that the occurrence of bursts is closely associated with the presence of a large transverse vortex in the outer layer. This vortex appears to arise as a result of a shear instability between accelerated and decelerated fluid and is very like the "typical eddies" that have been observed in a smoke filled boundary layer of Falco (1976). At the low Reynolds numbers characteristic of these experiments this vortex exists across most of the layer and it is not clear what its relative size would be at higher Reynolds numbers. Therefore although there is an implication of an outer layer influence, the details of the influence of the large structures are by no means clear. In addition the mechanisms discussed above suggest that the large structures are a consequence of the repeated pairing

of the small scale bursting fluid. While not sufficient to contradict this view, the great disparity in scale between the two kinds of motions, particularly at high Reynolds numbers, is certainly hard to reconcile with such an idea.

A quite different view from that in which the large structure in the outer layer is a result of the amalgamation of small scale bursts near the wall, has been taken by Coles and Barker (1975) in which it is proposed that a large scale structure is the basic building block of the boundary layer and the burst-sweep cycle of events is part of the signature of this large structure. They maintain also that this large structure may have characteristics not unlike those of the turbulent spot observed during transition (Emmons, 1951, Elder, 1960). In such a model the burst-sweep cycle of events may feed turbulent energy to a large structure but the bursts do not amalgamate directly to form a new large structure.

The presence of the large structure in the boundary layer and the second kind of organized motion referred to above has been inferred from correlation measurements. In particular those measurements that take advantage of the well defined intermittency in the outer part of the layer have provided some insight into the behaviour of these structures. The correlations of Kovasznay et al (1970) have shown that the large structures have a streamwise length scale of the order of 2δ and a spanwise length scale of the order of δ. They are tilted away from the wall and can be correlated over streamwise distances of the order of 20δ or more, suggesting that they have long lifetimes. They are responsible for the turbulent bulges at the outer edge of the layer. Structures of this kind have been photographed, at low Reynolds numbers, by Falco (1976). The conditional sampling work of Kovasznay et al (1970) and Antonia (1972)

has shown that there is a general rotation within the structure. On the back, or upstream side of the structures, there is a flow away from the wall, and toward the wall on the front or downstream side. At the outermost edge of the layer, these structures are found to have a streamwise velocity less than the local mean so that the irrotational free stream rides over them giving rise to potential velocity fluctuations that can be detected at distances from the wall in excess of 2δ.

Both the large and small scale structures of the boundary layer evidently give rise to fluctuation in the wall pressure. Because of the importance of these fluctuations as a source of both acoustic noise and structural vibration they have been extensively studied using spectral and correlation techniques. A review of this work has been presented by Willmarth (1975b). The work of Willmarth and Wooldridge (1962) and Bull (1967) has shown that the wall pressure may be divided into two groups of families characterized by different wavenumbers. One is a low wavenumber grouping which displays convection at velocities typical of the outer part of the layer. The other is a high wavenumber grouping which displays convection at speeds typical of regions closer to the wall. These groupings are consistent with the two scales of turbulent motion that have been discussed. Because of the attenuation resulting from the finite size of the transducers used in such measurements, the importance of the small scale contributions to the wall pressure has, however, been underestimated in the past. The work of Emmerling (1973) has indicated that intense small scale pressure fluctuations can be identified and that these occur with a mean period that is close to the burst rate determined by Rao et al (1971). It seems likely therefore that they are related to the burst-sweep cycle of events

near the wall. The role of the pressure in these events and the relation, if any, between the small scale and large scale fluctuations is, however, not clear.

Within the context of this brief discussion it is to be seen that there are essentially two features of boundary layer turbulence. One is the flow near the wall characteristic of all bounded wall flows. The other is the outer flow (the wake component) which has in the past thought to have the properties of non-bounded turbulent flows. The mean and fluctuating quantites of each region scale differently and as Kovasznay (1970) has pointed out, it is the attempted matching of the two regions that makes the problem of boundary layer turbulence both interesting and challenging.

1.1. Aims of the Research Programme

The discussion of the last section raises many questions. In particular the mechanisms behind the generation of wall streaks and the cyclical regeneration of bursts are not clear. There is also an implication of a role of the large structures that exist in the layer but the causal relationships are unknown. The large structures may generate the bursts and sweeps at the wall, but it is not clear whether or not these small scale motions ultimately lead to a new large structure. The large structures may alternatively exist in their own right and give rise to the occurrence of small scale events at the wall. The correct representation is not known and it is evident that detailed measurements are required to shed light on these processes.

It has also been indicated that the pressure may be the link between the events in the outer layer and those at the wall. This question can only be answered by undertaking careful analysis of the

wall pressure signal at times when the turbulent bursts are thought to be occurring. Such measurements, using both pressure transducers and hot wire anemometers are usually made at a fixed point and allow only a brief view of a complex and evolving structure as it is convected by. Useful information could certainly be gained if it were possible to follow the evolution of a structure in its passage downstream. Such an experiment would be difficult to undertake in practice and one must be content with measurements made at a fixed point. Point measurements by themselves, however, will not describe the simultaneity of occurrence of a structure at different points in the layer. It is apparent therefore that useful results might be obtained using arrays of probes of the kind used by Blackwelder and Kaplan (1976).

Furthermore because of the apparent importance of the events very near the wall in the dynamics of the flow, it is clear that detailed measurements need to be made in that region. Even at moderate Reynolds numbers, however, great care is required in the placing of hot wires very near the wall. A possible way to overcome this difficulty is by the use of suitably designed flush mounted hot film shear stress gauges of the kind described by Bellhouse and Schultz (1966).

With these general remarks in mind, the aims of this research programme may be summarized into the following categories:

(i) The relationship between the small scale events at the wall and the outer layer is implied largely through scaling trends. By simultaneous recordings of the outputs of a flush mounted hot film and an array of many hot wires it was felt that this relationship could be more accurately defined.

(ii) By further use of arrays of hot wires it was hoped to shed light on the nature of the large structures themselves and the extent to which they are organized. Additionally it was hoped to find out to what extent they dominate the mechanics of the flow and the way in which they determine the Reynolds stress. A crucial feature of boundary layer turbulence is the three dimensionality of the phenomenon, and by use of a spanwise array of wires it was felt that some details of the spanwise geometry could be determined.

(iii) The role of the wall pressure in the turbulent bursting process is not clear. By use of flush mounted pressure transducers it was felt possible to clarify this role and determine the significance of the turbulent pressure field on the motions at the wall.

2. DESCRIPTION OF THE EXPERIMENTAL FACILITIES.

2.1 The Variable Section Boundary Layer Wind Tunnel.

The wind tunnel used for the present investigation is of the open circuit type driven by a centrifugal compressor situated downstream of the working section with a discharge external to the building. The system is described in some detail by Lim (1971), from which the schematic view in figure 2.1 is taken.

Air is drawn into the contraction through a contoured bellmouth leading to two sets of honeycombs and six fine wire mesh screens. The contraction is 1.15m square at inlet and reduces to 230mm square at the start of the working section, providing a contraction ratio of 25:1.

The working section is a rigid structure of extruded aluminium sections and is mounted on a heavy steel frame. It is 4.5m long by 230mm square, and has fifteen accurately machined circular instrumentation ports at 30cm intervals on the upper surface. The ports are fitted with numbered and individually matched instrumentation plugs in which the probes and transducers can be mounted. The boundary layer that develops on the upper surface is used in the experiments.

An important feature of the working section is that the lower floor is a thin flexible stainless steel sheet which may be moved up or down within the main section so as to allow any desired pressure gradient to be impressed upon the flow. Control of the floor position is achieved by a series of screw jacks mounted below the flexible floor between instrumentation ports and passing down into the rigid steel structure supporting the test section. Rubber edge strips run the full length of the edges of the panel to prevent air leaks. Longitudinal tension is maintained in the panel by means of a clamp at the downstream end.

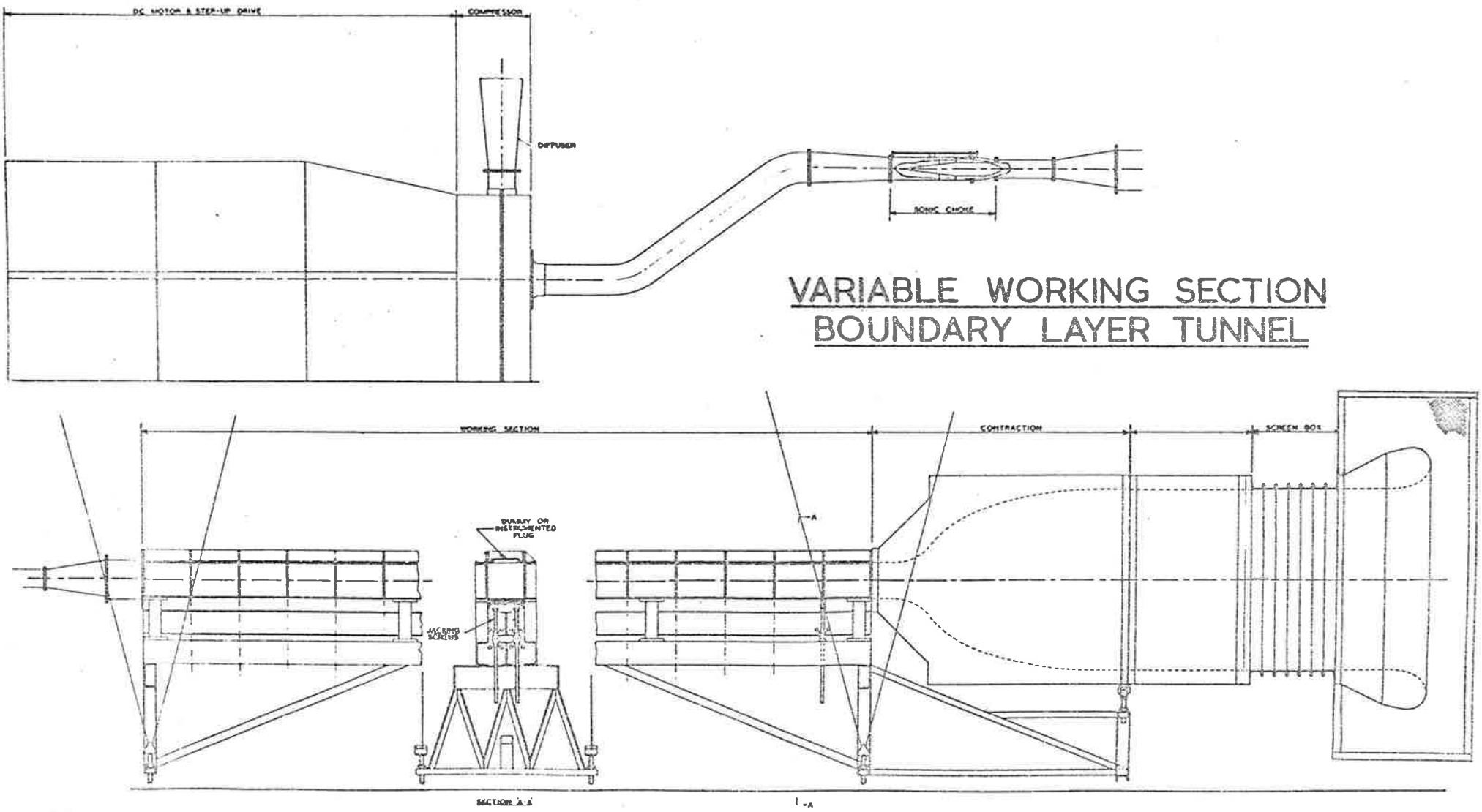

Figure 2.1 General arrangement of the variable working section boundary layer wind tunnel.

Downstream of the test section the flow is choked in a variable section sonic throat which provides good flow regulation and stability as well as significantly reducing the acoustic noise propagated into the test section. The flow then passes to the centrifugal compressor and diffuser and is discharged outside the building. The prime mover of the system is a 60 kw d.c. motor powered from the rectified three phase mains supply. The ductwork and housing surrounding the drive mechanism are acoustically insulated with sheet lead and fibreglass wool so as to reduce the noise levels within the laboratory. To reduce the transmission of vibrational energy into it, the structure of the working section is suspended from the ceiling on cables fitted with vibrational isolation units. Such precautions were found necessary when using the piezo-electric pressure transducers, which respond to vibrational stresses causing a degradation in their signal to noise ratio.

Natural transition from laminar to turbulent flow within the boundary layers on the tunnel wall, while being most desirable, is difficult to implement in practice due to the low inlet velocities which give rise to the need for large inlet lengths. In addition the strong favourable pressure gradients that exist within the contraction tend to stabilize the flow and for these reasons artificial trips are used in two locations in the tunnel. Each of these consists of a 5cm strip of coarse sandpaper, the first being located 28cm before the start of the test section along the region of concave curvature of the contraction and the second at the start of the test section. The first trip was used to prevent a wandering separation at the contraction and the second was used to bring about turbulence transition at the start of the test section.

Without such trips the mean properties of the boundary layers in the test section were found to vary with time due to what appeared to

be a wandering transition point giving rise to a variable effective origin of the turbulent boundary layers. There was also an apparent unsteadiness of the flow into the inlet of the bellmouth itself. This problem was alleviated by the removal of a one metre length of settling chamber introduced by Lim (1971) downstream of the bellmouth, thereby moving the inlet further away from the end wall of the laboratory. In addition, the entire bellmouth was housed in a box of fine terylene mesh so as to prevent stray drafts from affecting the flow into the tunnel. Extensive tests on the mean flow within the boundary layer in the test section showed these precautions to be particularly effective.

2.2 Transducers for Fluctuating Wall Pressure Measurements.

2.2.1. The Piezo-electric Transducers and Preamplifier.

The transducers used for the present work are essentially the same as those used by Lim (1971) except that some modifications were made to provide an improved signal to noise ratio. The heart of the device is a small cylindrical lead zirconate-titanate piezo-electric crystal of both diameter and thickness of 0.75mm, mounted on a brass stem set in a plug of insulating material (silicon loaded ebonite), which is in turn housed in a 6.35mm diameter brass shell. The details of the device are shown in figure 2.2(a). The designation for the piezo-electric material is PZT-5H; it is manufactured by the Brush Clevite Company of Southampton, England.

The clearance between the crystal and the surrounding body is filled with silicone moulding rubber so that an electrical contact of conducting silver paint may be placed on the top surface of the crystal without the possibility of the paint flowing down the sides of the crystal.

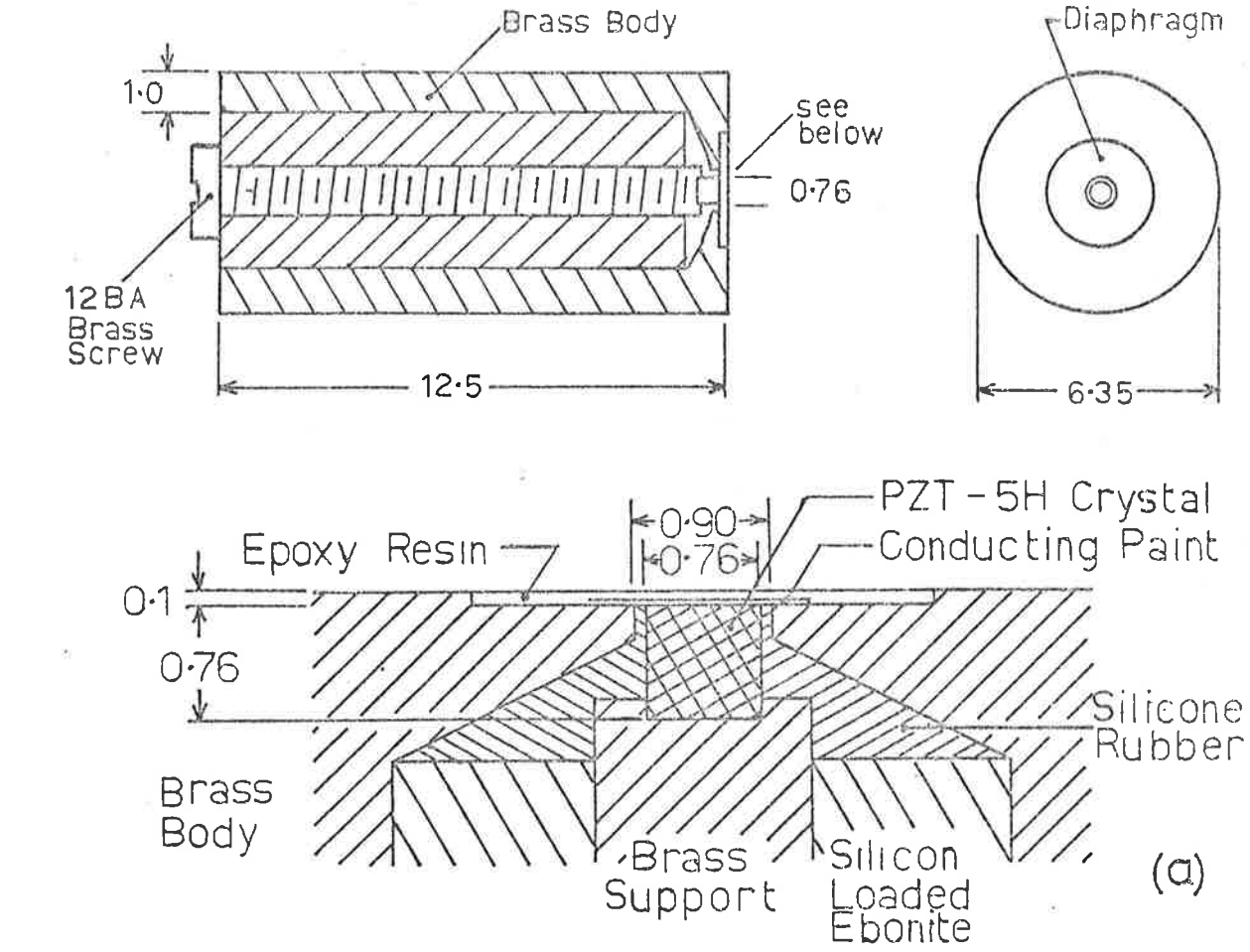

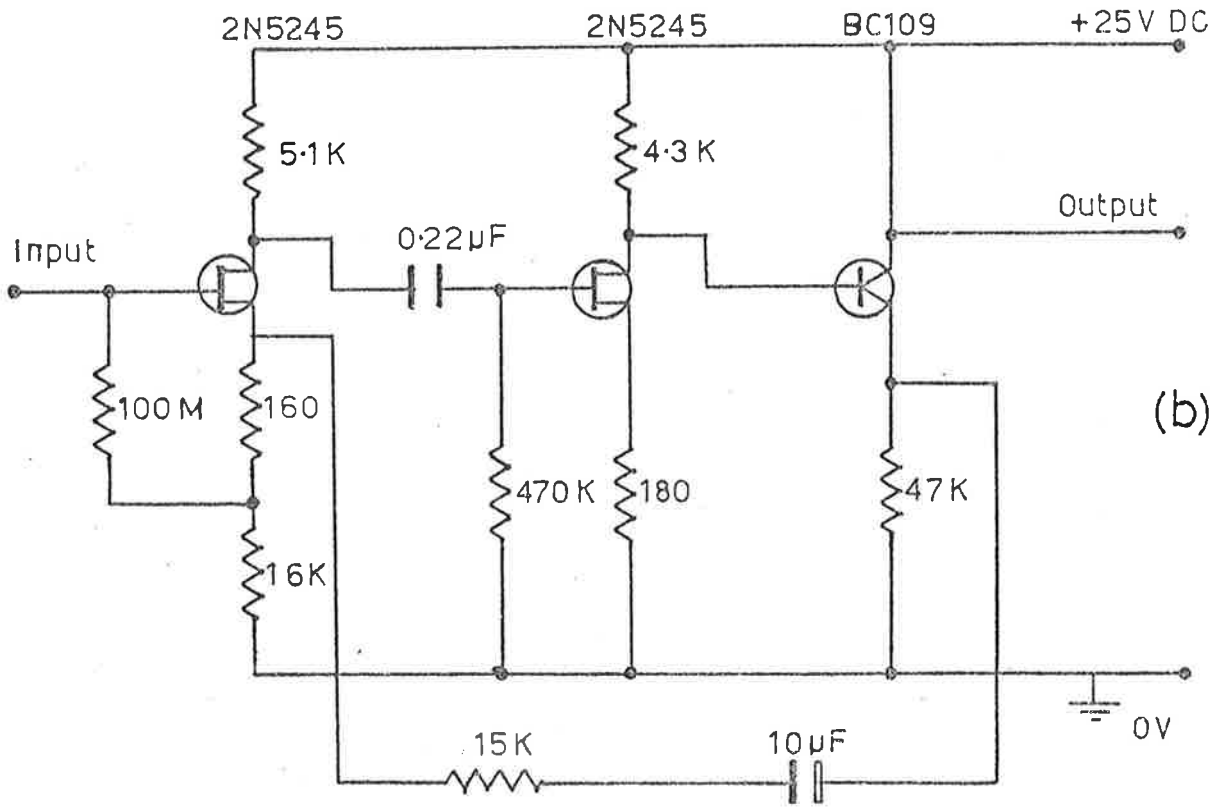

Figure 2.2 (a) Details of the piezo-electric pressure transducers. All dimensions in mm.

(b) Circuit diagram of the pre-amplifier for use with the piezo-electric transducers.

The first step in the manufacture of the transducers is the machining of the brass shell and brass stem. For the latter a 12BA screw is used and a small register is machined on one end into which the crystal is mounted using, as an adhesive, a thin coating of conducting thermosetting silver paint (type FSP 36-002 made by Johnson Matthey of Hatton Garden, England). Any excess paint on the sides of the crystal is carefully scraped away. Next a tube of silicon loaded ebonite, with its central hole threaded to take the 12BA brass stem, is glued inside the brass shell with epoxy cement. After all the adhesives have set, the threaded hole is partially filled with silicone moulding rubber and the crystal is also lightly coated with the liquid rubber. The brass stem with the crystal attached is then screwed into the transducer body so that the excess rubber is squeezed out leaving a thin layer of rubber between the sides of the crystal and the surrounding body.

Once the rubber has set, the excess from the top of the transducer is cut away and a thin layer of conducting silver paint applied to the crystal face and over the insulating rubber on to the brass body to complete the necessary electrical connection. After the paint has dried a thin diaphragm of epoxy cement is applied to the transducer face to offer some degree of protection and to ensure a surface free of discontinuities.

Since the piezo-electric transducers are very high impedance devices a pre-amplifier for impedance matching is required. For this purpose the devices described by Lim (1971) and shown in figure 2.2(b) were used. These are two stage devices using low-noise field-effect transistors with an emitter follower output. When in use they were mounted immediately above the transducers on the wind tunnel plug so as to reduce any lead capacitance effects. The frequency response of the pre-amplifier was checked and found to be flat within 1dB from 20Hz

to more than 100 kHz with no detectable phase shifts, and the gain was about 5.8.

2.2.2 The Pinhole Microphone Transducers

The piezo-electric transducers have the advantage that they present a surface to the flow free from discontinuities. However they also have the disadvantage that they respond to vibrations of the structure in which they are mounted and this, in addition to their low sensitivity, can give rise to a poor signal to noise ratio.

Because of such problems, some studies of wall pressure fluctuations, in particular those of Blake (1971) and Burton (1974), have been made using pinhole orifice microphones employing small commercially made condenser microphones. These were used in the early stages of the present work in the hope of providing a better signal to noise ratio at low flow speeds. Their use was later discontinued when they were found to give substantially different results from the flush mounted piezo-electric devices.

The design of the pinhole system centres on the Bruel and Kjaer 1/8 inch condenser microphone type 4138, and is shown in figure 2.3. A carefully machined plastic cap with a 0.75mm pinhole is placed over the microphone; the clearance is kept as small as possible so as to reduce the cavity volume and thereby improve frequency response. On the other hand the smaller the cavity, the greater is the possibility of accidental damage to the delicate microphone diaphragm, so that extreme care must be exercised during manufacture of the plastic cap. In the present case the cavity in the plastic cap was formed by first machining a cutting tool to the image cross section of the desired profile. Only after the geometrical accuracy of the tool had been verified under a measuring microscope was the cavity cut in the

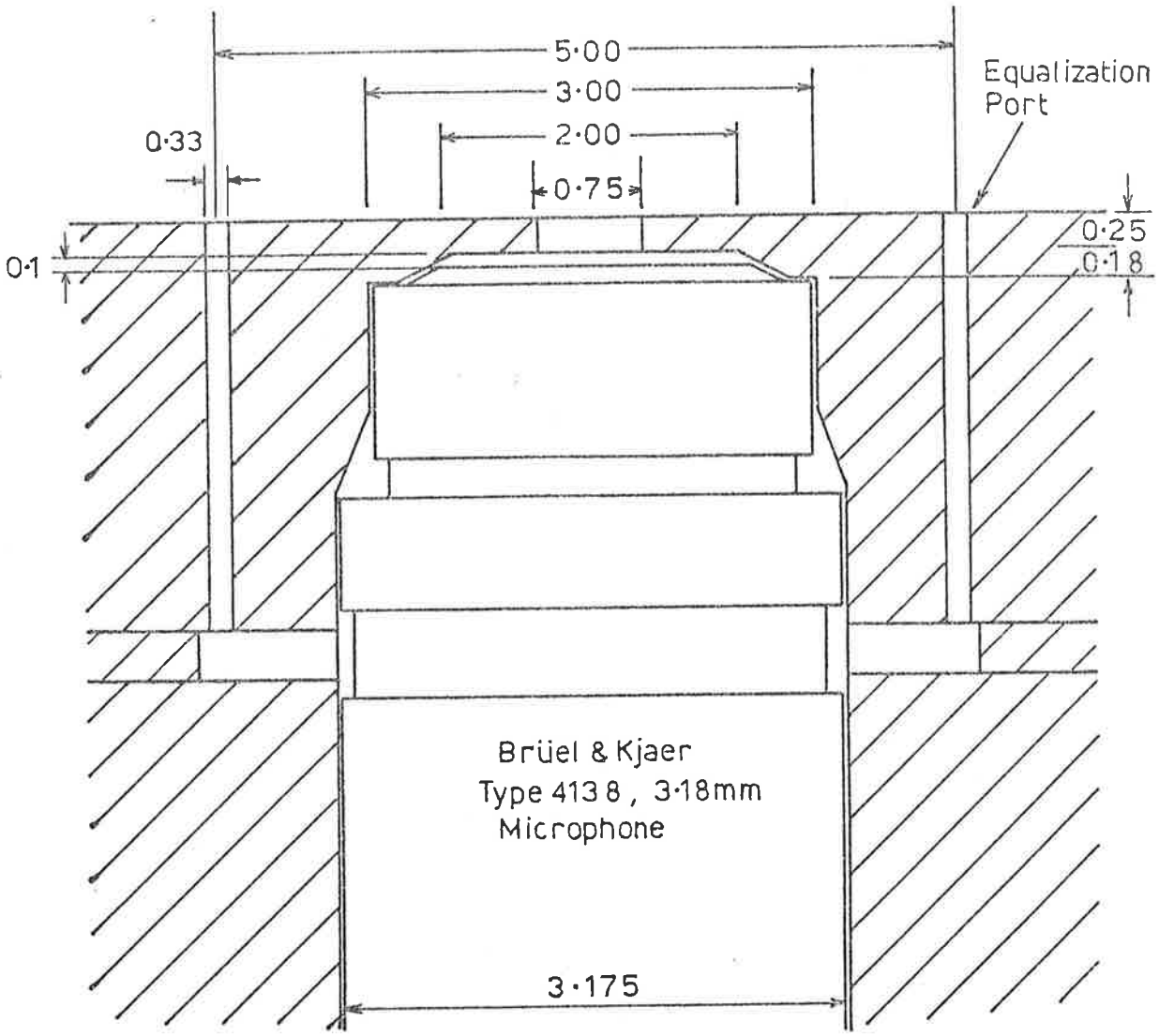

Figure 2.3 Details of the pinhole microphone pressure transducers. All dimensions in mm.

plastic cap. By this means very small cavity volumes could be obtained with minimal risk of damage to the condenser microphone.

Because the devices are required to operate in a region of mean static pressure below atmospheric, it is necessary to make provision for the mean pressure to be equalized across the microphone diaphragm. For this purpose two small 0.33mm holes were drilled on either side of the pinhole and these led to the pressure equalization hole in the microphone itself. Because of the size of this hole relative to the dimensions of the cavity behind the diaphragm, only very low frequency pressure fluctuations can be transmitted to the back of the diaphragm so that degradation of frequency response will occur only in the very low frequency region of the spectrum. The microphone manufacturers place an upper limit on this region at about 30 Hz which was considerably lower than the frequencies of interest in the experiments.

It is well established that for a small hole of radius a, and length ℓ leading to a cavity of volume V, a so-called Helmholtz resonance phenomenon may be expected to occur at a frequency given by (see for example Beranek, 1971)

$$f_o = \frac{c}{2\pi} \left[\frac{\pi a^2}{V(\ell + 2\Delta\ell)} \right]^{\frac{1}{2}} \qquad (2.1)$$

where c = speed of sound in air, a = radius of the pinhole,

$\Delta\ell$ = correction to ℓ to allow for end effects on the hole.

The generally accepted estimate for $\Delta\ell$ is $\Delta\ell = 8a/3\pi$.

Using these relationships with the known cavity dimensions gives a value of f_o of 65 kHz. Later experiments showed the actual value to be nearer 30 kHz, the difference probably resulting from the inapplicability of the above equation to the case where the hole leading to the cavity and the cavity itself have comparable volumes. In any case

this frequency is still well above the range of interest.

2.2.3. Calibration of Pressure Transducers

Two methods were employed to calibrate both the piezo-electric crystals and pinhole microphones. The first method was based on the passage of a shock wave of known strength across the transducer face and the second method on comparison of the transducer response with that of a reference microphone when the two are subjected to the same cyclic pressure variations in a small volume. In both cases the devices were calibrated while mounted in the wind tunnel plug in which they were used and calibrations were checked before and after each tunnel run.

In the first method of calibration the transducer and wind tunnel plug are mounted so as to form part of one of the walls of a shock tube. The passage of a shock wave across the transducer face causes a voltage rise at the transducer output; measurement of the voltage rise for various shock strengths allows a calibration curve to be obtained. Oscilloscope traces of typical transducer shock wave responses are shown in figure 2.4(a) and (b) for a piezo-electric device and in figure 2.4(c) for a pinhole microphone. The progressive decrease of output voltage after the shock wave has passed, which is most noticeable on the piezo-electric crystal, can be attributed to the lack of low frequency response of the transducer/pre-amplifier combination. In addition the very high frequency oscillations apparent on the trace in figure 2.4(b) can be attributed to the fundamental longitudinal resonance of the brass stem upon which the crystal is mounted. Likewise the component with a period of about 20 μsec which is evident in figure 2.4(b) can be attributed to a similar resonance in the wind tunnel plug itself.

The pinhole microphone response shown in figure 2.4(c) is of

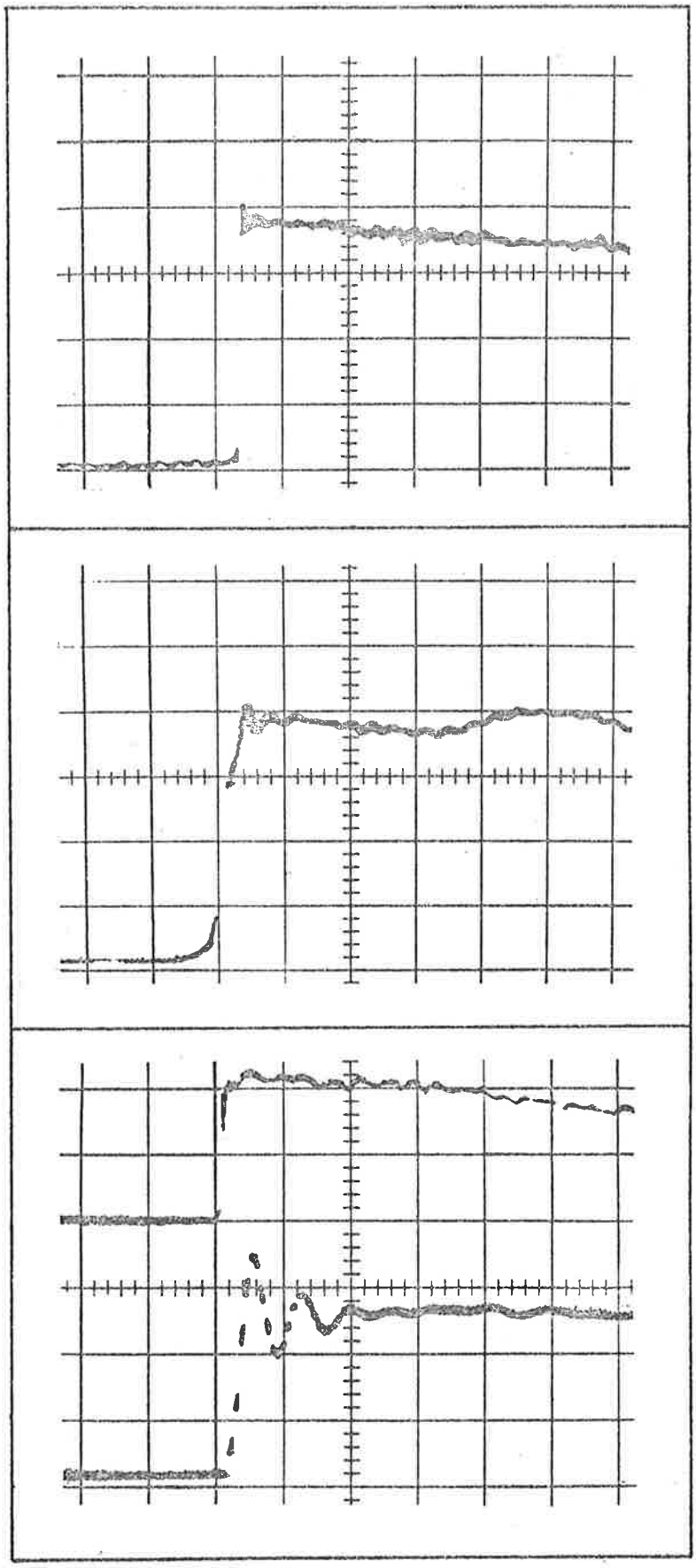

Figure 2.4(a), (b). Oscilloscope traces of the response of a piezo-electric transducer to the passage of a shock wave.

(c) Simultaneously recorded oscilloscope traces of the response of a piezo-electric pressure transducer (upper trace) and a pinhole microphone transducer (lower trace) to the passage of a shock wave.

a rather different nature and shows the response typical of a somewhat underdamped second order system. As already mentioned this arises because of the Helmholtz resonance phenomenon associated with the pin-hole and the cavity behind it. It is clear from figure 2.4(c) that the resonance frequency is about 30 kHz which was adequate for the proposed experiments.

The magnitude of the pressure rise across the shock may be calculated using the well-known relation,

$$\frac{P_2-P_1}{P_1} = \frac{2\gamma}{\gamma-1}(M_s^2-1), \tag{2.2}$$

or alternatively the approximate shock tube relation

$$\left(\frac{P_2}{P_1}\right)^{\frac{1}{7}} = \frac{2}{1+\left(\frac{P_1}{P_4}\right)^{\frac{1}{7}}} \tag{2.3}$$

where P_1 = static pressure ahead of the shock,

P_2 = static pressure behind the shock,

P_4 = initial pressure in the high pressure chamber of the shock tube,

γ = Specific heat ratio of gas used in low pressure chamber,

M_s = Shock Mach number = U_s/a_1,

U_s = Speed of progression of shock front,

a_1 = Speed of sound in gas ahead of shock front.

The first of these equations allows the pressure rise to be computed from the speed of the shock and second makes use of knowledge of the initial pressure ratio across the diaphragm of the shock tube.

The speed may be found by timing the shock as it passes between two piezo-electric crystal transducers and accurate measurements can be made if an oscilloscope fitted with a variable, precision, time delay unit is used. Great care is, however, required in measuring the time of flight as the resulting percentage error in the determination of the pressure rise can be shown to equal the percentage error in the estimation of speed multiplied by a factor of $2M^2/(M^2-1)$ which is large for a Mach number near unity. Consequently the shock diaphragm pressure method (equation 2.3) was used in preference to the shock timing method although checks were made to show that both yielded similar results.

The typical calibration curves that result from these procedures are shown in figure 2.5(a) for the crystal transducers and in figure 2.5(b) for the pinhole microphones. For the piezo-electric devices the curves are well defined straight lines, with good agreement between the two methods used to determine the shock strength. No non-linearities in the calibration can be seen. The response of the pinhole microphone system on the other hand, shows marked non-linearity, the sensitivity of the device increasing with shock strength. This phenomenon also occurs on a standard Bruel and Kjaer 1/8th inch microphone (figure 2.5(b)) and is not related to the pinhole and cavity in any way. The microphones themselves consist of a thin metallic sheet placed close to an electrode so as to form a small capacitor. Pressure waves cause the metallic diaphragm to flex with a consequent change in capacitance and the device can be expected to be linear provided the amplitude of the diaphragm motion is much smaller than the mean spacing between the diaphragm and electrode. In the shock tube, because the pressure step across the shock is much greater than the acoustic pressures for which the microphones are designed, this situation no longer occurs; the consequence is undoubtedly the non-linearities

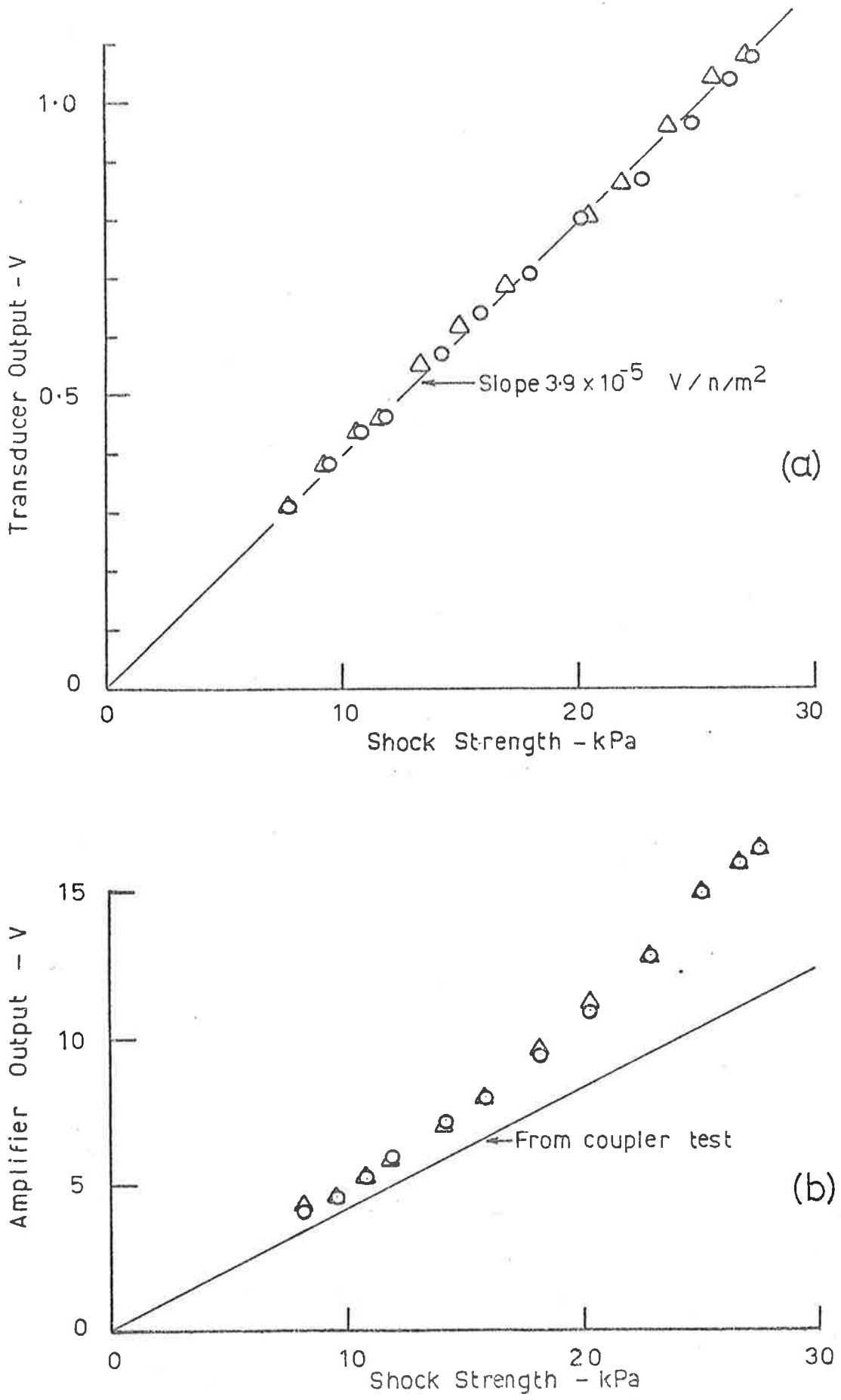

Figure 2.5(a) Typical shock tube calibration curves for a piezo-electric transducer using the shock timing method (Δ) and the diaphragm pressure method (o).

(b) Typical shock tube calibration of a pinhole microphone transducer (Δ) and a standard Bruel and Kjaer 1/8th microphone (o).

depicted in figure 2.5(b). Such non-linear effects would of course not affect the use of the device in a wind tunnel where the pressures are much lower than those encountered in the shock tube.

The shock tube calibration is therefore suitable only for flush mounted piezo-electric pressure transducers.

The second calibration procedure is to compare the pressure transducer with a known reference microphone, using a small coupler into which they both face, and in which cyclic pressure variations are created. The device used is shown in figure 2.6(a) with a pinhole microphone and in figure 2.6(b) with a piezo-electric crystal; it consists essentially of a small cavity of diameter 3.5mm and length 3.5mm which can be placed over the pressure transducer being tested.

The pressure oscillations are provided by means of a small earpiece speaker which is driven by a signal generator and Silicone grease is used throughout to ensure that no air leaks are present. As shown in figure 2.6(a) the use of the device is quite straight forward with pinhole microphones. Both pressure signals can be observed on an oscilloscope to determine the frequency and phase characteristics of the pinhole microphone being tested; an absolute pressure calibration is obtained by calibrating the reference microphone with a Bruel & Kjaer pistonphone type 4220.

When calibrating piezo-electric transducers by this method, vibration isolation is required, otherwise the transmission of vibrational energy from the earpiece driver to the crystal can give rise to an apparent spurious frequency response. For the present tests this was achieved by using thick layers of silicone grease as shown in figure 2.6(b), the mass of the coupler being carried by a separate support. Without such precautions consistent calibration data could not be obtained.

Valid calibration with the acoustic coupler requires that at

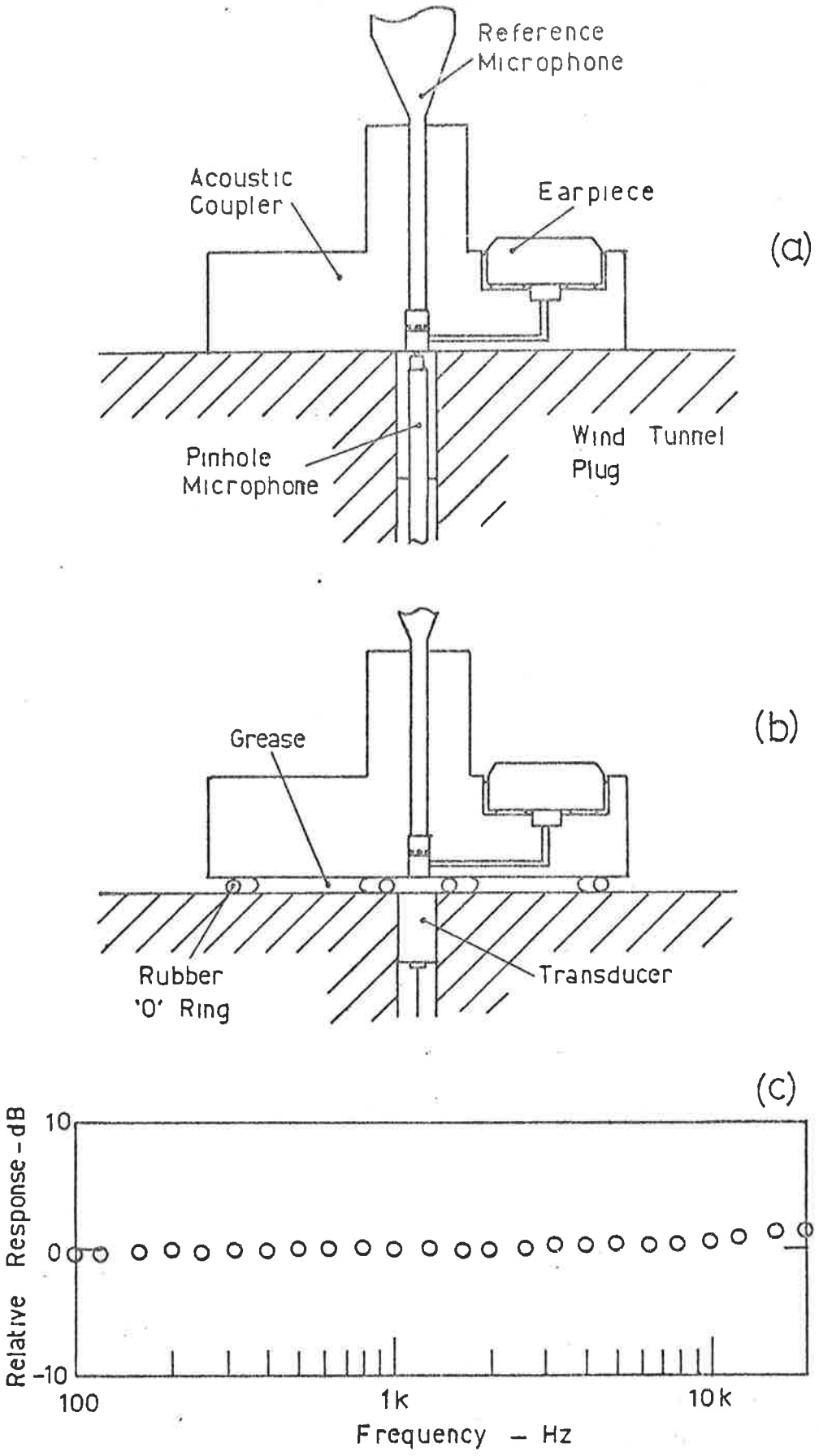

Figure 2.6(a) Arrangement for acoustic coupler calibration of a pinhole microphone.

(b) Arrangement for acoustic coupler calibration of a piezo-electric pressure transducer.

(c) Response of coupler using two standard microphones.

any given frequency and at any instant there is a uniform pressure within the cavity. Clearly at high frequencies where the acoustic wavelength is small this may not be the case and following Lim (1971) this may be expected to occur at a wavelength λ such that $\lambda/10 \approx d$, where d is a typical cavity dimension. For the present case where d = 3.5mm this yields an upper frequency limit of 10 kHz. In figure 2.6(c) are shown the results obtained when the pressure transducer is replaced by another standard 1/8" microphone. It can be seen that a flat response from the coupler is indeed obtained for frequencies up to about 10 kHz with small deviations occurring at higher frequencies.

Figures 2.7(a) and (b) show the frequency behaviour of each device at a fixed pressure amplitude and in both cases their response is flat to within less than 1dB from 100 Hz to 10 kHz. No phase shifts could be detected over this range. Figures 2.8(a) and 2.8(b) show the linearity of both transducers with pressure amplitude at a frequency of 1 kHz. A direct comparison may be made between these results and the shock tube results of figure 2.5 in which the amplitude of the pressure was 1000 times greater than in figure 2.8. The accurate linearity of the piezo-electric transducer over this range is notable. The departures from linearity of the pinhole microphone are due to the non-linear response described previously.

When taking boundary layer pressure data the acoustic calibration method was used, careful checks being made before and after each run to ensure that no calibration drift had occurred. The shock tube test was used to check the behaviour of new piezo-electric transducers and to determine the resonance frequencies of the pinhole microphones.

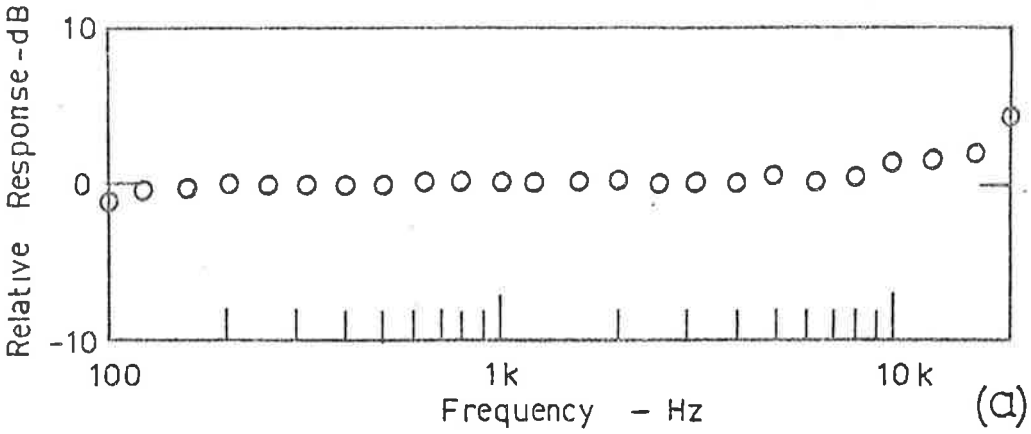

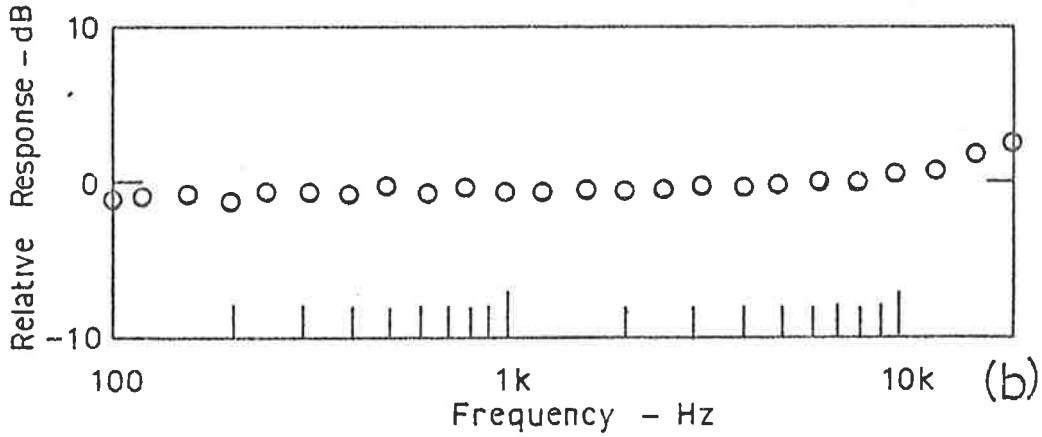

Figure 2.7(a) Frequency response of a pinhole microphone as measured with the acoustic coupler.

(b) Frequency response of a piezo-electric transducer as measured with the acoustic coupler.

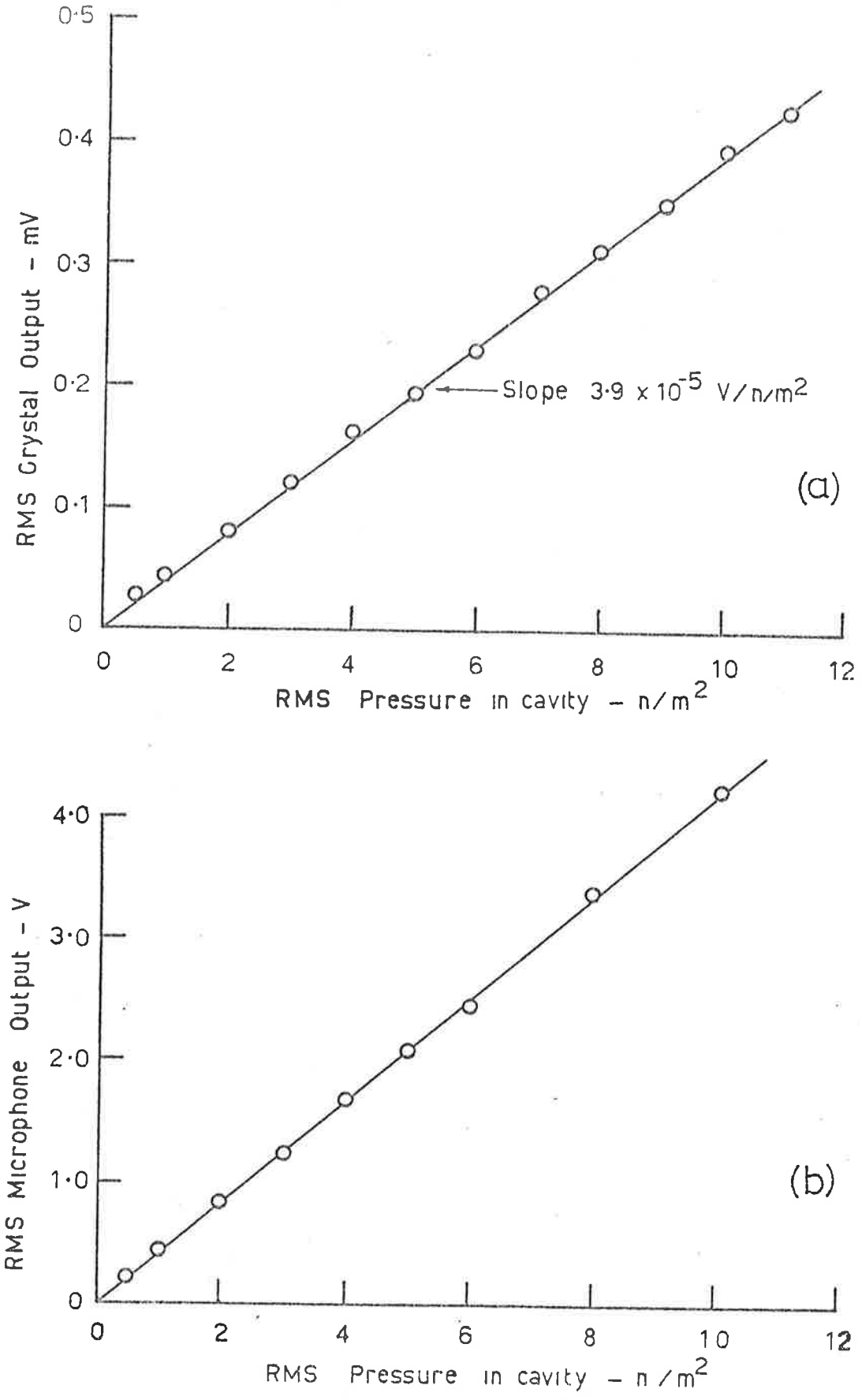

Figure 2.8(a) Calibration of a piezo-electric transducer at a frequency of 1 kHz using the acoustic coupler.

(b) Calibration of a pinhole microphone at a frequency of 1 kHz using the acoustic coupler.

2.3 Sensors for Velocity and Shear Stress Measurements

2.3.1 The Hot Wire Anemometers

The single hot wire probes used for this work are shown in figure 2.9(a). The needles for these probes were 0.3mm diameter steel jeweller's broaches set at a 2.0mm spacing.

For the measurement of the transverse or v component of velocity smaller cross wire probes shown in figure 2.9(b) were used. The needles for these probes were 0.13mm diameter steel jeweller's broaches set at a spacing of 1.0mm. To avoid possible thermal interferences the cross wire pair was separated by 0.5mm (i.e. half the wire length, Bradshaw, 1971). It may be noted that this separation represents 1.25% of the thickness of the boundary layer in which they were used and corresponds to a scale of $43\nu/U_\tau$ which was adequate for the large scale motions being studied.

The wires used in the experiments were of 5×10^{-6}m diameter tungsten and were soft soldered to the needles. To facilitate soldering, the ends of the wires were copper plated so as to leave an unplated active portion 1.0mm long giving a length to diameter ratio (ℓ/d) of 200. Constant temperature operation was used at an overheat ratio of 1:2; the cold resistance of the wires was typically 6.0 ohms. Prior to operation the time response of the wires and the associated feedback loop was set using the square wave injection technique.

2.3.2. Calibration of the Hot Wire Anemometers

The single hot wires were calibrated in the free stream against a Pitot tube. The form of the calibration law used was

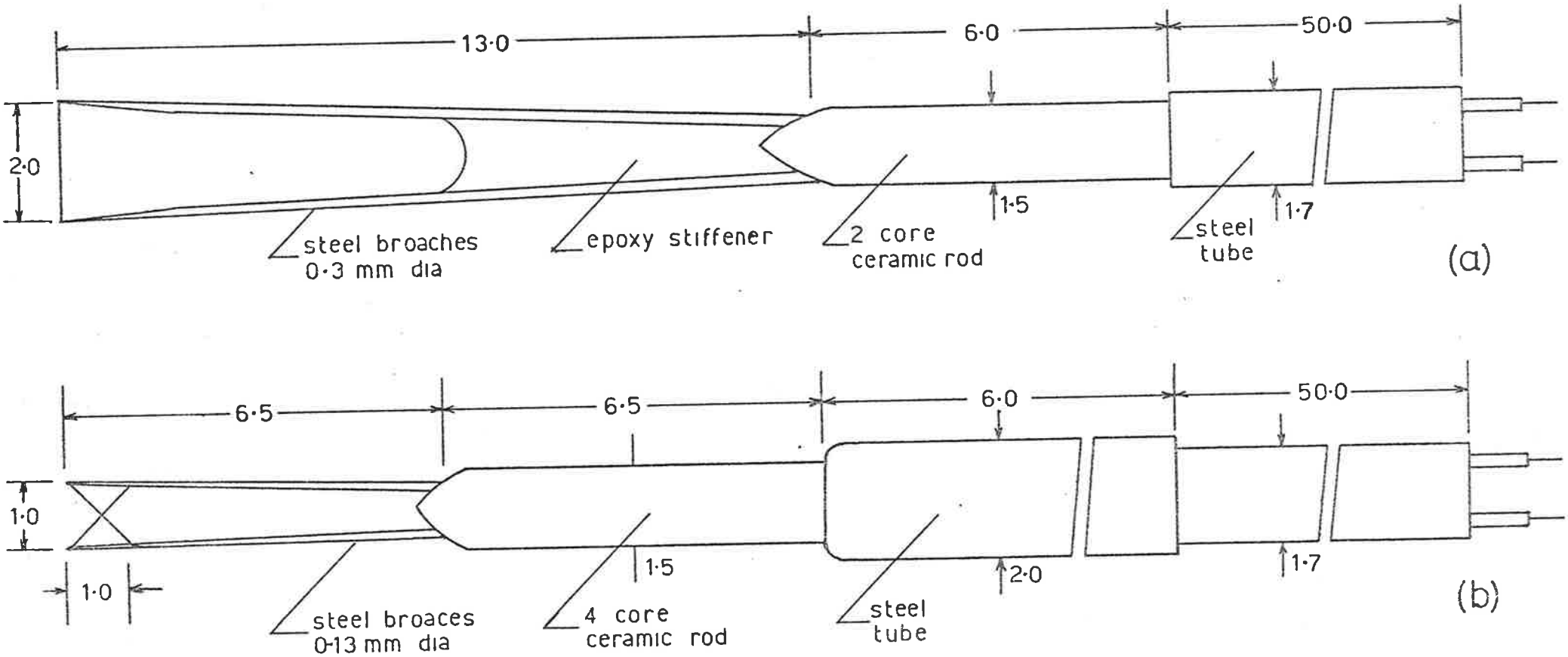

Figure 2.9(a) Design of hot wire probe for measurement of the streamwise component of velocity.

(b) Design of cross wire probe for measurement of streamwise and normal component of velocity. All dimensions in mm.

$$V^2 = V_o^2 + BU^n, \qquad (2.4)$$

where V is the measured bridge voltage and the exponent n was found to be 0.45 for optimum linearity over the calibration range.

The calibration of the crossed wires was more difficult but was again performed in the free stream, calibration data for each wire being taken at several yaw angles within the range $\pm 10^o$. To facilitate such measurements the crossed wire pair was mounted on a pivot and could be rotated about the pivot. The calibration technique follows that described by Bradshaw (1971) and is based on the assumption that a "cosine" cooling law is valid and that an effective value of the wire angle can be determined. This method makes an attempt to take account of the longitudinal cooling of the wire and, correspondingly, yielded wire angles that differed from the measured angles by about 2^o. This difference arises because the longitudinal velocity component has the effect of making the wire appear to lie closer to the direction normal to the flow.

Shown in figure 2.10(a) are the typical yaw calibration curves that result for a given member of a crossed wire pair and in each case the linearity can be seen to be good. For determination of the effective wire angle these curves have been cross plotted in the form suggested by Bradshaw (1971) namely

$$\left[\frac{V^2-V_o^2}{V^2-V_o^2}\bigg|_{\Delta\psi=0}\right]^{\frac{1}{0.45}} \text{—} \cos\Delta\psi = -\tan\psi_{eff}\sin\Delta\psi$$

and are shown in figure 2.10(b). The linearity of these curves suggests, as Bradshaw points out, that the probes are reasonably free from prong interference and other spurious effects.

Later experiments demonstrated that the resulting values of u', v' and $-\overline{uv}$ measured at various points in the boundary layer agree very

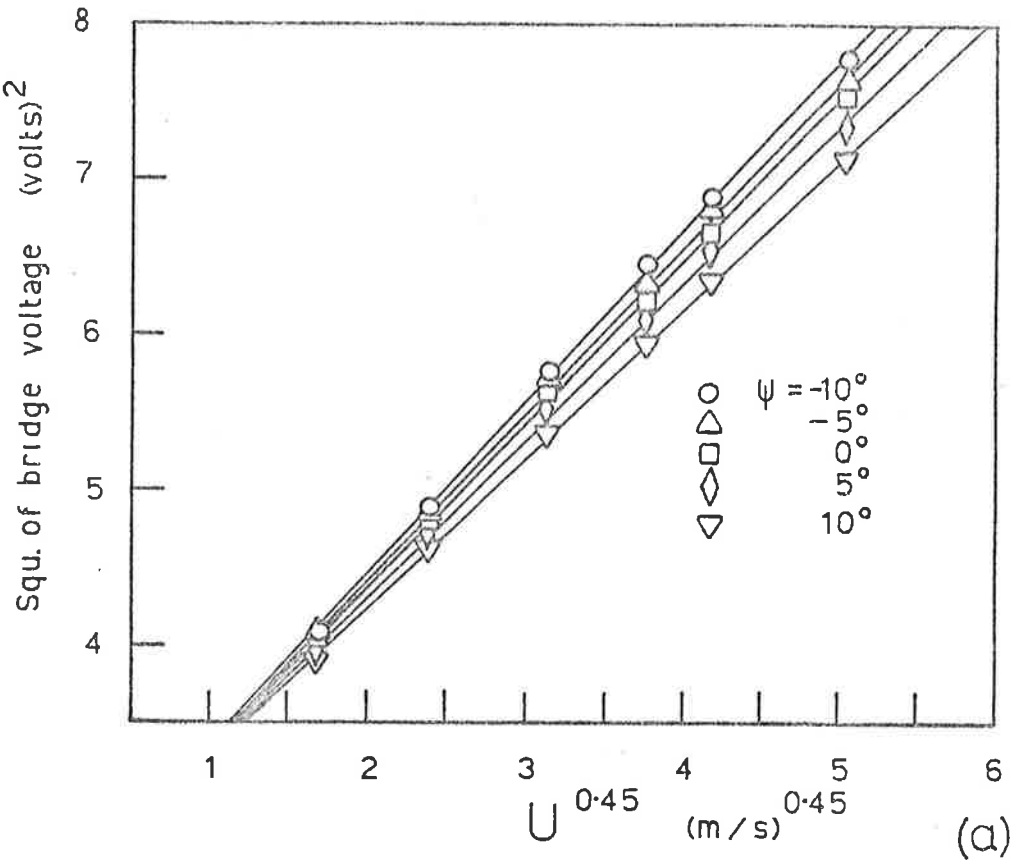

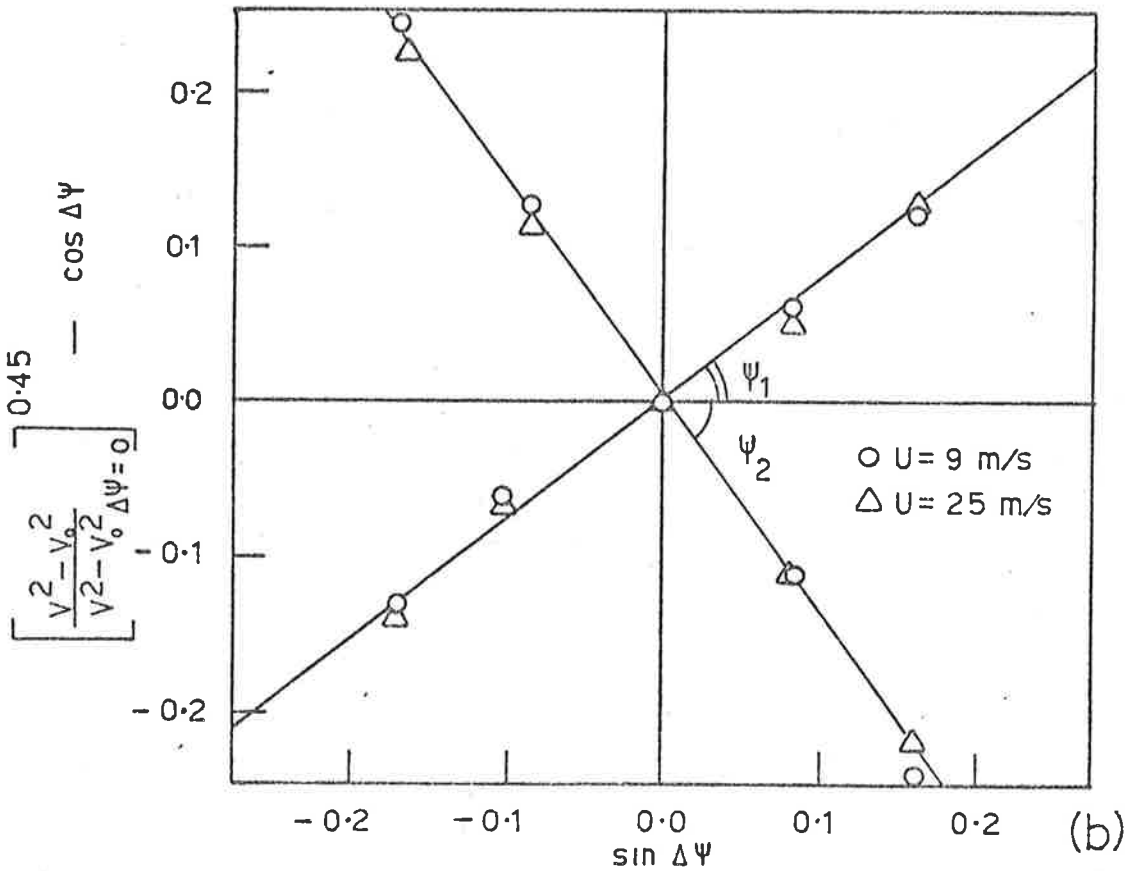

Figure 2.10(a) Typical yaw calibration curves for one member of a crossed wire pair.

(b) Cross plot of yaw calibration data in the form suggested by Bradshaw (1971).

well with previously published data suggesting that the calibration procedure is adequate.

2.3.3. The Constant Temperature Feedback System.

The circuitry used to drive both the hot wires and hot films in the constant temperature mode is shown in fig. 2.11. The system is based on a high speed National Semiconductor LM 318 operational amplifier. The current output of this unit is boosted by the high performance 2N 2270 power transistor. The bridge ratio is 1:1 with 20Ω resistors in the upper two arms. Because of the compact design and high bandwidth of the LM 318, no trimming inductances were required. Output offset was controlled by means of a 200KΩ potentiometer connected to the internal offset control of the LM 318 and no compensation networks were used on the amplifier. A square wave could be injected into one side of the bridge with protection provided by a 10KΩ resistor and 1.0μF capacitor.

The system was very compact and could be placed close to the probes so that long cables did not have to be used, thereby reducing the possibility of oscillations through lead inductance effects.

2.3.4 The Hot Film Shear Stress Sensors.

The use of flush mounted hot films in turbulence research is by no means new although the devices of course are not as popular as the hot wire anemometer. The use of films of certain geometries is also a well established technique for velocity measurements in liquids and in environments intolerable to hot wires. The use of films as dynamic shear stress gauges can therefore be viewed as a somewhat specialized anemometry technique.

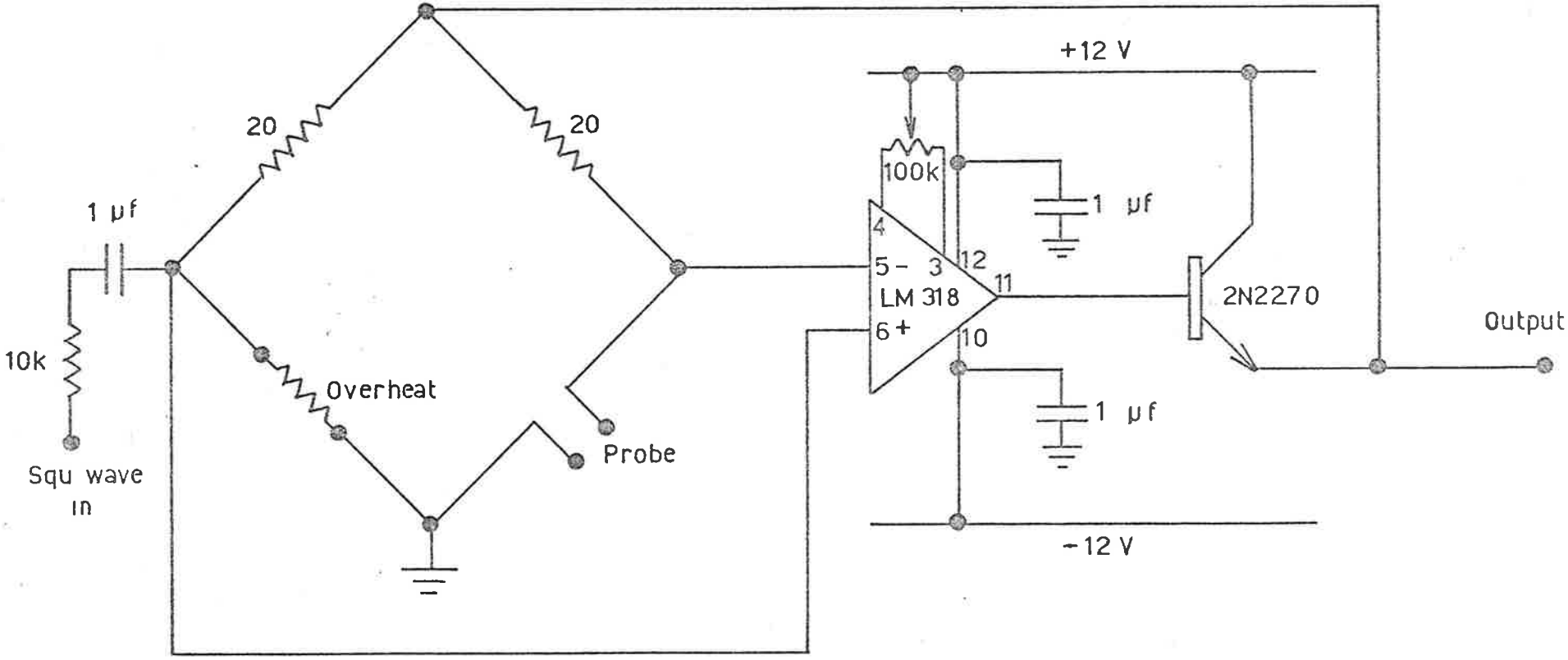

Figure 2.11 Circuit diagram of the constant temperature feedback bridge.

Fage and Falkner (1931) used the heat transfer from a heated element to determine skin friction and Ludwieg (1950) used a heated copper block for skin friction measurements in a turbulent boundary layer. Liepmann and Skinner (1954) used a hot wire near the surface for similar measurements and showed that a one third power law shear stress calibration could be expected. Lighthill's (1954) analysis of the heat transfer to a linear velocity profile also showed that such a calibration might be expected.

Bellhouse and Schultz (1966) used thin heated films of platinum for mean and dynamic friction measurements in both laminar and turbulent flows and verified the applicability of the one third power calibration law. Brown's (1967, a, b) detailed analysis of the heat transfer from a wall with a "top hat" wall temperature distribution shows that the Nusselt number depends on the one third power of the wall shear stress and depends only weakly on the pressure gradient. His experiments in both laminar and turbulent flows once again verified this result and demonstrated rather remarkably that identical mean calibration could be expected in both flow situations.

Quite recently Armistead and Keys (1968) performed correlation and spectral measurements using thin gold films in turbulent pipe flow, and Simpson (1975) has used commercially available platinum films to determine details of the quasi-periodic flow known to exist in the sublayer region of a turbulent boundary layer. In neither of these series of measurements however was a calibration of the thin film gauges attempted.

2.3.5 Manufacture of the Hot Film Sensors.

Bellhouse and Schultz (1966) manufactured their films by the heating of a thin strip of metallic based paint which had been applied to

the substrate material. The reader is referred to their report for a more detailed discussion of this method. The main shortcoming of such a technique is that there is little control over the electrical and geometrical properties of the film that finally results; it is for this reason that an alternative method was used to produce the films for this work.

The production technique was based upon vacuum deposition of the required film material on to the substrate medium. The metal is raised to melting point on an electrically heated tungsten filament and allowed to evaporate. Condensation will occur on all nearby surfaces and by a suitable arrangement of shrouds and shields a thin metal film of any desired shape can be formed on almost any surface. The technique is therefore suitable for the production of flush mounted hot films and with some care it is possible to produce several almost identical films in one evaporation process.

The evaporation of metals has been used for many years to produce electronic components and as such is a well-documented technique. An excellent treatise on the subject can be found in Holland (1966).

For the substrate of the films, ceramic or glass may be used. Glass was used for the present films as some early experiments indicated that the ceramic materials chipped rather easily and that the porosity of the ceramic surface tended to give rise to weak areas of high electrical resistance in the films.

Nickel was chosen for the film metal particularly because of the high resistance to abrasion of nickel on glass (compared with gold and platinum, Holland, 1966), because of its relatively high temperature coefficient of resistivity (6.7×10^{-3} / ^{o}C) compared to gold (3.9×10^{-3}) and silver (1.6×10^{-3}), and because of its quite adequately slow rate of oxidation.

In view of the above considerations films using nickel on a glass

substrate were produced by the following means:

(i) Small lengths of 2mm dia glass rod were cut and their end faces ground and polished to give a 10mm length. Their corners were then chamfered at two diametrically opposite points on one end as shown in figure 2.12(a). This small chamfer lends strength to the film which has to be deposited around the sharp corner. These rods were then cleaned ultrasonically in alcohol for about 2 minutes.

(ii) The rods were then placed face up in a row in the vacuum chamber and a screen with a 0.25mm wide slot (2 razor blades side by side) placed over them to form a shield for the first evaporation. They were then heated to 300°C and the pressure reduced to 5×10^{-5}mm of mercury. The effect of the heating is twofold. Firstly the films tend to bond better to a hot substrate; and secondly after the metal condenses the atoms still have some mobility on the hot glass which allows a more even grain growth, resulting in a more stable film. It was found that if the heating was not used the films suffered from a sudden and irreversible resistance drop during subsequent operation.

Fine nickel wire wrapped on a tungsten filament was then evaporated to leave a film 0.25mm wide running across the end faces of the glass rods. (fig. 2.12a).

(iii) The first shield was removed and a second shield 0.5mm wide was placed centrally across the faces of the rods to form a mask for the evaporation of the side films. As shown in figure 2.12(a) two stages were used for this and very thick films were deposited on the ends of the glass rods and allowed to run over the chamfered corner and down the sides of the rod. This resulted in films ready for mounting.

(iv) The details of the mounting are shown in figure 2.12(b). Two wires were glued on to the side of the glass rod and conducting epoxy

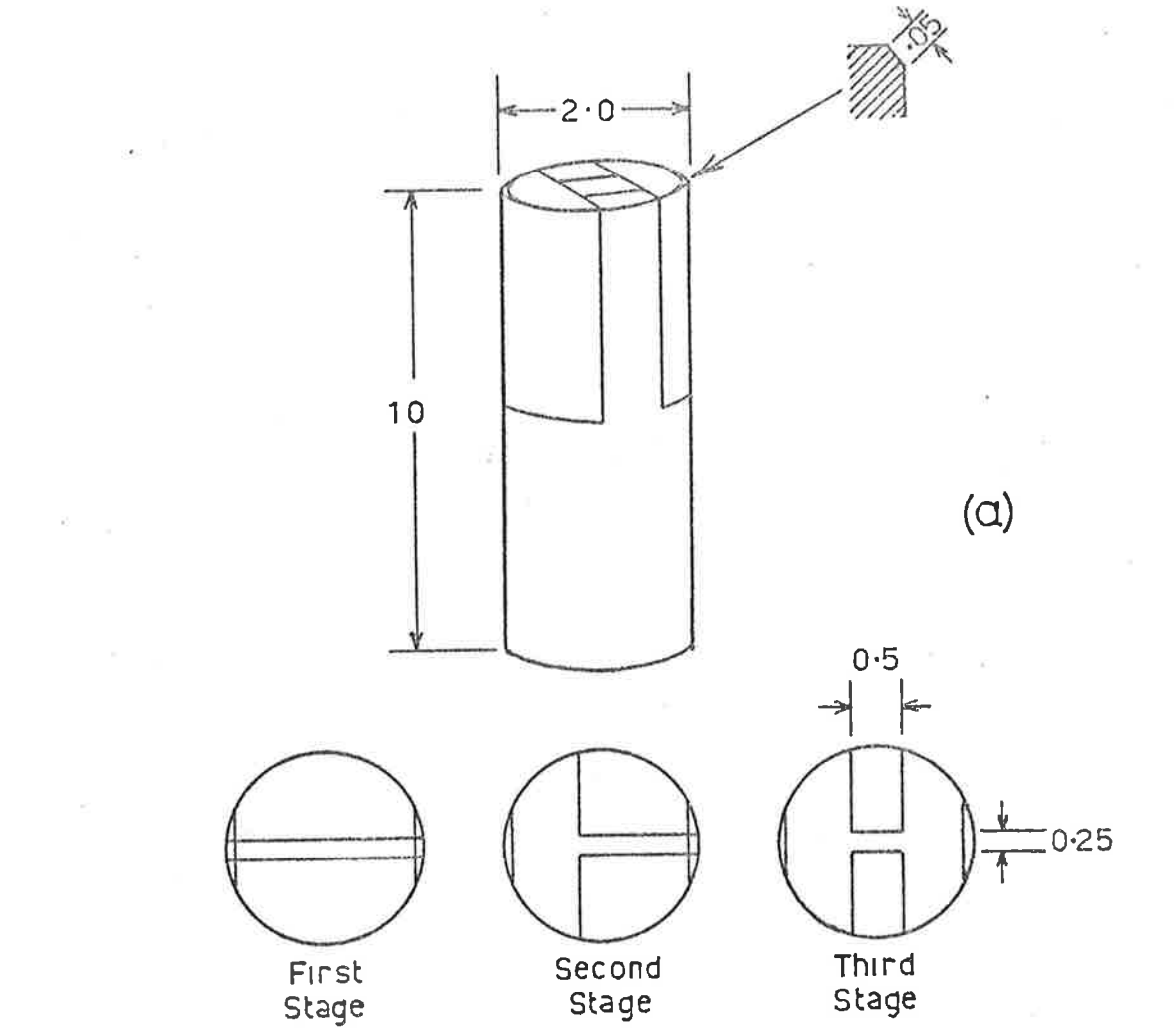

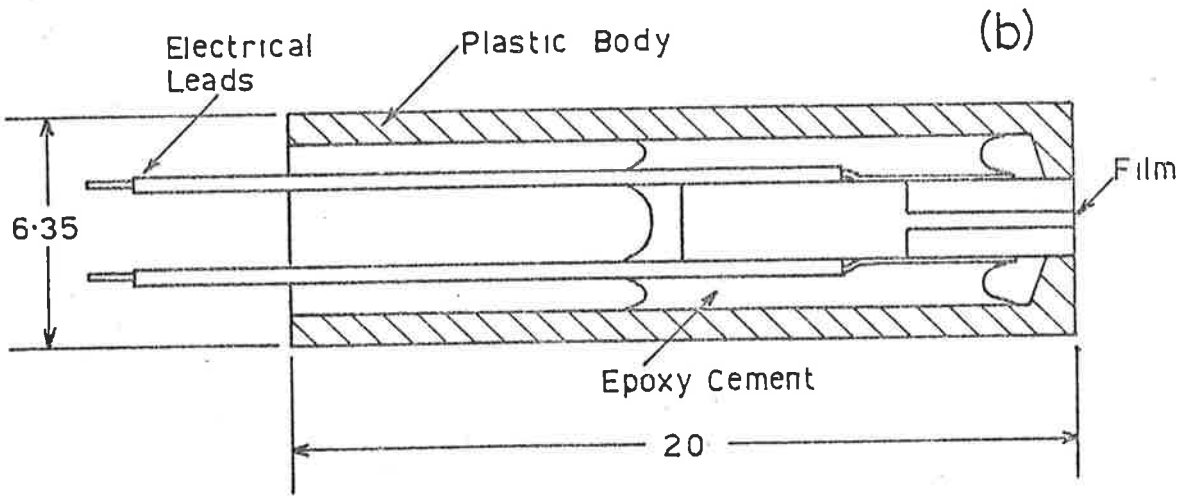

Figure 2.12(a) Diagram of the glass rods used as a substrate for the hot films and the three stages of evaporation used when depositing the films.

(b) Arrangement of the mounting of the hot films. All dimensions in mm.

resin applied liberally to ensure good electrical contact from the wires to the side films. The unit was then fixed into the plastic body as shown in figure 2.12(b).

With this technique batches of films were produced with cold resistances of typically 15 ohms and very closely matched characteristics. These characteristics were so closely matched in fact that the raw uncalibrated turbulent spectra from various films of one production run were sometimes quite indistinguishable from each other.

The temperature coefficient of resistivity of the films was typically $2.7 \times 10^{-3}/^{o}C$ which is about 40% of the value of the bulk metal and, as Holland (1966) points out, is typical of small films.

The films were operated in the constant temperature mode at an overheat ratio of 1.2 and a mean film current of about 50mA. This represents an overheat temperature difference of about $75^{o}C$.

2.3.6 Static Calibration of the Hot Film Sensors

In the past films for shear stress measurements have been calibrated in a wind tunnel by placing them beneath a laminar boundary layer and comparing the film output with the output of a Stanton tube or Preston tube. Brown and Davey (1971) describe an alternative calibration method using the flow between a flat plate and a disk rotating in a plane parallel to the plate. This flow is an asymptotically exact solution of the Navier-Stokes equations for small gaps and offers a very simple means of calibration.

A device similar to that described by Brown and Davey was made and is shown schematically in figure 2.13(a). The design allowed a variable disk-to-plate spacing and the film could be traversed beneath the disk on the slide to vary the shear stress at the film.

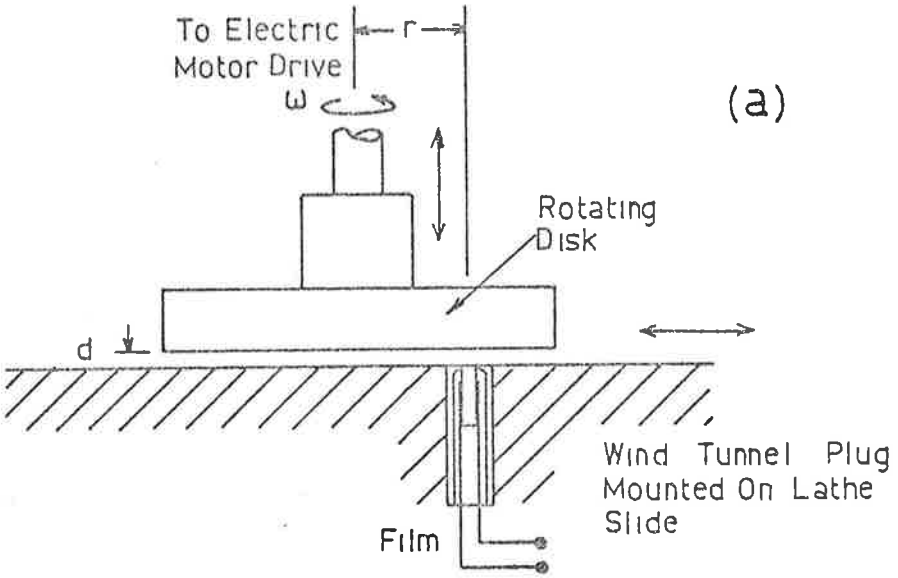

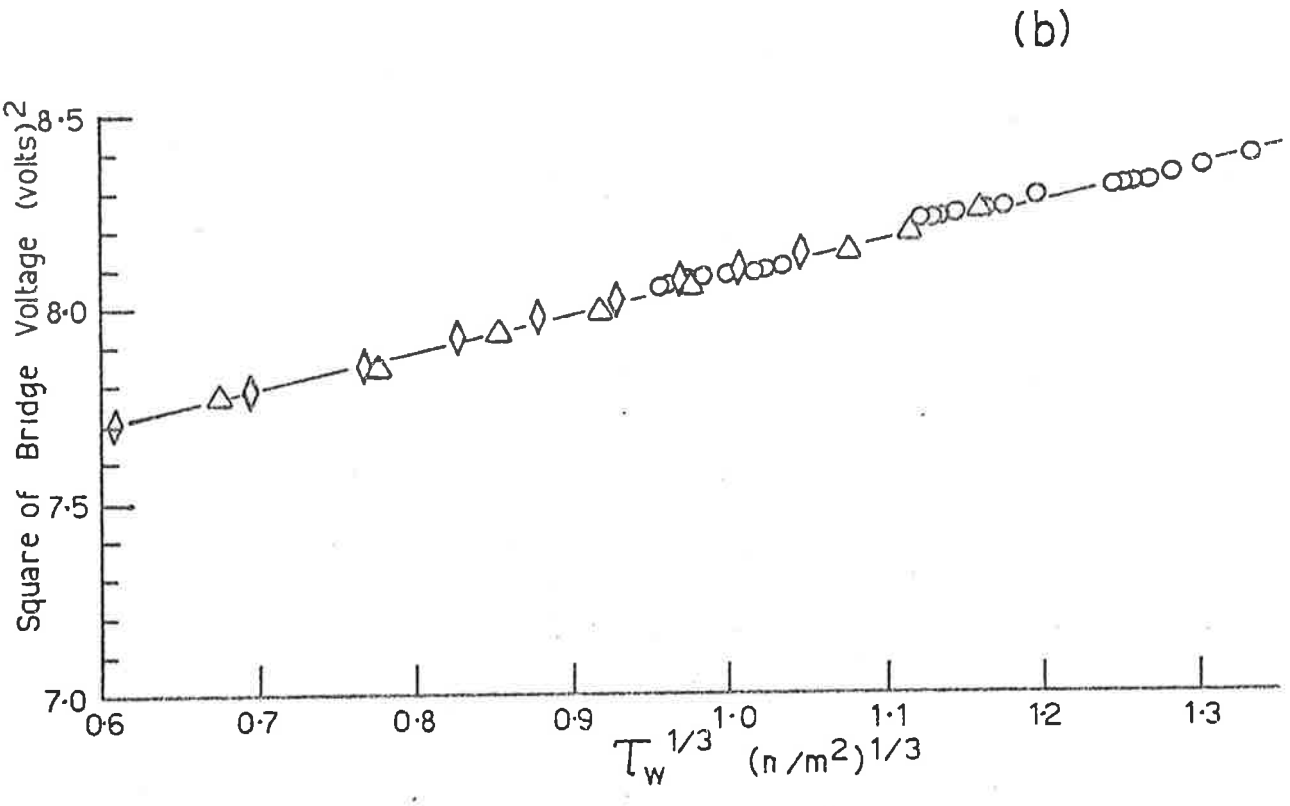

Figure 2.13(a) Arrangement of the spinning disk used to calibrate the hot films.

(b) Typical calibration curve of a hot film transducer. ◊, ω = 940 rad/sec, d = 0.3mm; Δ, ω = 1260 rad/sec, d = 0.3mm; o, calibration points inferred from Preston tube measurement in the wind tunnel.

A typical calibration is shown in figure 2.13(b). The films were also used in the boundary layer wind tunnel to measure the mean wall shear; these results are also presented in figure 2.13(b) as a calibration curve where the wall shear stress as measured by a Preston tube has been used to define the curve. The data points lie precisely on the mean curve obtained from the spinning disk calibration.

This would appear to be a significant finding as it demonstrates that films such as these may be calibrated externally in this laminar flow device and then used directly to measure skin friction in an unknown turbulent boundary layer where calibration in situ is not possible.

The 1/3rd power calibration law depends on, amongst other things, the existence of an essentially linear velocity profile above the film and validity of the boundary layer approximation to the thermal energy equation. Under such circumstances Spence and Brown (1968) show that the calibration law can be reduced to

$$\frac{I^2 R_w}{\Delta T} = \lambda W \left(\frac{1}{1.9} \quad \frac{\rho \sigma L_e^{\,2}}{\mu^2} \right)^{\frac{1}{3}} \tau_w^{\frac{1}{3}} + B, \qquad (2.5)$$

where I = mean film current,

R_w = mean film operating resistance,

ΔT = overheat temperature difference,

λ = conductivity of fluid being used,

σ = Prandtl number,

ρ = Fluid density,

μ = Fluid viscosity,

W = width of the film in the spanwise direction,

L_e = effective length of film in streamwise direction.

Clearly however, due to the spreading of the heat into the substrate, W and L_e will be larger than the geometrical values and must be experimentally determined. If W were known accurately (as would be the case for films of large W/L_e) then L_e could be determined from the above equation in conjunction with the slope of the measured calibration curve. For the 0.5mm x 0.25mm films used in this investigation, W and L_e are comparable so that an uncertainty exists in any estimation of L_e. This is demonstrated by the following values of L_e computed for a typical film from equation 2.5 with various possible values of W;

W(mm)	L_e(mm)	L_e/W	L_e/L_a
0.5	0.86	1.72	3.44
0.6	0.66	1.10	2.60
0.7	0.52	0.74	2.08

Here L_a is the actual film length (0.25mm). Clearly large values of W lead to small values of L_e and conversely, so that a compromise value has to be selected. In view of the fact that the actual width is 0.5mm, it is reasonable to assume an effective width of approximately 0.6mm giving an effective length which is 2.6 times the actual length. In his experiments, Brown (1968) found this ratio to be close to three also.

Spence and Brown (1967) also found that for the 1/3rd power law calibration to be applicable the following inequality must be satisfied;

$$\frac{6.6}{\sigma^{\frac{1}{2}}} < \frac{U_\tau L_e}{\nu} < 64\sigma$$

The lower limit is a consequence of the requirement that the streamwise temperature gradients be small compared with vertical gradients so that a boundary layer type of approximation is valid. The upper limit follows from a requirement that the thermal

boundary layer due to the film lie within the linear viscous sublayer of the turbulent boundary layer so that a linear mean velocity profile is an accurate approximation to the velocity profile. For air with Prandtl number $\sigma = 0.72$ the inequality becomes

$$7.8 < \frac{U_\tau L_e}{\nu} < 46$$

For the two flow extremes used in most of these experiments ν/U_τ ranged from 1.2×10^{-5} to 1.7×10^{-5}. The inequality is then

$$0.09 < L_e < 0.53\text{mm}$$

and $$0.14 < L_e < 0.81\text{mm},$$

for these two cases. Thus the films with an effective width of 0.66mm are well within the limits for the lower speed and not seriously beyond the limit at the higher speed.

Given these considerations in addition to the smooth and very linear calibration curves that result (figure 2.13(b)) it seems reasonable to assume that the films give a valid measure of the mean wall shear.

2.3.7 Deduction of Dynamic Calibration of Hot Film Sensors

The dynamic response of the films is of course significantly different from the static response due to the reduction in effective length of the film at high frequency. This is a consequence of the reduced penetration of the dynamic heat flux into the substrate. The frequency at which this phenomenon becomes significant is in fact quite low. Indeed a simple analysis based on an unsteady one dimensional conduction equation (or simply dimensional analysis) shows that for a glass substrate the fluctuating heat flux will penetrate to distances much less than L_a if $\omega L_a^2/\kappa >> 1$. (κ = thermal diffusivity of glass). At frequencies satisfying this criterion the film effective length will be the same as the geometrical length. The implication is then that for these frequencies

the slope of the one-third power calibration line (equation 2.5) must be decreased in the ratio $(L_e/L_a)^{\frac{2}{3}}$ or by a factor of about 1.9 for the given values of L_e and L_a.

There is also an upper limit to the frequencies for which this quasi-steady behaviour can be assumed, and this limit is determined by flow conditions. In more precise terms one must consider the significance of the time dependent term $\partial T/\partial t$ in the heat equation in relation to the convective terms such as $u\partial T/\partial x$. This is discussed in more detail by Brown (1967) and he demonstrates that this leads to the requirement that the frequencies be such that

$$\omega << \frac{U_\tau^2}{\nu} \cdot \sigma^{-\frac{1}{3}} \cdot \left(\frac{\nu}{U_\tau L_a}\right)^{\frac{2}{3}}$$

Taken with the previous requirement, for a quasi steady behaviour to be valid, the frequencies must therefore lie within the following range.

$$\sigma^{-\frac{1}{3}} \left(\frac{U_\tau L_a}{\nu}\right)^{\frac{4}{3}} > \frac{\omega L_a^2}{\nu} > \frac{\kappa}{\nu}$$

For the flows used in the present investigation these limits correspond to about 5 kHz and 50 Hz. This is adequate for the present study since virtually all the turbulent energy exists within this frequency range.

Direct measurement of the dynamic sensitivity of the devices would be preferable, but no reliable method exists at present which satisfies the constraints discussed in the last section.

Bellhouse and Schultz (1966) attempted such a calibration by mechanically oscillating the film beneath a boundary layer, but were limited to low frequencies. Acoustic oscillations superimposed on a mean boundary layer flow could in principle be used, were it not for the fact that acoustic boundary layers tend to be very thin so that the length

requirements cannot be satisfied.

2.3.8 Hot Film Time Response.

The discussion in the previous section does, of course, assume that the film and its associated constant temperature feedback loop, is capable of response at the desired frequencies. The question of the dynamic behaviour of such a system is complex and requires careful consideration of the effect of the spread of heat into the substrate below the metal element. In addition, as is the case with hot wires, the dynamic response of the feedback loop itself is subtle, due to the active element within the feedback loop.

In an analysis taking account of these and other problems, Brown in a private communication, has shown that the problem of determining the time response given a step change in heat transfer at the film, reduces to finding a solution of an integral equation. A brief summary of the important points of this analysis is presented in Appendix A and it is demonstrated that a solution is possible yielding the following rather simple result for the time constant of the film and the feedback system:

$$T^{\frac{1}{2}} \approx \frac{3.2\, A_f \pi^{\frac{1}{2}} \lambda}{2 I_f^{\,2} R_f \kappa^{\frac{1}{2}}} \cdot \frac{E_{off}}{E_o} \cdot \frac{(R_1 + R_f)^2}{R_1 R_o\, \alpha} , \qquad (2.6)$$

where A_f = Film area,

λ = Thermal conductivity of glass,

I_f = Mean film current,

R_f = Film operating resistance,

R_o = Film cold resistance,

E_{off} = Output offset voltage,

E_o = Mean bridge voltage,

α = Temperature coefficient of resistivity of film,

R_1 = Bridge resistances,

κ = Thermal diffusivity of glass.

This relationship clearly demonstrates the need for small films operating at large overheat ratios and with carefully tuned offset voltages. Perry and Morrison (1971) have also demonstrated the importance of offset voltage in the case of hot wires.

To check the time response of the present films a shock wave was passed across the face of the film and the offset voltage adjusted to give a critically damped output free from overshoot. The step response determined in this way was typically 50 μsecs which is clearly adequate for the proposed experiment. Because of the importance of correctly setting the time response of the film and the feedback system, this procedure was adopted before each tunnel run; without these precautions spectral distortion was found to occur for frequencies greater than about 10 kHz.

Additionally, the film time response depends upon the ratio E_{off}/E_o which decreases as the flow is applied to the film. These changes are however quite small (7%) so that they do not lead to significant changes in the time response of the device when used in the wind tunnel.

2.4 The Digital Data Acquisition Facilities

Except for the power spectral measurements, all the data analysis was performed on the Control Data Corporation 6400 computer of the University of Adelaide. The measurements were recorded on computer tape using a multiple input channel data acqusition system designed by and built in the Department of Mechanical Engineering at the University of Adelaide. The system enables simultaneous measurements to be made on twelve analogue and four digital channels at total rates of up to three million per second. These measurements (each of eight bit precision) are written into a 16K shift register memory that is hard wired within the system. Different quantities of the memory can be allocated independently to each of the 16 channels according to requirements. Likewise the sampling rates on each channel can be independently varied up to a maximum of 0.5 MHz.

When the allocated memory is filled its contents are dumped onto standard 9 track computer tape as a continuous block with a preamble on each record providing information such as sampling rates, memory block sizes etc. This process of acquiring the data and writing to tape can be repeated any selected number of times.

The entire operation of this system is controlled from a series of front panel switches and it is apparent that such versatility enables experiments with multiple arrays of probes to be undertaken with relative ease.

For the experiments that follow, the sampling rate was 12.5 kHz and each record consisted of 2560 words of memory allocated to each input channel with typically 16 such records being acquired for each run of a particular experiment. The analogue to digital

converters used within the data acquisition system were the ADC10Z (20 μsec conversion time) and the ADC10QU (8 μsec conversion time) 10 bit converters manufactured by the Analog Devices Corporation with the most significant 8 bits being used. Whenever possible the higher speed converters, of which four were available, were used although this was not entirely necessary as negligible energy existed within the turbulence signals at frequencies corresponding to the slower conversion time.

The analogue to digital converters were set for a bipolar operating mode with an input range of -5 to +5 volts; since the turbulence signals were typically of the order of a few hundred milli-volts in amplitude, some signal amplification was necessary prior to the conversion process.

For this purpose a series of signal amplifier units were made with carefully matched phase and frequency characteristics and continuously variable gain from 1 to 100. The bandwidth for these units as given by the half power points extended from 20 Hz to 70 kHz and as such, adequately covered the range of frequencies within the turbulence signals. These units were AC coupled and the DC levels on the hot wires and hot films were, therefore, not recorded digitally. A digital multimeter with resolution to 1 mv and 1 second averaging time was used to record manually all DC levels; checks were made before and after each run to ensure that no calibration drift had occurred.

It is a well known fact that if a signal of broadband frequency content is sampled at a frequency of f cycles/sec, then any frequency content within the signal greater than f/2 will be "folded" about this frequency during the sampling process so as to appear as

energy in the digitized signal at a lower frequency. This phenomenon of "Nyquist frequency folding" is well described by Bandat and Piersol (1966) and can give rise to an inaccurate digital reproduction of the original analogue signal.

For the present case where a 12.5 kHz sampling rate has been used, we require that the signals contain negligible energy above 6.25 kHz. For the thinnest boundary layer at the highest speed in these measurements (δ = 27mm, U_o = 36 m/sec) this corresponds to a non-dimensional frequency of $\omega\delta^*/U_o = 4.2$ or $\omega\nu/U_\tau^2 = 0.34$ and the energy content above this frequency within a signal depends upon whether the signal is one of pressure, velocity or wall shear stress. Estimations of the energy content of the various signals above 6.25 kHz as a percentage of the total mean square energy (including the various noise sources present in each signal type) have been made by integration of power spectral data (obtained from analogue measurements). Taking the velocity at $y^+ = 30$ as being representative, there is a one percent contribution to the mean square energy of the velocity and wall shear stress signals, and a seven percent contribution to the pressure signal above this frequency. Therefore only a little Nyquist folding is to be expected and subsequent analysis showed negligible signal distortion to arise from this phenomenon.

3. PROPERTIES OF THE MEAN FLOWS

For the investigation three zero pressure gradient turbulent boundary layers were used with free stream speeds of nominally U_o = 36, 30 and 24 m/sec. This speed range was set by the available maximum operating power of the wind tunnel drive mechanism at high speeds and the low signal levels of the piezo-electric pressure transducers at low flow speeds.

In order to ensure that the pressure was uniform in the test section of the wind tunnel and that the flexible floor was free of surface waves, the floor was initially pulled flat and clamped at the downstream end so as to provide longitudinal tension. It was then slowly and evenly raised using the turnbuckle screws until the static pressure was approximately constant at the desired value along the test section. Thereafter very careful adjustments were made to bring the pressure at all points to the required value. The pressure was measured using a 0.33mm diameter static hole drilled in one of the circular instrumentation plugs and a water filled TEM micromanometer capable of resolution to 0.1mm of water gauge.

Careful checks were made to ensure that the pressure was constant in all directions and not just the longitudinal direction and that the floor was free from waves and surface distortion.

This procedure was carried out accurately for the flow with a free stream speed of 30 m/sec, and because of the very weak dependence of boundary layer growth rate with Reynolds number it was found that the static pressure was also accurately constant for the other two flow speed cases, any deviations being less than 1% of the free stream dynamic head.

The resulting floor shape is shown in figure 3.1(a) and the resulting distribution of free stream velocities are shown in figure 3.1(b) for the three cases considered. As can be seen the free stream velocity is constant from a streamwise distance x of 1.6m to 3.8m, where x is measured from the start of the test section.

The mean boundary layer velocity profiles were measured using a small circular Pitot tube of outside diameter 0.8mm, and internal diameter of 0.4mm which was electrically driven across the layer by means of a lead screw traverse mechanism. This mechanism is described in detail by Lim (1971) and was fitted with a dial indicator (resolution of 0.01mm) for determination of position. The zero point was determined by winding the Pitot tube up to the wall until it just met its own reflection in the surface of the wind tunnel instrumentation plug.

The resulting mean velocity profiles are shown in figure 3.2, expressed in the usual law of the wall form, namely

$$\frac{U}{U_\tau} = \frac{1}{K} \ln \left(\frac{yU_\tau}{\nu}\right) + B \qquad (3.1)$$

The results conform well to this relation with K = 0.4 and B = 5.5, the values suggested by Coles (1968).

The value of U_τ used to non-dimensionalize the profiles shown in figure 3.2 is that which has been obtained from the reading of the Pitot tube when positioned at the wall, i.e. when used as a Preston tube in conjunction with the calibration form suggested by Patel (1965). A value for U_τ can also be obtained by the slope fitting method suggested by Clauser (1956) which is based on the assumption of the existence of a universal logarithmic relationship (equation 3.1). For the present case both methods have been used and yielded results that were typically within 5% of each other. To preserve

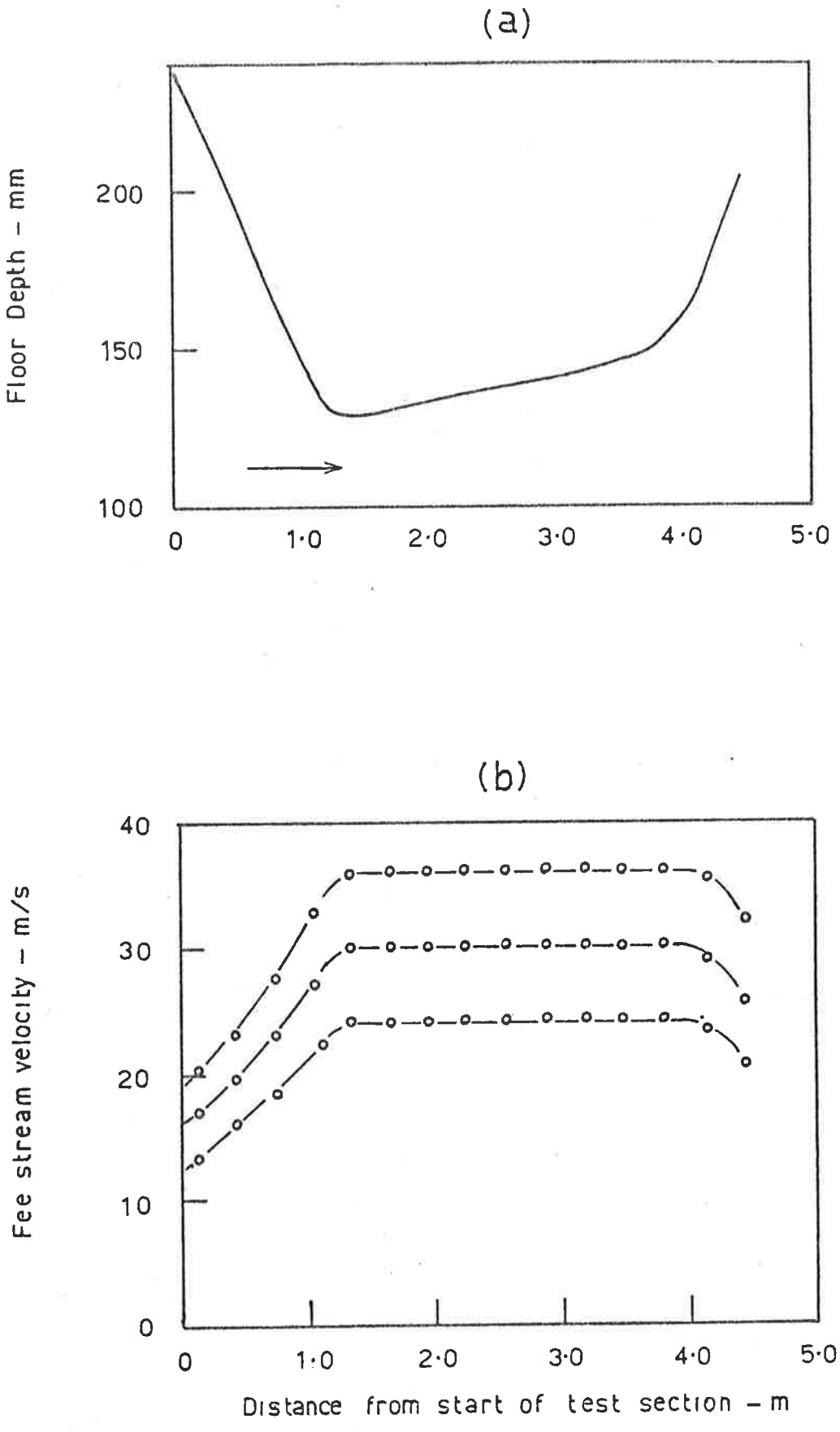

Figure 3.1 (a) Profile of the wind tunnel floor for a constant pressure boundary layer with U_o = 30 m/sec.

(b) Distribution of the free stream velocity along the test section for the three flows considered.

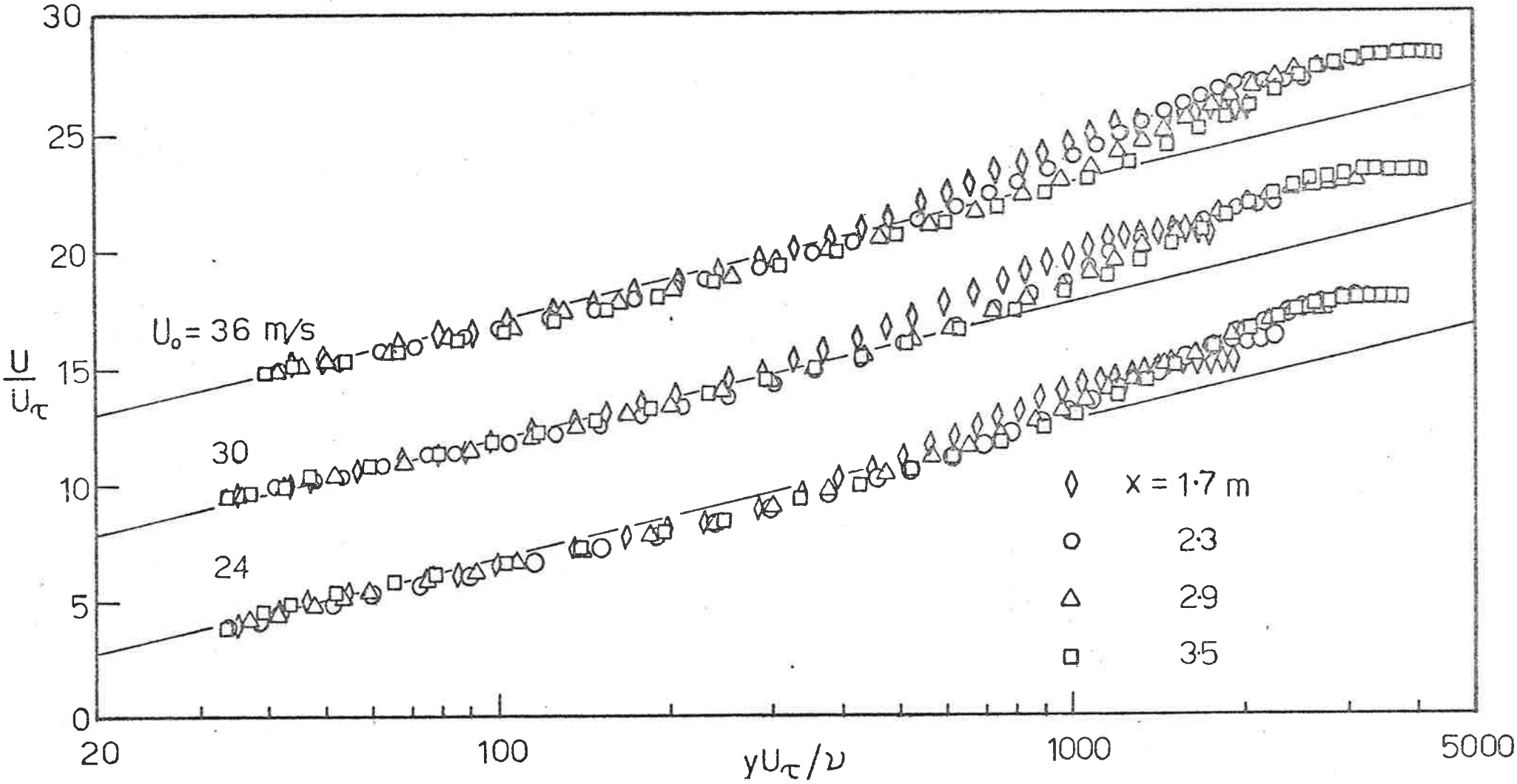

Figure 3.2 Mean velocity profiles along the test section for the three flows considered. Note shifted origins for the upper two curves. The solid lines correspond to the law of the wall (equation 3.1).

consistency the values of U_τ quoted in this and following sections are those obtained from the Preston tube and are shown in figure 3.3(a). The same data are presented as non-dimensional skin friction coefficients versus Re_θ in figure 3.3(b) and there is good collapse of the data and agreement with the form suggested by Coles (1968).

By integrating the mean velocity profiles, the boundary layer displacement thickness, momentum thickness and shape parameter $H = \delta^*/\theta$ have been determined and are shown in figure 3.4. The total boundary layer thickness has been found using the relationship determined by Coles (1956) i.e.

$$\frac{\delta^*}{\delta} = 3.88 \frac{U_\tau}{U_o}$$

and this value was consistently found to agree very well with the point where $U/U_o = 0.98$.

From figure 3.4 it can be seen that the growth of the boundary layers is smooth and regular, although between x = 1.5m and x = 2.2m the shape parameter H shows a slight increase with distance in all three cases (H is expected to fall with increasing Reynolds number, although only weakly). This region corresponds to just downstream of the contraction in the working section (figure 3.1) and it appears that at this point the flow has still retained some memory of the massive accelerations to which it has been subjected in passing through the inlet portion of the tunnel. To remain free of such pressure gradient effects, no measurements were carried out at these points, and the farthest upstream point that was studied was at x = 2.59m.

Reynolds numbers based on total boundary layer thickness, displacement thickness and momentum thickness have been computed and are shown in figure 3.5 and again reflect the smooth and steady

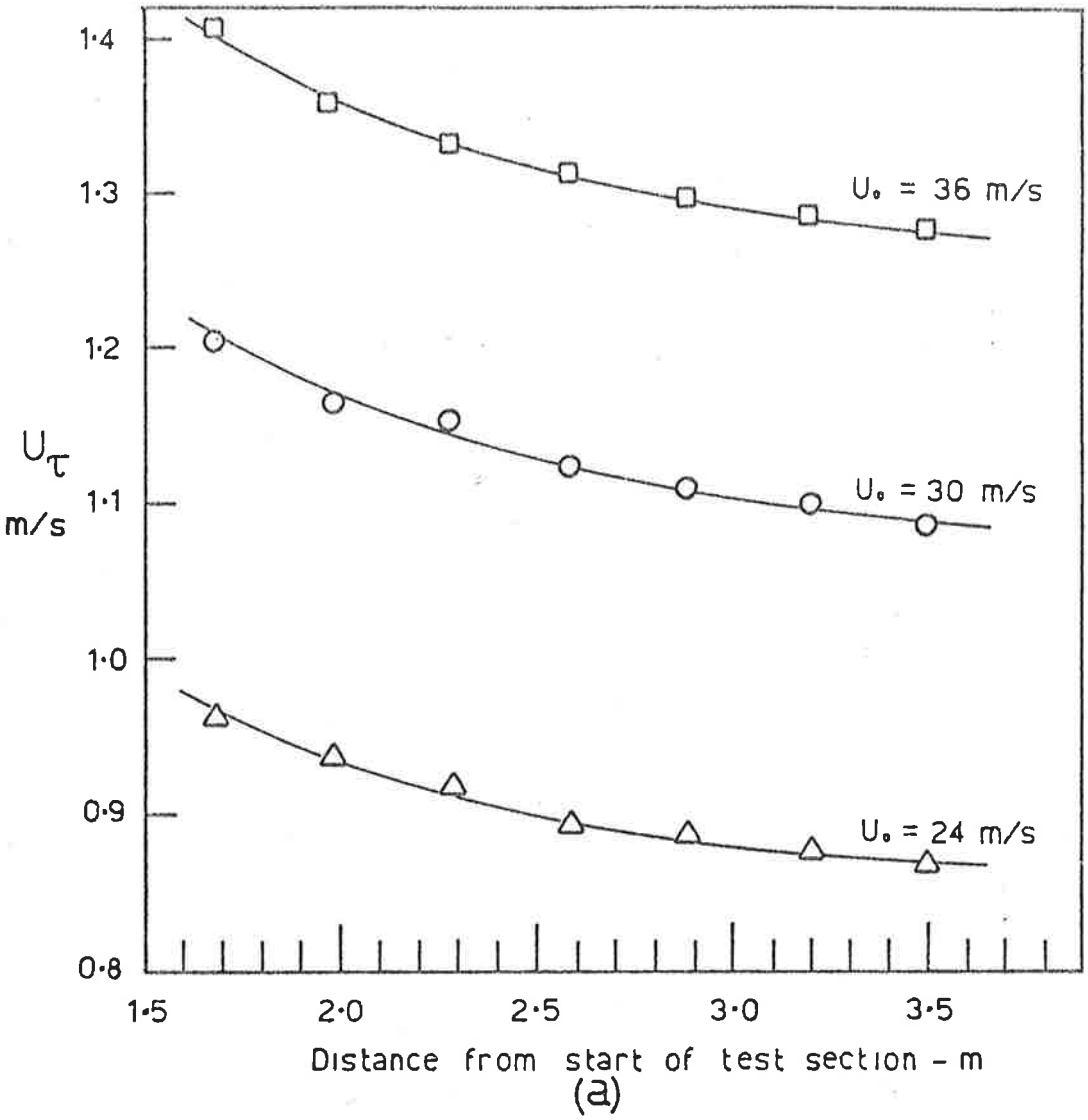

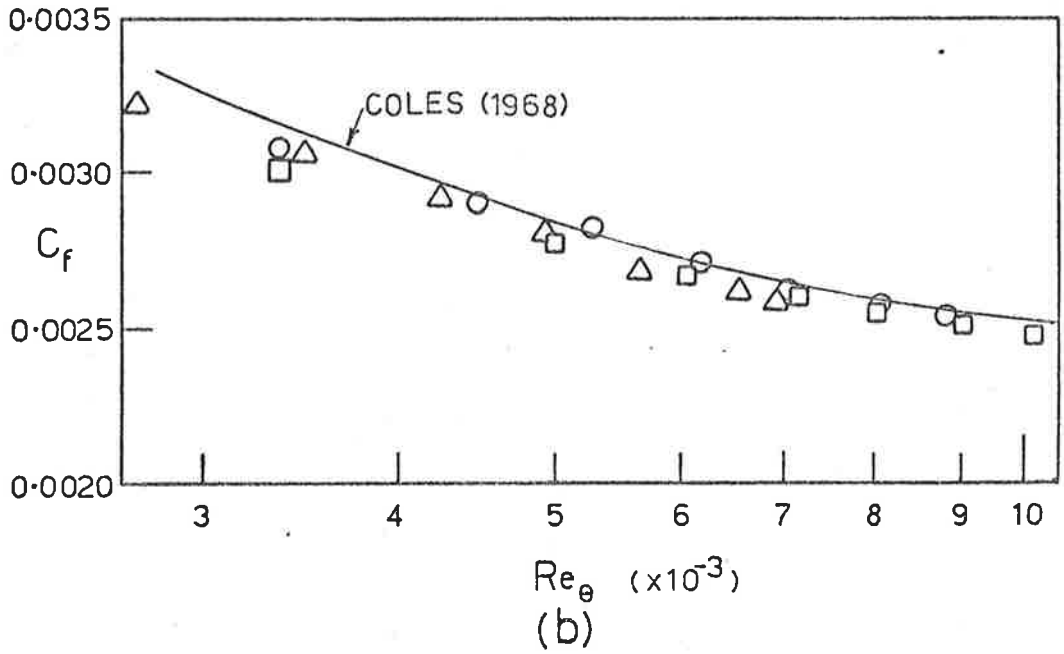

Figure 3.3(a) Variation of friction velocity U_τ along the test section as measured with a Preston tube.

(b) Corresponding non-dimensional skin friction coefficients versus Reynolds number.

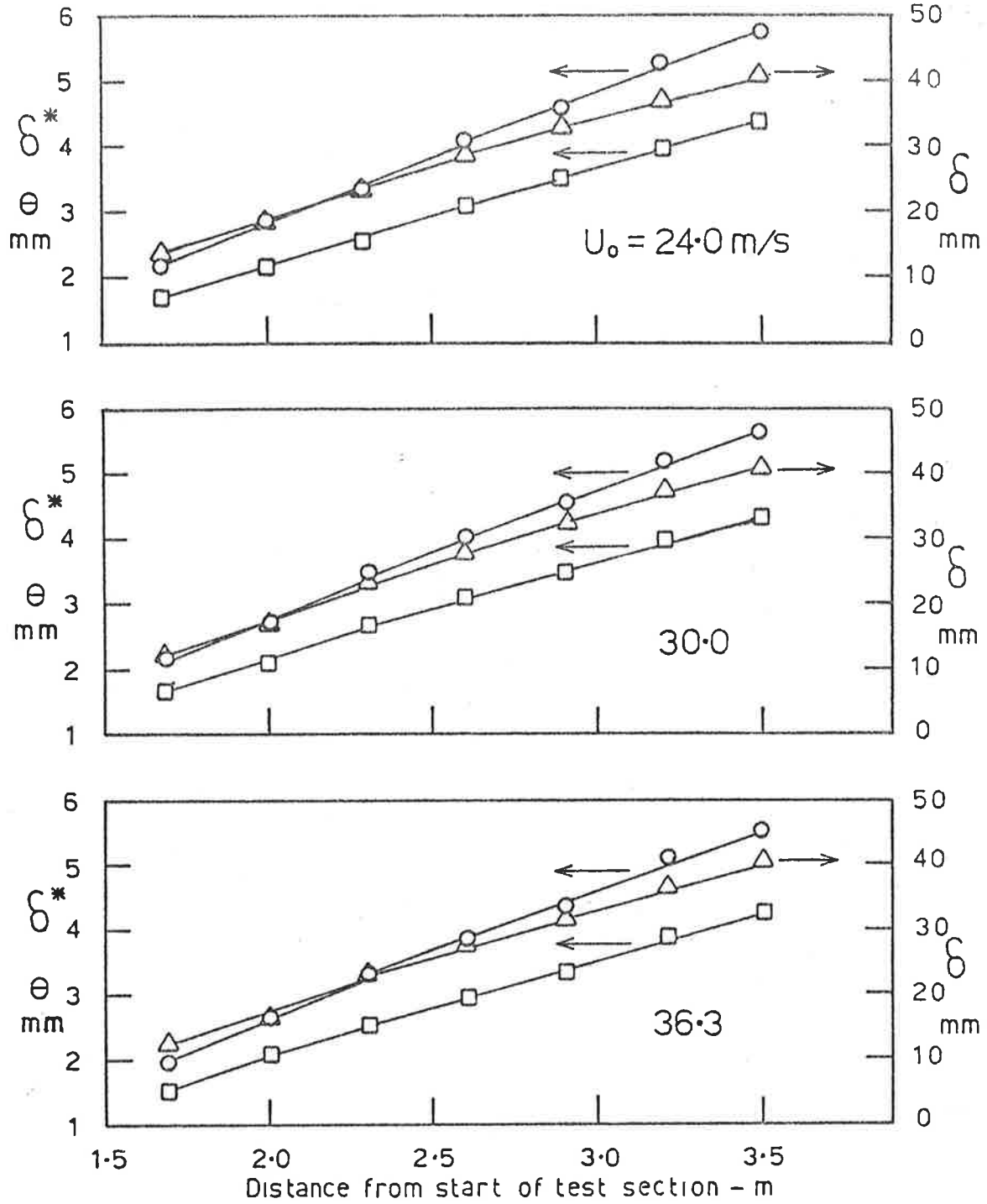

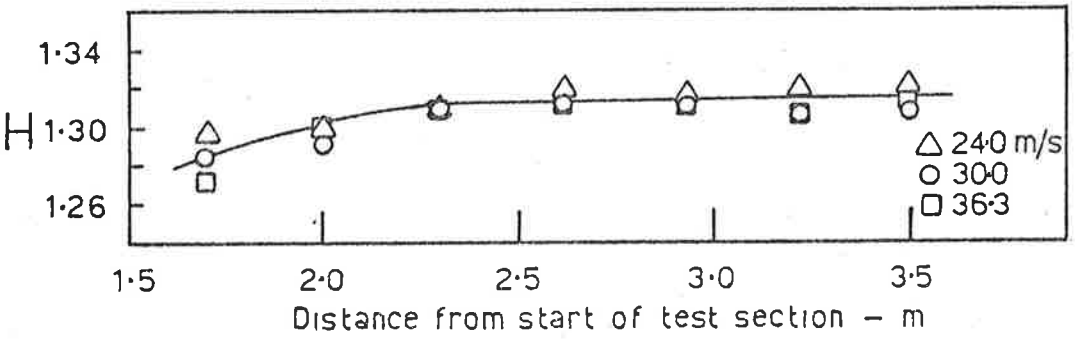

Figure 3.4 Variation of displacement thickness (o), momentum thickness (□), total boundary layer thickness (Δ) and shape parameter along the test section.

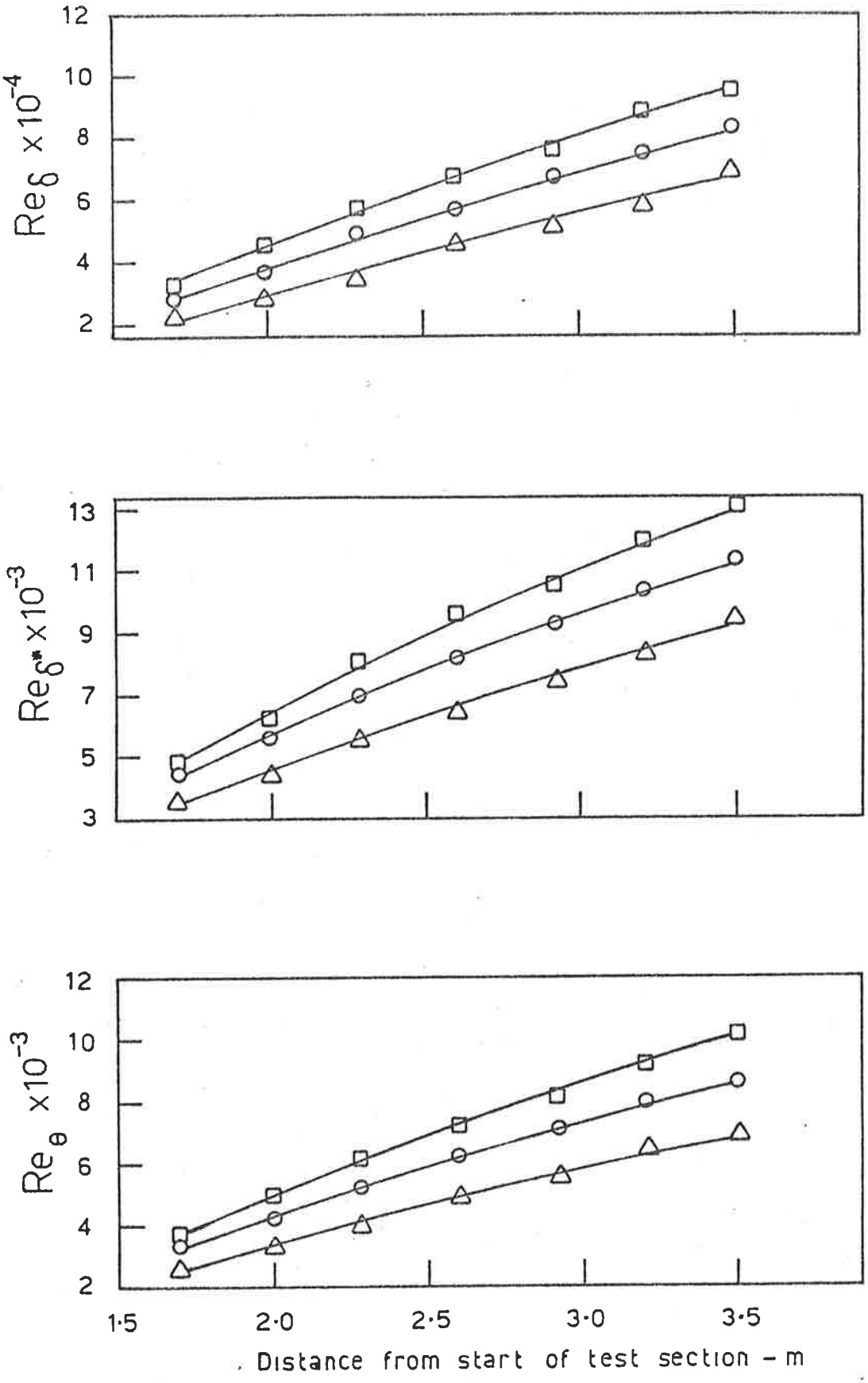

Figure 3.5 Variation of Reynolds numbers based on boundary layer thickness, displacement thickness and momentum thickness for the three flows considered; □, U_o = 36 m/sec; o, U_o = 30 m/sec; Δ, U_o = 24 m/sec.

growth of the layer within the tunnel.

Naturally during the course of the experimental work upon the turbulence structure itself, it was not possible to examine all the flows because of limitations of time, although trends found at one speed were verified where possible at other speeds. It is made clear in the text which flows were used in each particular experiment; the bulk of the work was carried out at the highest and lowest Reynolds number flows.

These correspond to a streamwise position of x = 3.5m for a free stream velocity of U_o = 36 m/sec and x = 2.60m for U_o = 24 m/sec. These are referred to in the text as the high Reynolds number flow and low Reynolds number flow respectively and the corresponding mean flow properties are listed in table 3.1.

Table 3.1

Mean Flow Properties

	High Reynolds Number	Low Reynolds Number
U_o m/sec	36.3	24.0
U_τ m/sec	1.28	0.89
δ mm	40.3	28.1
δ^* mm	5.5	4.1
θ mm	4.2	3.1
Re_θ	10,200	4,920
x m	3.5	2.6

4. AVERAGED STATISTICAL PROPERTIES OF TURBULENCE

In what follows are described various measurements of time averaged quantities such as power spectral data and mean square fluctuation values as measured for the wall pressure signal and fluctuating wall shear stress signal. These results are included to provide information about the turbulence structure itself and to show that the various devices being used were operating correctly and that they yielded results in agreement with previously published data.

For various experimental reasons it was found to be easier to compute the spectra by analogue means rather than by a Fourier transformation of the digital records and the power spectra are defined in the sense that the mean square value of a quantity q is given by

$$\overline{q^2} = \int_0^\infty \phi_q(\omega)\, d\omega \qquad (4.1)$$

Spectral data were recorded using a Bruel and Kjaer 1/3rd Octave Spectrometer type 2112 in conjunction with a Bruel and Kjaer Level Recorder type 2305, the raw data from these devices being punched on cards for computer reduction.

4.1 Power Spectra of the Fluctuating Wall Pressure

Spectra have been recorded at the three different flow speeds at x = 2.59m and x = 3.5m, using both the piezo-electric transducers and pinhole microphones. The calibration procedures adopted have been described previously. Because surface continuity is maintained, the piezo-electric transducers are to be preferred when making such

measurements, however the use of pinhole microphones has also been considered with a view to improvement of the signal to noise ratio. Their use was, however, later discontinued because of uncertainties of the effect of the hole itself and this point is described in more detail in a following section.

When making such spectral measurements several sources of noise are present and are a result of the following effects:

(1) Acoustic noise within the test section resulting from both the turbulence pressure fluctuations in the side wall boundary layers and from noise generated by the tunnel drive mechanism.

(2) Electronic noise on the output of the pressure transducers. This is a problem only with the less sensitive piezo-electric devices.

(3) Piezo-electric crystals in particular have a significant sensitivity to acceleration so that further degradation in their signal to noise ratio will occur if vibration is present in the structure of the working section in which they are mounted. This is not a significant problem with the pinhole microphones where signal levels arising from this source are 20 dB or more below the turbulent signal levels.

The importance of acoustic noise has been estimated by placing a Bruel and Kjaer 1/4 inch microphone (type 4136) fitted with a nose cone in the free stream at the measuring points considered and recording spectra of its output. These spectra indicated that acoustic noise was a severe problem at the very low and very high frequencies and tended to dominate the pressure signals below 150 Hz and above about 15 kHz. Measurements are therefore presented only in the

interval of 200 Hz to 12.5 kHz with corrections for acoustic noise applied to the transducer outputs in this frequency range. Integration of power spectral data shows that the resulting corrections to the mean square wall pressure represent about 15% for the low speed case and 6% for the high speed case. These figures apply to the piezo-electric transducer and are reduced by a factor of about 1.6 for the pinhole microphones.

The importance of vibration-induced noise and electronic noise on the crystal signal has been determined by measuring the output of the device when it is blanked off from the flow. The levels recorded in this way indicate that the signal is dominated by these effects only at frequencies less than about 200 Hz; and this is another reason for rejecting the data in this frequency range. Integration of power spectral data suggests that for the most severe case of the lowest flow speed this source of noise gives rise to a correction of 2% to the mean square pressure and 1% for the high speed case.

The measured power spectra as recorded by both the pinhole microphones and piezo-electric devices with the corrections for noise applied are presented in non-dimensional form based on inner layer parameters in figure 4.1. An outer layer scaling has been used to replot the same data in figure 4.2 and a mixed scaling has been used in figure 4.3. Only the piezo-electric crystal data are presented for these last two cases.

Ignoring for the moment the question of appropriate scaling of such data, the most interesting result to be seen from figure 4.1 is that the data form two distinct sets according to transducer type. It should be noted that the pinhole results agree very well

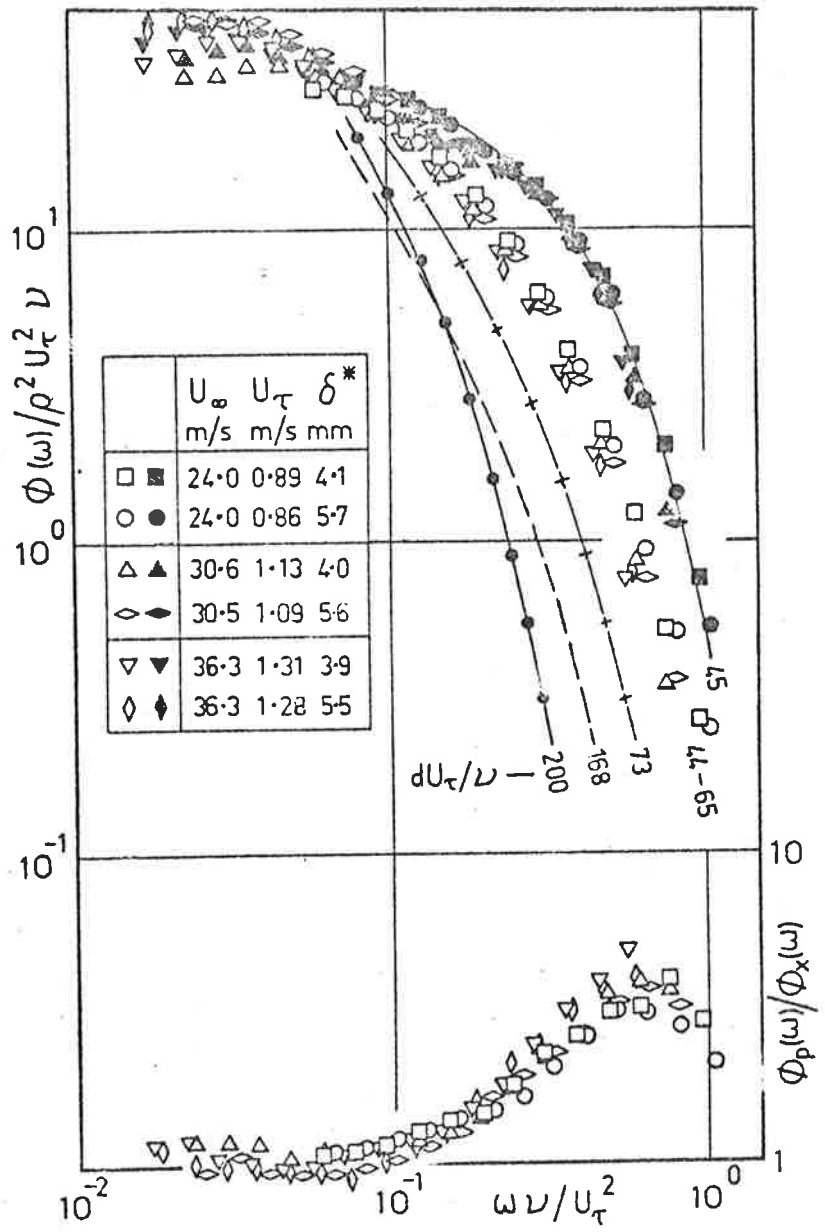

Figure 4.1 Power spectra of the fluctuating wall pressure as measured with piezo-electric transducers (open symbols) and pinhole microphones (closed symbols). The curves are scaled on wall variables; —o—o— Willmarth and Roos (1965); — — —, Bull (1967); —+—+—, Lim (1971); ————, Blake (1971).

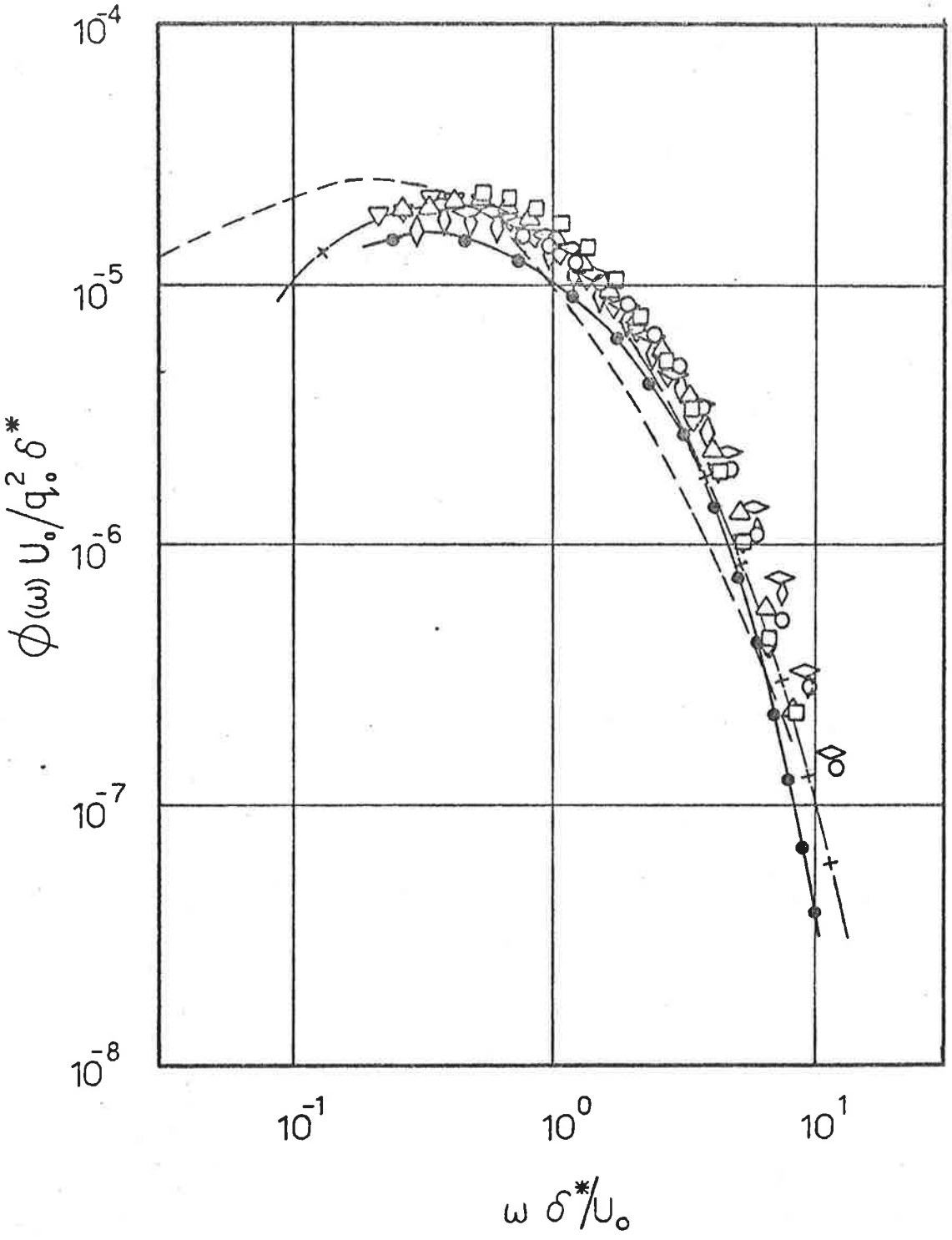

Figure 4.2 Power spectra of the fluctuating wall pressure as measured by the piezo-electric transducers. The symbols are as in figure 4.1. An outer layer scaling has been used.

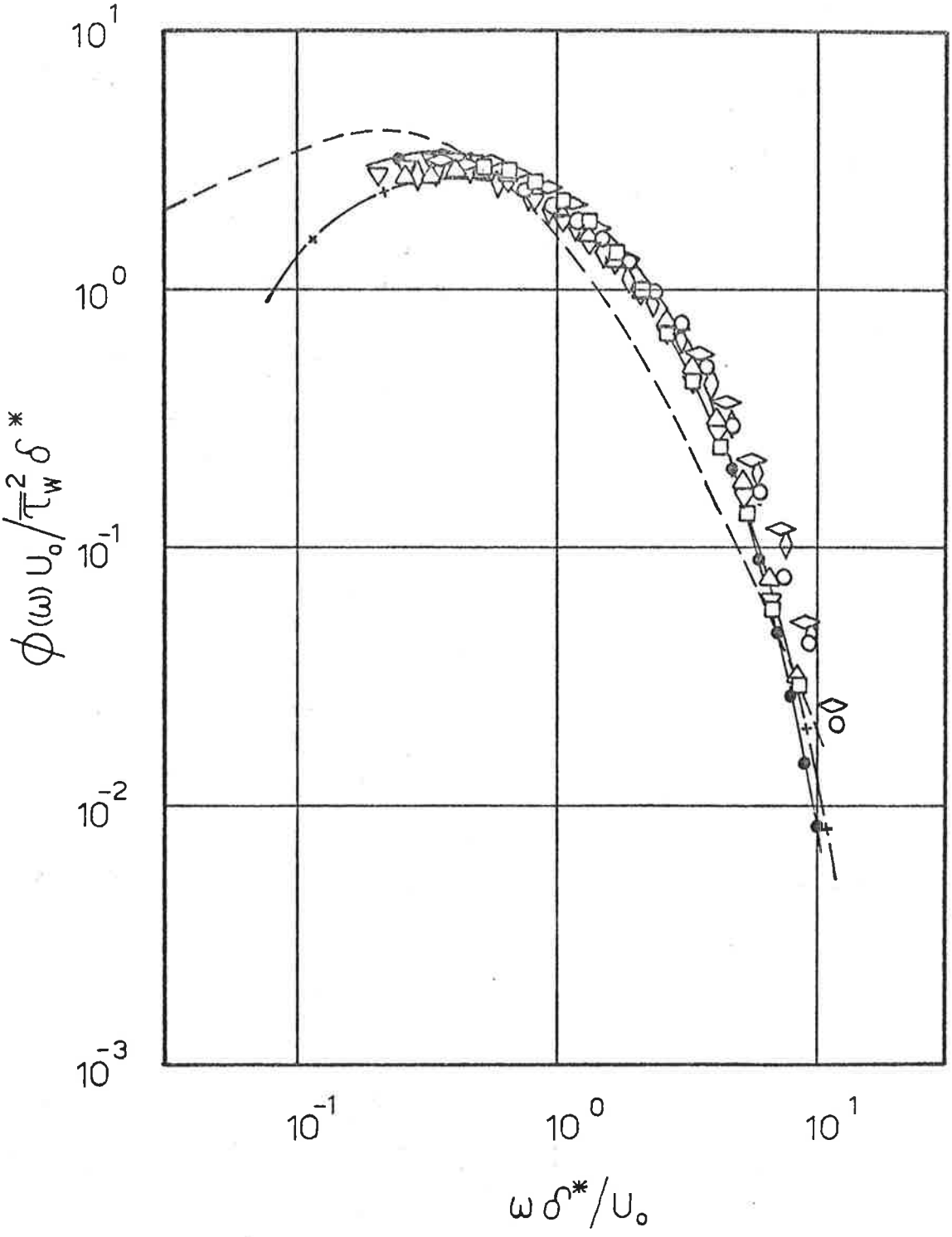

Figure 4.3 Power spectra of the fluctuating wall pressure as measured by the piezo-electric transducers. The symbols are as in figure 4.1. A mixed scaling has been used.

with those of Blake (1971) taken with similar instrumentation. The piezo-electric results are considerably lower in the high frequency region despite the fact that both transducers had the same nominal sensing area. In the lower portion of figure 4.1 is shown the ratio of these two spectral curves and it can clearly be seen that at the highest frequency the pinhole results are nearly a factor of 4 higher, whereas there is a general agreement at the low frequencies. These differences are significant and further tests were undertaken to try to shed light on the mechanism behind the discrepancies. The results of these tests are presented in the next section; the discussion that follows refers only to the data from the piezo-electric devices.

The spectral data from the piezo-electric devices may also be compared with similar measurements by Willmarth and Roos (1965), Bull (1967) and Lim (1971) shown in figure 4.1 and it can be seen that the present spectral levels are somewhat higher at the high frequencies. These differences are possibly an effect of transducer resolution as there can be seen a trend in the data according to the size parameter dU_τ/ν. This effect becomes more dramatic as dU_τ/ν becomes smaller and clearly indicates the need for very small transducers. The apparent improved collapse between the different measurements at high frequencies with the different scaling in figures 4.2 and 4.3 may, under these circumstances, be misleading. It follows, therefore, that any conclusions about physical scaling must be made cautiously in view of the rather severe transducer resolution effects present which may be more significant than the work of either Corcos (1963) or Willmarth and Roos (1965) has suggested.

Considering the question of scaling such spectral data, a problem of some interest is how the various wave-number components of the spectra scale with flow parameters. Strictly, frequency

wave-number spectra of the kind computed by Wills (1967) and Bradshaw (1967) are therefore required. In practice, of course, a great deal of labour is required to obtain such information and the measurements are still subject to the effects of inadequate transducer resolution of the high wave-numbers. Nonetheless some interesting information can be obtained from the frequency spectra presented in figures 4.1, 4.2 and 4.3.

As is the case with most quantities relevant to boundary layer turbulence, there is a problem of two length scales depending upon whether the region of interest is the inner or outer part of the flow.

Since the pressure at a point on the wall can arise from sources in either region, it is to be expected that no single scaling law will be appropriate. In addition, as the Reynolds number changes the relative strengths of the two types of source will change, so that a ratio such as that of the root mean square pressure to the wall shear stress will not necessarily remain independent of Reynolds number. That the wall pressure can be thought of as being produced by sources in either of these regions is consistent with the high and low wave-number groupings suggested by Bull (1967) and the same idea is implicit in Bradshaw's (1967) concepts based on Townsend's ideas of active and inactive motions.

With this view there is a possibility that the high frequency region of the spectra would scale with wall variables. Whether or not such a conclusion is correct cannot be determined directly from the spectral data presented, however, because of the dominance of the transducer resolution effects discussed previously. On the other hand, the low frequencies do not suffer from such effects, and if the

same argument is followed, this region of the spectra might be expected to scale on outer flow variables. However, as pointed out by Bull (1967), self preservation of mean velocity profile occurs in velocity defect form so that the velocity scale is U_τ. In addition, as the irrotational free stream flows over the turbulent bulges in the outer edge of the layer fluctuations will be generated with a velocity scale of U_o. Therefore, two possible scaling schemes exist and are shown in figures 4.2 and 4.3. From these curves it would appear that the mean wall shear stress is possibly the more appropriate scaling parameter than the free stream dynamic head q_o at least in the frequency range $0.2<\omega\delta^*/U_o<2.0$, although considerable scatter is evident in both diagrams. At much lower frequencies q_o is likely to be more appropriate; however, the high levels of acoustic noise within such regions make reliable measurements impossible.

It is, of course, also to be recognized that these conclusions are based on a rather limited range of Reynolds numbers.

4.2 Comparison Experiments Using Pinhole Devices

As noted in the previous section serious discrepancies arise when identical measurements are made using pressure transducers based on a pinhole principle as opposed to flush mounted piezo-electric devices, and it is tempting to relate these to flow disturbances associated with the pinhole.

For the calibration procedures adopted, in order to determine which device gives the better indication of the wall pressure, a comparison was made using a normal piezo-electric transducer and a pinhole transducer based on a piezo-electric sensor. This is the

same series of experiments described by Bull and Thomas (1976) and a copy of that report is given in Appendix B. Only a brief discussion of that work will be presented here.

As shown in figure B2 the spectral data from the pinhole system based on the piezo-electric crystal are identical to those of the pinhole microphone system. This suggests that the reason for the discrepancies does not lie with the capacitor microphones themselves but is probably associated with either the pinhole or the cavity or both.

A pinhole system based on a piezo-electric transducer but without a cavity was then made and showed a normal response to shock wave and acoustic testing. As can also be seen from figure B2 this device yielded spectral results similar to those of the original pinhole microphone suggesting that the spectral discrepancies are associated with the pinhole itself.

As a final test, the pinhole and cavity of the first pinhole-piezo-electric crystal device were filled with soft silicone grease to once again retore surface continuity. This device still showed a normal response to shock and acoustic testing, although its sensitivity was considerably reduced. Referring once again to figure B2 it can be seen that this device now yields spectral results that are similar to those of a flush mounted piezo-electric transducer.

These experiments therefore lead to the following conclusions in relation to the power spectral density measurements of wall pressure fluctuations.

(1) Measurements using a pinhole device based on either a capacitor microphone or a piezo-electric element yield significant errors, which for the values of dU_τ/ν used in

the present case occur at frequencies $\omega\nu/U_\tau^2 > 0.1$.

(2) The flow disturbances caused by the pinhole are localized so that the spectra from such devices appear to scale on wall variables at high frequencies.

Also, as pointed out by Bull and Thomas (1976), the spectral discrepancies could be interpreted in terms of a difference in response kernels and any flow modification by the pinhole would be reflected in the response kernel of that device.

The physical reason for this result is not altogether clear. Evidently the difference is due to a change in impedance of the hole with grazing flow past the hole. Ronneberger (1972) has demonstrated that the acoustic impedance of a hole can change signficantly under such circumstances.

Some uncertainty therefore exists in the interpretation of the results taken with a pinhole device. For this reason no digital recordings of its output were taken and all subsequent pressure measurements were made with flush mounted piezo-electric transducers.

One final comment should perhaps be made concerning the shape of the spectrum of the wall pressure fluctuations. Bradshaw (1967) has shown by dimensional reasoning that a region of the pressure spectrum up to a wave-number of the order of the inverse of the sublayer thickness may vary as τ_w^2/k, and he supports this with some unpublished pinhole microphone data presented by Hodgson in 1967 at a meeting in Southampton. As can be seen in figure 4.1 it is possible for such an apparent dependency to arise from the uncertainty of the response of the pinhole microphone itself. The piezo-electric results do not show such a variation but this may be a consequence of inadequate transducer resolution.

4.3 Root Mean Square Values of the Wall Pressure

The rms wall pressure value has been computed by direct integration of the power spectral data after the corrections for the various sources of noise have been made and are shown in figure 4.4 as a function of Reynolds number. As can be seen the results show a slight decrease with Reynolds number when normalized by the free stream dynamic head (in direct contrast to the findings of Bull, (1967) despite similar values of d/δ^*) and when normalized by the mean wall shear stress appear to be nearly independent of Reynolds number. In addition, the results from the pinhole microphone are 25% or more higher than the piezo-electric crystal data, is to be expected from the spectral differences discussed previously.

As was also demonstrated in section 4.2, and as has been concluded by Emmerling (1973) and Willmarth (1975b), any comparison of the various published values of the rms wall pressure should also take account of the transducer size. Such a conclusion was first demonstrated by Emmerling (1973) on the basis of a curve similar to that in figure 4.5(a) which shows values of p'/q_o as a function of transducer size expressed as dU_τ/ν. In addition, flush mounted transducer results from other published sources are presented, and a similar curve which also presents pinhole microphone data is given in Appendix B. Referring to this second curve, it can be seen that the pinhole microphones yield higher values of p'/q_o consistent with the discussion of spectra presented previously. These differences are a reflection of the response of the pinhole itself so that it is not, therefore, appropriate to include them when making comparisons of various published results. The results of figure 4.5(a), which apply to piezo-electric devices only, indicate that there is a

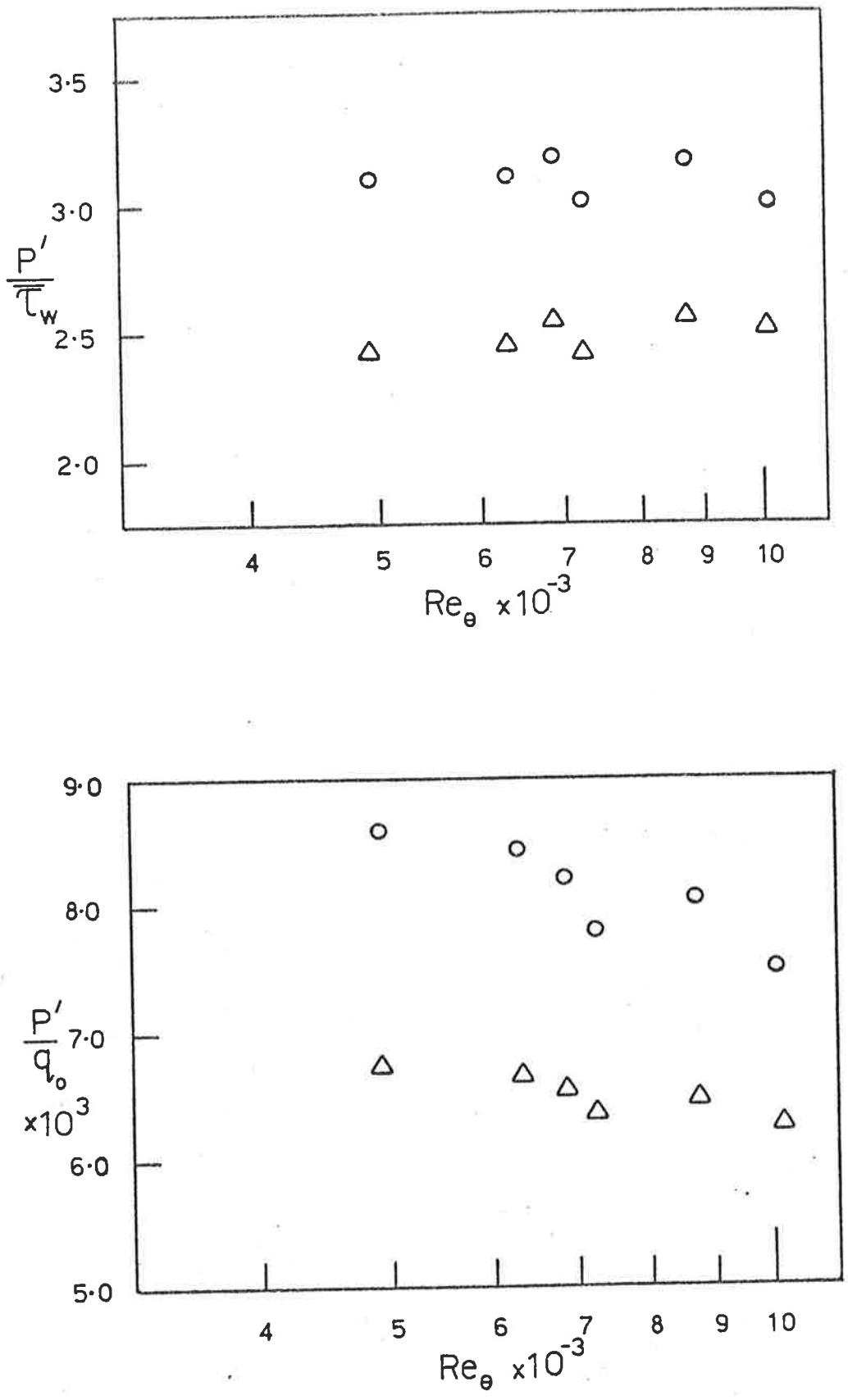

Figure 4.4 Root mean square values of the fluctuating wall pressure as a function of Reynolds number; o, pinhole microphones; Δ, piezo-electric crystals.

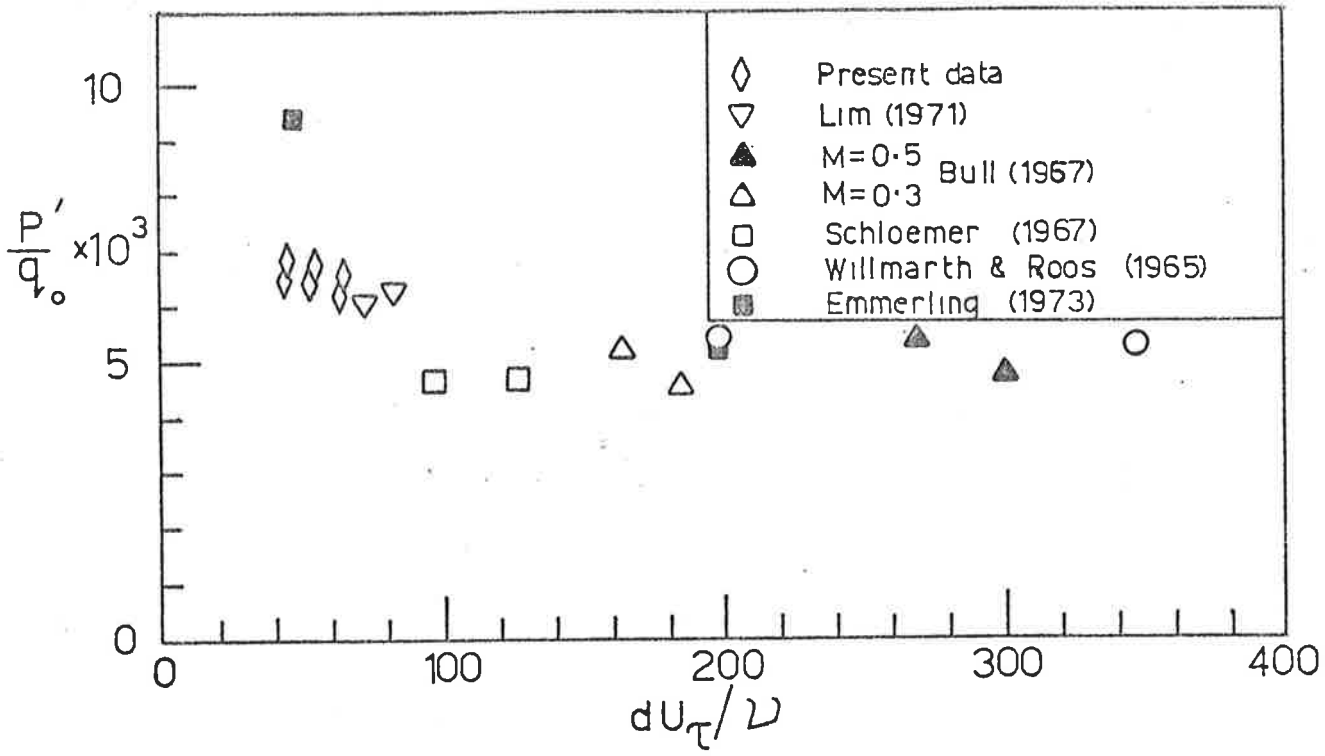

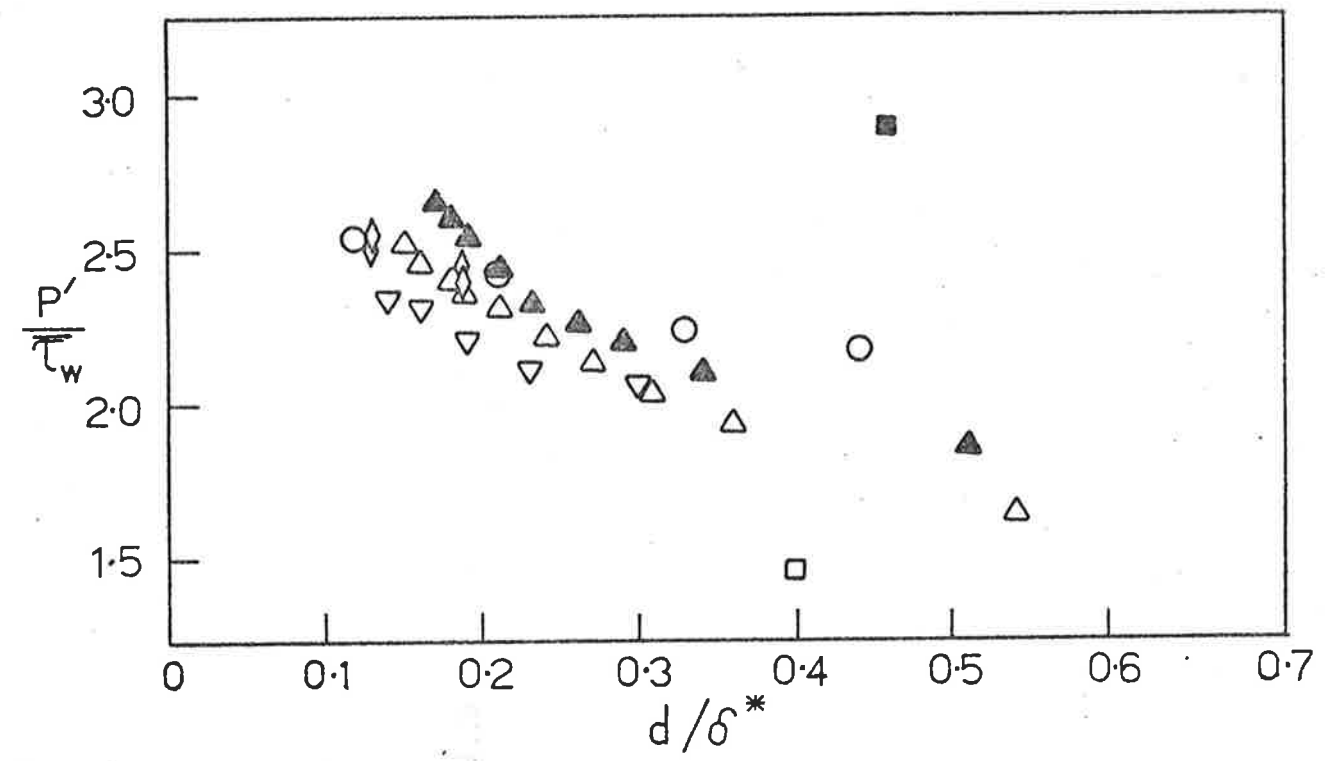

Figure 4.5(a) Variation of p'/q_o vs dU_τ/ν for flush mounted transducers only.

(b) Variation of $p'/\bar{\tau}_w$ vs d/δ^* for flush mounted transducers only.

general increase in measured rms pressure as the transducer is made smaller, but this increase is not as great as Emmerling's (1973) original analysis or Willmarth's (1975b) discussion of it would suggest. Furthermore it is on the basis of such a curve that Willmarth (1975b) concludes that the smallest pressure fluctuations scale on wall variables; however such a conclusion based on a curve such as figure 4.5(a) alone may not necessarily be correct. The data have been replotted in figure 4.5(b) except that they are now presented as $p'/\sqrt{\tau_w}$ as a function of d/δ^*. This leads to the same conclusions regarding the effect of transducer size except that now there is perhaps an indication that the small fluctuations scale on outer layer variables. The apparent contradiction is a consequence of the way the data are presented and the fact that Reynolds number has been ignored. Also it is not strictly appropriate to characterize the resolution of the transducer by either d/δ^* or dU_τ/ν alone.

If the comments in section 4.1 regarding the possibility of an essentially two wave-number form of the spectrum are correct, with the inner and outer parts of the layer containing the sources for the low and high wave-number pressure fluctuations respectively, then it may be possible to write for the spectrum measured by a finite transducer:

$$\phi(k) = \phi_{1m}\,(k/\delta^*,\ d/\delta^*) + \phi_{2m}\,(k\nu/U_\tau,\ dU_\tau/\nu)$$

where, at a given Reynolds number either ϕ_{1m} or ϕ_{2m} dominates depending on the wave-number. An overlap region would exist and ϕ_{1m} may be expected to make a larger relative contribution to the mean square pressure level at a low Reynolds number than at higher Reynolds numbers. In such circumstances the parameter d/δ^* may be important at low Reynolds numbers whereas at higher Reynolds numbers dU_τ/ν

becomes significant.

Now figures 4.6(a) and (b) show curves of p'/q_o and $p'/\overline{\tau_w}$ versus Reynolds number from various published sources and only results for flush mounted transducers are shown. Also indicated are the various values of d/δ^* and dU_τ/ν or ranges of values, the lower numbers, of course, being the d/δ^* values. It can be seen that while the present values of p'/q_o and those of Lim (1971) show a decrease with Reynolds number, the extensive results of Bull (1967) show a marked increase despite the fact that both the Reynolds number and d/δ^* values are not very different. The dU_τ/ν values are markedly different, however, and also these different data sets show rather similar behavior when expressed as $p'/\overline{\tau_w}$ as in figure 4.6(b). These facts suggest that for the limited data available $p'/\overline{\tau_w}$ is the relevant non-dimensional parameter with resolution depending on dU_τ/ν rather than d/δ^* for the Reynolds numbers and values of dU_τ/ν of the data that are presented. In addition, the data at any one Reynolds number tend to group themselves according to the values of dU_τ/ν as shown by the solid lines in figure 4.6(b).

If such a grouping is indeed valid, with lines of constant dU_τ/ν being straight lines on a logarithmic plot, then it is possible to write

$$p'/\overline{\tau_w} \sim \left(\frac{(d'+d)U_\tau}{\nu}\right)^m Re_\theta^n, \quad m < 0, \; n > 0 \qquad (4.2)$$

where d' is some very small transducer size, below which resolution effects are unimportant. It can then be demonstrated that the same data when presented as curves of p'/q vs dU_τ/ν or $p'/\overline{\tau_w}$ vs d/δ^* will be nearly independent of Reynolds number if reasonable values of m and n are used which is consistent with figures 4.5(a) and (b).

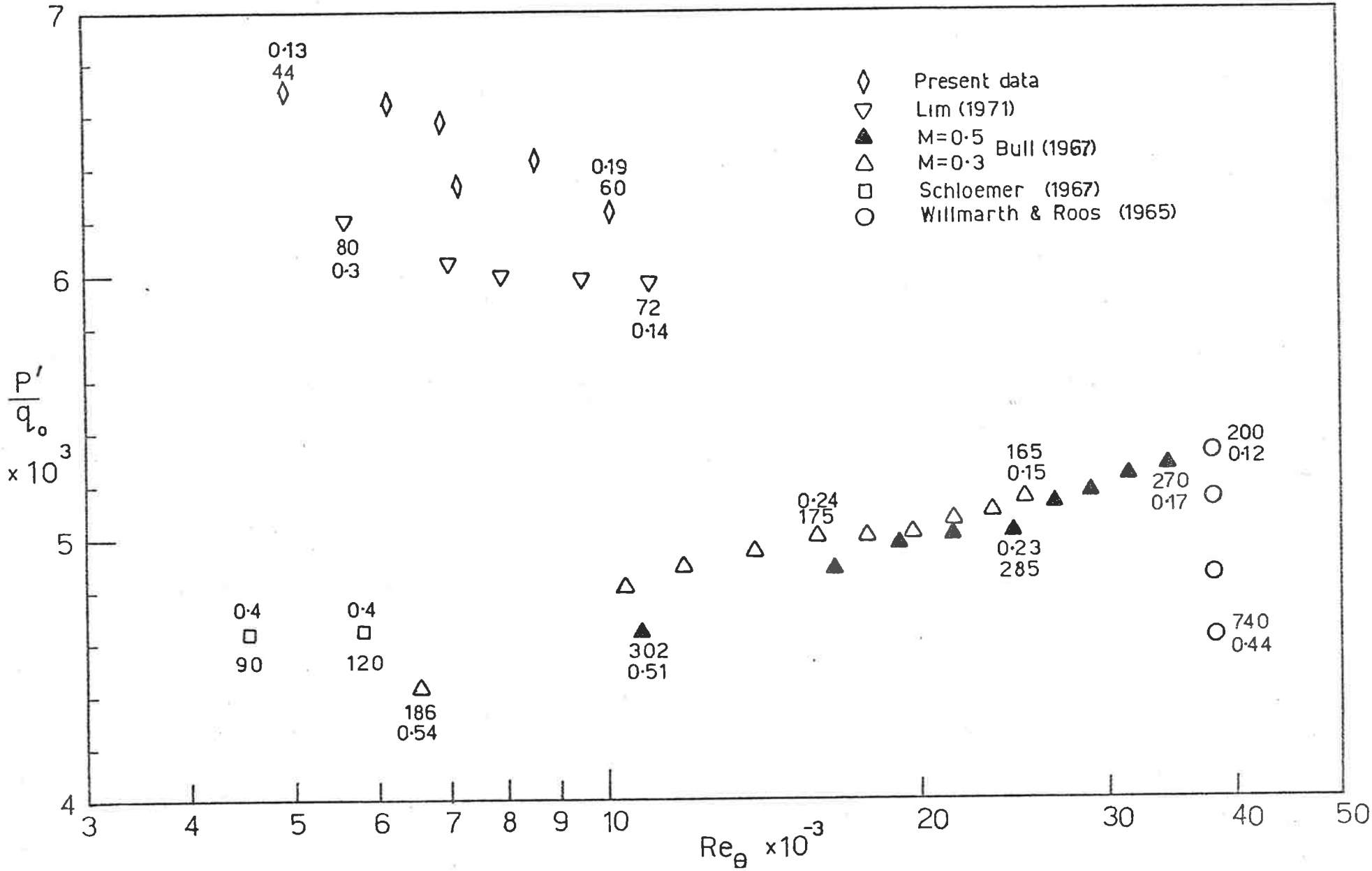

Figure 4.6(a) Variation of p'/q_o versus Reynolds number from various published sources. The larger numbers shown refer to values of dU_τ/ν and the smaller numbers refer to values of d/δ^*.

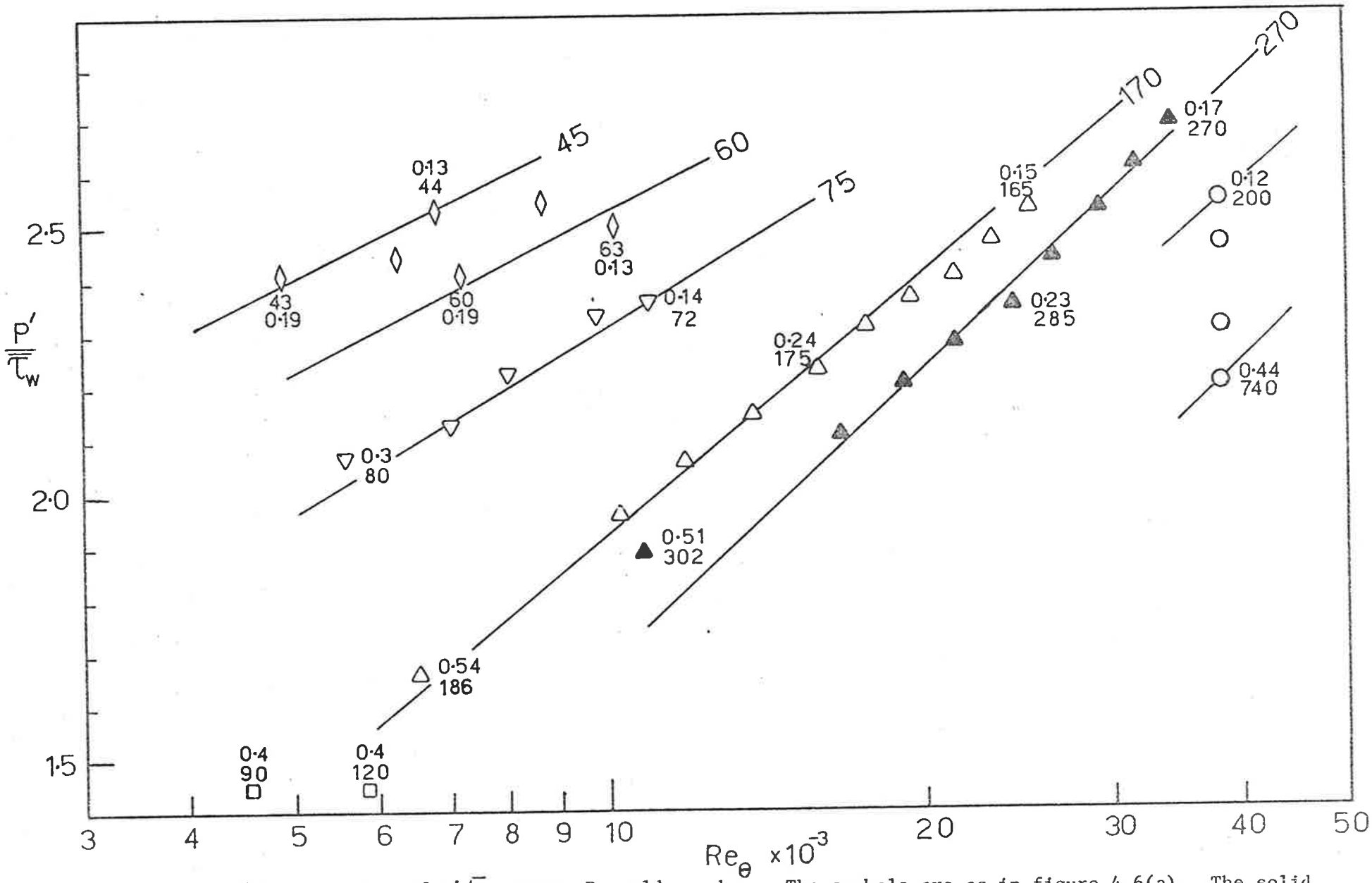

Figure 4.6(b) Variation of $p'/\bar{\tau}_w$ versus Reynolds number. The symbols are as in figure 4.6(a). The solid lines represent lines along which dU_τ/ν appears to be nearly constant.

The conclusions of this section are, therefore, that $p'/\overline{\tau_w}$ appears to be the more appropriate non-dimensional parameter and that at any given value of dU_τ/ν greater than about 40, $p'/\overline{\tau_w}$ increases with Reynolds number. If the Reynolds number is fixed, dramatic increases in measured $p'/\overline{\tau_w}$ will occur as dU_τ/ν is reduced below about 100. This implies that the small scale pressure fluctuations do indeed scale on wall variables as Willmarth (1975b) suggests and may be related to the well documented burst-sweep cycle of events observed near the wall and which exist on a spanwise scale of this order.

It is clear from this work that the behavior of the wall pressure is complex and that inadequacies of measurement technique (even with the very small transducers used in this work) add further difficulties. The spectral data are useful as a guide when making engineering estimations but it is clear that they shed little light upon the subtle structural features that exist in boundary layer turbulence. The work that follows in later sections represents a more detailed study of the various signals in an attempt to determine the character of the structures present.

4.4 Power Spectra of the Fluctuating Wall Shear Stress

The power spectra of the unlinearized signals from the hot films have been measured using the same apparatus used for the pressure spectral data and are shown for two points in each of the three flow speeds in figures 4.7 and 4.8, using two possible scaling schemes and a small perturbation linearized calibration law.

From figure 4.7 which is scaled entirely on wall variables, it is to be seen that there is quite good collapse of the data at the high frequency end of the spectrum with $\omega\nu/U_\tau^2 > 0.03$, but a poorer

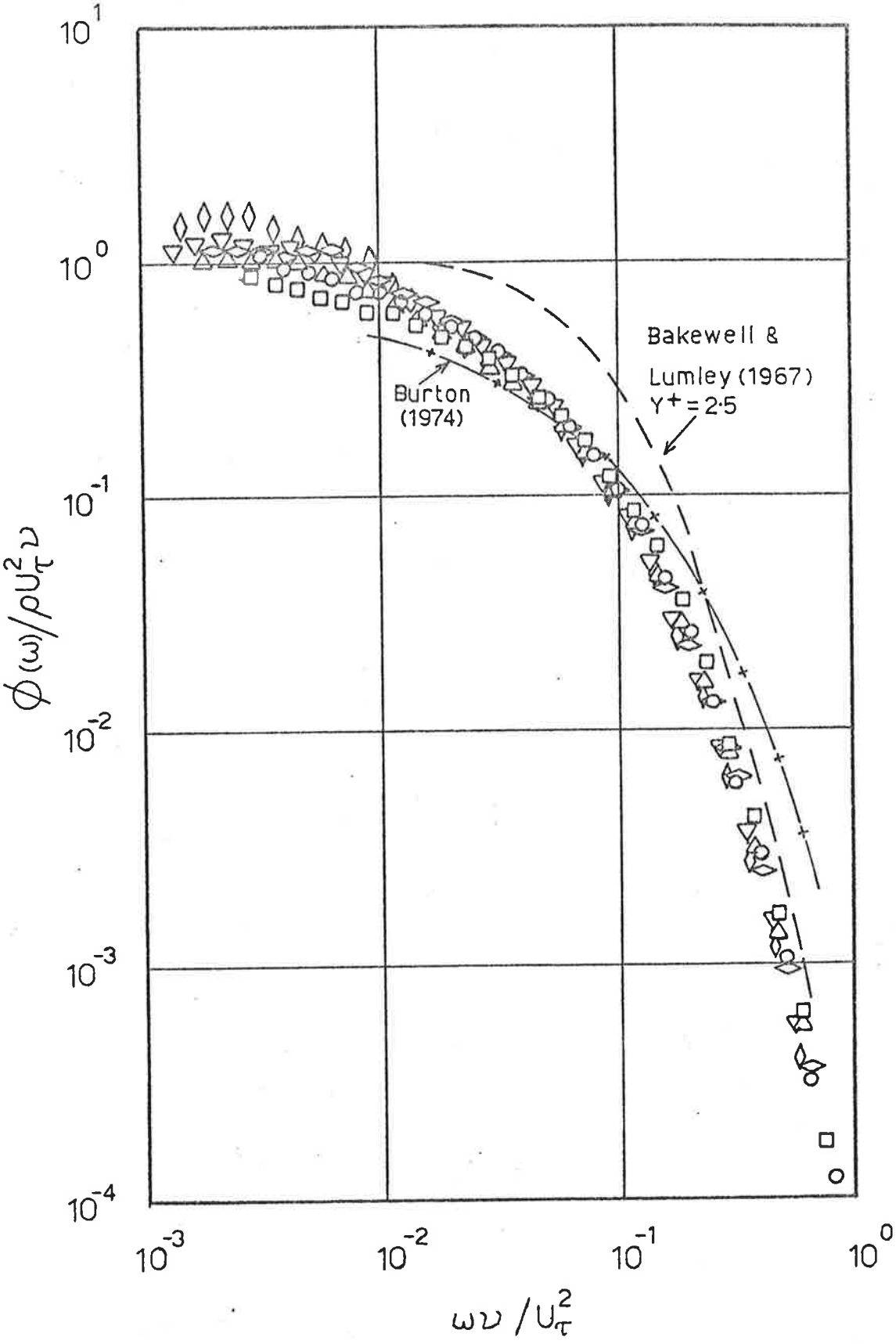

Figure 4.7 Power spectra of the fluctuating wall shear stress scaled on wall variables. The symbols are as in figure 4.1.

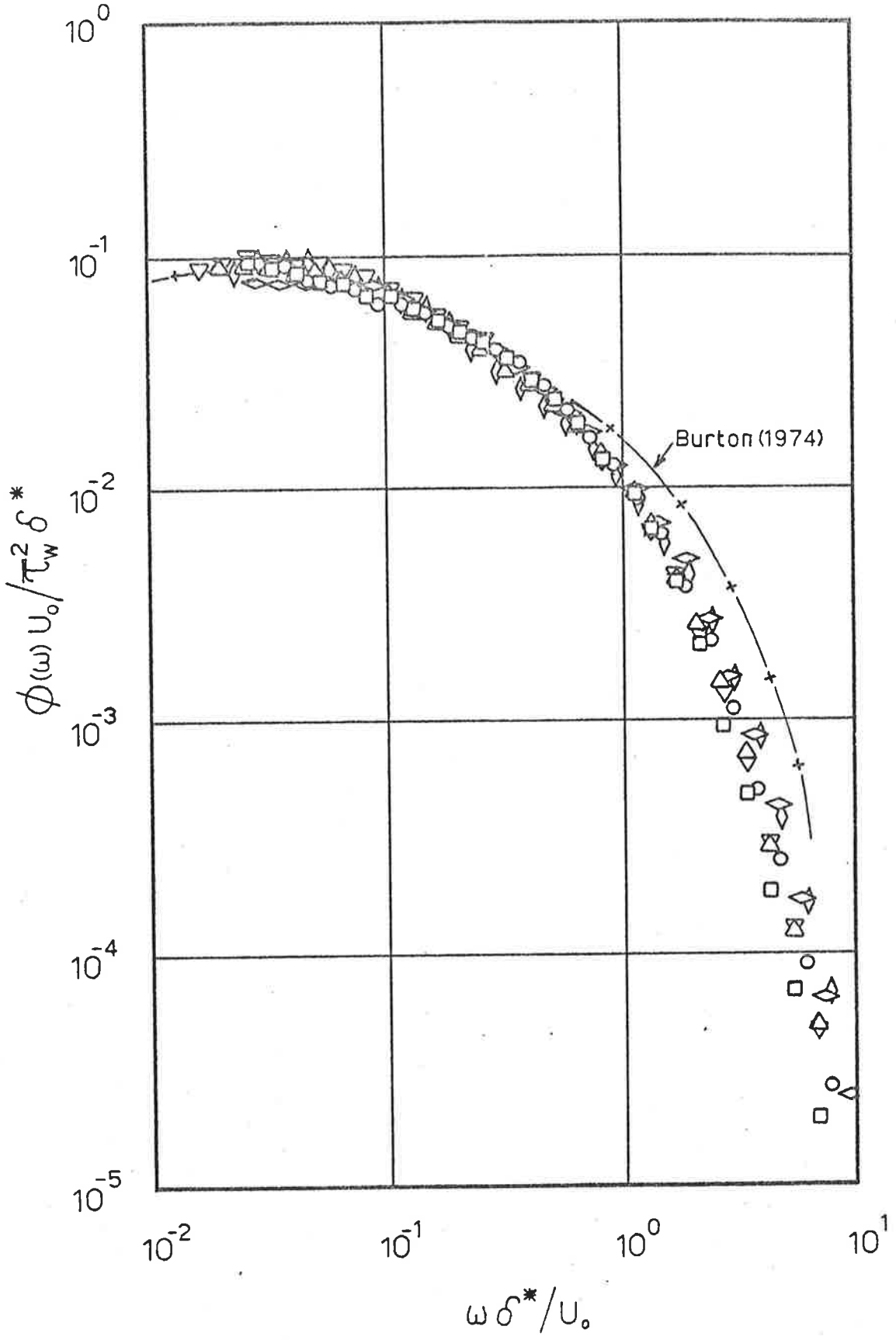

Figure 4.8 Power spectra of the fluctuating wall shear stress using a mixed scaling. The symbols are as in figure 4.1.

collapse at the low frequency end. On the other hand as shown in figure 4.8 the same data collapse very well in the low frequency region at least for frequencies $0.02<\omega\delta^*/U_o<1.0$ when an outer layer scaling scheme is used.

Also shown in figure 4.7 and 4.8 are similar spectra of the wall shear stress as were reported by Burton (1974) in a similar boundary layer; in each case, the agreement with the present data is quite reasonable in view of the uncertainties involved in the dynamic calibration of the devices, and supports the suggested scaling schemes.

It is possible to compare wall shear stress data with velocity measurements made in the sublayer using the assumption of a quasi steady, instantaneously linear velocity profile in the sublayer. This is, as Bakewell and Lumley (1967) point out, equivalent to a Taylor series expansion of the streamwise fluctuating velocity as a function of the distance normal to the wall with all terms except the second ignored. Measurements made by Willmarth and Lu (1971) and Eckelmann (1974) using hot wires in the sublayer have shown this representation to be quite valid so that it is possible to convert a velocity spectrum at sufficiently small y^+ to a shear stress spectrum.

This has been done for the glycerine pipe flow spectra reported by Bakewell and Lumley (1967) taken at $y^+ = 2.5$ and is shown in figure 4.7. Once again the agreement can be seen to be good at the high frequency end of the spectrum indicating that the hot films in the present series of experiments are correctly measuring the dynamic shear stress.

It should perhaps be mentioned that it would have been extremely difficult to position a 5μm diameter hot wire at $y^+ = 2.5$

(or 24 μm) which further demonstrates the usefulness of the hot film technique.

The power spectral data of the dynamic wall shear stress have been integrated to find the rms wall shear. A value of the ratio of rms wall shear to mean wall shear $\tau_w'/\overline{\tau_w}$ was obtained as 0.22 with no apparent Reynolds number dependency. This value may be compared with values of the slope of the u'/U_τ versus y^+ curves measured near the sublayer and various published results are included in the table 4.1 below. Also shown are the values of $\tau_w'/\overline{\tau_w}$ reported by Burton (1974) using hot films.

Table 4.1

Reported values of $\tau_w'/\overline{\tau_w}$ and $u'/U_\tau y^+$ near the wall

Source	$\tau_w'/\overline{\tau_w}$, $u'/U_\tau y^+$	Re_θ, Re_d	Type of Flow
Laufer (1954)	.30	5.0×10^5	Pipe Flow
Klebanoff (1954)	.28	84×10^3	Boundary layer
Mitchell & Hanratty(1966)	.32	4×10^4	Pipe flow, Electro-chemical Technique
Bakewell & Lumley (1967)	.30	8.7×10^3	Glycerine Pipe Flow
Eckelmann (1974)	.24	8.2×10^3	Oil Channel Flow
Burton (1974)	.29	5.1×10^3	Boundary Layer
Present Results	.22	$6.7\text{-}10.1 \times 10^3$	Boundary Layer

These results in various flow configurations and at various Reynolds numbers do indicate values similar to the present values. The present value of 0.22 must be considered to be in reasonable agreement, particularly in view of the uncertainty involved in deducing the

dynamic calibration of the hot films.

The spectral data suggests then that the films are indeed giving a reliable indication of the dynamic wall shear stress and that as was suggested for the spectra of the wall pressure, the high wave-number region appears to scale on wall variables and the low wave-number region appears to scale on outer variables. Such scaling is consistent with the findings of Rao, Narasimha and Badri Narayanan (1971) that the events near the wall can scale outer flow variables and there is an implication of a large structure of scale δ passing the wall and giving rise to long time scale fluctuations in the wall shear stress. Superimposed on these fluctuations are small scale disturbances of local origin and with time scales of the order of TU_τ^2/ν of 10 to 100. As is the case with pressure transducers such small scales must be somewhat attenuated by the finite size of the hot film ($\ell U_\tau/\nu \approx 20$).

From the spectral data presented in figures 4.7 and 4.8 it can be seen that the spectral region which scales on outer layer variables extends up to frequencies of about $\omega\delta^*/U_o \approx 1.0$ and integration of the spectra shows that the region below this point makes about an 85% contribution to the mean square dynamic wall shear for the highest Reynolds number case and a 90% contribution for the lowest Reynolds number case considered. In terms of an outer layer influence, however, these figures represent overestimates because a significant portion of the same region also scales quite well on wall variables. Examination of the spectral data indicates that a better estimation of the regions which appear to scale only on wall variables extend to non-dimensional frequencies of the order of $\omega\delta^*/U_o \approx 0.50$ and integrations of the spectra below this point indicate

that these regions make a 50% contribution to the mean square wall shear stress for the highest Reynolds number and about a 60% contribution for the lowest Reynolds number considered. Regardless of precisely where the changeover point is defined it would appear, however, that a significant portion of the mean square dynamic wall shear stress can be related to outer flow events. In subsequent work, this changeover frequency ($\omega\delta^*/U_o \approx 0.5$) will be used as a basis for the selection of a low pass filter cutoff in an attempt to separate the two scales of motion.

The spectral data presented have provided some useful statistical information, but as was the case with the pressure spectra, the subtle details of the flow structures remain hidden. The remainder of this work follows a somewhat different reasoning and was prompted in an attempt to resolve, in an unambiguous manner, the more detailed features of boundary layer turbulence.

5. STRUCTURAL FEATURES OF THE LARGE SCALE MOTIONS.

It is significant that a region of the spectrum of the dynamic wall shear stress scales on outer layer variables in that there is, perhaps, a suggestion of an influence at the wall by a large scale structure of the kind described by Kovasznay et al (1970). From the flow visualization studies of Kim et al (1971) and Corino and Brodkey (1969) however, it is apparent that a most significant feature of the flow near the wall is the well documented burst-sweep cycle of events which exist on a smaller scale. An essential issue that has not yet been resolved is the connection between the bursting phenomenon and the large scale motions.

As discussed in the introduction, Offen and Kline (1973) have described a model based on flow visualization studies which suggests that the circulatory flow, or vortex, in a burst can impose an adverse pressure gradient on the wall as it passes downstream. It is this pressure gradient, they maintain,which acts on a new wall streak and stimulates the lift up of this new streak. A significant part of this hypothesis is that the pairing of the vortices of initial bursts leads to the origin of new bursts. In this way the processes at the wall are regenerative and the large scale motions in the outer part of the layer are a consequence of the repeated pairing process as the vortices associated with bursts are convected into the outer part of the layer. There is an implication that the large scale structures play a passive role in the process as a whole and that the wall flow is self-sustaining.

A shortcoming of such an idea is that the mean period between bursts as measured by Rao, Narasimha and Badri Narayanan (1971) and Lu and Willmarth (1973) appears to scale on outer flow variables. In addition it is difficult to reconcile such a hypothesis with the

great disparity in scales, particularly at high Reynolds number, between the initial wall streak and the motions in the outer part of the layer.

Coles and Barker (1975) have described a significantly different model in which it is proposed that the large scale structures are the building blocks of the turbulent boundary layer. They suggest that these structures have a character not unlike those of the turbulent spot observed during transition and that the bursting phenomenon is a signature of this large scale structure. Such an idea is also implied by the model proposed by Badri Narayanan, Rajagopalan and Narasimha (1974).

It is not clear as yet which of these two hypotheses is a most accurate description of the boundary layer structure and each hypothesis makes a different statement about cause and effect.

In order to uncover more of the causal relationships and to try and resolve which of the two hypotheses discussed above is appropriate, a series of experiments were undertaken in which correlations were computed between the flow at the wall and the outer layer. These are described in the following sections.

5.1 Wall Shear - Velocity Correlations

For the first experiment the outputs of an array of four hot wires at y/δ = 0.05, 0.25, 0.50 and 0.75 placed directly above a hot film were recorded digitally. Long time averaged correlations were computed between the velocities at various points and the wall shear stress, the sense of the time delay being such that

$$R_{\tau_w}(\tau) = \lim_{T_{AV} \to \infty} \frac{1}{T_{AV}} \int_0^{T_{AV}} \frac{\tau_w(t) \cdot u(t+\tau)dt}{\tau_w' u'} ,$$

where τ_w' and u' are the conventional rms levels of the signals. These results are presented for the high and low Reynolds numbers in figures 5.1(a) and (b) and some features are worth noting. Firstly as the point of measurement is moved further from the wall, the correlations peak at an increasing time delay. Secondly, the correlations, while not large, are quite perceptible out to $y/\delta = 0.75$. (In order to verify that the weak correlation at $y/\delta = 0.75$ is indeed real, a data set was taken using a large number of samples (163,840) and it is the results from this set that are shown). Blackwelder and Kovasznay (1972) report similar measurements but with a wire at $y^+ = 24$ instead of a wall shear probe; however they present correlations only to $y/\delta = 0.5$. The similarity in correlation is significant because their experiment was performed at a considerably lower Reynolds number ($Re_\delta = 27,500$ as opposed to 97,000 for the present case). If the flow at the wall was indeed driving the outer flow then their correlations might be expected to be larger and of greater extent because of the greater parity between the two scales of motion.

Favre et al (1957) have reported similar correlation measurements based upon a wire at $y/\delta = 0.06$ and at a Reynolds number of $Re_\delta = 12,800$. Their correlations do extend to the outer layer but that is perhaps not surprising since for their flow one boundary layer thickness corresponds to 600 wall units ($600\nu/U_\tau$) or 6 streak spacings. In the high Reynolds number experiment of this investigation one boundary layer thickness corresponds to 34 streak spacings and under these circumstances it is significant that the present correlations can be perceived across the entire layer. It seems unlikely that the correlations could be generated by an event on the scale of the wall flow being convected into the outer flow. A more appealing suggestion is that the correlations are generated by the presence of a large

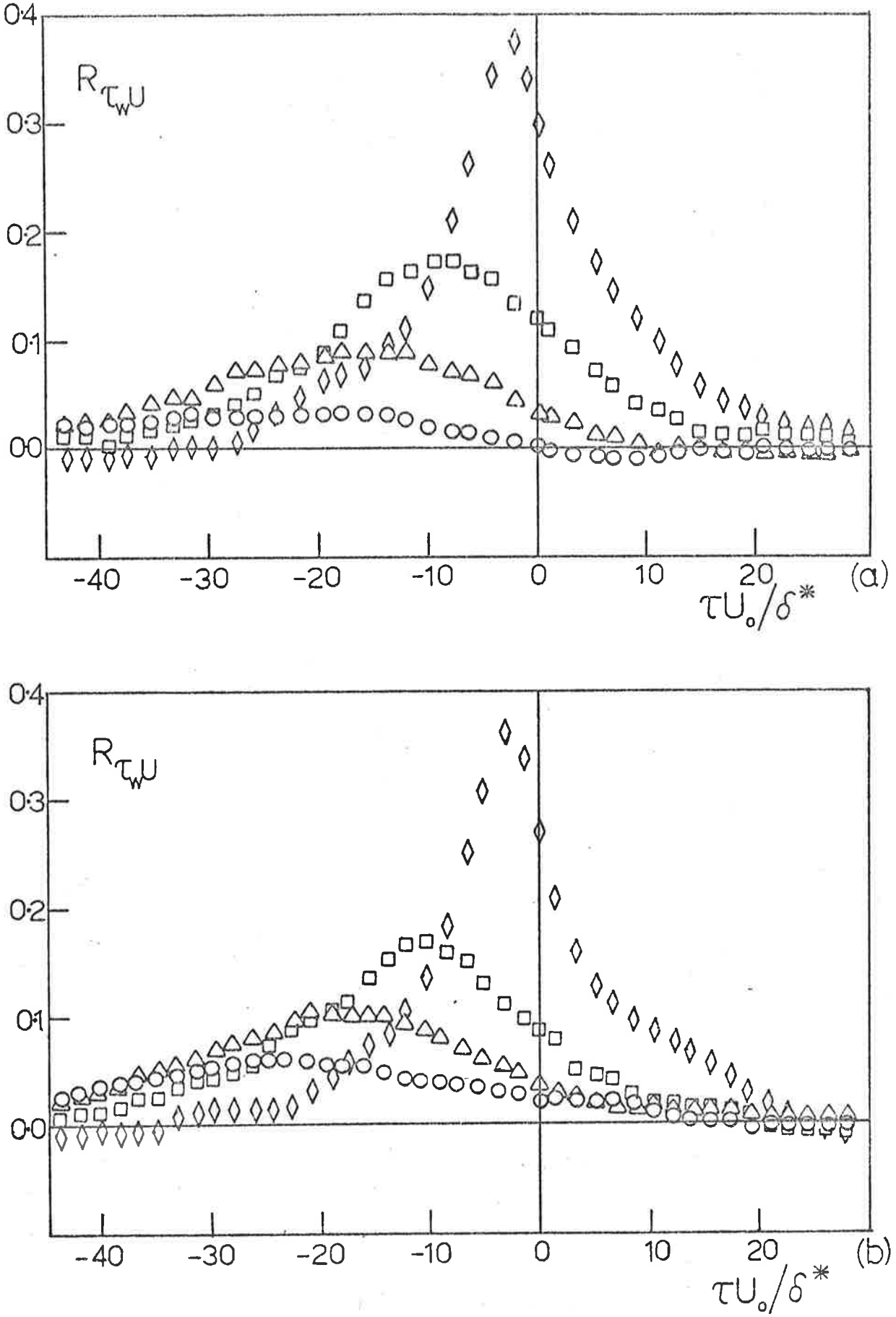

Figure 5.1 Long time averaged correlations between the wall shear and velocity directly above the hot film for high Reynolds number case (a) and low Reynolds number case (b). ◊, y/δ = 0.05; □, y/δ =0.25; Δ, y/δ = 0.50; o, y/δ = 0.75.

structure lying at an oblique angle to the wall. Blackwelder and Kovasznay (1972) suggest the former, although their correlations give little indication of this suggestion being any more appropriate than the latter.

To try and resolve this question the wires were moved to various downstream distances in an attempt to find the positions at which the correlations peak at $\tau = 0$. To do this a straightforward iterative procedure was adopted, the initial estimation of the wire positions being made on a basis of a convection velocity of 0.7 U_o. The correlations that were computed were found not to peak at exactly zero time delay and positional adjustments were made until a peak at zero time delay occurred on all the correlation curves. The correlation curves that resulted are shown in figure 5.2 and the required positions of the wires are shown in 5.3(a).

It is apparent that at the larger y/δ values there is some uncertainty in locating the wire position because of the broad flat nature of the correlation curve. This is not particularly serious as far as the present discussion is concerned and once again a very large number of samples (163,840) was used to check the final wire positions.

Comparison of figures 5.1 and 5.2 shows that the correlations obtained at the downstream position are almost exactly the same shape and amplitude as those found with the wires vertical except for the translation in time, (certainly with the experimental accuracy - see Appendix D for further discussion). If the correlation in figure 5.1 were due to the passage of fluid from a burst event near the wall then the correlation at $\tau = 0$ would surely be expected to be larger because the probes are nearer to the oblique trajectory of the bursting fluid.

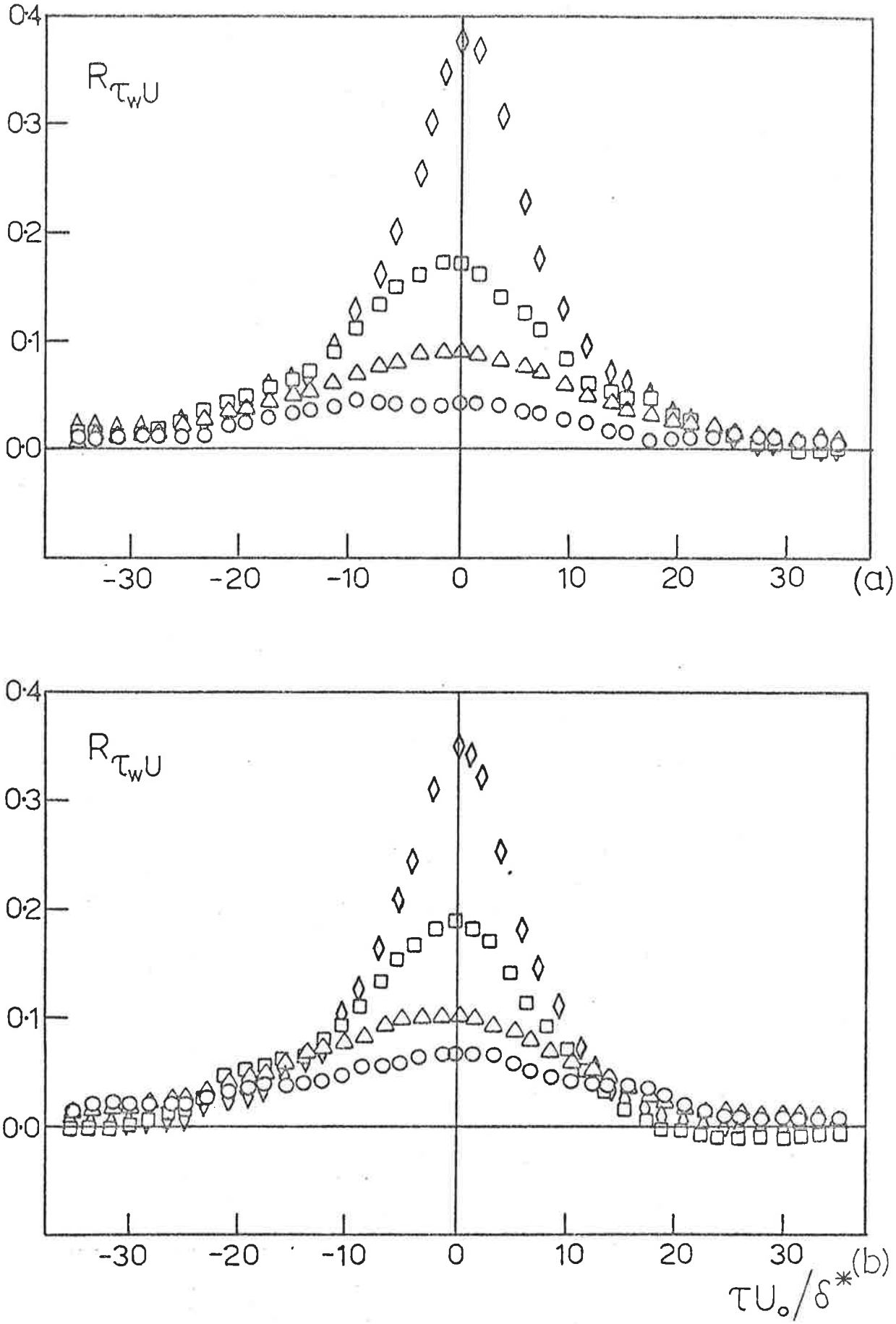

Figure 5.2 Long time averaged correlations between the wall shear and the velocity at various points downstream of the hot film such that the correlations peak at $\tau = 0$, for the high Reynolds number case (a), and low Reynolds number case (b).
◊, $x/\delta = 0.24$, $y/\delta = 0.05$; □, $x/\delta = 0.89$, $y/\delta = 0.25$;
Δ, $x/\delta = 1.72$, $y/\delta = 0.50$; o, $x/\delta = 2.40$, $y/\delta = 0.75$.

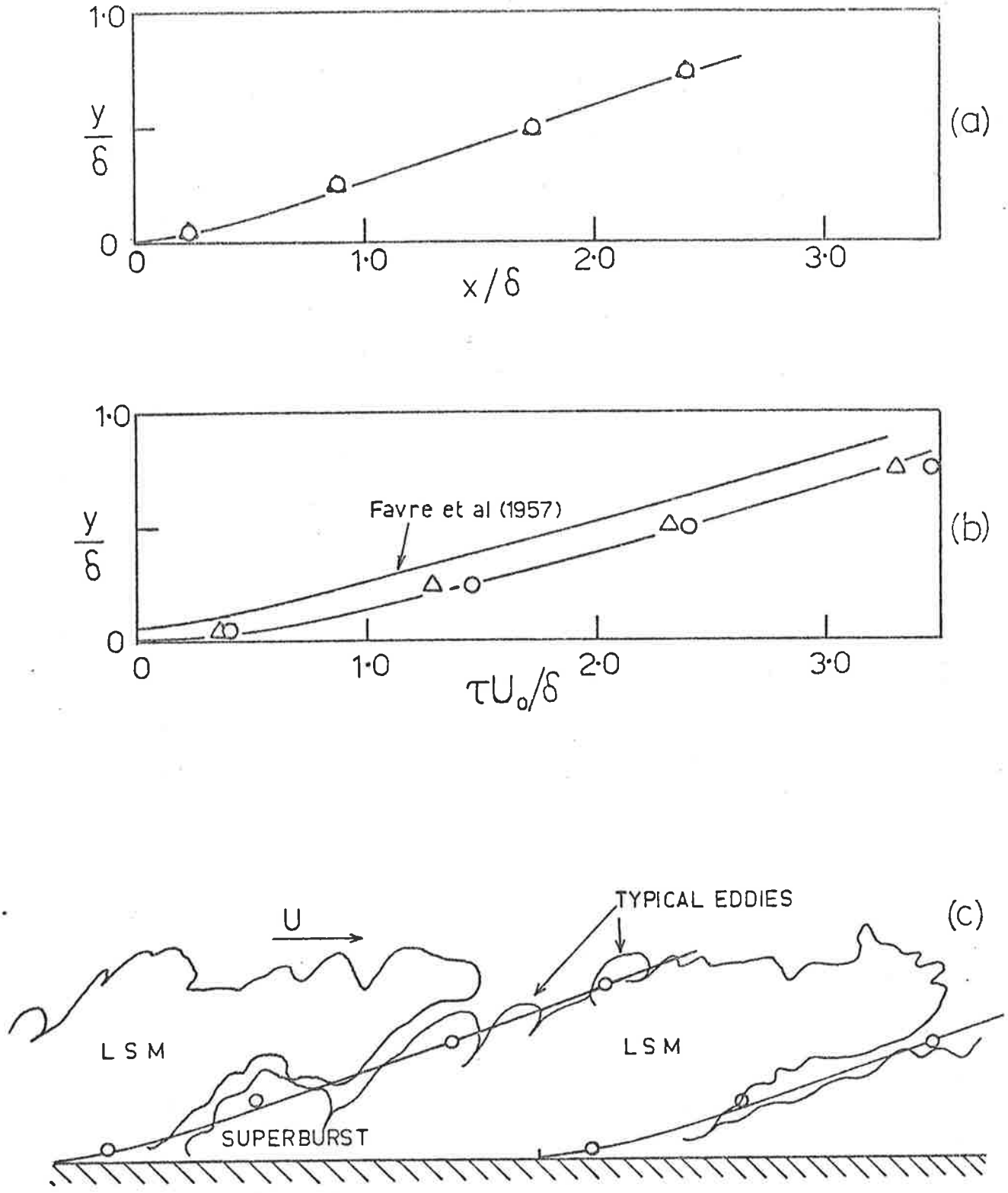

Figure 5.3(a) Spatial positions of the hot wires used to obtain the curves of figure 5.2.

(b) Time delays at which the correlations of figure 5.1 peak; o, low Reynolds number case; Δ, high Reynolds number case.

(c) Comparison of the wire positions required for the correlations to peak at $\tau = 0$ (shown —o—o—) with a tracing of a smoke picture from Falco (1976).

The conclusion on this evidence alone is that of the two hypotheses discussed in this and the previous section, it is the second that most likely accounts for the results presented here; that is, the correlations are produced by the passage of a large structure lying at an oblique angle to the wall. The points shown in figure 5.3(a) show this angle to be about 18^{o} to the wall.

Also shown in figure 5.3(b) are the values of time delay at which the correlations at $x = 0$ peaked. These are compared with similar values taken from the data of Favre et al (1957) and in each case the temporal angles of the structures are remarkably similar.

Recently and independently of this work, Falco (1976) has reported a series of flow visualization experiments using smoke in a wind tunnel. He has observed the frequent appearance of a large slowly rotating structure of width corresponding to the boundary layer thickness. Such a structure could account for the correlations observed in the present work. A tracing of one of Dr. Falco's smoke pictures is presented in figure 5.3(c) (the structural features indicated are in Falco's terminology) and superimposed on this is the line corresponding to the wire positions for which the correlations peak at $\tau = 0$. It can be seen that there is quite a remarkable similarity between the angle of the depicted structure and the angle inferred from the wall shear velocity correlations despite the large differences in Reynolds numbers.

If, as these results suggest, a large structure is responsible for the large scale variation in the wall shear stress then the structure evidently exists for a large streamwise distance when travelling downstream because the shear-velocity correlations change so very little, even over distances as large as 2δ. This is also

supported by the space - time correlations of streamwise fluctuating velocity reported by Blackwelder and Kovasznay (1972) where detectable correlation between the velocity at points separated only in the stream direction can be found for separations as large as 20δ or more.

Kovasznay, Kibens and Blackwelder (1970) have carefully mapped out correlation contours of the streamwise velocity with a fixed probe at $y/\delta = 0.5$ and their correlation contours which take the form of a large upward tilted ellipsoid are of the same form that would be produced by a structure inclined to the wall in the manner depicted in figure 5.3(c). The suggestion that structures are inclined to the wall is also consistent with the findings reported by Blackwelder and Kaplan (1976) although their study was limited to the wall region.

With regard to the curves presented in figure 5.3(a) and (b), there is a temptation to compute a convection velocity of a large structure on a basis of the time delays corresponding to each streamwise separation distance. If this is done values ranging from 0.65 U_o near the wall to 0.80 U_o at $y/\delta = 0.75$ are obtained, suggesting that the structure is convected at a speed less than the local mean velocity. This is, however, not necessarily so, since such a convection velocity is accurate only if the structure is frozen. Structures of the kind depicted in figure 5.3(c) are unlikely to be frozen but are presumably slowly growing and rotating. Therefore the computed convection velocities may be dominated by points near the hot film and only approximately reflect the convection velocity of the large scale structure. It is likely that the convection velocity of the large structure is of the order of 0.8 U_o which as Willmarth and Wooldridge (1962) and Bull (1967) find is the convection velocity of

the large scale or low frequency pressure field.

5.2 Ensemble Averaged Short Time Correlations

The conclusions in the last section regarding the presence of a large structure in the boundary layer rest upon a set of rather weak correlations. Therefore more stringent tests of the large structure hypothesis were sought with the aim of showing more conclusively that the wall shear velocity correlations are not produced by smaller scale disturbances convected from the wall to the outer flow.

Such tests could make use of higher order correlations of the kind described by Fulachier, Giovanangeli, Dumas and Kovasznay (1974), but in what follows the same conclusion has been found by a more direct means based on conditional ensembled averaging of short time estimations of the correlation. One of the shortcomings of long time correlations is that the correlation is an ensemble of all events and is averaged over all times, including those times when the event may not be present. Clearly, if one could discriminate upon the presence of the event of interest, then a more meaningful correlation could possibly be generated. Unambiguous event discrimination in turbulent boundary layer flow is notoriously difficult but in the present case there is an implication that the large structure can be characterized by locally large values of $R_{\tau_w u}$, suggesting that a search should be made upon such a basis.

Therefore in what follows the time records of data were broken up into a series of short time records of length $T_{AV}U_o/\delta^* = 50$, and corresponding short time correlations computed between the wall shear stress and velocity at those various positions in the layer found previously to maximize the correlations at $\tau = 0$. The correlations

are computed in the sense

$$R_{\tau_w u} = \frac{1}{T_{AV}} \int_0^{T_{AV}} \frac{\tau_w(t, x) \cdot u(t + \tau, x + x', y + y') \cdot dt}{\tau_w' \, u'}$$

where unlike the conventionally defined correlation, T_{AV} may be quite small and τ_w' and u' now refer to the local short time estimations of the rms values. A similar correlation technique has been used by Gupta, Laufer and Kaplan (1971) to determine spatial details of the low speed streaks known to occur near the sublayer and Simpson (1975) used the same method to determine the time scales of events near the wall. The choice of averaging time is not completely arbitrary; if it is too large, the detailed events will become obscured and if too small, there will be doubt as to the significance of any correlations found. In the present case it should be chosen, so as to be of the same order as the correlation extent of the events being studied - hence the value of $T_{AV} \, U_o/\delta^* = 50$ chosen on the basis of the results in figure 5.2.

A conditional procedure was applied to the short time correlations which selected those times when a large correlation occurred between the wall shear stress and the velocity at $y/\delta = 0.25$ and a discrimination level was chosen such that this correlation should exceed about twice the long time averaged value or, more precisely, exceed 0.3 at $\tau = 0$. This was found to occur in 26% of the cases studied and when the curves were ensemble averaged the results shown in figure 5.4 were obtained. Naturally the ensemble averaged curve has a level greater than 0.3 but in all other respects is similar to the long time averaged curve.

A test of the large structure hypothesis is now evident; if the correlations result from the presence of a large structure, then

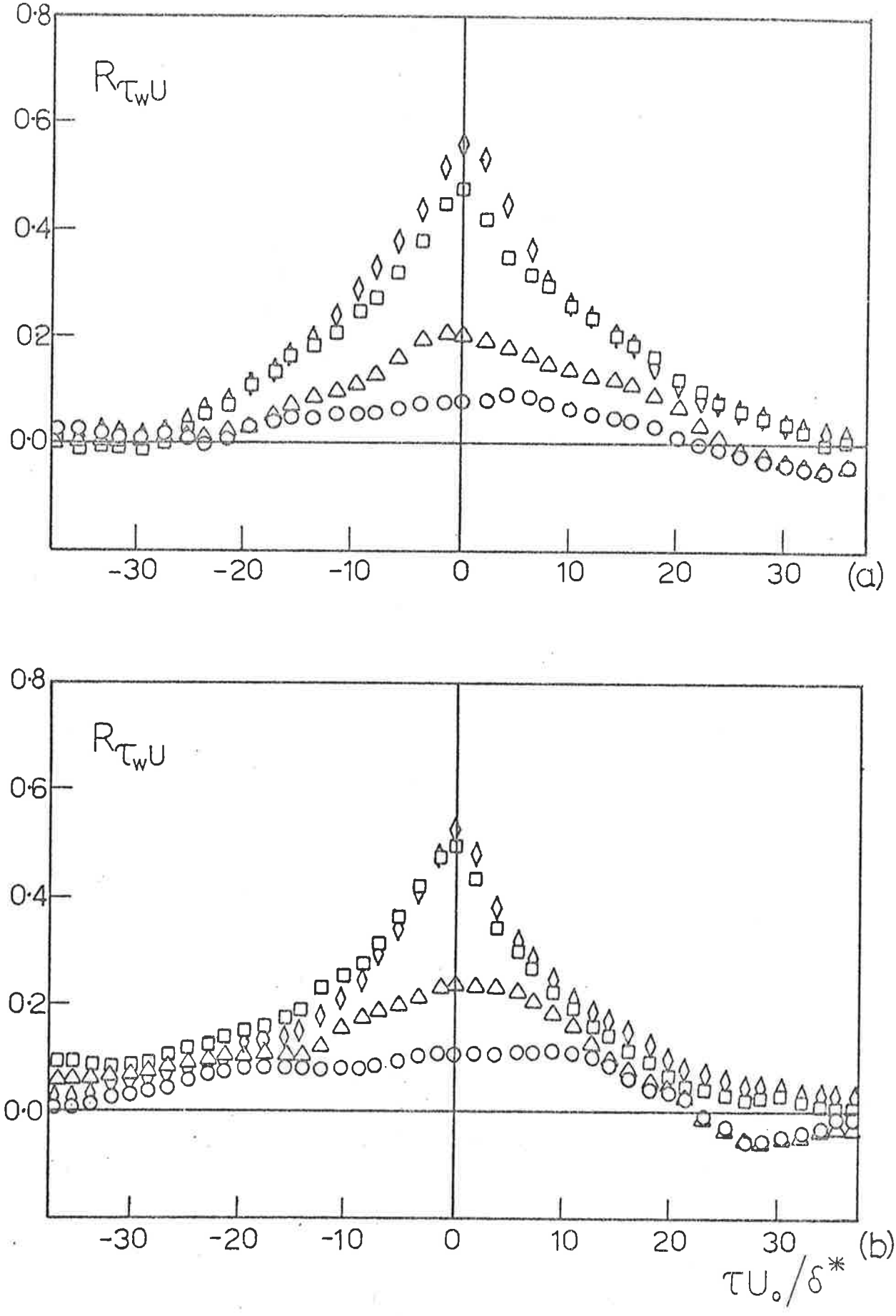

Figure 5.4 Conditional ensemble average of short time wall shear-velocity correlations for the high Reynolds number case (a) and low Reynolds number case (b). The symbols are as in figure 5.2. Note change in ordinate scale from figure 5.2.

at those times when there is a locally large correlation between the wall shear and velocity at $y/\delta = 0.25$, the correlations between the wall shear and velocity at other points should also be large. These correlations were therefore computed for that subset of times when the detection criterion was satisfied and the results are also shown in figure 5.4. It may be seen that the amplitude of the correlations across the entire boundary layer in both Reynolds number flows has been simultaneously increased. Such behavior can only be reconciled with the idea of a large structure which causes simultaneous effects at all measuring points.

The discrimination amplitude applied to the correlation at $.25\delta$ was changed to a correlation level of 0.45 and 0.60 which reduced the subset of times which satisfied the criterion to 15% and 7% respectively but in every other way only substantiated the above result. The same technique has been used with the averaging time, both halved and doubled, and the same behavior is observed.

Given that these correlations are a result of a large structure, it is of interest to inspect the time records used to generate the correlations in an attempt to identify those parts of the signals which characterize the structures. There was little obvious indication of a large structure in the long time records themselves, but it is clear that the place to look is at the times when the discrimination was successful. Presented in figure 5.5 are some of the short time records of the signals (for the high Reynolds number case) selected from the subset of times when the discrimination process was successful. They do show a strong visual correlation of events across the entire layer.

Closer examination of these records shows identifiable features which appear to characterize the large structure. In particular, the velocity records show a relatively sharp step from a low value to a

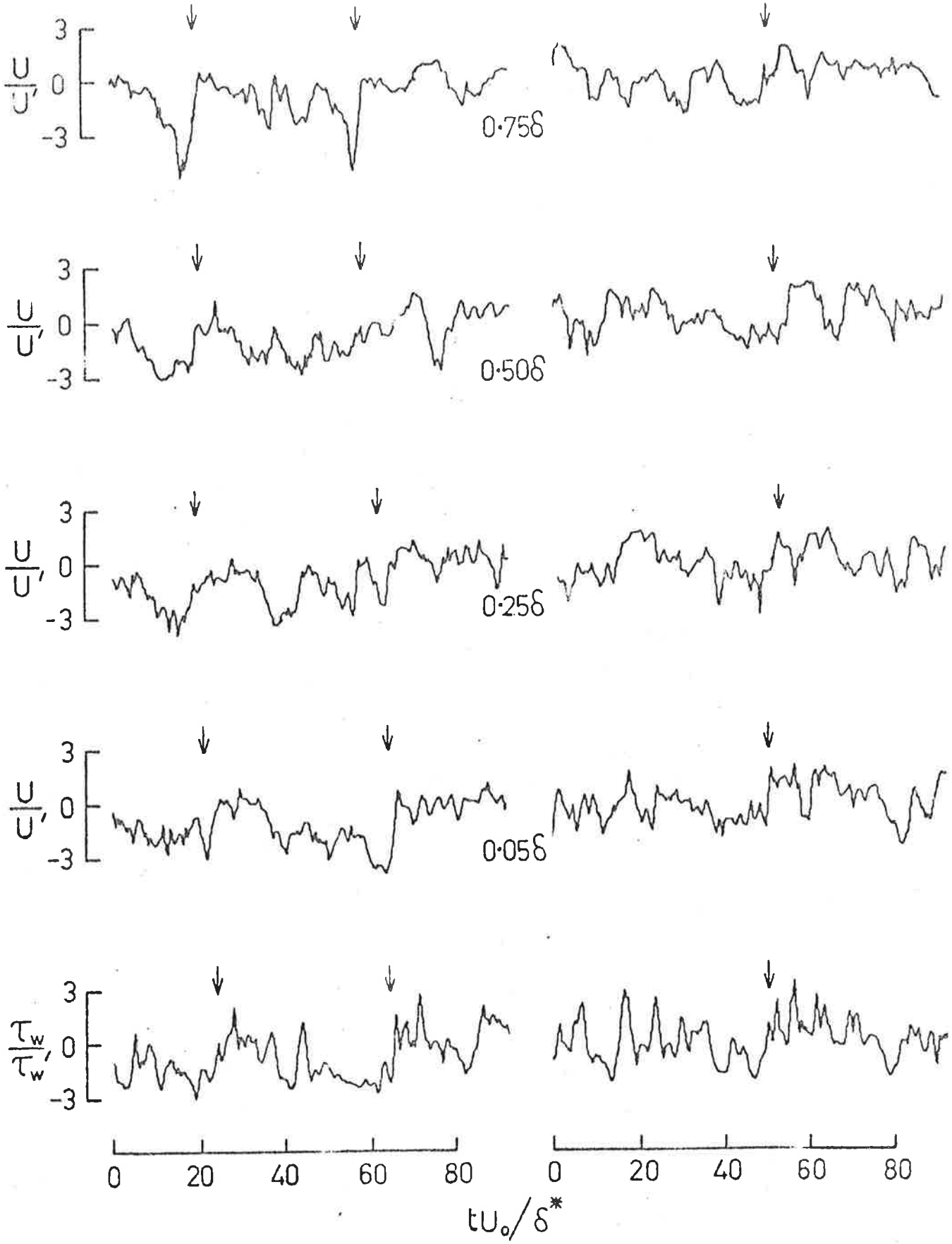

Figure 5.5 Simultaneous time records of the wall shear and velocity at other points in the layer for the high Reynolds number flow at the times when the detection scheme used to generate figure 5.4 was satisfied.

high value followed by a slow decrease thereafter. Typical examples of this effect are flagged in figure 5.5 and it can be seen that the effect may be observed across the entire layer. Laufer (1975) has recently reported some simultaneously recorded traces of the outputs of a rake of temperature probes placed in a boundary layer above a slightly heated wall, and a similar sawtooth character is evident in that data also. Such behavior is also consistent with the findings of Ueda and Hinze (1975) and others, that the time derivative of the fluctuating velocity is a quantity with positive skewness. The same event at the outer regions of the layer shows large negative excursions, representing in broad terms a turbulent zone, and the sudden change in velocity can be seen to occur on the upstream or trailing edge of such zones. In addition to this step in the velocity, it is important to notice a similar positive step in wall shear stress and in particular the high frequency fluctuations following this step. If this is a characteristic feature, then it is clearly important, as it implies that the high frequency fluctuations are the response of the region near the wall to the passage of the large structure. Such a finding would also account for the scaling of the wall shear stress spectrum discussed in section 4.4. This point will be taken up again in more detail in section 6.1.

These typical structural signatures are not always apparent, and while they may be present on one signal, there are times when they cannot be simultaneously identified at other points. Likewise the relative phase of an event on one signal to its counterparts on other signals varies by significant amounts, indicating a variation in the mean angle of the structure relative to the wall. It is this randomness in angle and length scale that apparently accounts for the weak long time averaged correlations that have been presented.

5.3 Correlations of Velocity in the Spanwise Direction

A most significant feature of boundary layer turbulence and of turbulent flows in general is the complex three dimensional nature of the phenomenon. The features discussed in the previous section imply the existence of a structure with a width of one boundary layer thickness in the direction normal to the wall; it is then reasonable to expect this structure to have a significant lateral extent. The extensive correlation data of Kovasznay, Kibens and Blackwelder (1970) in the intermittent region of the boundary layer suggest that the lateral width of the large scale motions is also of the order of a boundary layer thickness.

To try to resolve more details of the three dimensionality of the motions, the array of five hot wires was placed transversely, that is with the wires at the same x and y positions but separated in the lateral direction by distances of 0.15δ or about $1.1\delta^*$. Simultaneous recordings of the signals from each wire were taken with the array placed at various positions above the wall. The cross correlations between the signals were computed and the resulting correlations for three values of y/δ for the high and low Reynolds number flows are shown in figures 5.6 and 5.7.

The correlations can all be seen to be symmetrical about $\tau = 0$, a consequence of the spanwise homogeneity. At small spanwise separations and distances far from the wall the correlation is positive but as the separation increases the correlation becomes zero (somewhere between $\Delta z = 0.3\delta$ and $\Delta z = 0.45\delta$ for $y/\delta = 0.75$) and negative thereafter. This form of correlation is precisely the same as given by Kovasznay et al (1970) who found the zero crossing to

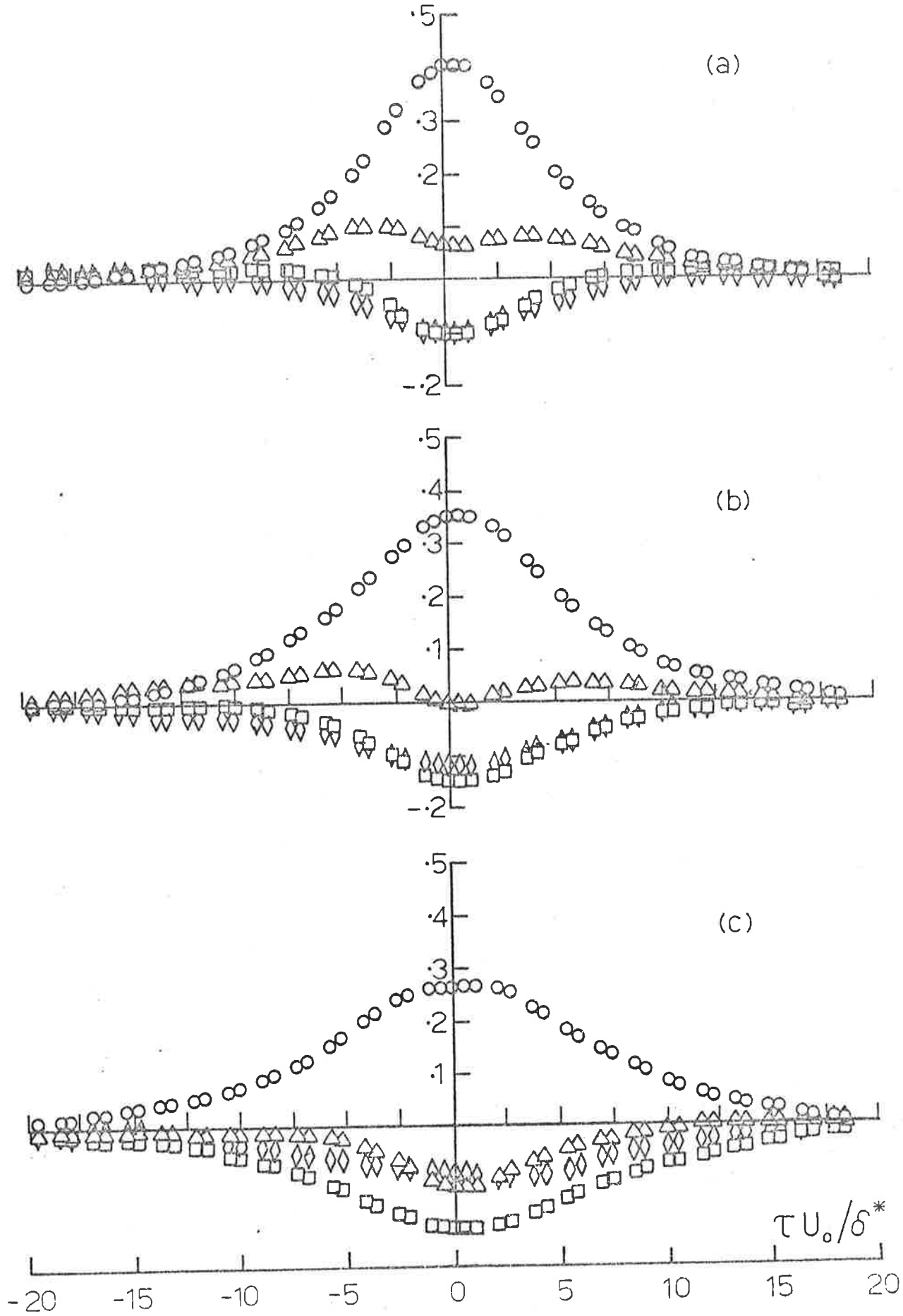

Figure 5.6 Correlations of the velocity at points separated only in the spanwise direction for the high Reynolds number flow; (a), $y = 0.75\delta$, (b) $y = 0.5\delta$, (c) $y = 0.25\delta$; o, $\Delta z = 0.15\delta$, Δ, $\Delta z = 0.30\delta$, $\square$, $\Delta z = 0.45\delta$, $\Diamond$, $\Delta z = 0.6\delta$.

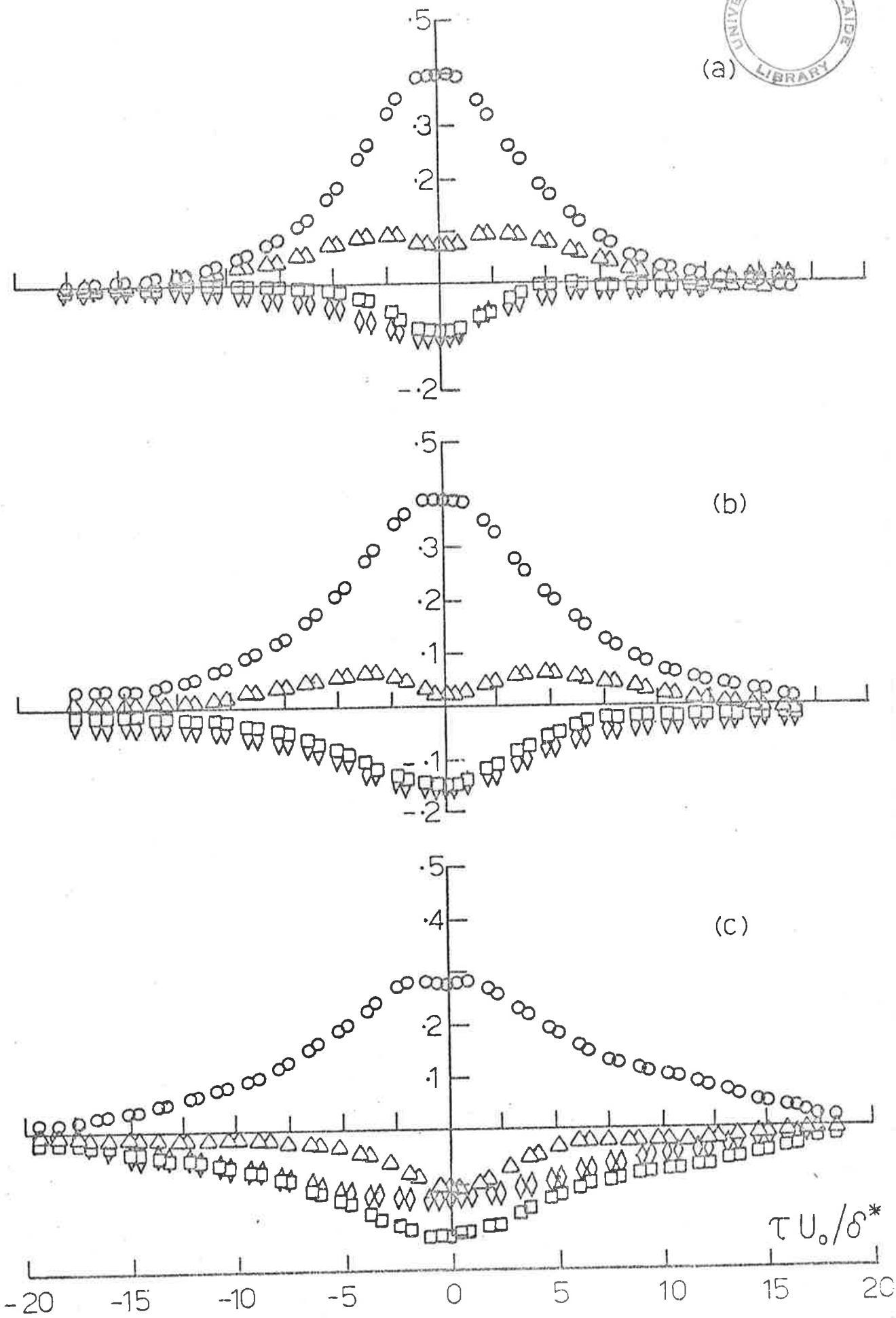

Figure 5.7 Correlations of the velocity at points separated only in the spanwise direction for the low Reynolds number case. The symbols are as in figure 5.6.

occur at about $\Delta z = 0.4\delta$ at a similar y/δ also. As the wall is approached the correlations become negative at smaller spanwise separations and the region of negative correlation is more extensive. At $y/\delta = 0.25$ the change in sign of correlation occurs somewhere about $\Delta z = 0.25\delta$. The time extent of the correlations is large being of the order of $20\delta^*/U_o$ or nearly $3\delta/U_o$ which compares favourably with a similar value which can be seen in the curves of Kovasznay et al (1970).

A very significant feature, however, which cannot be seen in their data, is that the curves corresponding to $\Delta z = 0.3\delta$ at $y/\delta = 0.5$ and 0.75 show a clear indication of twin maxima with symmetry about the axis at $\tau = 0$. This correlation effect, although of small amplitude, is larger than the error bars on the correlations themselves (see Appendix D). The result seems unmistakable in this data, but as it was not evident in previously reported work, special studies were undertaken to prove that it was not spurious and did not result, for example, from the presence of the rake. It is noted that the same results were obtained at other flow speeds and in thinner and thicker regions of the boundary layers occurring in the wind tunnel. The mean flow was checked for spanwise homogeneity and found to be genuinely two dimensional. The effect was found when any pair of wires separated by 0.3δ in the rake of 5 wires were used. All the various tests undertaken indicated that twin maxima in the correlations are certainly real.

The possible implication of these twin maxima is that they result from significant correlation at positive time delay for half the time and at negative time delay for the other half of the time. That is, the structure has a characteristic angle in the transverse direction.

In order to demonstrate this and account for this unusual series of correlation curves, simultaneous traces of the signals from the array of five wires are presented in figure 5.8 for the high Reynolds number case at $y/\delta = 0.75$. The intermittent nature of the flow can clearly be seen by the large negative velocity excursions which give rise to a highly skewed signal (because the mean velocity has been substracted out, the non-turbulent regions show a small positive streamwise velocity). Careful examination of these signals demonstrates the way the correlations are formed. Consider for, example, one of the turbulent regions at $z/\delta = 0.0$ shown by the arrows in the figure. Once again the same steep fronts identified in the last section can be seen; a very similar pattern can frequently be seen on the signals of adjacent wires, except that it occurs at a different time from the initially identified disturbance (this time shift is quite small in relation to the time scale of figure 5.8). Sometimes it occurs at a later time and sometimes at an earlier time, and as the wire separation increases so the time difference appears to increase. A long time correlation, therefore, at small separations will show an essentially positive correlation and at larger separations the regions of positive correlation will occur less often at zero time delay and more often at positive and negative time delays giving rise to the possibility of twin maxima in the correlation. As the separation increases further these maxima lose definition because of the increased randomness in the time delay at which the peak correlation occurs as a result of large variations present in the structural geometry.. The most probable correlation event is then one of turbulent zones ($u < 0$) and non-turbulent zones ($u > 0$) (and vice versa) giving rise to the negative and symmetrical correlation observed.

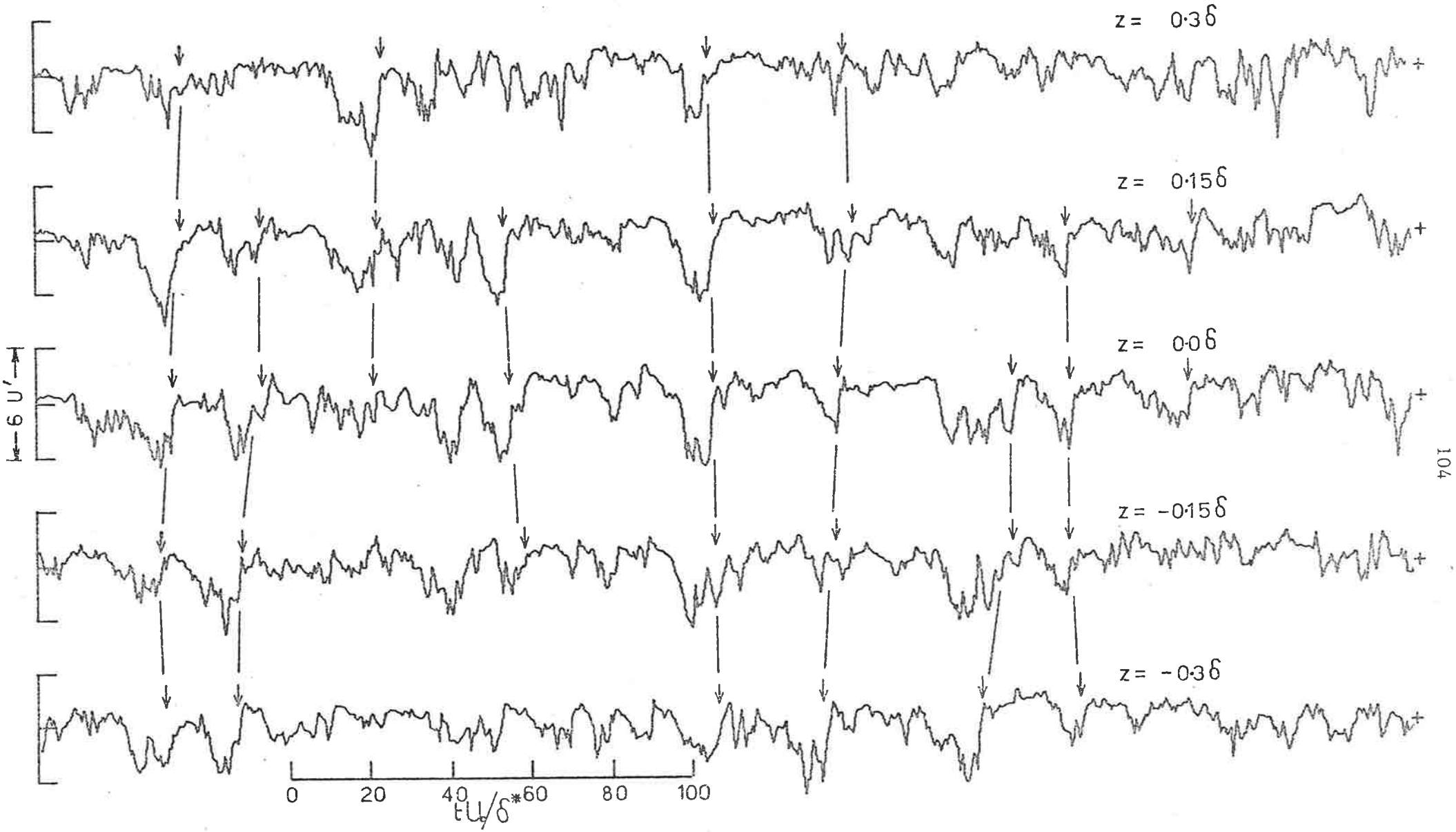

Figure 5.8 Simultaneous time records of the velocity at five points separated only in the spanwise direction and at $y/\delta = 0.75$ for the high Reynolds number case.

The implication is therefore one of an interesting three dimensional structure which has regions lying laterally oblique across the flow, and one possible structure that has such a feature is, of course, the turbulent spot whose edges lie at an angle to the mean flow direction. As already mentioned, Coles and Barker (1975) have recently used the spot as a model for a synthetic turbulent boundary layer. This kind of flow structure, which was first recognized in the transition studies by Emmons (1951) and has been studied by Elder (1960) and most recently by Zilbermann et al. (1977), has a broadly triangular shape in plan view and it is plausible that a similar structure exists in a fully turbulent boundary layer.

The positions of the time delays corresponding to the twin maxima suggest that the structure has regions at quite an acute angle to the mean flow and the negative correlation at large separations is also a reflection of this angle. The included angle between the structures and the flow direction is about 25° at $y/\delta = 0.75$ and 0.50 if it is assumed that the structures responsible for the generation of these curves are convected at the local mean velocity. The question of this angle, and the correct interpretation of these correlations will be discussed more fully in the discussion of the conditionally sampled measurements in section 7.

Finally, in view of the large spanwise scales present and the almost identical results at the two Reynolds numbers, it is perhaps worth reiterating that the structures present are quite unlikely to arise as a direct result of small scale events nearer the wall. It is more plausible that the turbulent bursts, for example, represent a small scale response of the wall region to the passage of a larger structure.

In this sense these results support the earlier findings and add further weight to this conclusion.

5.4 Spanwise Correlations of Wall Shear Stress

Given the substantial correlation between the wall shear and the velocity in the vertical plane (section 5.1) and the transverse velocity cross-correlation (section 5.3) it is natural to expect some wall shear correlation over substantial transverse distances. Of course, the wall region is dominated by the small scale bursting phenomenon and the intensity of this activity perhaps accounts for the apparently small scale transverse velocity correlation in this region (Gupta, Laufer and Kaplan, 1971, Grant, 1958). Despite this fact it seemed important to establish the extent of the transverse wall shear cross correlation.

Digital records from two hot films, separated by various amounts in the spanwise direction were obtained. Long time averaged correlations have been computed from these data and are shown in figure 5.9(a) for the high Reynolds number case. The same data at $\tau = 0$ are presented as a space correlation in figure 5.9(b). These correlations are clearly very weak but do show a similar behavior to the velocity correlations presented previously. They are symmetrical in time, again a consequence of spanwise homogeneity. At small separations there is positive correlation and as the separation increases to about $\frac{1}{4}\delta$ the correlations become negative and slowly return to zero thereafter. It is notable that the wall shear stress may be correlated (albeit weakly) over distances as large as 0.7δ which for the high Reynolds number of this work corresponds to a distance of $2400\nu/U_\tau$.

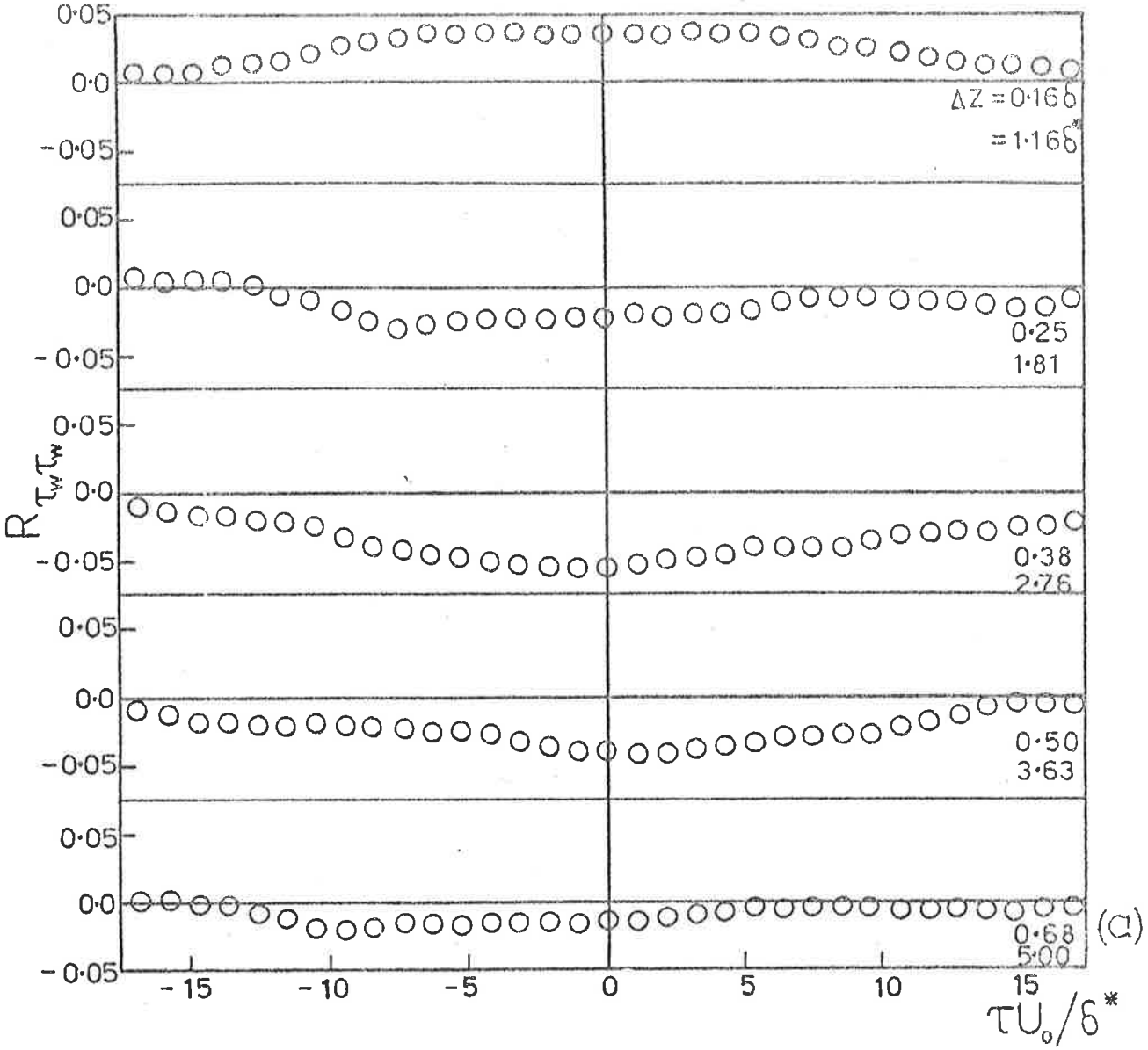

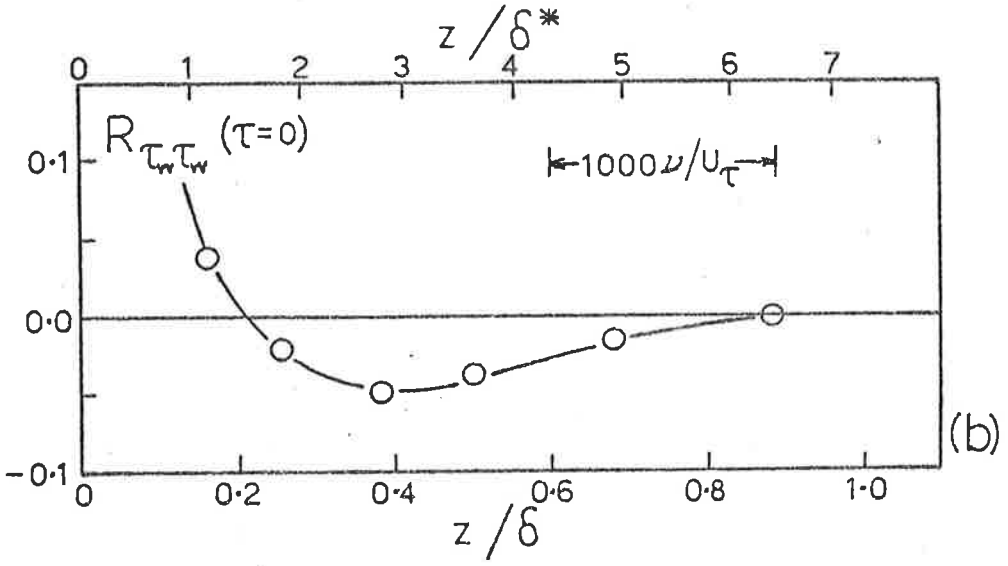

Figure 5.9(a) Long time averaged correlation between the wall shear stress at points separated only in the spanwise direction. High Reynolds number flow.

Figure 5.9(b) Cross plot of the spatial wall shear correlation value occurring at $\tau = 0$.

Gupta, Laufer and Kaplan (1971) have reported some measurements of the spanwise correlation of the streamwise velocity at the edge of the sublayer and at lower Reynolds numbers than in this case. Their correlations also decay very quickly and show nearly zero correlation beyond separations of about $zU_\tau/\nu = 300$. However, some of their correlations do maintain small positive values for larger separations. There is no evidence of the small nevative correlation at large separations found here, but they did not carry their correlations far enough for this to show up, presumably because of the weak values encountered.

The weakness of the correlations is evidently a reflection of the fact that the flow near the wall is dominated by the intense small scale fluctuations of the bursting phenomenon. These make a large contribution to the rms shear so that the normalized correlations are small. (If it were possible to normalize by an rms level arising from the large scale structure alone, a more meaningful correlation amplitude could be generated. The discussion of the scaling of the spectra of the wall shear stress has suggested that outer layer influences account for about a 70% contribution to the mean square wall shear. If the correlations of this section were normalized by this component alone, their amplitude would be doubled.)

In section 5.2 correlations were reported between the wall shear and the velocity at various points in the layer. It was found that these correlations were increased throughout the layer by confining the correlation to those times when the correlation between the wall shear and the velocity at $y = 0.25\delta$ was larger than

the long time average value. A further test of the large structure hypothesis is that if this discrimination process does discriminate the presence of a large structure for a certain subset of times, then for the same subset of times, an enhanced set of spanwise wall shear correlations should be obtained.

When the digital records of wall shear data used to generate the information in figure 5.9 were recorded, a hot wire was also positioned at $y/\delta = 0.25$ and at $x/\delta = 1.72$ relative to one of the hot films. This position corresponds to the point at which the wall shear - velocity correlation peaks at zero time delay. As before, the data were broken up into a series of short records and short time correlations computed between the wall shear and the velocity at $y/\delta = 0.25$. The averaging time used was once again $50\delta^*/U_o$. The spanwise wall shear correlations have been re-computed at those times when the discrimination was successful and ensemble averaged. The results are presented in figures 5.10(a) and (b) which may be compared directly with the curves in figure 5.9. It is clear that the correlations have been nearly doubled, even at separations as large as 0.7δ. This is evidence that a proportion of the dynamic wall shear stress is a direct consequence of the passage of a large structure. It is of significance that the discrimination requirements can be satisfied by structures which are only of the order of 0.25δ in normal extent, and yet the spanwise scale of the same events appears to be of the order of 0.7δ. However since the same discrimination technique showed a significant correlation between the wall shear and velocity at $y/\delta = 0.75$, then the large structures would appear to have comparable spanwise and normal extent.

In order to resolve more details of the structure which

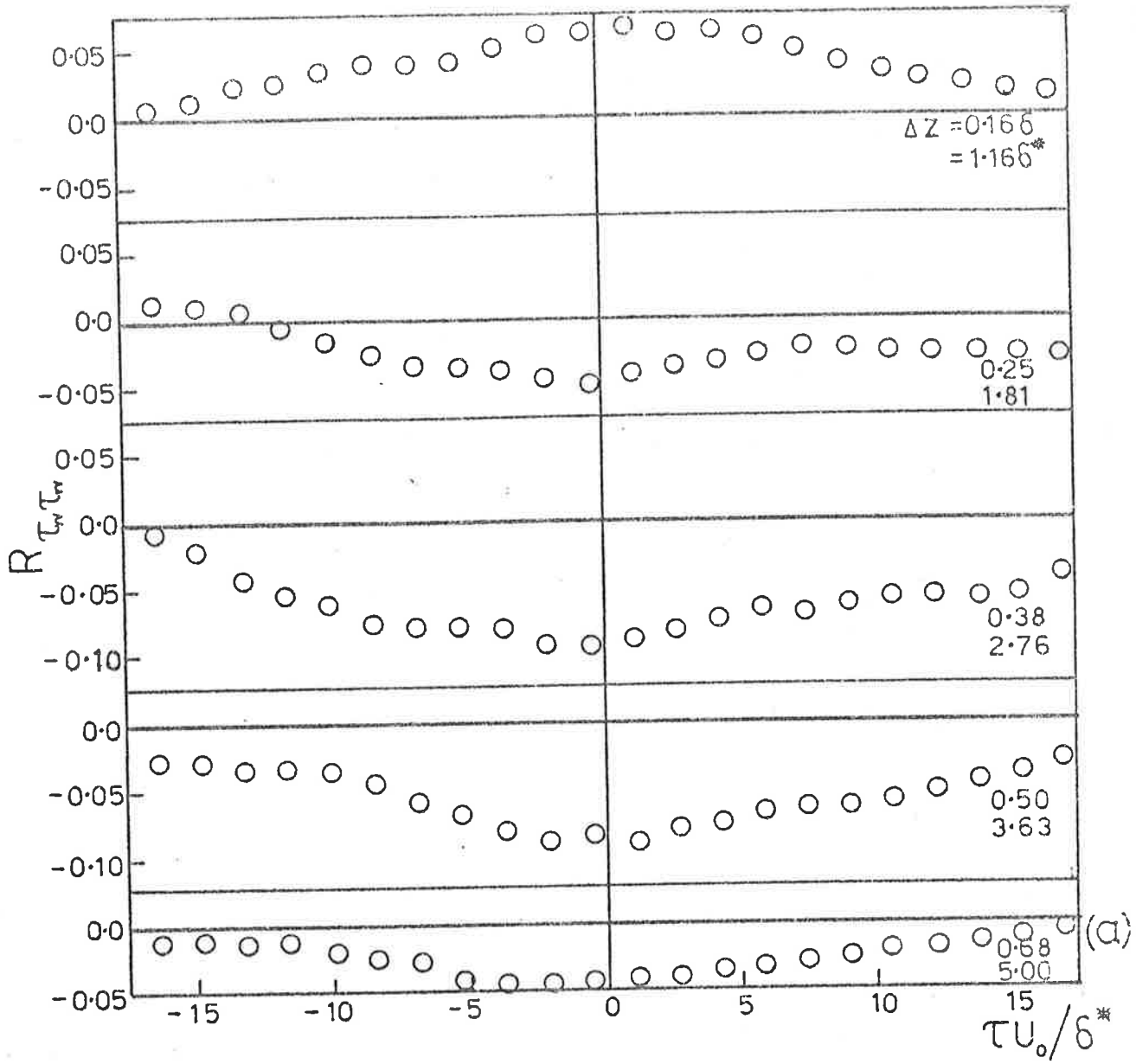

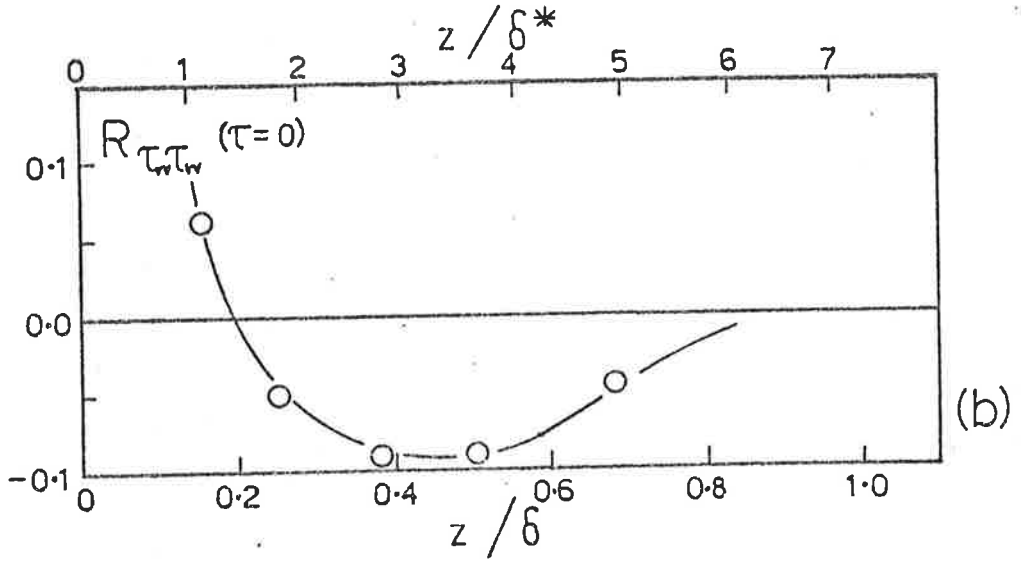

Figure 5.10(a) Ensemble average of short time spanwise wall shear correlations computed only at those times when the short time correlation between the wall shear at $x = 0$ and the velocity at $x = 1.72\delta$, $y = 0.25\delta$ exceeded 0.3 at $\tau = 0$.

Figure 5.10(b) Cross plot of the above correlation values occurring at $\tau = 0$.

generates the spanwise wall shear correlations, a quadrant breakdown of the correlation at zero time delay has been determined. The results are presented in table 5.1 for both the long time averaged correlation and the enhanced ensemble averaged result. As before, the short time correlations have been normalized by the short time estimation of the rms value and then averaged. Also shown in table 5.1 are the results obtained when using two uncorrelated wall shear signals.

Table 5.1

Quadrant Breakdown of Spanwise Wall Shear Correlations

Spanwise Separation $\Delta z/\delta$	Long Time Average				Enhanced Ensemble Average			
	1 $\geqslant 0$ $\geqslant 0$	2 $\geqslant 0$ < 0	3 $\leqslant 0$ $\geqslant 0$	4 < 0 < 0	1 $\geqslant 0$ $\geqslant 0$	2 $\geqslant 0$ < 0	3 $\leqslant 0$ $\geqslant 0$	4 < 0 < 0
0.16	0.17	-0.15	-0.15	0.17	0.18	-0.15	-0.15	0.18
0.25	0.16	-0.17	-0.17	0.15	0.16	-0.18	-0.18	0.16
0.38	0.15	-0.17	-0.17	0.15	0.14	-0.19	-0.19	0.15
0.50	0.15	-0.17	-0.17	0.15	0.15	-0.19	-0.18	0.15
0.68	0.16	-0.16	-0.16	0.15	0.16	-0.18	-0.17	0.15
Uncorrelated Signals	0.16	-0.16	-0.16	0.16	0.16	-0.16	-0.16	0.16

The long time correlations show that at a separation of 0.16δ, the small positive correlations result, not surprisingly, from both an increase in contribution from the first and fourth quadrant and a decrease in contribution from the second and third. When enhanced, however, the larger positive correlation obtained results almost entirely from a further increase in contribution from the first

and fourth quadrant with the values in the other two quadrants being unchanged. At larger separations the situation is reversed. The negative long time correlation is generated from decreased contributions from the first and fourth quadrants compared to the case of uncorrelated signals and increased contributions from the other two quadrants. When enhanced, however, the larger negative correlation results almost entirely from further increases in the contribution from the second and third quadrants as opposed to decreases in the first and fourth.

The long time correlations can, of course, only result from signals which are predominantly in phase at small separations and out of phase at larger separations. When the presence of the large structure is discriminated upon, however, it is notable that the enhanced correlations result only from the in phase components at small spanwise separations and only from the out of phase components at larger separations. The contributions from the other quadrants are little different from what might be expected through random associations of events. Blackwelder and Kaplan (1976) have remarked that a similar in phase - out of phase behavior can be visually observed in the signals from a spanwise rake of hot wires placed at the edge of the sublayer.

A model of the large structure that accounts for such a behavior will be discussed in section 8.

6. STRUCTURAL FEATURES ASSOCIATED WITH THE SMALL SCALE MOTIONS

Up to this point the discussion has clearly been concerned with the evidence for large scale structures in the boundary layer. The scaling of the spectrum of the wall shear stress has, however, indicated that one spectral region (the high frequencies) scales on wall variables and the other region (low frequencies) scales on outer layer variables. It was also mentioned in section 5.2, that from visual observations of the signals there appeared to be significant correlation between the occurrence of intense small scale shear stress fluctuations and the passage of a large structure. This appeared to be an important finding and the work of the following sections is a result of an effort to quantify this conclusion.

6.1 Correlation Between High Frequency and Low Frequency Activity.

It is apparent from this that the wall shear stress may consist of essentially two scales of motion. To represent a turbulent signal in this way is a considerable simplification as many scales are present with large overlap, however, it will shortly be demonstrated that such a breakdown of a signal can lead to considerable information regarding the way the large structures and small scale events are related to one another.

Given a time record of any turbulent signal, in order to try to quantify any relation between the two scales of motion it is clearly necessary to split the signal into one part representing, in the present case, the large scale motions and another part

representative of the small scale motions. A way to achieve this is by the use of a low pass filter with the cutoff being chosen at a point which is assumed to separate the two scales of motion reasonably well. The effect of low pass filtering a signal is best described by example and shown in figure 6.1(a) are time records of the wall shear stress and velocity at $y/\delta = 0.25$ for the high Reynolds number case. It will be recalled that the presence of the large structure was discriminated upon by the local short time estimations of the correlation between these two signals. Superimposed on the unfiltered traces are the traces obtained when the signals are low pass filtered with a filter whose cutoff frequency is $\omega_c \delta^*/U_o = 0.43$. A running average summing filter was used to generate this trace and the filter had zero phase delay. Its characteristics are described in Appendix C.

It can be seen from this figure that this filter does indeed give an acceptable smoothing of the signals. Figure 6.1(b) shows the high frequency portion of the signals that remain when the smoothed signal is subtracted from the unfiltered records. This high frequency record evidently represents the small scale motions while the low frequency records clearly represent large scale motions. One reason for the selection of this filter cutoff frequency is that it corresponds to the region where the spectrum of the wall shear stress appears to change from outer layer scaling to inner layer scaling. A further reason for choosing it is that the period at the cutoff frequency is about twice the mean time interval between bursts ($TU_o/\delta^* \approx 30$) as determined by Rao, Narasimha and Badri Narayanan (1971). As this period was found to scale

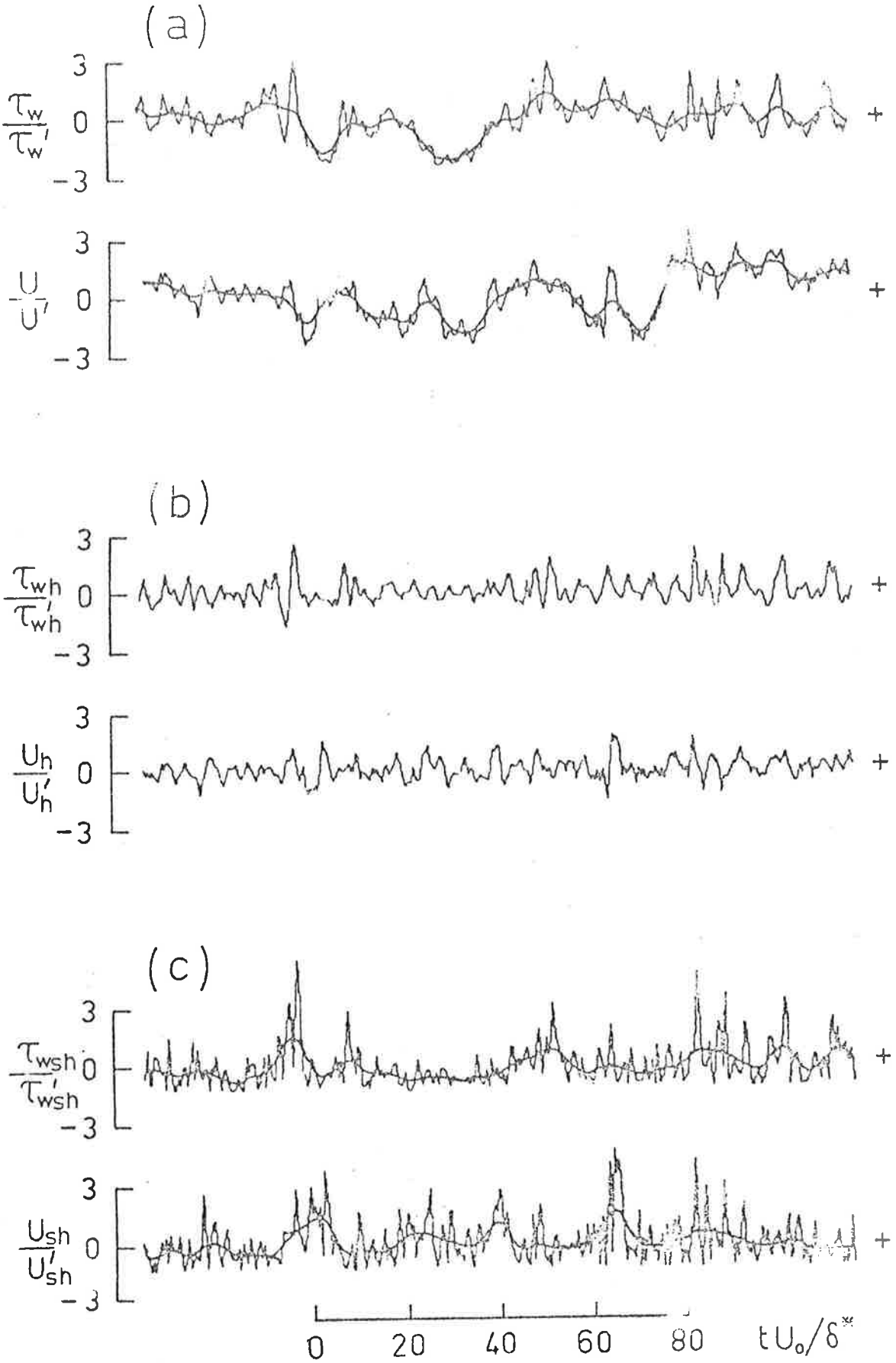

Figure 6.1(a) Time records of the low pass filtered and unfiltered wall shear and velocity at $y/\delta = 0.25$.

(b) Wall shear and velocity signals that remain after the low frequencies are subtracted out.

(c) Rectified high frequency wall shear and velocity and smoothed rectified components.

with outer layer variables, it is perhaps a suitable characteristic time scale for the large structure.

Finally, further support for this choice of filter cutoff frequency was sought in the long time averaged wall shear correlations of section 5. It was felt that since these evidently resulted from a large structure, the high frequency content of the signals should contribute little to the correlation. That is, if the signals are filtered and then correlated one would expect, for acceptable filtering, to produce a negligible change in the correlation (using the same rms values for normalizing the results). This test was undertaken and indeed there was negligible change in either the extent or amplitude of the long time correlations. (This is, by itself, perhaps an important result and does raise the question of what role the small scale disturbances play).

With reference to figure 6.1(b) it can be seen that when there is small scale activity on the high frequency wall shear then the slowly varying part of the wall shear is invariably high. It is this result which the work of this section attempts to quantify. Any effort to mark the large amplitude regions of the high frequency signal and, for example, obtain some sort of intermittency function is clearly problematical and definitions of amplitude discrimination levels and hold times are required. It seemed more appropriate to achieve the same end by rectifying the high frequency signal and then placing an envelope over, or more accurately, smoothing this rectified signal. Figure 6.1(c) shows the result (the non-dimensional filter cutoff was again $\omega_c \delta^*/U_o = 0.43$). Qualitatively this whole process can be seen to achieve the original aim, namely to separate the two scales of motion and generate a signal representative of

high frequency activity.

The resulting low frequency shear stress signal and its smoothed rectified high frequency component have been correlated and the results are shown in figure 6.2 for both the high Reynolds number and low Reynolds number cases. The sense of the time delay is the smoothed rectified high frequency at time t and the low frequency at time $t + \tau$. Also shown are the results obtained when the filter cutoff is halved and when it is doubled.

There are some significant features to be seen in these curves:

(i) The correlations are all very large, the peak value being near 70% and this value is only very weakly dependent on the value of the filter cutoff used. It appears that the small scale disturbances occur mostly when the low frequency part of the wall shear is high.

(ii) The major effect of changing the filter frequency is simply to produce an expected change in the width of the correlation curves.

(iii) The correlations peak at a non-zero time delay indicating a definite phase relationship between the low frequency signal and the generation of small scale high frequency wall shear stress fluctuations. The value of this positive time delay is small and depends slightly on the filter frequency.

Thus it appears from this and the results of section 4 that the boundary layer is dominated by a large scale structure and the passage of this structure gives rise to small scale activity at the wall. It seems likely that this high frequency activity in the

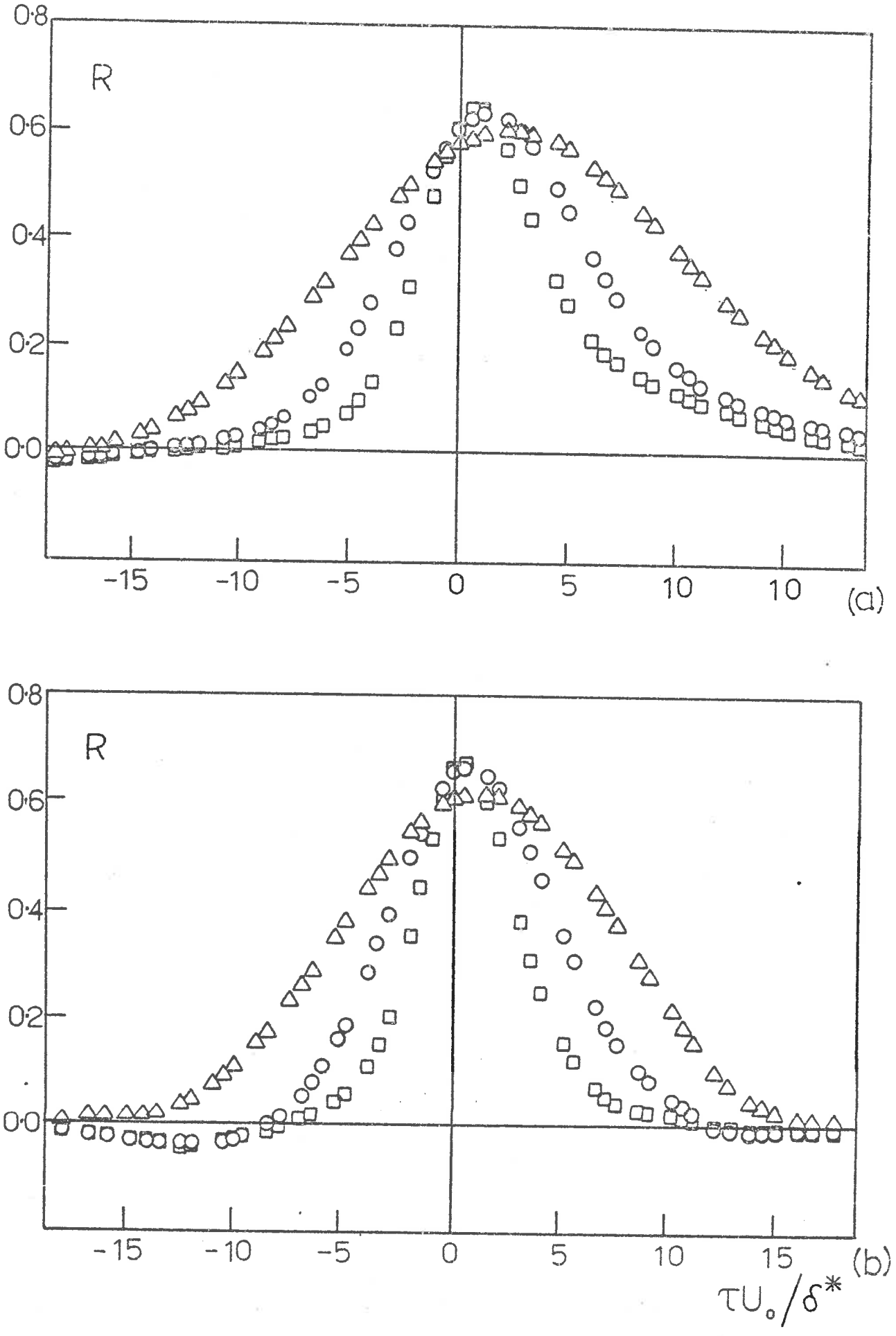

Figure 6.2 Correlation between the low frequency wall shear and the smoothed rectified component of high frequency wall shear for the high Reynolds number flow (a) and the low Reynolds number flow (b). The filter cutoffs used are; $\Delta, \omega_c \delta^*/U_e = 0.9$; o, 0.43; □, 0.21.

wall shear stress, i.e. the small scale disturbances near the wall are related to the burst-sweep cycle of events observed near the wall by Kim et al. (1971) and Corino and Brodkey (1969). Bursts are characterized by outward migrations of low momentum fluid and sweeps are characterized by inward rushes of high momentum fluid (Willmarth and Lu, 1971). Since the small scale shear stress fluctuations are usually positively going disturbances on a high shear level, it would appear that these fluctuations are related to the sweep motions in the burst-sweep cycle of events. That their occurrence is intimately related to the passage of a large structure is also consistent with the findings of Lu and Willmarth (1973) that the mean period between such sweeps scales on outer layer variables.

As the technique that has been used is novel and has no formal mathematical basis it is important to establish that the apparent correlation was not inherent in the technique. It was, therefore, applied to two artificial signals, namely white noise and white noise which had been filtered to have the same power spectra as the high Reynolds number wall shear. The correlations that result are shown in figure 6.3(a) and (b) and can be seen to be quite negligible.

These tests are, however, not entirely satisfactory in that these signals do not have the positive skewness of the wall shear. Skewness can give rise to an apparent correlation through the impulse response of the filter. A more stringent test was therefore sought.

An artificial signal was generated by taking the low frequency shear stress signal from one data run and adding to it the high frequency signal from an entirely different run. The resulting signal, however, did not have the correct

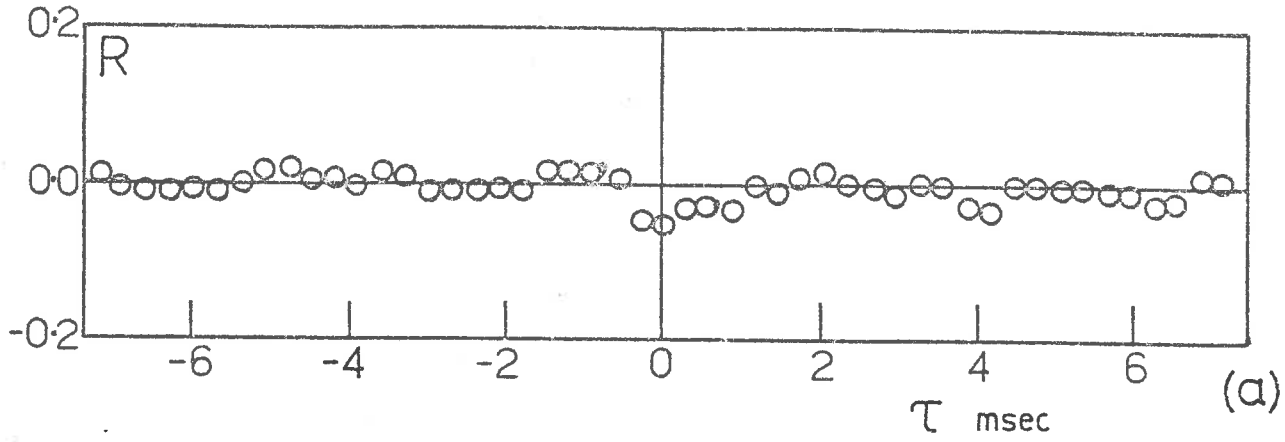

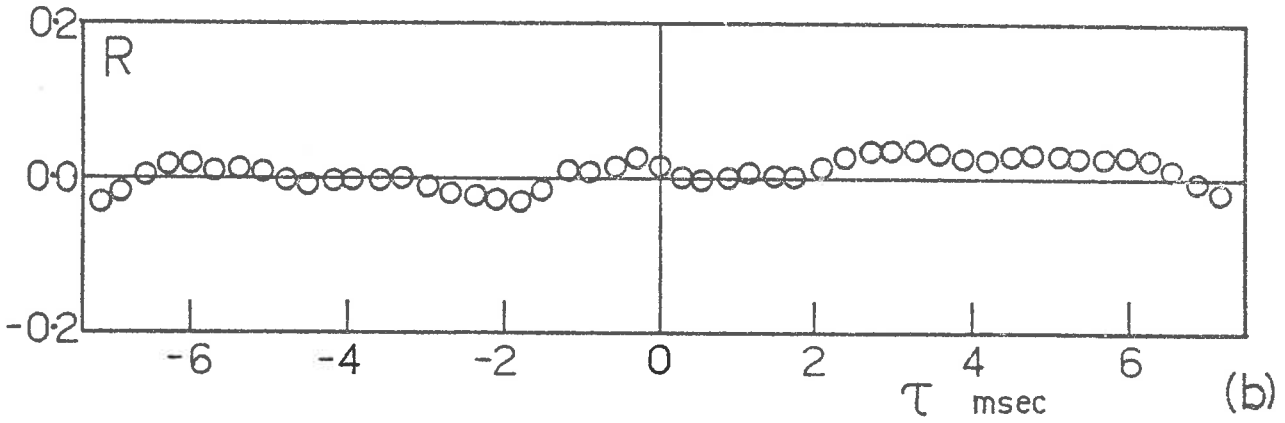

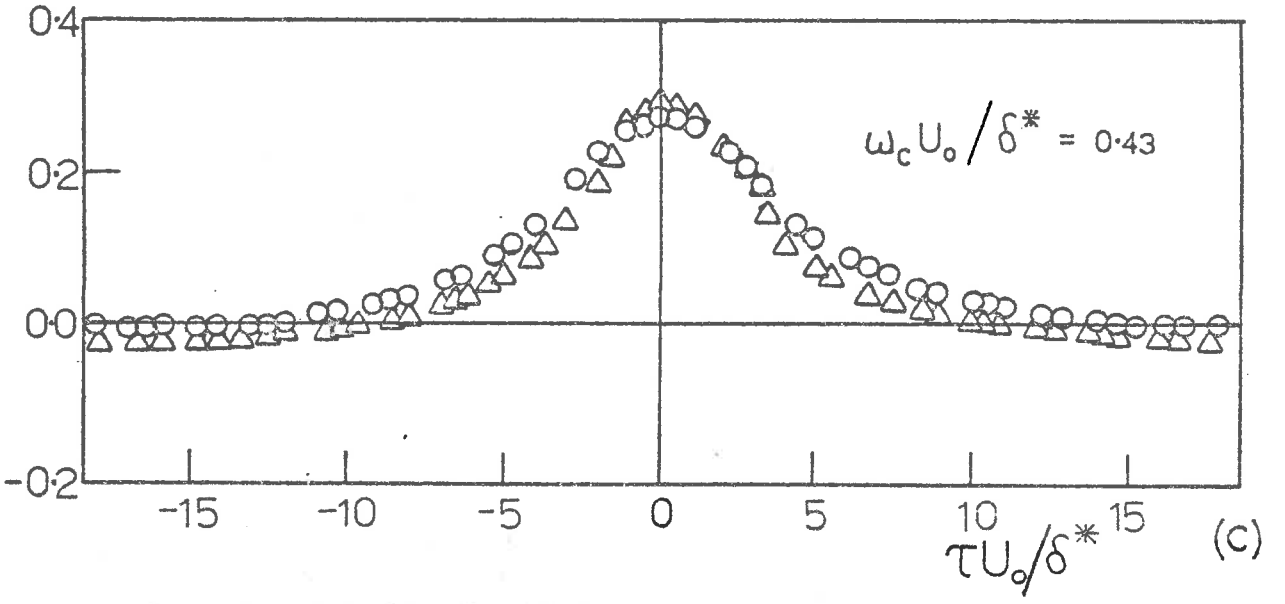

Figure 6.3 Result obtained when the technique of correlating between the high and low frequencies is applied to (a) white noise; (b) white noise filtered to have the same power spectrum as the high Reynolds number wall shear; (c) synthetic wall shear signal (see text); o, high Reynolds number flow, Δ, low Reynolds number flow.

skewness. Indeed it would have been disturbing if it had, as it would contradict the present conclusion that small scale large amplitude shear stress fluctuations occur mostly when the shear stress is high. To generate the correct skewness it was found by trial and error that all positive values had to be multiplied by a factor of 1.4. Clearly other means could be used to generate the correct skewness, and as far as the present discussion is concerned it may not be correct to characterize the effect of skewness by a single parameter such as the third central moment of the signal. However, the correct choice is unknown and some interesting results can be found by synthesizing signals in this way.

This procedure was used to generate artificial signals corresponding to the low and high Reynolds number flows considered, and the technique of correlating the high and low frequencies then applied to them. The results are shown, for one filter cutoff only, in figure 6.3(c); they show that skewness can indeed cause an apparent correlation to appear. It is however significant that the level is very much less than that obtained for the genuine signals (.3 instead of almost .7); and, importantly, the curves peak at precisely zero time delay whereas for the genuine signals a non-zero time delay was found. Finally it is to be noted that in order to generate a correlation level of nearly 70%, as found for the genuine signals, all positive values of the artificial signal had to be multiplied by a factor of 4.2; the resulting signal had skewness and flatness factors which were more than double the real values, and the correlation still peaked at zero time delay.

These tests confirmed that the technique does yield meaningful results and has established quantitatively that the correlation between the high frequency shear stress fluctuations

and the low frequency shear stress associated with the large structures, is both real and large.

This result implies an intimate connection between the two scales of motion and it is now of interest to apply the technique to the velocity signals that were recorded at y/δ = 0.05, 0.25, 0.50 and 0.75. An example of the generation of the smoothed rectified velocity signal was previously given in figure 6.1. The results obtained when the correlating technique is applied to such signals are shown in figure 6.4(a) and (b) for the high and low Reynolds numbers where a filter cutoff of $\omega_c \delta^*/U_o$ = 0.43 has been taken as being representative. The following features of these curves are also particularly worth noting:

(i) Even at small values of y/δ (i.e. 0.05) the curves are significantly different from those obtained for the wall shear stress. The region of positive correlation is reduced and a region of negative correlation has appeared at negative time delays. This suggests that the small scale disturbances that occur on the wall shear only have a limited normal extent.

(ii) As the distance from the wall is increased the region of negative correlation begins to dominate the curves. These changes are consistent with the change in the skewness factors of the velocity signals themselves but it is apparent that such effects cannot be produced by skewness alone.

These curves could possibly reflect the increasing appearance of a steep fronted positive step (in time) occurring in the velocity signals. It will be recalled that visual inspection of

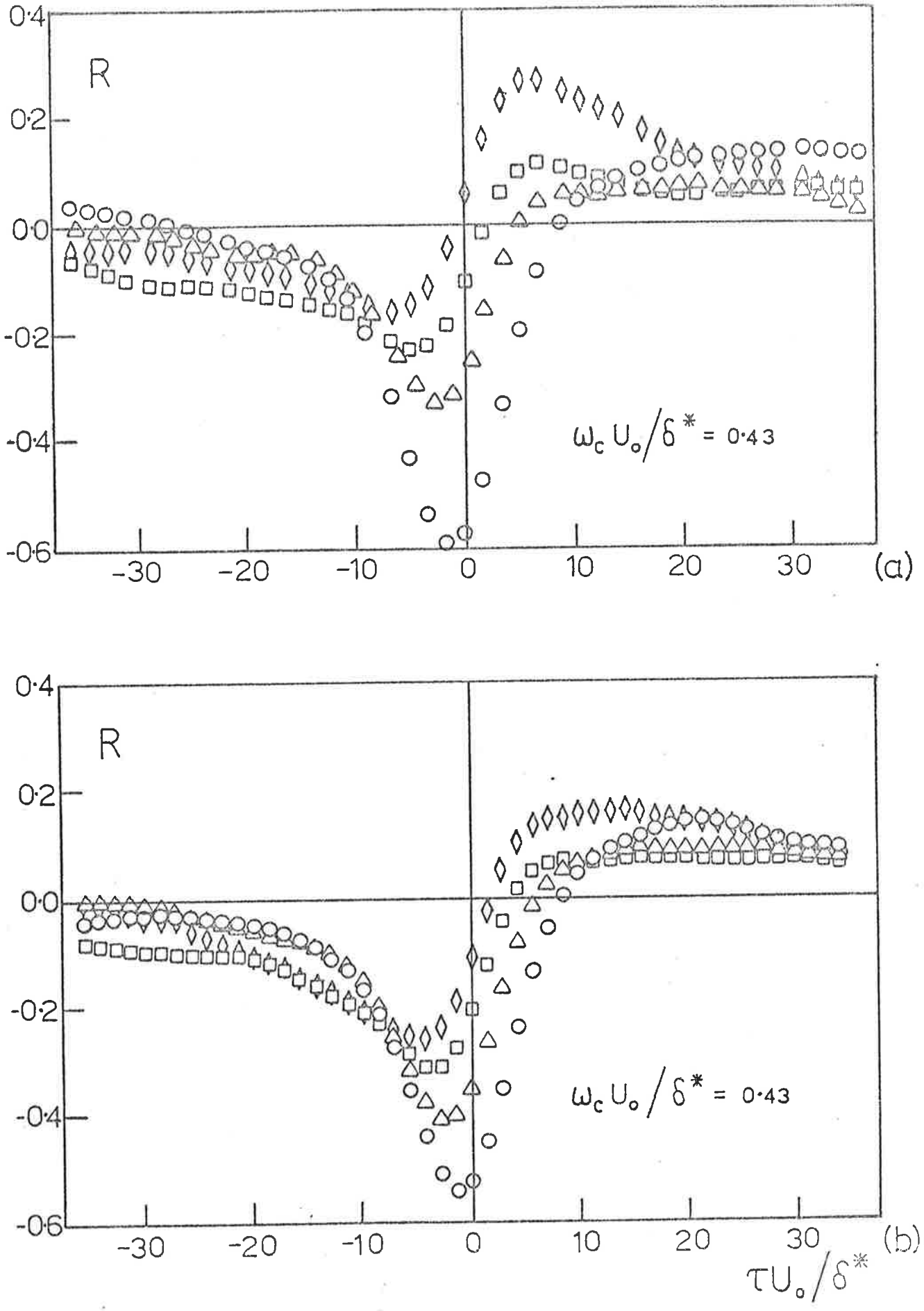

Figure 6.4 Results of correlating between the high and low frequencies when applied to the velocity at various points in the layer; (a), high Reynolds number case; (b), low Reynolds number case. ◊, $y/\delta = 0.05$, □, $y/\delta = 0.25$; Δ, $y/\delta = 0.50$; o, $y/\delta = 0.75$.

the signals in figure 5.6 showed such a feature to be a signature of the rear of the large structure. The same large structure gives rise to the high levels in the slowly varying part of the wall shear. Experimental results based on a conditional sampling technique will be presented in section 7 which will further demonstrate the way these correlations are formed. It will also be demonstrated that these steep fronts in the signals, which are a signature of the large structure, are associated with large contributions to the Reynolds stress.

The response of the wall region to this structure consists of small scale fluctuations and it was expected that these disturbances could perhaps be identified in the turbulent wall pressure. Figure 6.5 presents some simultaneously recorded signals of wall shear stress and wall pressure for the high Reynolds number flow. The pressure transducer was placed at a distance of $1.2\delta^*$ upstream of the hot film; however, the convective delay between the two devices is small in relation to the time scale of figure 6.5 and may be ignored. In order to make the smaller scale disturbances stand out, the low pass filtered signals have once again been subtracted out. The regions of intense small scale shear stress fluctuations can be visually identified and at the same time the wall pressure can be seen to show small scale, large amplitude fluctuations (these are flagged in figure 6.5). These small scale pressure fluctuations are probably the same as those that have been identified by Emmerling (1974) using an optical means and do not appear to have any repeatable form. They are a signature of the small scale response of the wall region and it is of interest to apply the correlating technique of this section to the wall pressure in order to see if there is simultaneously a large scale variation in the wall pressure associated

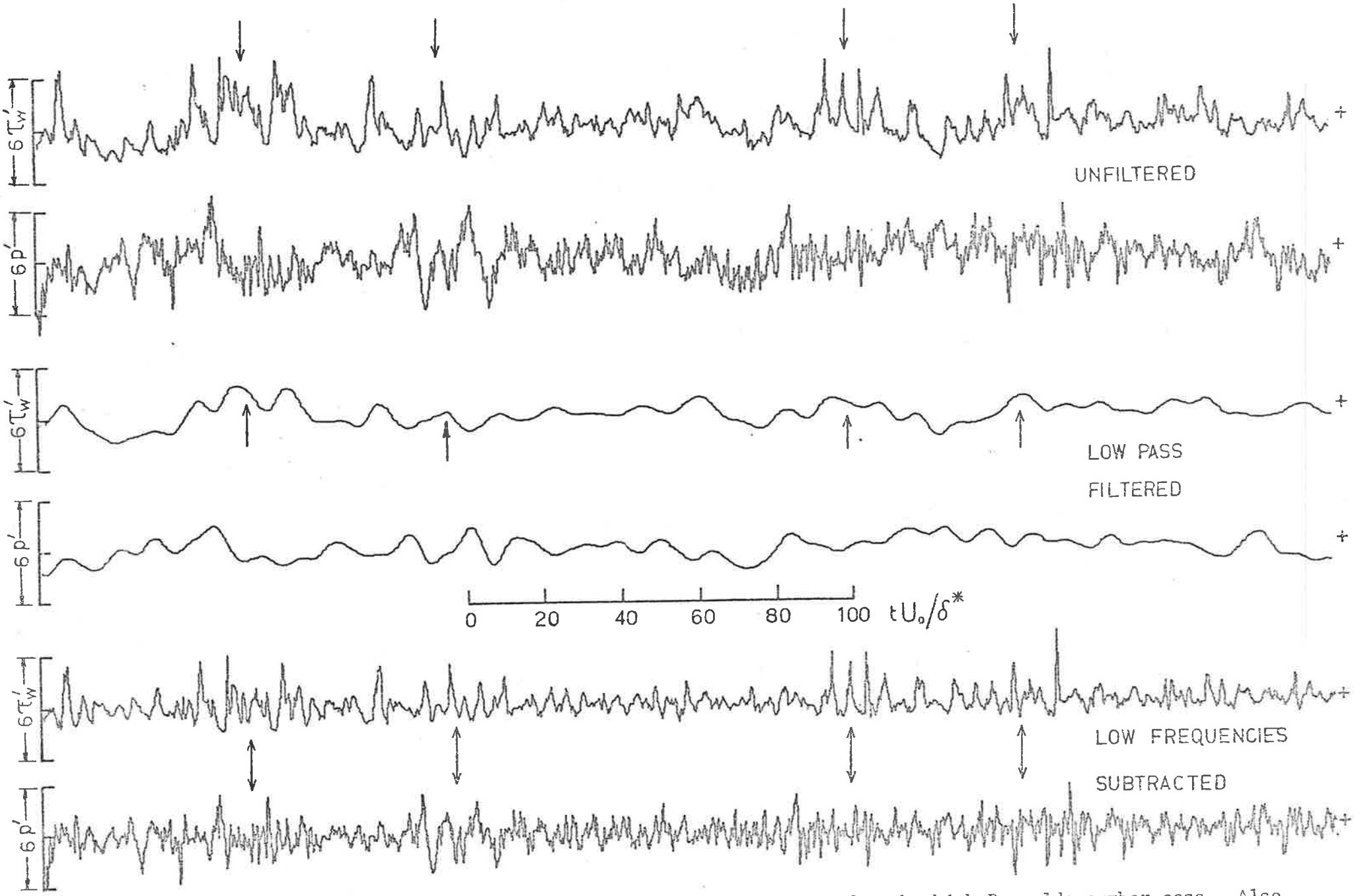

Figure 6.5 Simultaneous recordings of wall shear and wall pressure for the high Reynolds number case. Also shown are the low pass filtered signals and the high frequency signals obtained when the low frequencies are subtracted out.

with the passage of the large structure.

The results that are obtained for the high and low Reynolds number flows are shown in figures 6.6(a) and (b). The filter cutoff of $\omega_c \delta^*/U_o = 0.43$ has once again been used. For the high Reynolds number case in figure 6.6(a) there is a positive peak at negative time delays and a negative region at positive time delays. The curve for the low Reynolds number case (figure 6.6(b)) is similar although there is no negative region. The small amplitudes of the correlations are a reflection of both the poor signal to noise ratio that exists at low frequencies and the fact that a point measurement of the pressure contains the effects of sources across the entire layer.

The dissimilarity of the two curves in figures 6.6(a) and 6.6(b) is also apparently a result of the poorer signal to noise ratio occurring at the lower flow speed. The sources of this noise are acoustic, electronic and vibrational influences and occur predominantly at low frequencies of the order of 100 Hz. If the raw signals are low pass filtered with a cutoff at 100 Hz (which is a factor of 5 lower than the cutoff used in the correlating technique) the results shown in figure 6.6(c) and (d) are obtained. In this case the results for the high Reynolds number are almost unchanged, but the results for the low Reynolds number are now rather similar to the high Reynolds number case.

Clearly such correlations could, although it is not the only possibility, result from large scale pressure excursions characterized by a steep fall in pressure (in time) from a high value to a low and negative value. Conditional sampling experiments which will be presented in a later section will show that such

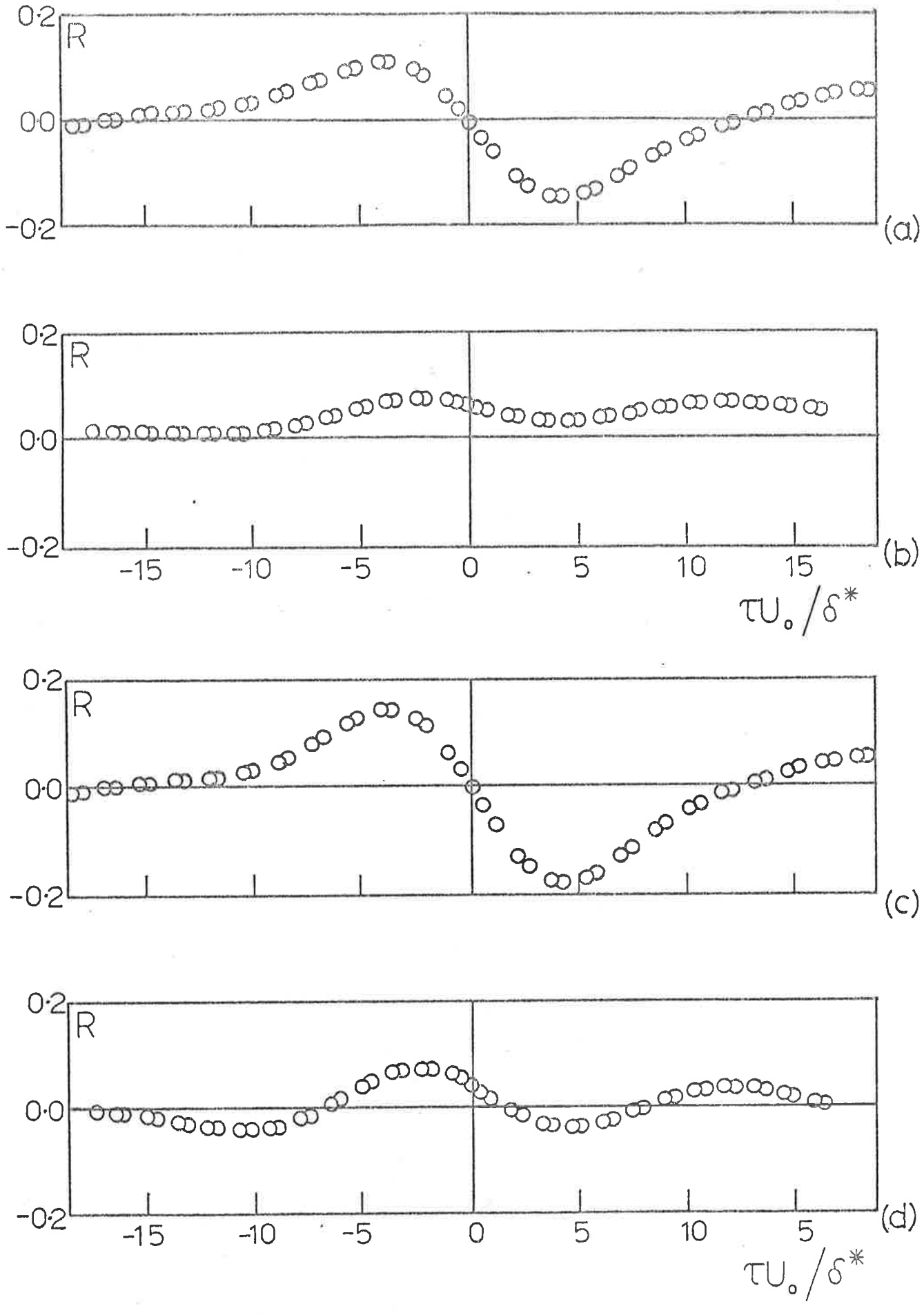

Figure 6.6 Correlation between the high and low frequency wall pressure for the high Reynolds number case (a), (c) and the low Reynolds number case (b), (d). The lower two curves (b) and (d) show the results obtained if the very low frequencies (<100 Hz) are first filtered out.

behaviour can be detected in the signals.

Because the correlations for the pressure are weaker than those obtained for the wall shear it would appear that the wall shear is a better indicator of the presence of the large structure than the wall pressure.

6.2 Correlations of High Frequency Activity Across the Layer

The results of the previous section have indicated that there is a relationship between the small scale velocity fluctuations and those fluctuations generated by larger scale motions. This behaviour could be found to occur across the entire layer, but the results do not necessarily imply that the occurrence is simultaneous. In order to see if the occurrence was indeed simultaneous the smoothed rectified high frequency components of the wall shear stress and the velocity at various points in the layer have been correlated with the same component of the velocity signal at $y/\delta = 0.25$. The array of wires was positioned vertically above the hot film and the results for the high and low Reynolds number cases are shown in figure 6.7(a) and (b).

The correlations are all rather weak, but it is apparent that when the signal at $y = 0.25\delta$ is taken as reference, then a region of positive correlation extends from $y/\delta = 0.05$ to 0.75. The time delays at which the correlations peak are non-zero and reflect the way the structures are inclined to the wall. These findings are important; use will be made of them at a later stage when creating a streamline pattern from conditionally sampled data.

Another feature of figure 6.7 is that there is a negative correlation between the smoothed rectified high frequency component of velocity at $y = 0.25\delta$ and the corresponding component of the wall shear

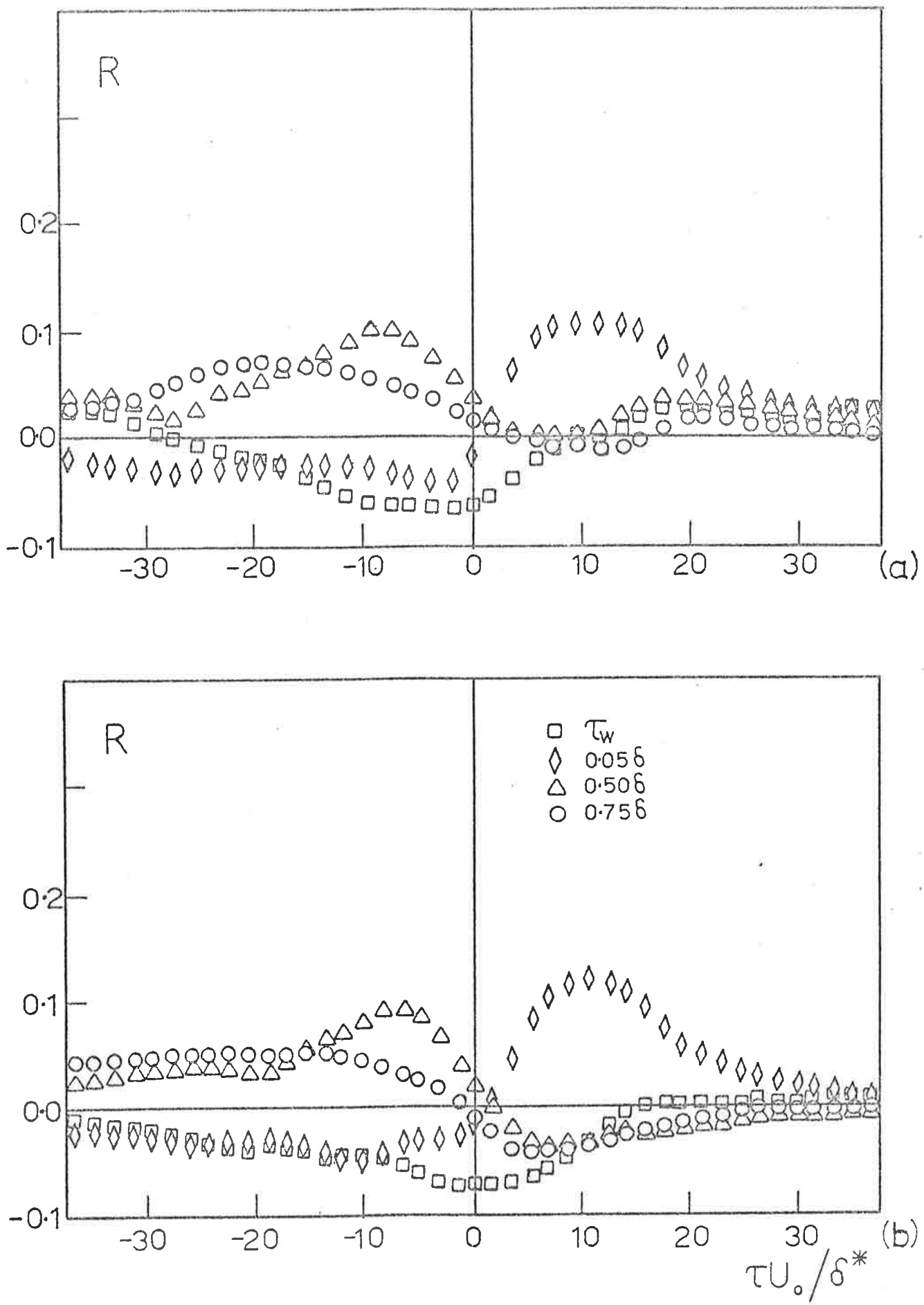

Figure 6.7 Correlation between the smoothed rectified component of velocity at $y/\delta = 0.25$ with the corresponding components of wall shear and velocity at other points in the layer; (a) high Reynolds number case, (b) low Reynolds number case. The velocities were measured at points which were directly above the hot film.

and this occurs quite near the zero time delay point.

The predominance of a region of negative correlation as opposed to a positive correlation, is due to the change in character of the flow as the wall is approached. In physical terms it suggests that small scale activity near the wall is associated with quiescence directly above and further from the wall. This implies, nor surprisingly, that the small scale fluctuations at the wall have a limited normal extent. Conversely, the same correlation can arise from small scale activity at $y/\delta = 0.25$ being associated with quiescense directly below at the wall. Both this and the previous case can be attributed to an inclined large structure causing small scale disturbances near the wall, and with the structure being characterized by steep velocity gradients over most of the layer. The flow is, by comparison, rather more quiescent within the structure itself.

A more detailed discussion of this is presented in section 8.

7. DETAILED CONDITIONAL AVERAGING EXPERIMENTS

The work presented in the previous sections has indicated the existence of a large deterministic structure within the boundary layer which appears to play a significant role in the dynamics of the turbulence process and has quite detectable influences at the wall. From visual observation of the signals some of the details of the structure are also known. It is a highly three dimensional structure with regions apparently lying skewed across the flow. The dominant visual feature of the structure is a steep interface on the rear or upstream side of the structure where steep velocity gradients occur. Further details of the structure are, however, not yet clear. For example, the streamline pattern of flow within the structure is not known. Also it would certainly be of interest to know the pressure field that is associated with the passage of the large structure so that the role of the pressure might be determined. Additionally, it would be useful to know the contribution made to the Reynolds stress by the organized motions.

In order to extract this kind of information from the digital records a conditional signal analysis is required in which ensemble averaged statistics of various quantities are determined only at those times when the organized large structure is known to be present. This in turn would require the generation of some kind of detection procedure which would discriminate reasonably well upon the presence of a large structure. The work of the following sections represents an attempt at such an analysis.

This kind of signal analysis is not new and Townsend's (1949) early definition of an intermittency function associated with

intermittent turbulent flow respresents a special case of conditional signal analysis. Extensive use has been made of conditional techniques by Kovasznay et al (1970) to determine the statistics of the large turbulent bulges existing at the outer edge of the boundary layer. Similarly Lu and Willmarth (1973) have used a conditional signal analysis to determine the relative contributions made to the Reynolds stress by the turbulent burst and sweep motions.

Conditional signal analysis is, however, a difficult and subtle process. There are problems associated with the generation of a detection criterion and these will be mentioned in the next section.

Aside from this there is often some question as to whether the ensemble average signal obtained represents genuine features in the original flow or is a consequence of random variations in phase and signal amplitude in each supposed realization of the feature being considered. The extent to which this is the case can sometimes be judged by comparison with results obtained by applying the technique to synthetic signals and may be assisted by a direct visual comparison between the original signal and the ensemble average signal obtained. This problem will be discussed in relation to the present work in the following section.

7.1. Detection of the Presence of the Large Structure

In the present context one wishes to discriminate upon the presence of a large organized structure. It is possible that its presence could be detected by some characteristic excursion in the velocity, Reynolds stress or vorticity. The problem, of course, is in the definition of a characteristic excursion. Aside from the obvious fact that the character of the excursion is not yet known another

difficulty arises from the fact that the supposed organized motion is in fact also partly random due to the variations in amplitude and scale of this motion. Nevertheless it is described as organized in the sense that apart from this randomness, there is some recognizable similarity between one structure and the next. The problem is then somehow to define this recognizable similarity (for example by correlation techniques). In this way various sections of the time history of the signals can be found which do satisfy some criterion which measures this similarity. Evidently, however, because of the difficulties in accurately defining either the recognizable pattern or allowing for variation in scale or amplitude of a particular realization of this pattern, there will be occasions when a section of signal which should have been included is omitted, and similarly included when it should have been omitted. The latter is termed a false detection and results basically because of a detection criterion which is not ideal, i.e. in practice does not discriminate against those events which would be omitted by the "ideal" detector. This whole question can be better understood by a consideration of the examples which follow.

Various detection schemes have been suggested in the literature, and although each attempted to detect different phenomena, they are worth considering in the present context as they may be useful in determining the presence of the large structure. A brief review of these schemes is perhaps appropriate.

(i) Kovasznay, Kibens and Blackwelder (1970).

This detection scheme was based upon one component of the vorticity (or more precisely of $\partial u/\partial y$) exceeding a given threshold level for a certain hold time. By this means the presence or otherwise of

turbulent flow at the outer edge of the boundary layer could be determined.

(ii) Antonia (1972).

This scheme was also aimed at the making of turbulent/non-turbulent decisions and was based on the square of the time derivative of the instantaneous uv product exceeding a given level over a suitably chosen hold time.

(iii) Willmarth and Lu (1971).

This detection scheme was aimed at detecting the turbulent bursts and sweeps near the wall and was based upon the low pass filtered streamwise velocity component at $y^+ = 15$ passing through a given level with a given sign of slope.

(iv) Lu and Willmarth (1973).

This series of measurement was based on the instantaneous uv product exceeding a certain level with u and v having predetermined signs. The quadrant breakdown is clearly necessary because two quite different structural forms can generate values of uv with the same sign and amplitude.

(v) Blackwelder and Kaplan (1976).

This detection scheme was used to detect the presence of the turbulent bursting phenomenon. It was based upon the short time variance of a velocity signal exceeding a given level, where the variance was calculated using a short time estimation of the local mean signal level. It will become apparent that this scheme is very similar to the one that was finally adopted here.

This brief review demonstrates a point which is perhaps axiomatic in this kind of work. Having decided upon the nature of the detection signal, two remaining variables exist. These are the setting of a discrimination level and the application of a hold time or alternatively the use of a filter (both are similar statements about time scales). The settings of these two variables represent decisions about the scale and amplitude of the structures of interest. Ideally one would like to demonstrate that the averages that are generated are independent of these variables. Similarly the mean time interval between detections should, if possible, be independent of the settings of these variables. In this way the settings of these parameters could be objectively decided upon. In the works outlined above, however, it appears that the latter independence could not be demonstrated. Under these circumstances the best that can be done is to demonstrate that the ensemble averages generated do not change significantly with these variables.

A further shortcoming of the detection schemes that have been outlined is that they assume prior knowledge of the character of the structures of interest, i.e. they assume that the structures whose presence were being detected do have large excursions in vorticity or Reynolds stress etc. In the present context, however, the amplitude and character of these excursions is unknown and it seems, therefore, inappropriate to consider only large excursions in Reynolds stress or velocity as the characteristic feature of the large structure.

In considering alternatives it was noted in section 5 after visual inspection of velocity records that the large structure was apparently characterized by a steep change in velocity on the back or trailing surface of the structure. Furthermore in section 6 it was demonstrated that an intimate relation exists between the large scale

or low frequency features of a signal and the small scale or high frequency component of the signal. Evidently a significant contribution to the high frequency content of a signal arises from the steep velocity gradients that are characteristic of the rear of the large structure. This suggested that the smoothed rectified high frequency content of a signal should be used as a basis for the detection of the presence of the large structure.

This of course is similar to the Blackwelder and Kaplan (1976) scheme. By using the rectified high frequency signal there is evidently no bias toward either positive or negative going disturbances so that any ensemble averages obtained should reflect genuine features of a signal rather than a distortion due to the detection scheme.

In what follows therefore detection was based upon the generation of a smoothed and rectified high frequency signal. Those points were flagged that were at a local maximum in this signal and at the same time exceeded a certain level. An example of the detection signal generated from the wall shear stress was shown previously in figure 6.2. Various signals can be sampled at those times where this criterion is satisfied. Ensemble averages of segments of signals centred at the flagged points can then be generated in the form,

$$\langle q(t) \rangle = \frac{1}{N} \sum_{j=1}^{N} q(t_j + t),$$

where t_j represents the times at which each detection occurs and $q(t)$ is the signal of interest ($q(t)$ need not necessarily be the signal used to generate the detection signal).

Decisions need to be made as to which filter cutoff and which discrimination level should be used; these problems are best discussed with regard to a particular turbulent signal. Shown in figure 7.1 are various averages of the velocity signal at $y/\delta = 0.05$ for the high

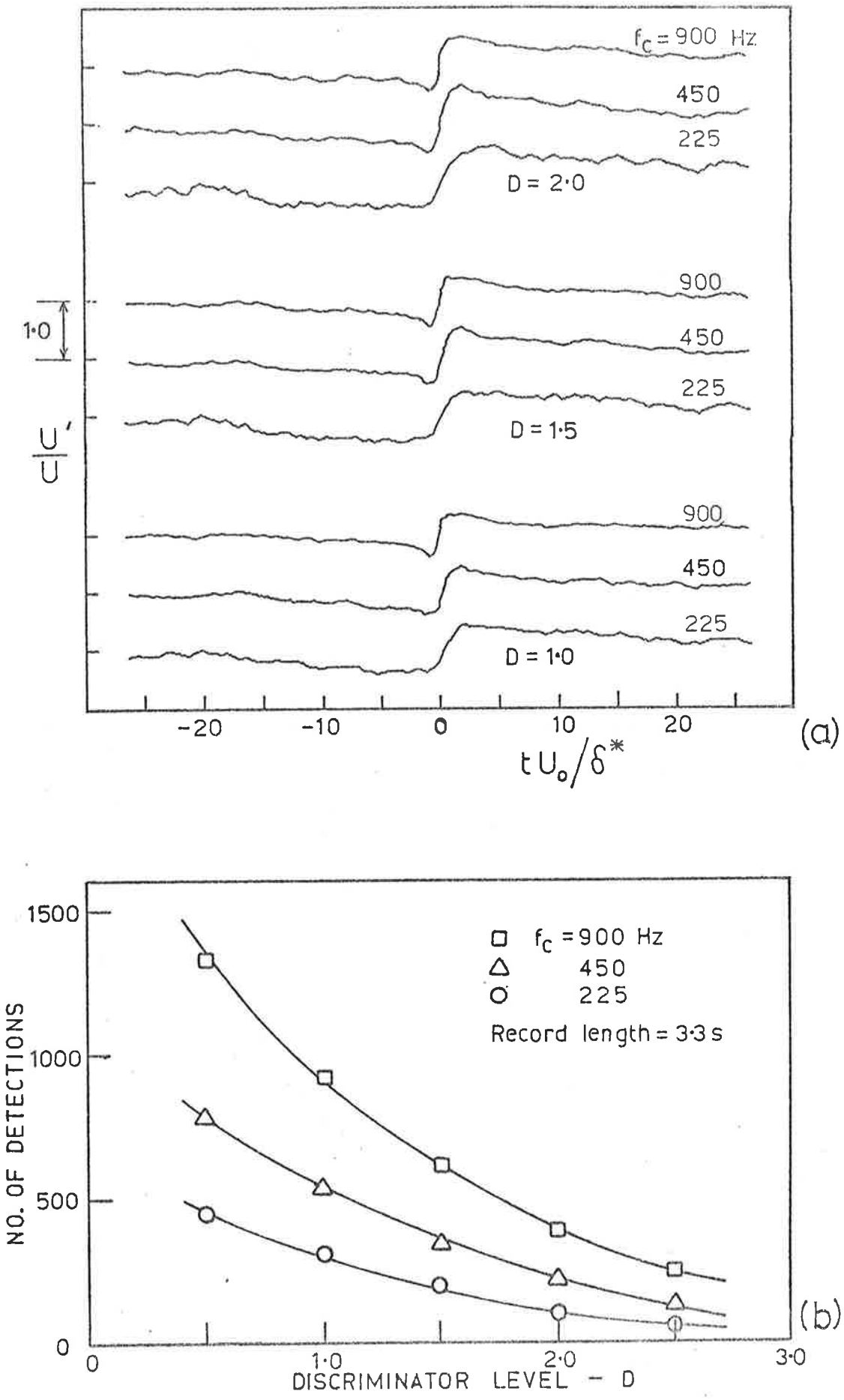

Figure 7.1 (a) The effect of various filter cutoffs and discriminator settings upon the ensemble averaged time history of velocity at $y/\delta = 0.05$.

(b) The corresponding number of detections for each choice of filter cutoff and discriminator setting.

Reynolds number case formed by the above means with various filter cutoffs and various discriminator levels D (D is expressed as a fraction of the rms level of the smoothed rectified high frequency signal). The filter cutoffs are the same as those used previously in the discussion of the correlation between the high and low frequency components of the signals.

Ignoring for the moment the nature of the average itself, it is significant that both the amplitude of the average and its general shape are independent of the settings of the filter cutoff and discriminator level. Given a fixed discrimination level, it can be seen that the only effect of a higher filter cutoff is to produce averages with a rather steeper zero crossing and not surprisingly an increase in the number of detections that occur (figure 7.1(b)). Using a rather similar detection process Blackwelder and Kaplan (1976) found that the amplitude of their averaged time histories near the wall depended linearly on their discriminator setting. This finding cannot be directly compared with the present results as their discriminator signal had a non-zero mean. The mean signal level generated during the rectification process has, in the present case, been subtracted out.

Also shown in figure 7.1(b) are the actual number of detections that were found to occur at various discriminator settings and filter cutoffs. Clearly each curve shows a monotonic decrease as the discrimination level is increased with no indication of a plateau or region where the detection rate becomes independent of the discrimination level. From these results which were also checked for various other signals, any filter-discriminator combination cannot be objectively favoured over any other combination. This seems to be a basic problem in most conditional sampling of this kind. The important point, however, is that the results themselves depend only weakly on

the filter cutoff and discrimination levels. Therefore, in some sense the conditional average does reflect a characteristic feature of the flow and the precise settings of these variables become less important. The values of the parameters that were finally settled upon were a filter cutoff of $\omega\delta^*/U_o = 0.43$ being used to generate the smoothed rectified high frequency detection signal and with a discrimination level of 1.5 times the rms level of the smoothed rectified high frequency signal. (By visually comparing detection points obtained using this choice with the original signals it did appear qualitatively to be more successful than other combinations).

This discrimination level is comparable to the value used by Blackwelder and Kaplan (1976) if allowance is made for the fact that their detection signal had a non-zero mean. Their averaging time, (comparable to the reciprocal of the filter cutoff in the present case) however, was quite small being set at $TU_\tau^2/\nu = 10$ or $TU_o/\delta^* = 2.2$. Such a small value was found in the present case to give rise to a significantly large number of very small scale disturbances being detected and was therefore not used.

Finally, in order to demonstrate the behaviour of this detection technique, it was applied to a synthetic signal created by filtering white noise, to yield a signal with the same power spectrum as the wall shear stress signal of the higher Reynolds number case. The corresponding conditional average was then generated and is shown in figure 7.2(a). Clearly except for some statistical scatter, an essentially zero average is the result and demonstrates that for a signal of zero skewness the detection and averaging technique does not lead to the identification of a signal pattern if none exists within that signal.

It is apparent, however, that skewness could give rise to

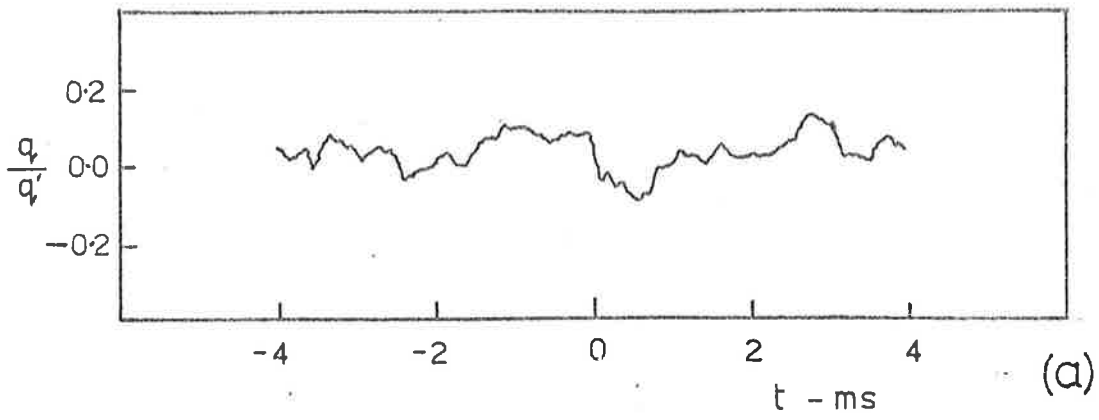

Figure 7.2 (a) Ensemble averaged time history obtained when the detection criterion is applied to white noise which has been filtered to have the same power spectrum as the wall shear.

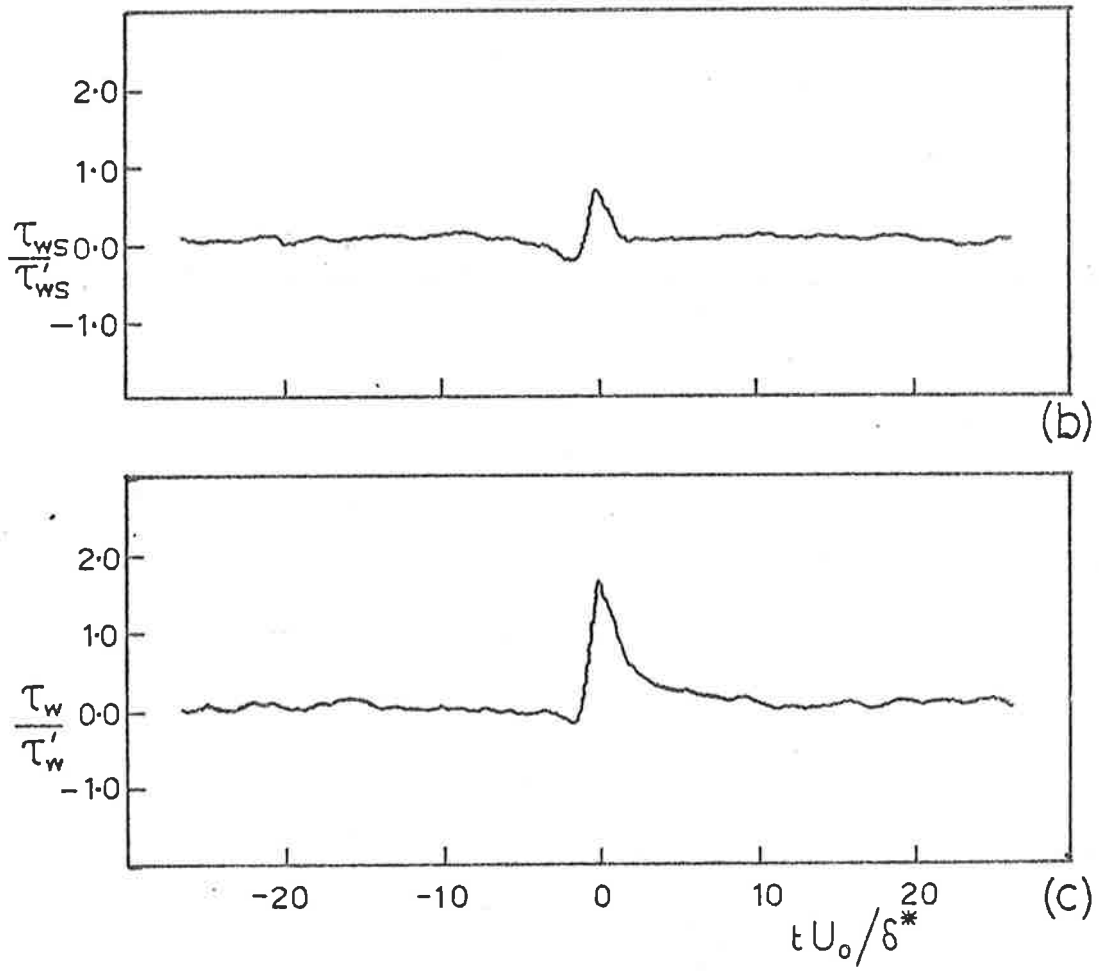

Figure 7.2 (b) Ensemble averaged time history obtained when the detection criterion is applied to a synthetic wall shear signal (see text.)

(c) Corresponding result for the real wall shear.

detections if the high frequency content of a signal tended to lie predominantly either in a positive or negative sense. The most severe skewness was found to occur in the wall shear stress signals, and, as a test, the synthetic shear stress signal used in a previous section was examined. This signal, it will be remembered, was created by the combination of high frequency and low frequency signals from different data runs, the correct skewness being generated by approximately scaling the positive values. When the detection and averaging technique is applied to this signal the results shown in figure 7.2(b) are obtained for the high Reynolds number case, which may be directly compared with the corresponding results of the real shear stress signal shown in figure 7.2(c). It is clear that skewness can indeed give rise to non-trivial averages although the average so formed is weaker than for the real signal. This test is really rather too severe however, because the synthetic signal has a character very like that of the genuine signal. It does nonetheless demonstrate that the average time histories that will be presented result not from skewness, but from genuine patterns within the signals.

The detection criterion has not been chosen in any attempt to detect specific events which may be called either bursts or sweeps, nor as a basis in making turbulent - non-turbulent decisions. The aim is to detect in an unbiased manner some specific structural feature associated with each signal which, if non-zero averages are formed, must have favoured occurrence within that signal. The correlations between high and low frequency presented in section 6 have suggested that this feature is associated with the presence of a large structure in the boundary layer.

7.2 Enhancement of Conditional Averages

Previously in figure 7.1, conditional averages of the velocity at $y/\delta = 0.05$ were presented all of which had amplitude levels rather lower than the typical levels encountered within the signal itself. It is likely that this reduced amplitude results from some randomness in the phase of the detection point relative to the structure and additionally from the inclusion of possible false detections (in the sense defined previously). The following technique was developed to minimize these problems.

Initially the ensemble averaged time history is formed from those points where the detection criterion is satisfied (as in figure 7.1). A time correlation is then computed between this average time history and each individual realization which contributes to this average. This time correlation is computed at various time delays and with a short averaging time T_{AV}. Each short time length of signal, including the initial ensembled average, has its local mean over this time removed. In addition, each correlation curve is normalized by the relevant local rms value. As will be seen shortly it is important to proceed in this way, otherwise large correlations may result which are a reflection of large signal amplitudes as opposed to a genuine correlation in the statistical sense. Next each correlation is scanned through the time delay range to find the local maximum level which is nearest the zero time delay point. The largest value occurring anywhere in the time delay range is clearly not used because that may be associated with an adjacent structure rather than the particular realization of interest.

Evidently if the maximum in the correlation is negative then that particular detection point may be regarded as being false

and therefore rejected. Usually about 30% of the initially detected points were rejected on this basis. If the maximum occurs at a non-zero time delay then the detection point is moved by an amount corresponding to this time so that the correlation peaks at zero time delay. This will minimize the problem of phase uncertainty. With the detection points redefined in this way a new ensemble average may now be generated and furthermore the entire process may be repeated until such time as no significant changes occur in either the average itself or the points at which the average is formed. In practice this was usually found to occur after the first two or three iterations although five were generally used. This technique can be seen to be a bootstrap operation in the sense that every iteration sharpens the definition of the detection criterion and reduces the set of events which now satisfy this more stringent condition.

In order to demonstrate that this technique is successful, typical results are shown in figure 7.3 using, as before, the streamwise fluctuating velocity at $y/\delta = 0.05$ and the wall shear stress for the high Reynolds number case. Also shown are histograms of the time increments between the initial and final iterations used to redefine the detection points after five iterations. The averaging time used was $T_{AV}\ U_o/\delta^* = 25$ in each case and this point is discussed further below. As can be seen there is a dramatic effect associated with this enhancing technique, the amplitude of the averages being nearly doubled. It can also be seen that the form of the averages is still the same but that the increased amplitude is now typical of actual signal levels. Furthermore the histograms demonstrate that only very small time adjustments are required to minimize the problem of phase uncertainty. The results will therefore be independent of the range of time delays used when generating the short averaging

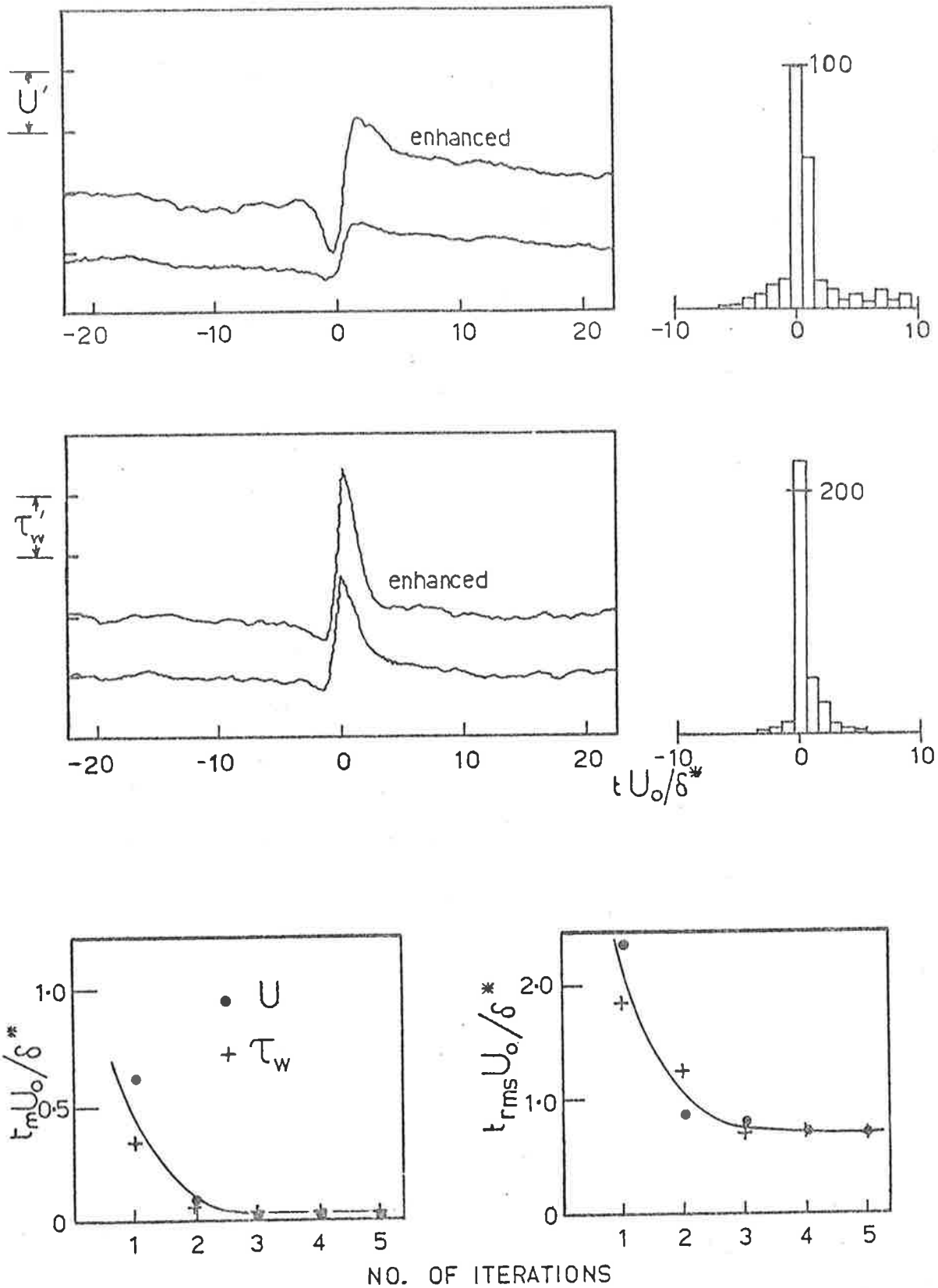

Figure 7.3 The effect of using the enhancing technique on the velocity at $y/\delta = 0.05$ and the wall shear. The histograms represent the time shifts used to redefine the detection points. Also shown are the mean and rms values of the time shifts between each iteration.

time correlations, provided of course the range is sufficiently large.

After each iteration the point of detection will be different from the previous iteration but, because of the inherent convergence of the technique, these differences may be expected to become small. Typical results for both the mean of these differences t_m, and the root mean square of the differences t_{rms}, are shown for each iteration in the lower portion of figure 7.3. These have been computed as differences between two successive iterations and both quantities are clearly always small in relation to the time scales of the flow and do not change after the first few iterations. Certainly after about 5 iterations further application of the technique can be seen to be redundant and redundancy frequently occurred after only two or three iterations.

A value for the averaging time T_{AV} must be chosen and it may be expected that its effect will be small once it has been made larger than the width of the non-zero portion of the average. Shown in figure 7.4(a) are the results obtained using four different averaging times on the sampling of the velocity at $y/\delta = 0.05$ used previously. These results clearly demonstrate that the effect, if any, of varying the averaging time is indeed small; the precise value is, therefore, somewhat arbitrary. In what follows a value of $T_{AV}\ U_o/\delta^* = 25$ was used. Higher values were not used because of the necessary increase in computing time associated with the process.

Finally in figure 7.4(b) are shown a few of the typical correlation curves that are usually produced during the first application of the process; these are presented to demonstrate that a maximum in the correlation can usually be unambiguously identified.

This process has been applied to most of the velocity averages that are presented in the following sections. Such averages will be

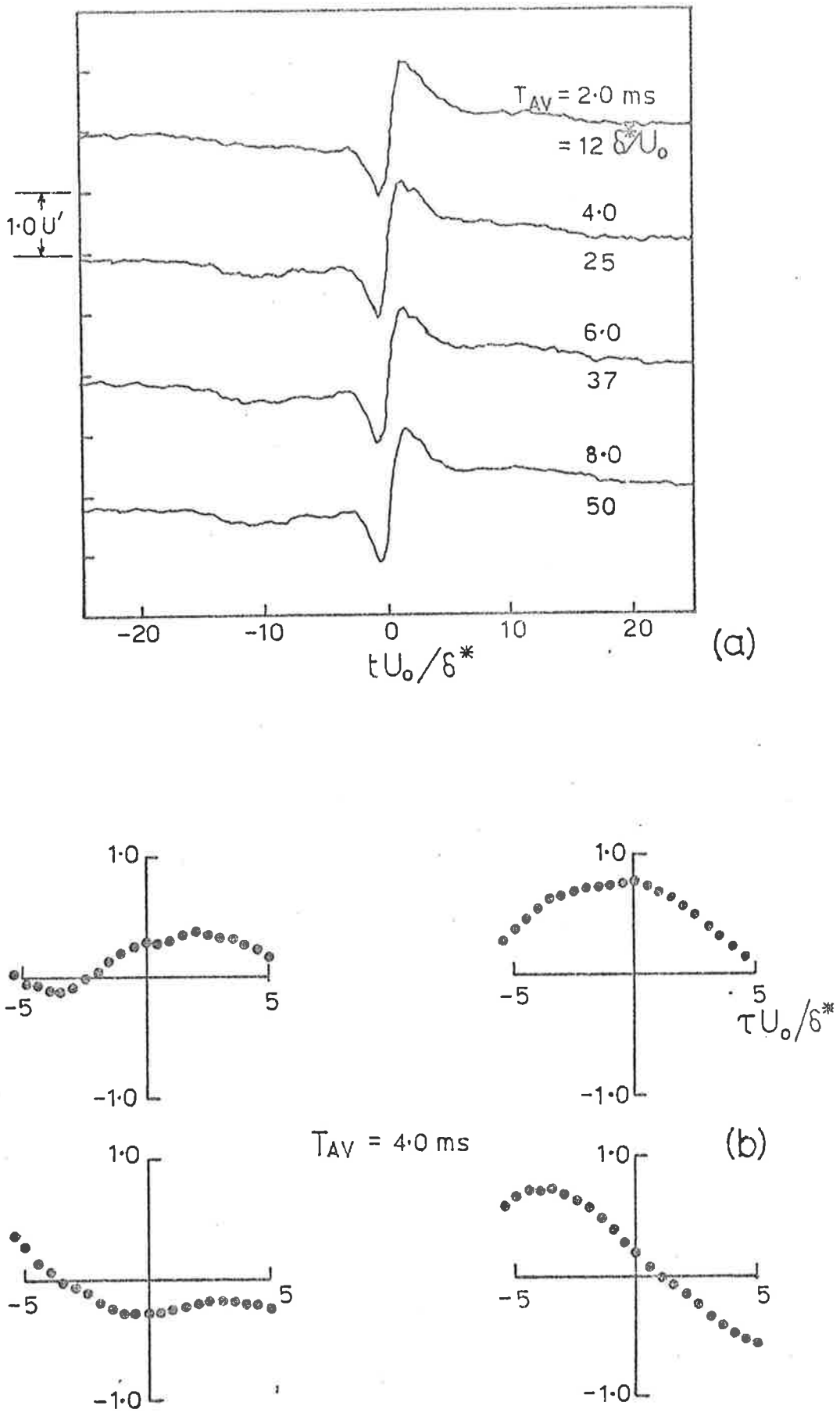

Figure 7.4 (a) The effect of various averaging times when used with the enhancing technique on the velocity at $y/\delta = 0.05$.

(b) Typical short time correlation curves generated during the application of the enhancing technique to the velocity at $y/\delta = 0.05$.

seen to represent patterns of large time scales and significant coherence. Under these circumstances the technique was found to be particularly useful to redefine the detection points. As will be demonstrated in a later section however, the ensemble averages of the wall pressure feature a steep negative fall in pressure, but because the pressure signal has a large high frequency content a positive correlation between the ensemble averaged time-history and the signal itself was found to occur even at times quite unrelated to the times when the detection criterion was satisfied. In this particular case there was considerable doubt as to the validity of the results obtained from the technique, and it was therefore not used for this case.

In all other cases the technique was successfully used and it is reiterated here that the technique consistently enhanced the amplitude of the averages and never introduced any obviously spurious behaviour in the averages themselves.

7.3 Sampling of the Streamwise Velocity in the Normal Direction

Ensemble averaged time histories of the streamwise component of velocity at various points in the layer, have been generated using the high frequency detection criterion and the enhancing technique (section 7.2), with the detection signal generated from the velocity signal being studied. The results of this test for two Reynolds numbers are shown in figure 7.5. Also shown are the results obtained for the wall shear stress.

In all cases the averages of the velocity do reflect the trends that can be observed visually in the signals shown in figure 5.5. They indicate that a dominant structural feature is one of a steep positive going step in velocity giving rise to the possibility of time records that have a sawtooth character. At times far from

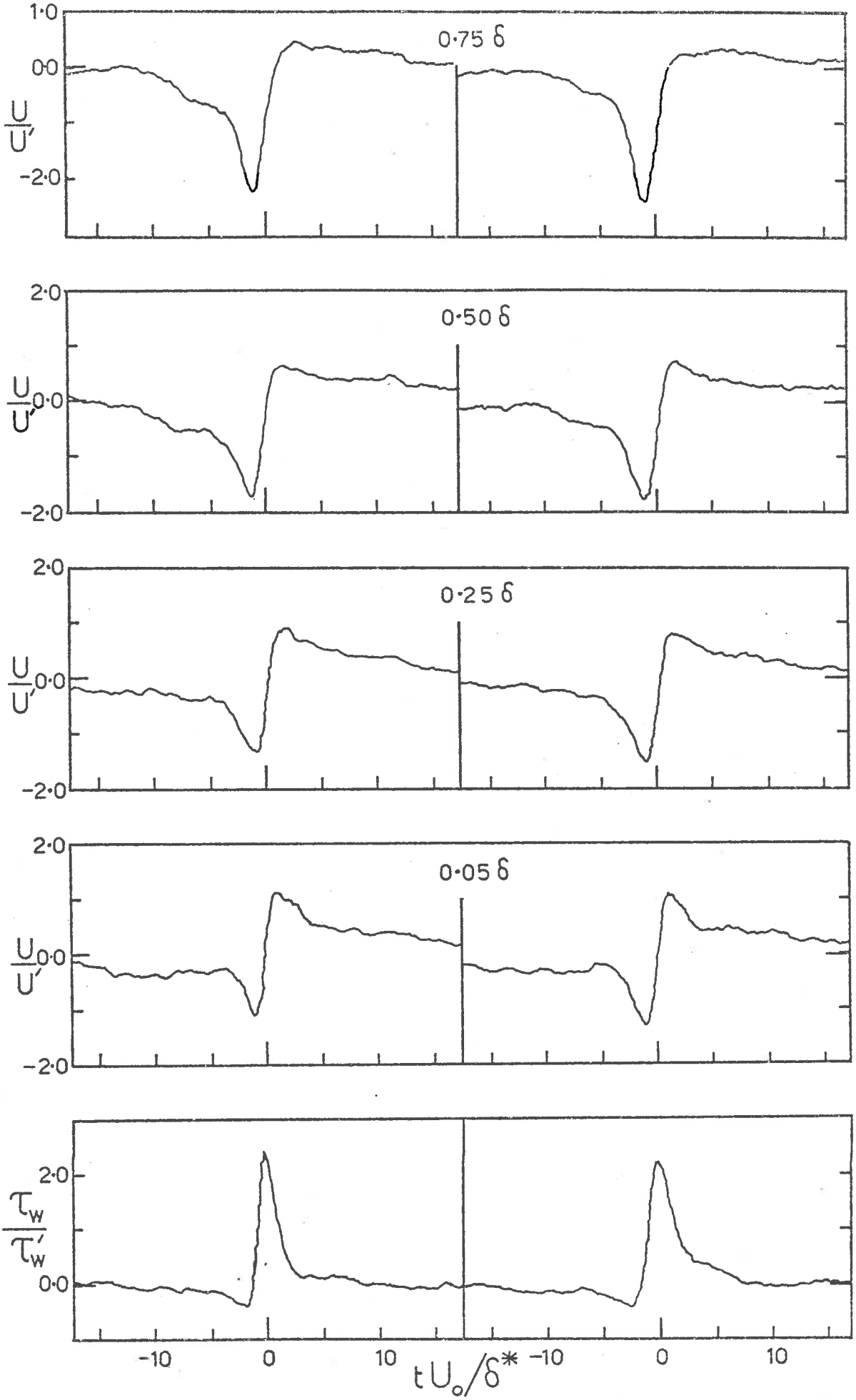

Figure 7.5 Ensemble averaged time histories of the streamwise velocity at various points in the layer, for the high Reynolds number flow (left) and the low Reynolds number flow (right). Detection is based upon the signal being sampled and averaged.

the point of detection, the ensemble averages become less and less representative of the signal itself due simply to the cumulative effect of the random variations in the time scales of each realization of the structure. In principle an enhancing technique could be developed to overcome this problem by time scaling each realization to maximize a correlation between each realization and the ensemble average. Although such a technique was tried, it did not prove to give reliable results and was not pursued.

In the region of the layer where the velocity signals have low skewness, the fact that the ensemble averaged time histories show a sharp positive slope (in time) is evidence that regions of sudden acceleration occur more frequently than regions of steep deceleration. The detection criterion is unbiased toward either case and the same behaviour can be observed across the entire layer. If these accelerations are the feature that in broad terms constitute a proportion of the high frequency activity, then the present results can be seen to be quite consistent with the correlations between high and low frequency presented previously. It is to be noted however, that while the same is partially true of the wall shear stress, the noticeable increase in high frequency activity near the wall which generally follows the regions of acceleration (figure 5.5) is lost within the averaging process used to generate the present results.

The scale of the events depicted in figure 7.5 is quite large. For example the averages of the wall shear stress have a temporal extent of $tU_o/\delta^* \approx 10$ which suggests a considerable streamwise extent in excess of typical wall scales. Further from the wall the averaged time histories have even a larger scale and is further evidence of a large structure with a streamwise extent of the order of 2δ.

Blackwelder and Kaplan (1976) have reported similar averages near the wall in a boundary layer using an analogous unbiased sampling technique. They argue that because the region of low velocity followed by a sudden acceleration is similar to the cycle of events observed by Corino and Brodkey (1969) and Kline et al (1967) then such averages may represent the bursting phenomenon near the wall. Since similar signal features can be identified across the entire layer, however, it is probably more correct to say that these features represent features of a large structure and that the occurrence of bursts is related in some way to the passage of this structure.

Shown in figure 7.6 are the same kind of results that are obtained across the layer when detection is based not upon a local event, but upon the velocity at $y/\delta = 0.25$. The wire positions used were those points where the wall shear velocity correlations were maximized at zero time delay.

A significant average is, of course, generated at $y/\delta = 0.25$ but the averages are barely perceptible at $y/\delta = 0.50$ and $y/\delta = 0.05$ and imperceptible at more extreme points. It will be recalled, however, that the smoothed rectified high frequency detection signal at $y/\delta = 0.25$ was positively correlated with the corresponding signals across most of the layer (section 6.2). The results of figure 7.6 therefore demonstrate a shortcoming of simple averaging techniques such as these and show that an ensemble averaged time history that is zero does not necessarily imply the lack of presence of the structural feature. It results from the randomness in phase (or what is sometimes called phase "jitter") between the different realizations.

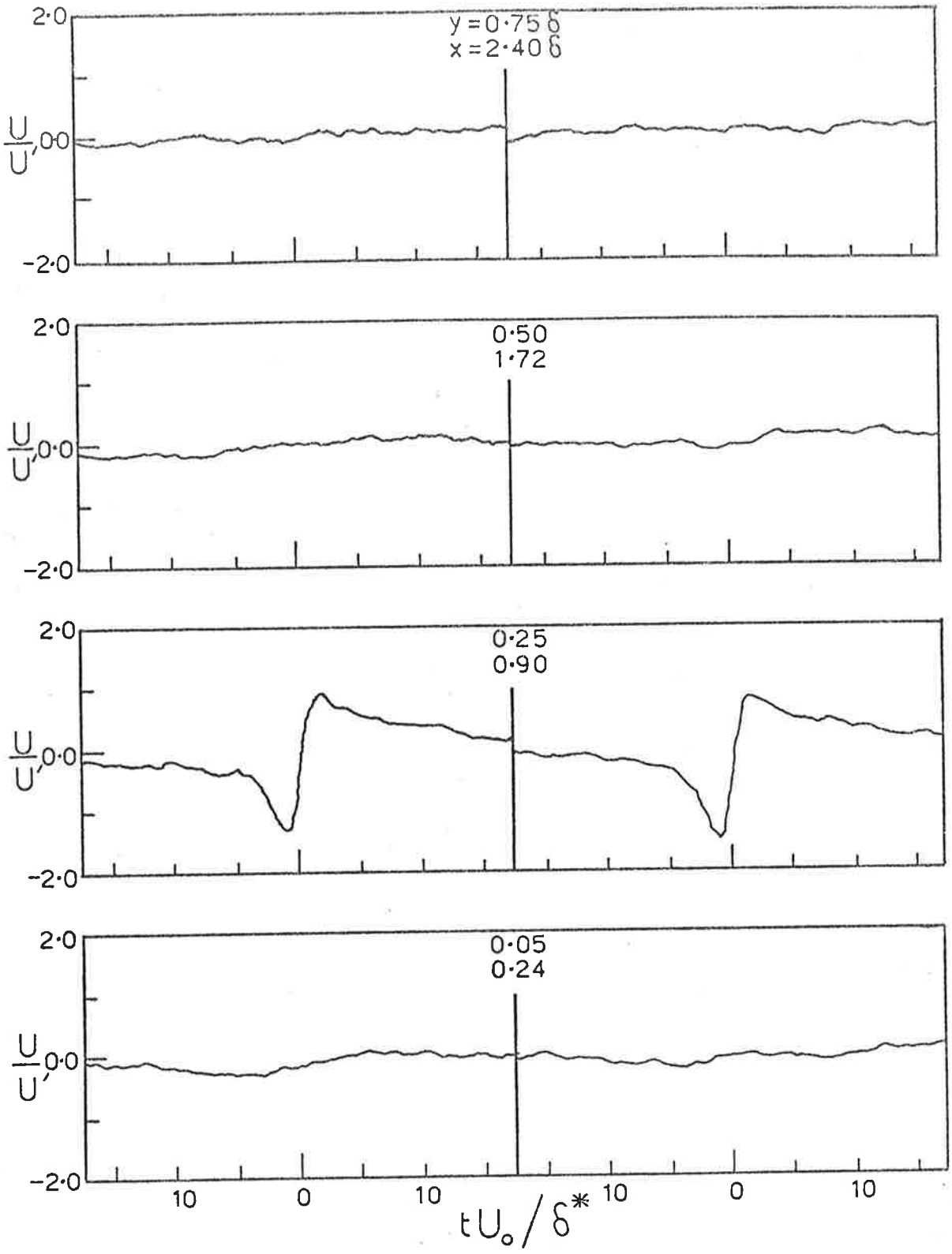

Figure 7.6 Ensemble averaged time histories of the streamwise velocity components at various points in the layer, for the high Reynolds number flow (left) and the low Reynolds number flow (right). Detection in all cases is based upon the signal at $y/\delta = 0.25$ and the wire positions correspond to those points which were found previously to maximize the wall shear velocity correlations at $\tau = 0$.

7.4 Sampling of Normal Component of Velocity and Reynolds Stress.

By undertaking careful recordings of the outputs of a cross wire probe at various positions above the wall, the normal component of velocity has been measured. The high frequency detection scheme has been applied to the corresponding streamwise component of velocity to generate an array of detection points which have then been used as a basis for the sampling of the normal component of velocity. The results of this procedure for the high Reynolds number case only are shown in figure 7.7 where the enhancing technique has been applied to the u signal to improve the ensemble averages. For comparison purposes, the corresponding streamwise velocity ensemble averages that resulted are also presented. The streamwise velocity averages can be seen to be of precisely the same form as those presented in figure 7.5, suggesting that the calibration methods used with the cross wire are satisfactory. It should also be noted that these averages are all non-dimensionalized by the local rms values which become small far from the wall so that the averages appear to have larger amplitude. Near the wall the averages are in fact of larger amplitude in an absolute sense.

A significant feature of the averages of the v component is a change in their form across the layer. Near the wall they show a predominantly positive region with a rather weaker negative region occurring at positive times. At that time when the strong acceleration occurs on the streamwise velocity, then there is correspondingly a strong fall in the normal component of velocity. This finding is also consistent with the results of Blackwelder and Kaplan (1976). As the point of measurement is moved farther from the wall, the region of negative velocity becomes reduced, until at about $y/\delta = 0.5$ the

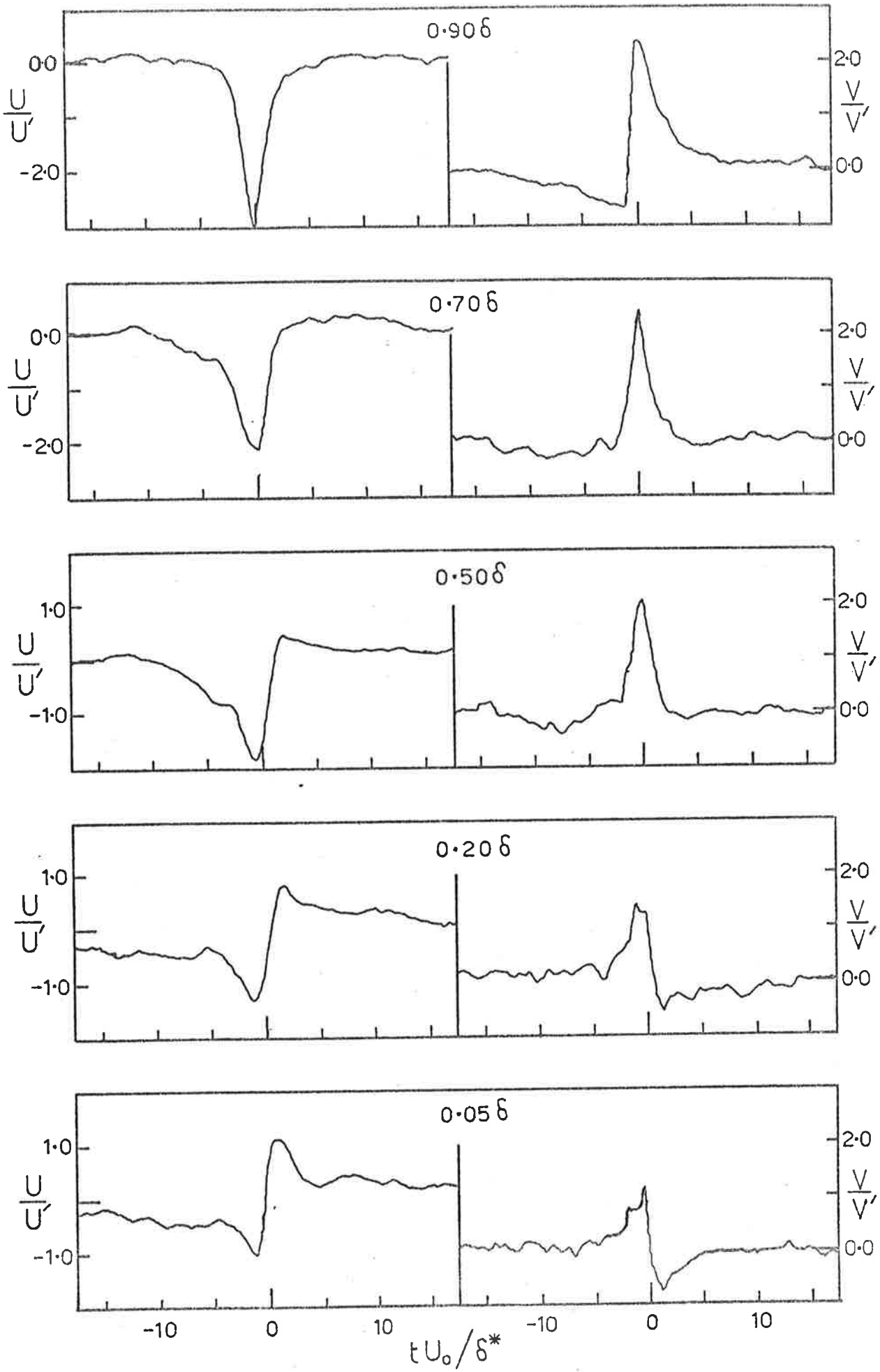

Figure 7.7 Ensemble averged time histories of the streamwise component (left) and normal component of velocity (right) for the high Reynolds

averages show mostly only a positive going region. Then at still larger y/δ values, the averages show a negative region once again, except that now it occurs at a negative time which, for a structure convected past a fixed measuring point, corresponds to the downstream side of the structure (i.e. at the front of the structure). The very interesting streamline pattern which can be drawn from the results will be discussed in section 8.1.

The averages of u and v at the outer edge of the layer are broadly similar to the zone averages presented by Kovasznay et al (1970) and Antonia (1972) except that no attempt has been made here to define the difference between turbulent and non-turbulent zones. Both those reports show that in the turbulent zones near the outer edge of the layer the v component is initially low and negative at the downstream edge of the zone and rises to a positive value within the zone and is near zero at the upstream edge of the zone. The u component is generally low within the turbulent region so that there is an implication of a slowly moving and rotating structure consistent with the averages presented in this section. Near the wall the situation is different because the rotation implied by the averages is of opposite sign to that in the outer layer; a model which takes this phenomenon into account will be presented in section 8.

The form of the averages of both u and v clearly implies a large negative correlation between u and v or large Reynolds stress and the averaged Reynolds stress data presented in figure 7.8 show that this is indeed the case. These curves have been generated by determining the detection points from the u component of velocity and the enhancing technique of section 7.2 has been used on this component to define detection points accurately. The instantaneous signal uv

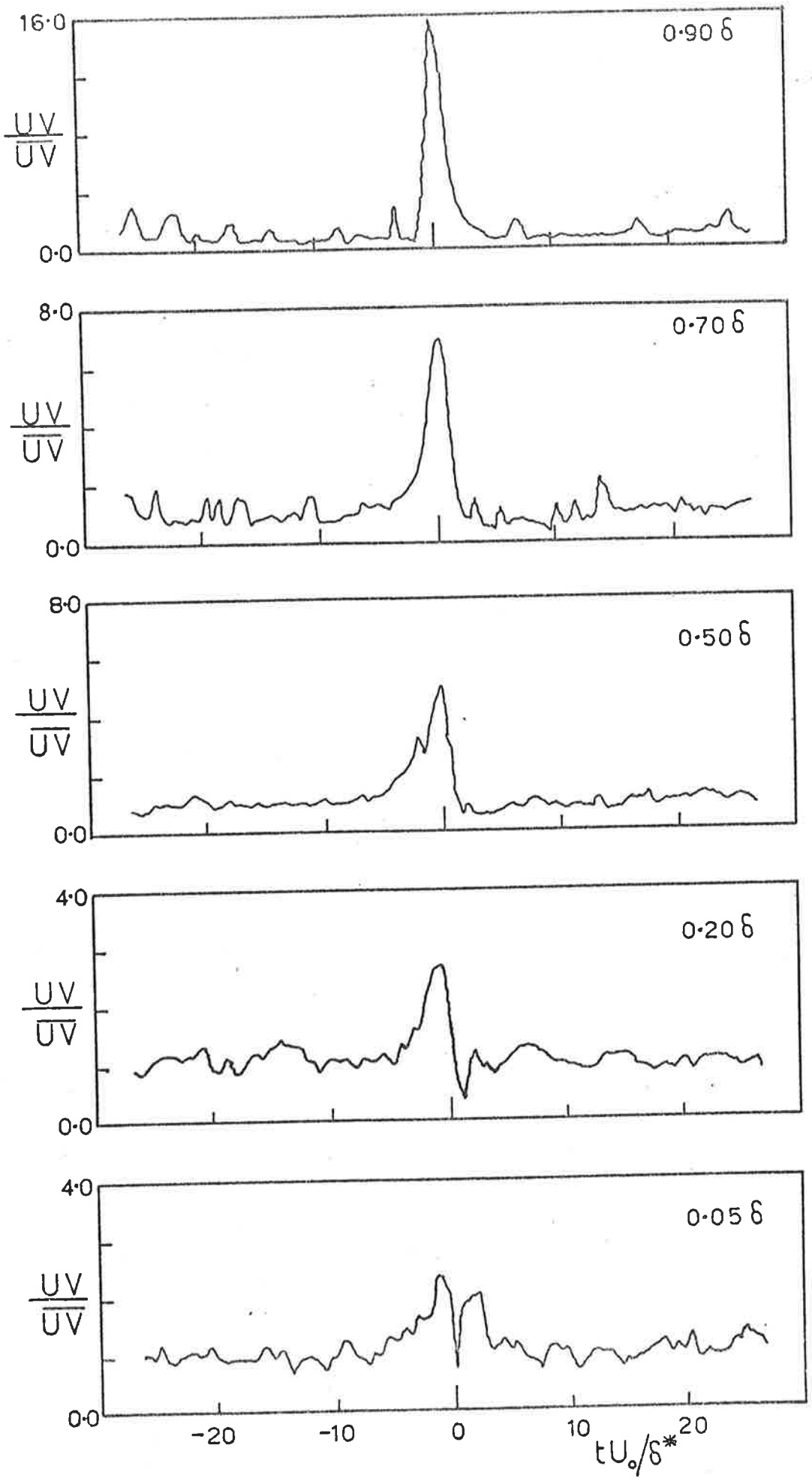

Figure 7.8 Ensemble averaged time histories of the instantaneous uv product for the high Reynolds number flow.

was then sampled at these points and an ensemble average generated.

It is clear from figure 7.8 that significant contributions are made to the Reynolds stress: the averaged values are typically an order of magnitude greater than the mean value near the outer edge of the layer and two to three times greater than the local mean near the wall. The particular results near the wall (i.e. at $y = 0.05\delta$ or $y^+ = 170$) are similar to those reported by Blackwelder and Kaplan (1976) whose measurements were restricted to wall region ($y^+ = 15$). Their results are of rather larger amplitude possibly because of their closer proximity to the wall or the lower Reynolds number of their experiment.

An important feature of the present Reynolds stress data and a feature that may be observed in the data of Blackwelder and Kaplan, is that particularly at $y = .05\delta$ the averages show twin maxima, one on either side of the low value at the time of detection. Such an effect is clearly a result of the steep negative to positive jump of the streamwise velocity component and the corresponding sudden fall in the normal component of velocity. The same effect cannot be discerned in the data of Willmarth and Lu (1971) and this is a reflection of the different sampling criterion that they used. It was based on a fixed level of the streamwise component of velocity and with such a scheme the detected points will not always bear the same phase relationship to the structure of interest from one realization to the next. Therefore the rather subtle effect that may be discerned in the present uv averages could become lost during the averaging process.

Despite this, the averages are not entirely inconsistent with the detailed and extensive set of data presented by Willmarth and Lu

(1971) in that the large contributions to the Reynolds stress are made by slow moving structures lifting away from the wall (bursts in their terminology) and faster structures moving towards the wall (sweeps). The present data show additionally that there is a clear relation between the occurrence of these two kinds of events which apparently arises from the presence of a large structure. Such a conclusion is also consistent with the work of Lu and Willmarth (1973) that the mean periods of these two kinds of events scale on outer flow variables, and are approximately the same across the entire layer.

7.5 Conditional Analysis of the Spanwise Geometry

Having established some of the features of the large structure in a plane normal to the wall, attention is now turned toward the three dimensionality of the structure. The correlations of section 5.3, between the streamwise components of velocity at points separated in the spanwise direction, have shown a characteristic feature of twin maxima at probe separations of the order of $\Delta z = 0.3\delta$. This is an important finding as it shows an unexpected degree of structural organization in the spanwise direction. Evidently the correlation curves are the result of a structure which has regions lying laterally oblique across the flow. Simultaneous measurement of the velocity at two points will record significant correlation at positive time delay for half the time and at negative time delay for the other half of the time. This behaviour is visually evident in the velocity time records and it is useful to follow a conditional analysis of

the same data to quantify the degree of this spanwise inclination.

Clearly, to conditionally generate an ensemble averaged time history of one signal on a basis of excursions in the other signal is not appropriate for this case. One must somehow discriminate between the occurrence of the two differently inclined parts of the structure. Since this feature of the structure was first highlighted by correlations, it would appear that the discrimination should be based upon short time estimations of the long time correlations, with the short time correlations being computed at those times when the large structure is thought to be present. Such correlations will be likely to show maxima at either positive or negative time delays depending upon the sense of the inclination of each realization. This kind of analysis has been undertaken and is described in more detail below:

(i) Initially the presence of the large structure in a given velocity record was discriminated upon using the high frequency detection criterion described in section 7.1. The enhancing technique was used to improve the definition of these points in the velocity record.

(ii) Short averaging time correlations centred on the flagged points were then computed between the first velocity time record (at time t) and the time record from an adjacent hot wire (at time $t + \tau$) which was separated from the first in the spanwise direction only. The correlations were normalized by the long time averaged rms signal levels and the averaging time used was $T_{AV}\ U_o/\delta^* = 25$ in each case. This is the same averaging time that was used with the enhancing technique and was selected because it is comparable to the apparent temporal extent of the large

structure whose ensemble averaged velocity time histories were shown in figure 7.7. Longer and shorter averaging times ($50\delta^*/U_o$ and $12\delta^*/U_o$) have been used and were not found to change the nature of the results.

(iii) Each short time correlation was then searched within some positive and negative search time T_s (i.e. from $-T_s$ to $+T_s$) for the maximum peak value that occurred nearest the zero time delay point. They were then sorted into two cases depending upon whether this value occurred at $\tau \leqslant 0$ or $\tau \geqslant 0$. Ensemble averages of the short time correlations were then computed for each case. This process represents an attempt to discriminate upon the occurrence of the two different structural forms which are evidently responsible for the twim maxima in the long time correlation.

It is apparent that because the search is based upon maxima in the correlations, then the ensemble averaged curve will show a maximum at some time delay. If, however, the results exhibit behaviour that is different from what might be expected from uncorrelated signals, then some significance may be attached to the time delay at which the ensemble averaged curve peaks. The position of this maximum will also depend upon the value of T_s, so that a range of values must be used to determine the importance of the search time.

The typical results that are obtained from such an analysis are shown in figure 7.9 for the high Reynolds number case. They are presented as the time delays $|\tau_m|$ at which the ensemble averaged correlation curves peak for different values of the search time T_s.

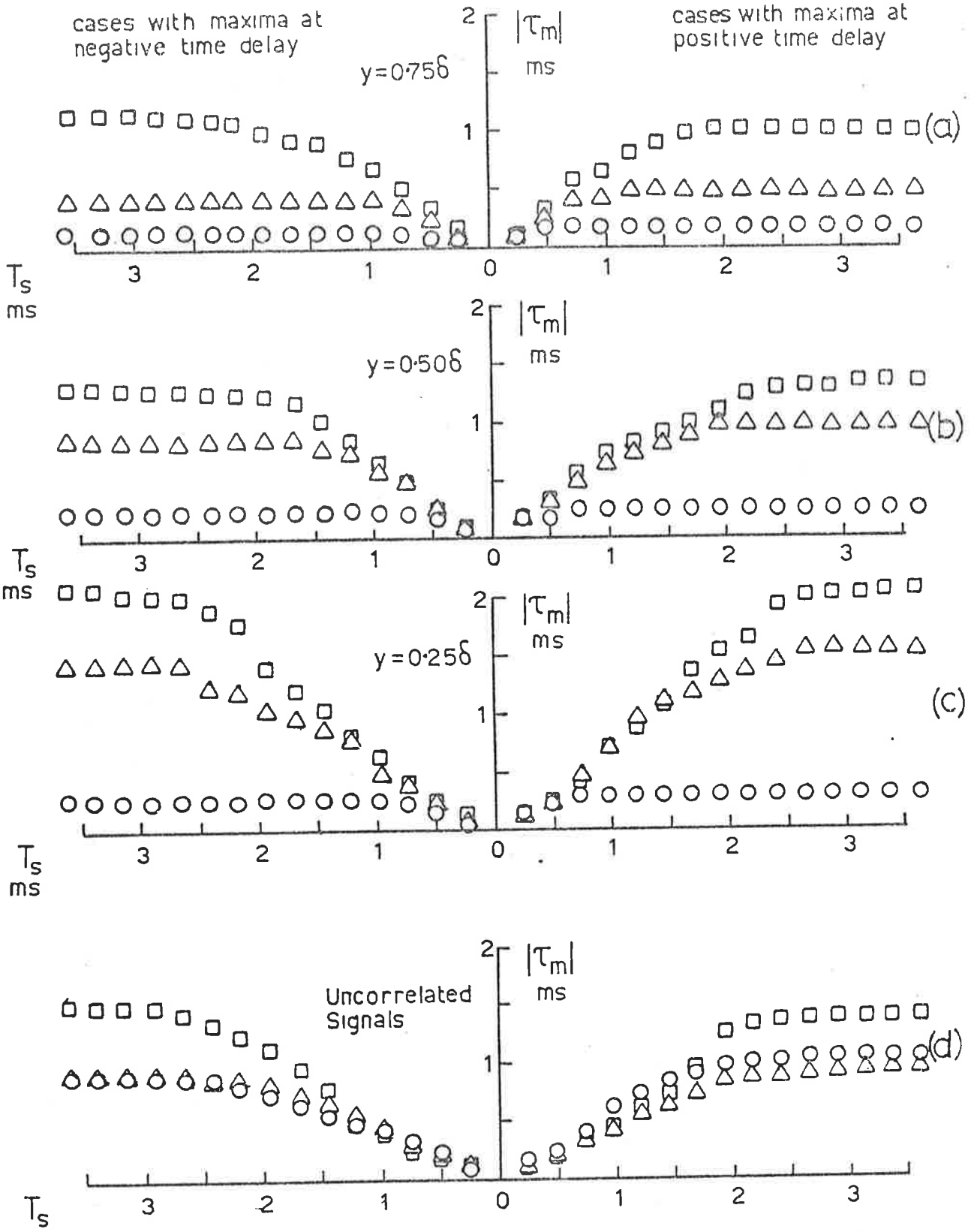

Figure 7.9(a)-(c) Absolute values of the time delay, $|\tau_m|$, at which the conditionally ensemble averaged velocity correlations peak, as a function of the search time T_s. Three positions in the boundary layer (y/δ = 0.75, 0.50, 0.25) and three spanwise separations (o, z = 0.15δ; Δ, z = 0.30δ; □, z = 0.45δ) have been used.

Figure 7.9(d) The corresponding results obtained when uncorrelated signals from the same position in the layer are used (o, y = 0.75δ; Δ, y = 0.50δ; □, y = 0.25δ). These results apply to the high Reynolds number flow.

Three different points in the boundary layer have been used (y/δ = 0.75, 0.50 and 0.25) and in the lower portion of the figure are shown the results obtained when the same process is applied to uncorrelated signals from the same regions of the layer. In all cases as T_s is increased from a small value, then $|\tau_m|$ increases monotonically. Eventually however a point is reached where $|\tau_m|$ no longer increases and becomes independent of T_s. This arises because the search time becomes large enough for the search process to always find the same peak in each short time correlation. When this occurs the curve corresponding to a negative time delay levels out at the same absolute value of time delay as the curve for a positive time delay. This is a consequence of the spanwise homogeneity. Furthermore, these values of $|\tau_m|$ increase with the spanwise separation which indicates that the large structure does indeed have regions lying laterally inclined across the flow.

Comparison of these results with those for the uncorrelated signals indicates a rather similar behaviour, however the time delays where independence of T_s is exhibited are not always the same as obtained for the correlated signals. There are occasions when they are higher and occasions when they are lower. At y/δ = 0.75 for example, the uncorrelated signals show the same time delay plateau as that for the largest separation studied (0.45δ). At y/δ = 0.25 however, they show a plateau at a time delay which is less than that for the largest separation. For this second case it would appear that the nature of the turbulence is such that a peak in the correlation is found, on average, later than would be expected through a random association of events. This lends some credibility to the discrimination technique that is being employed.

The time delays at which the curves of figure 7.9 indicate

a constant level are presented in non-dimensional form in figure 7.10(a) for the high Reynolds number flow. Figure 7.10(b) shows the results that are obtained when the analysis is applied to the data from the low Reynolds number flow. In both cases the various curves for different positions above the wall show similar behaviour and comparison with the correlations in figures 5.6 and 5.7 previously shows that the time delays from the present analysis are the same as those inferred from the long time correlations. The angle of the structure with the stream direction appears to be more acute nearer the wall but this is a reflection of differences in convection velocity. If the same data is non-dimensionalized by the local mean velocity U_m instead of the free stream velocity U_o, the curves shown in figures 7.10(c) and (d) are obtained. There is a tendency for the points to group themselves more nearly on a single curve so that it appears that different parts of the large structure are convected with a speed near the local mean. This suggests that the structure, which is also inclined to the wall, is slowly rotating.

The angle that the large structure apparently makes with the stream direction can be inferred from figure 7.10(c) and (d) and appears to be about 22° if the features of the large structure are convected at the local mean velocity. It was suggested in section 5.3 that the large structure responsible for these correlations might be similar to the turbulent spot that has been observed during transition. The photographs of the turbulent spot taken by Elder (1960) show the angle between the leading edge of the spot and the stream direction to be about 20°, although Schubauer and Klebanoff (1955) have reported the somewhat lower value of 15°. It would appear perhaps, that the large structure of the boundary layer does have some features in common with those of the

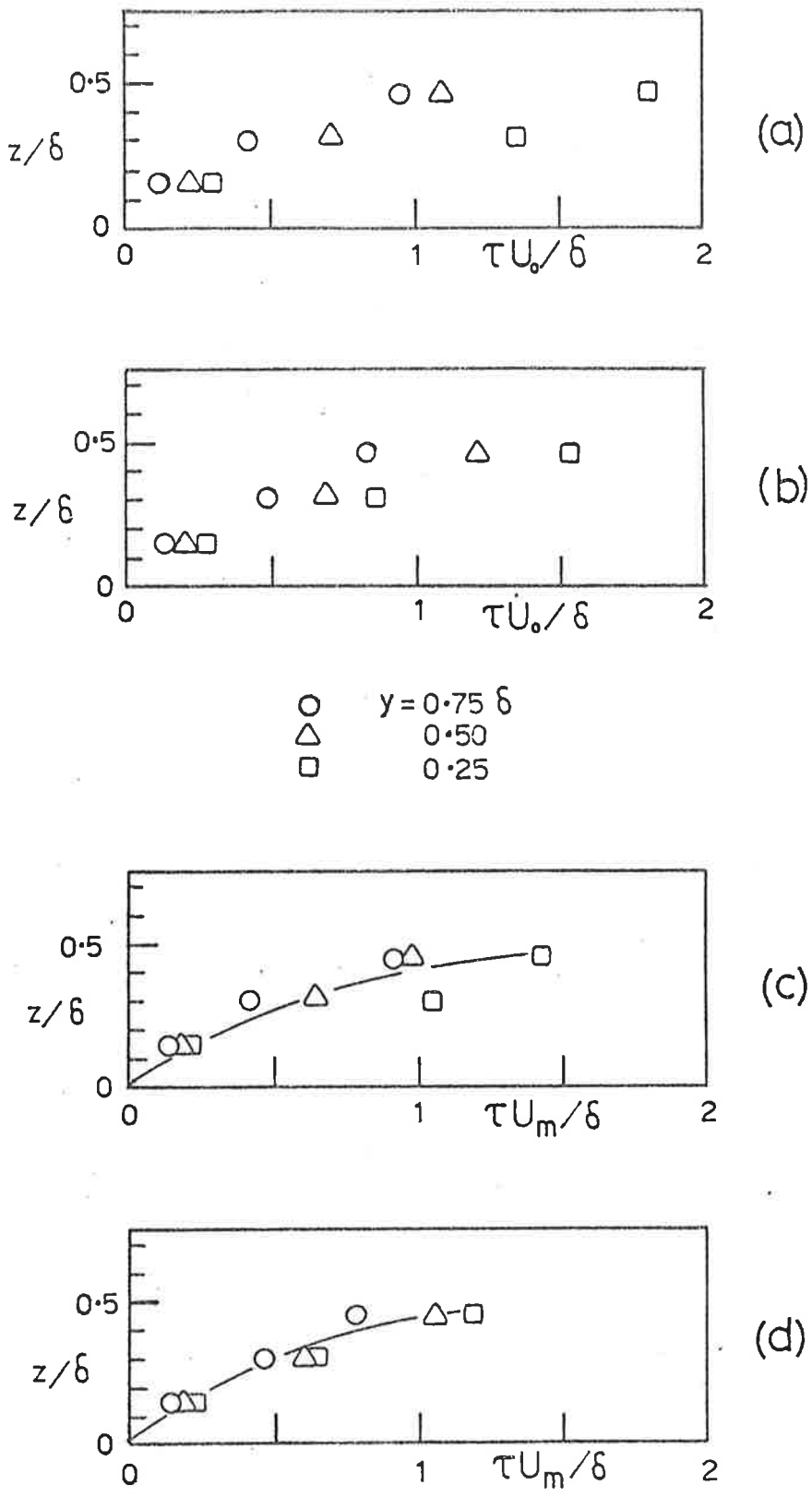

Figure 7.10 Time delays corresponding to the plateau of the curves such as those in figure 7.9; (a) high Reynolds number, (b) low Reynolds number. Curves (c) and (d) are the corresponding results when non-dimensionalized by the local mean velocity.

turbulent spot. The correct interpretation of this apparent angle is, however, rather more subtle as the results presented are an ensemble of many realizations and may not represent only the shape of the front or leading edge of the structure. The implied geometry could also be representative of the rear of the structure. It is of interest to make use of the simultaneously recorded outputs of a rake of three hot wires to determine more of the character of the individual members of the ensemble. If three wires are used (positioned, say at z/δ = 0.15, 0.0 and-0.15) two similar short time correlations may be computed between the signal of the central wire and those of the adjacent side wires. The time delays at which the maxima of these correlations occur may then take four possible combinations, each representing a different feature of the structure, and these will be referred to as the front, back or either of two sides. A search for each combination can be made and the relative frequency of occurrence of each structural feature determined. If, for example, the fronts (which presumably precede the backs) can be identified either more or less frequently than the backs, then the structure must have a definite streamwise asymmetry leading to a bias in detection of one region over the other.

Such a search has been made for the high and low Reynolds number data used previously and the results are summarized in Table 7.1 as the percentage of occurrence of each possible spanwise distribution. Ambiguous cases (i.e. those which display short time correlations that peak at $\tau = 0$) have been rejected. In all cases, for this probe separation, the most frequently occurring features are evidently the two sides of the structure. The rear surface is the next most commonly occurring feature and is apparently detected more frequently than the front of the structure. Such a bias is likely

TABLE 7.1

Percentage of occurrence different spanwise distributions determined by the short time correlation technique applied to the signals from a rake of 3 hot wires.

Possible flow Geometries		1 $\tau_1 < 0$ $\tau_2 < 0$	2 $\tau_1 > 0$ $\tau_2 > 0$	3 $\tau_1 > 0$ $\tau_2 < 0$	4 $\tau_1 < 0$ $\tau_2 > 0$
	y/δ	Back	Front	Side	Side
High Re	0.75	0.26	0.18	0.28	0.28
	0.50	0.26	0.14	0.28	0.32
	0.25	0.22	0.18	0.27	0.33
Low Re	0.75	0.26	0.17	0.27	0.30
	0.50	0.25	0.18	0.30	0.27
	0.25	0.24	0.12	0.31	0.33

since the detection of the presence of the large structure is based upon what appears to be the rear of the large structure and it is the rear surface which tends to dominate the structure. The front of the large structure appears to be rather poorly defined in relation to the rear surface.

If a simple model is followed in which the spanwise extent of the large structure is L and the width of the rake of three wires is ℓ, then the probability of detecting the centreline of the structure somewhere within the rake (i.e. a front or a back in table 7.1) is given by $\ell/(L - \ell)$. The values of table 7.1 show that this

is generally about 40% which for $\ell = 0.3\delta$ indicates that the spanwise extent of the large structure is of the order of 0.8δ. This represents an underestimate, however, because a proportion of the cases that resemble a front or a back may in fact result from two structures lying side by side and which satisfy the discrimination requirements.

7.6. Conditional Sampling of the Wall Pressure

It has been established that the small scale shear stress fluctuations near the wall are intimately related to the passage of a larger scale structure. The mechanism responsible for this relationship is, however, not clear. Offen and Kline (1973) and Willmarth (1975a) have suggested that it is the pressure field generated by a larger structure that gives rise to the small scale events (bursts and sweeps) near the wall and indeed a correlation has been found between the high frequency component of the wall pressure signal and the low frequency component (section 6.1). This suggests that there is a relation between the occurrence of the large scale pressure field and small scale events near the wall, but does not indicate whether one gives rise to the other. The experiments described below have been undertaken in an attempt to establish if such a causal relation is present by generating conditionally ensemble average time histories of the pressure signal. It will become apparent, however, that the data require a rather cautious interpretation.

The results of such an experiment are shown for the two Reynolds numbers in figure 7.11(a) - (d). The enhancing technique has not been used in either this or the following work. Figures

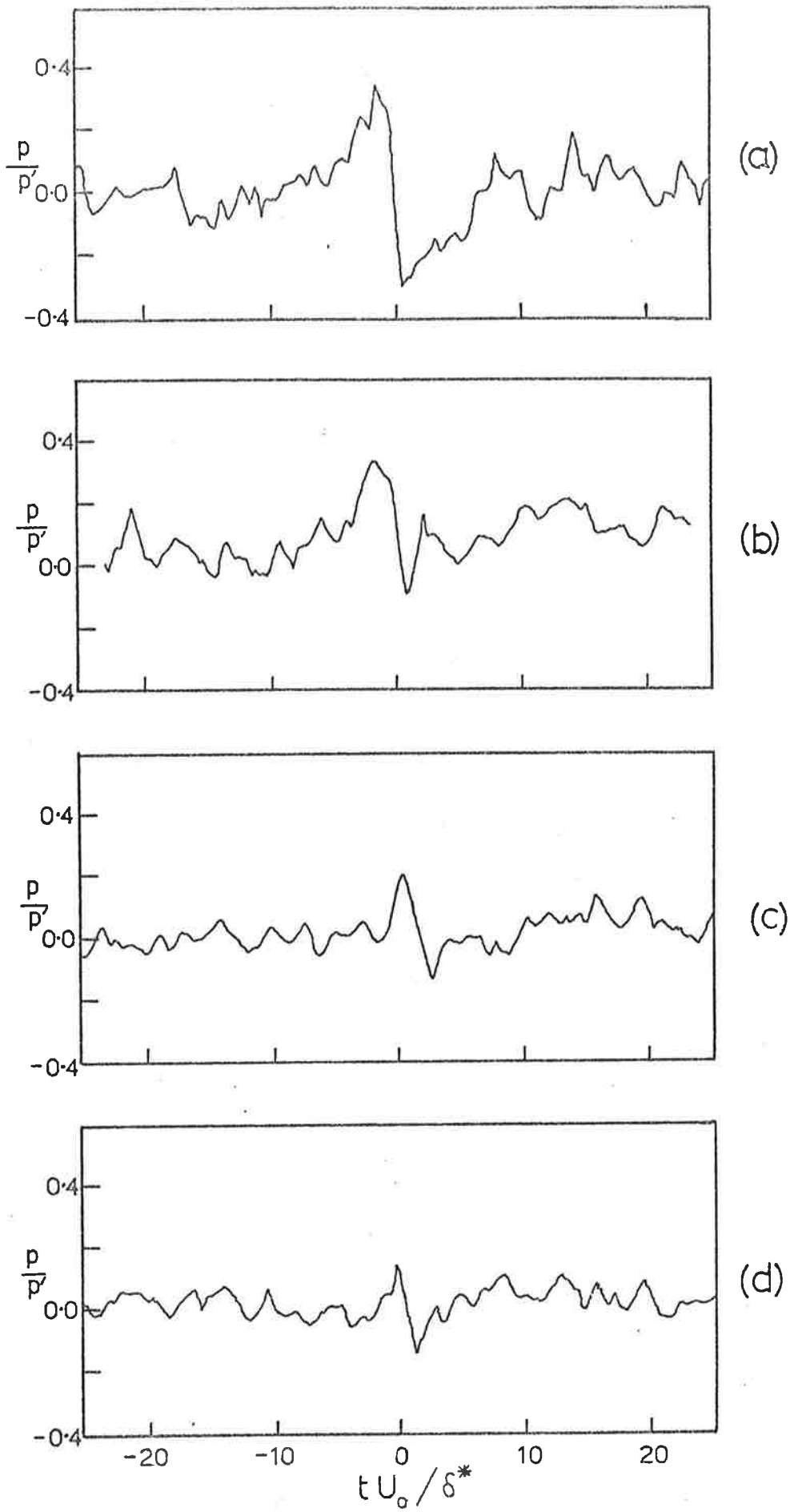

Figure 7.11 Ensemble averaged time histories of the wall pressure. The detection is based upon the wall pressure signal in (a) and (b) and upon the velocity at $y^+ = 30$ in (c) and (d). Curves (a) and (c) correspond to the high Reynolds number and (b) and (d) to the low Reynolds number flow.

7.11(a) and (b) show the ensemble averaged time histories that arise if the high frequency detection criterion is determined from the pressure signal itself. Figures 7.11(c) and (d) show the results obtained if the detection is based instead upon the velocity at $y^+ = 30$. (Care was taken when digitizing this data to ensure that the presence of the hot wire did not give rise to spurious wall pressure fluctuations; it was found necessary to place the wire slightly downstream of the pressure transducer by a distance of $x^+ = 60$. The convective delay between the two probes is, however, very small in relation to the scales of figure 7.11 and may be ignored.) When the detection is based upon the velocity signal, the amplitude of the averages is rather smaller than for the case where the detection is based upon the pressure signal itself. In each case, however, the shape of the averages are very similar and show the dominant feature to be a region of steep fall of pressure (in time). Burton (1974) has also remarked that such regions tend to be more significant than regions of rising pressure. Additionally when the detection is based on the pressure signal itself, the time width of the non-zero portion of the averages (figure 7.11(a) and (b)) is quite large being of the order of $20\delta^*/U_o$. Evidently these time histories are those due to structures of rather large scale and since they are based upon the excursions of the high frequency content of the pressure signal they reflect correctly the correlation between the two scales of motion that was found previously.

Willmarth (1975a) and Burton (1974) have also reported conditionally sampled and averaged wall pressure data and their results are reproduced in figure 7.12(a) and (b). They based detection on the low pass filtered velocity at $y^+ = 15$ being equal to $-2u'$ and decreasing; the basis being that this may represent the

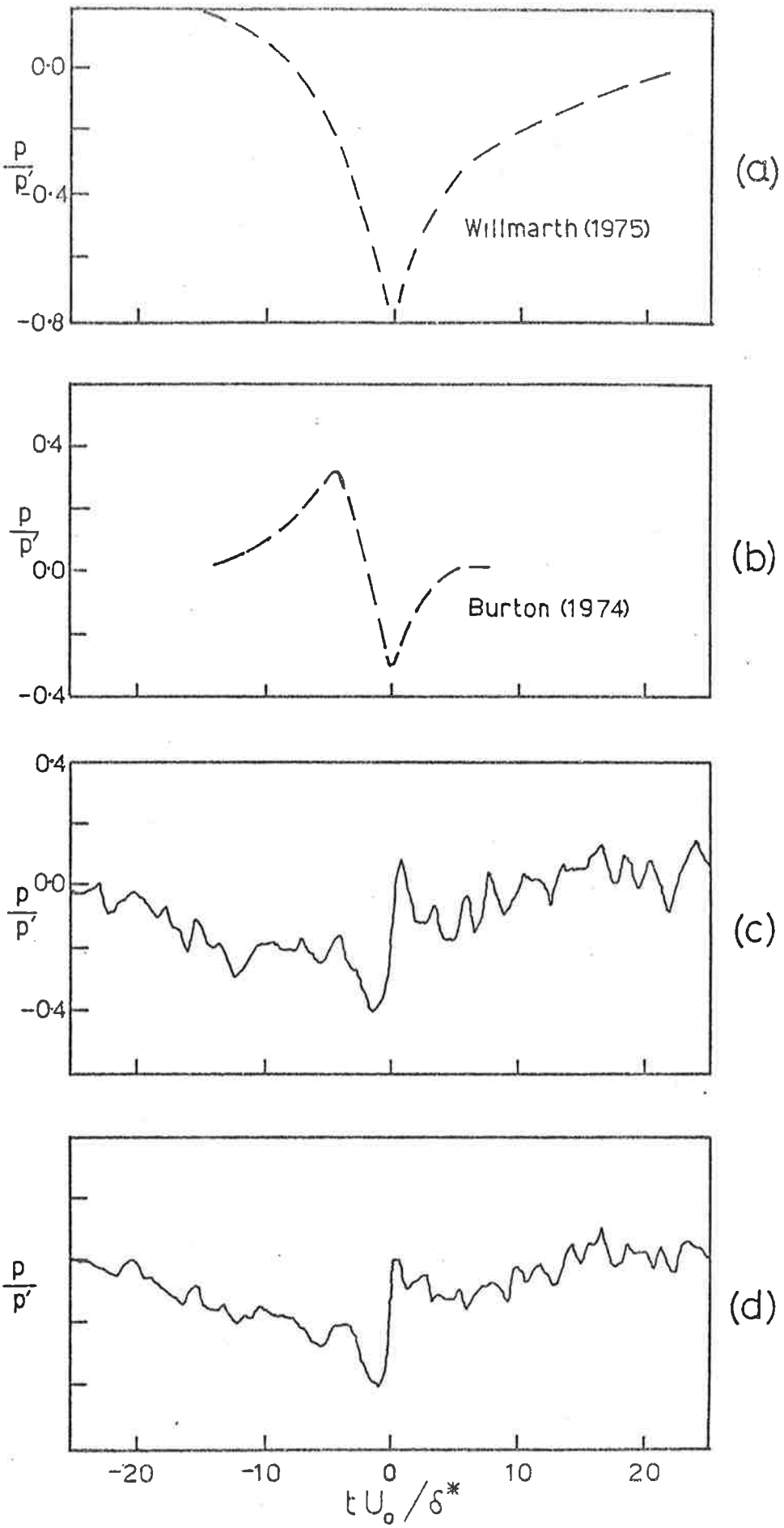

Figure 7.12 (a) Willmarth's (1975) ensemble averaged time history of the wall pressure.
(b) Burton's (1974) corresponding result.
(c) Repeat of Willmarth's experiment (high Reynolds number flow).
(d) Repeat of Burton's experiment (high Reynolds number flow).

turbulent bursts characterized by outward migrations of low momentum fluid. These two results both have the feature of being low at the time of detection although Burton's result shows a more significant region of positive pressure at negative times. Burton's result is, therefore, very similar to the present results of figure 7.11, however Willmarth's result is unlike the present data. Because of the differences in detection criteria, however, direct comparison is not strictly valid. Therefore, their experiments have been repeated for the high Reynolds number case and the ensemble averaged time histories that result are shown in figure 7.12(c) and (d) where in the present case detection has been based upon the low pass filtered velocity at $y^+ = 30$.

Willmarth (1975a) does not state what filter cutoff he used although it is likely to be the same as used by Willmarth and Lu (1971) i.e. $f_c = 0.2\ U_o/\delta^*$, which has, therefore, been used to generate figure 7.12(c). Burton (1974) used a filter cutoff of $f_c = 1.7\ U_o/\delta^*$ which in the present case could not be implemented directly because it represents a frequency greater than the Nyquist frequency of the data. The unfiltered velocity signal was, therefore, used. The similarity of the two ensemble averaged time histories in figures 7.12(c) and (d) demonstrates that the use of filtering has little effect upon the final results and in each case the dominant feature of the average is now a region of pressure increase with the pressure once again being low near the point of detection. Except for the more dominant region of pressure increase, the present results are very similar in character to that of Willmarth (1975a). He used a rather large transducer ($d^+ \approx 160$, $d/\delta^* = 1.7$) which may be the reason why the region of pressure increase is apparently attenuated

in his case. The present results are, however, rather different from Burton's in that a region of positive pressure at negative times is not apparent. The reason for this is not clear, but it may be a reflection of the response of the pinhole microphones that Burton used (see Appendix B).

The great dissimilarity of the results of figure 7.12 and those of figure 7.11 and the lack of agreement with Burton's result suggests that the conditionally sampled data needs to be examined in more detail. The sampling of the wall pressure on a basis of excursions in the velocity has therefore been extended to include the following specific cases:

(i) Points where $u = -u'$ and decreasing

(ii) " " $u < -u'$ and local minimum

(iii) " " $u = u'$ and increasing

(iv) " " $u > u'$ and local maximum.

Filtering of the velocity signal has not been used as it has been shown to have little effect upon the final results; a lower discrimination level has been used to reduce statistical uncertainty. Use of these detection criteria on the velocity at $y^+ = 30$ gives rise to the ensemble averaged time histories of wall pressure shown in figure 7.13 for the high Reynolds number case. It can be seen that a positive velocity is associated with a region of positive pressure followed by a sudden fall in pressure. Conversely a negative velocity is associated with a region of negative pressure followed by a sudden rise in pressure. The additional requirement that the velocity also be a local maxima or minima does not dramatically change the curves.

These averaged time histories indicate a considerable

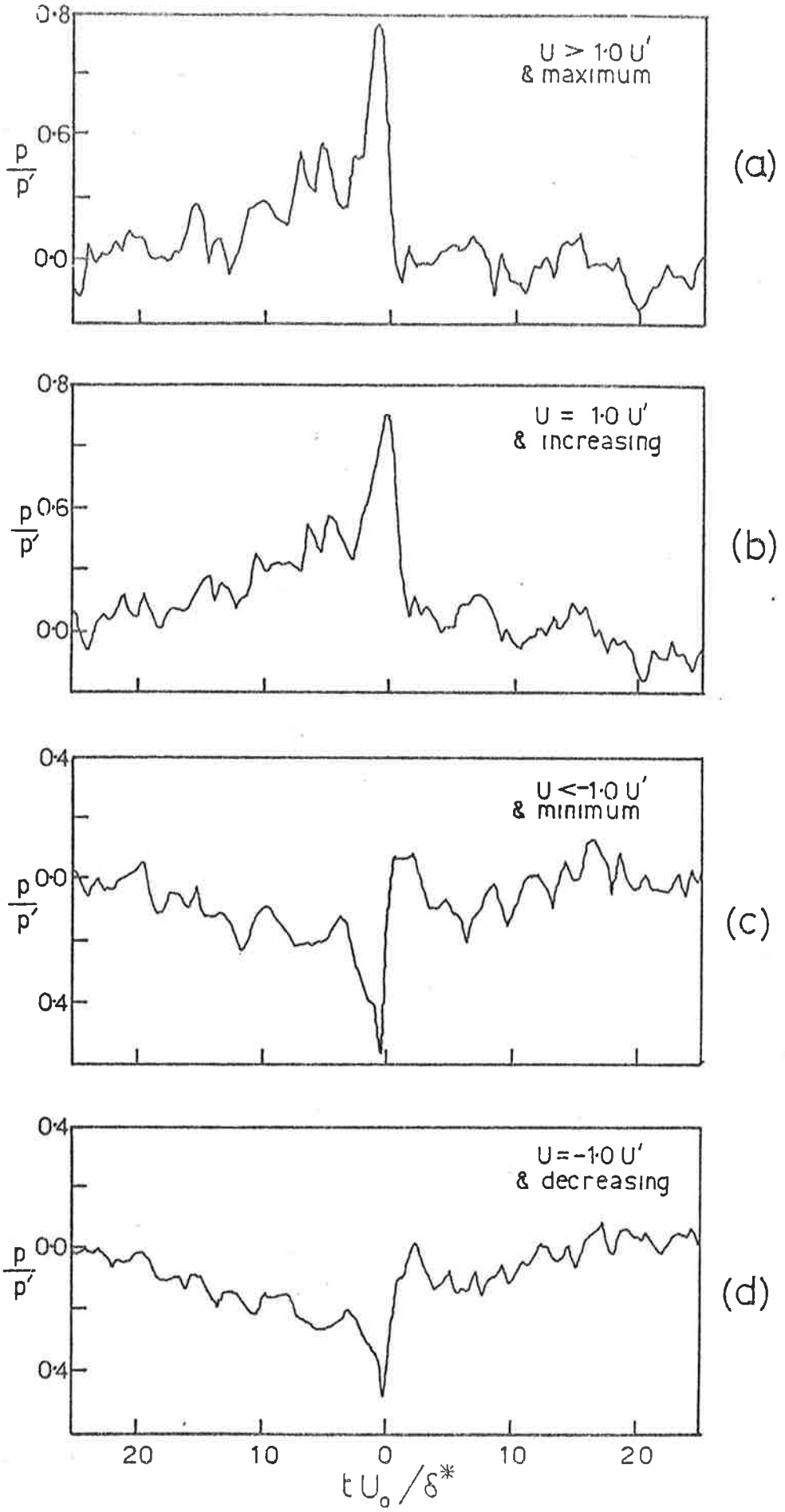

Figure 7.13 (a) - (d) Ensemble averaged time histories of the wall pressure determined with the four different detection criteria shown (high Reynolds number flow). The velocity is measured at $y^+ = 30$.

relation between the velocity at $y^+ = 30$ and the wall pressure but they do not indicate whether the time histories result from two different structural forms or represent different portions of the same more complex structural feature. In addition, a visual inspection of the original signals leads to little indication of any of the averages shown being representative of typical pressure signatures.

In section 7.3 it was demonstrated that a typical structural feature that could be observed in the velocity signals near the wall was characterized by a low velocity that rose steeply to a positive value and fell to zero thereafter. Such a time record is also likely to satisfy the four detection criteria used to generate figure 7.13 and this suggests that the curves shown in that figure represent different portions of the same more complex wall pressure signature. In order to see if this was so, a double detection procedure has been adopted which uses the four detection criteria outlined above, at points where the velocity signal is also known to satisfy, locally, the high frequency detection criterion. In more detail, the procedure that was as follows.

(i) The velocity signal at $y^+ = 30$ was searched to find these points where the high frequency detection criterion was satisfied, that is the points where the smoothed rectified high frequency component of the signal was a local maximum greater than 1.5 times its rms level. The ensemble averaged time history of the wall pressure generated at these points has been shown in figure 7.11 previously. The resulting averaged velocity time history showed the same sawtooth character as was shown in figure 7.5 for the velocity near the wall.

(ii) Having located the initial points, the velocity signal

was searched within positive and negative times around these points for the nearest positions where the four detection criteria of figure 7.13 were satisfied. The average of the time differences between the initial detection points and the second set of detection points was in all four cases quite small ($|t|U_o/\delta^* \approx 1.0 - 2.0$) suggesting that the points which satisfy the four criteria are now associated with the same structural feature.

The ensemble averaged time histories of the wall pressure generated at these points are shown in figure 7.14 for the high and low Reynolds number flows. They have been displaced in time by an amount corresponding to the average time at which the second detection occurred relative to the first and in all cases, except for this time shift, they can be seen to be rather similar to the results given in figure 7.13. Evidently these represent different portions of the same structural feature whose likely velocity and pressure signatures are of the kind shown in figure 7.15(a). Given a certain amount of random variation in the phase and scale of each realization, if the wall pressure is sampled at the points marked A, B, C and D in that diagram, then averaged time histories of the kind shown in figures 7.14(a), (b), (c) and (c) are likely to result. Additionally if the pressure time history is sampled and averaged at the points where only the high frequency detection criterion is satisfied by the velocity signal (i.e. where the velocity is rising steeply in time) then the averaged time histories shown in figure 7.11 (c) and (d) are likely to result. The dissimilarity between any one of these averages and the pressure time history proposed in figure 7.15(a) demonstrates a major shortcoming of simple averaging techniques such as these. As mentioned in section 7.3, as the poin

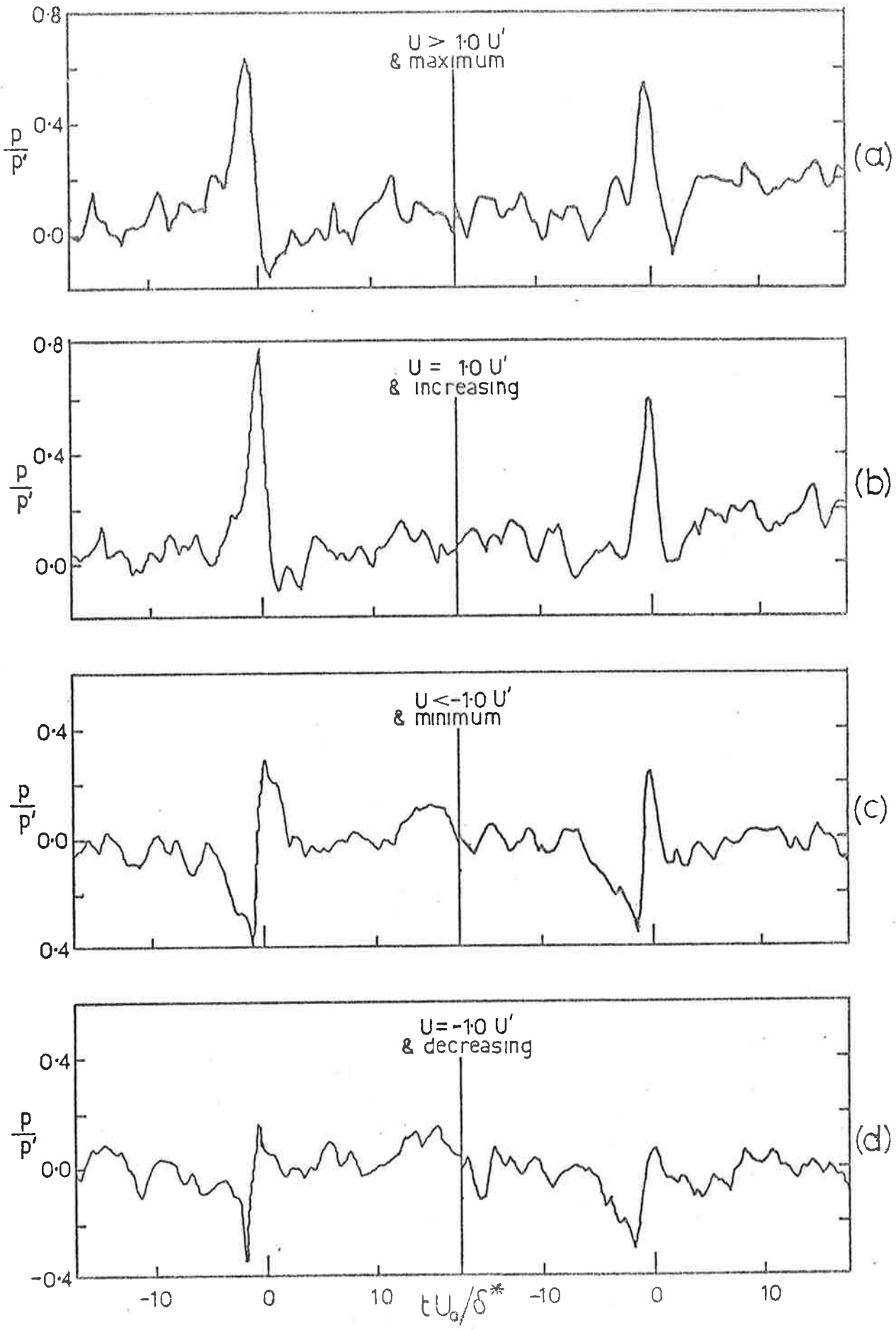

Figure 7.14 Ensemble averaged time histories of the wall pressure for the high Reynolds number flow (left) and the low Reynolds number flow (right). A double detection criterion, described in the text, has been used to generate this data.

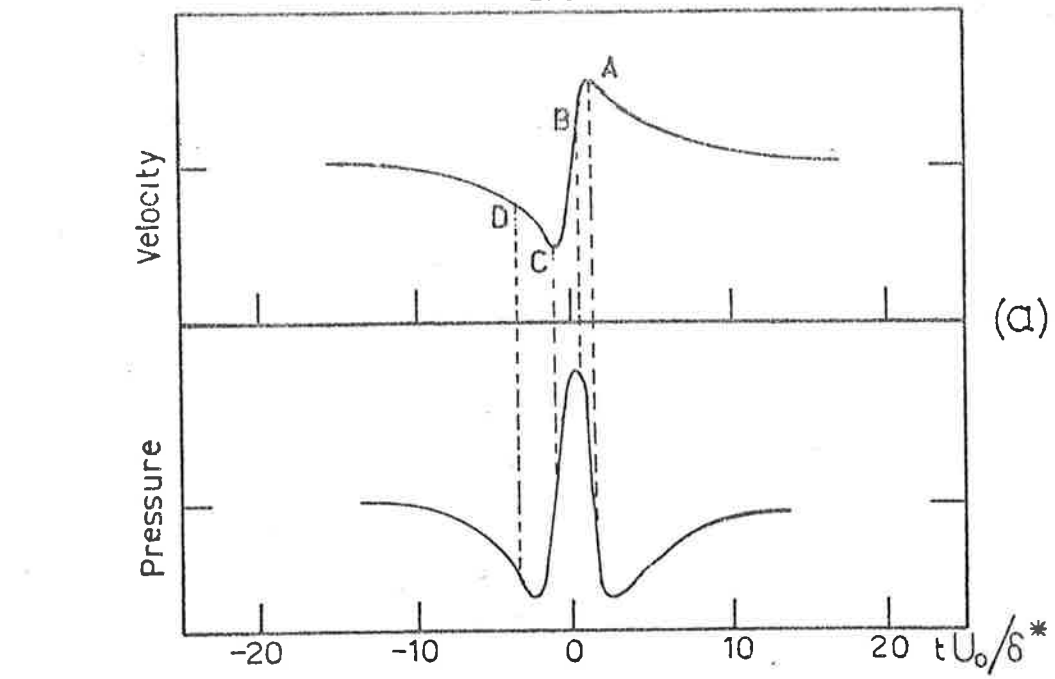

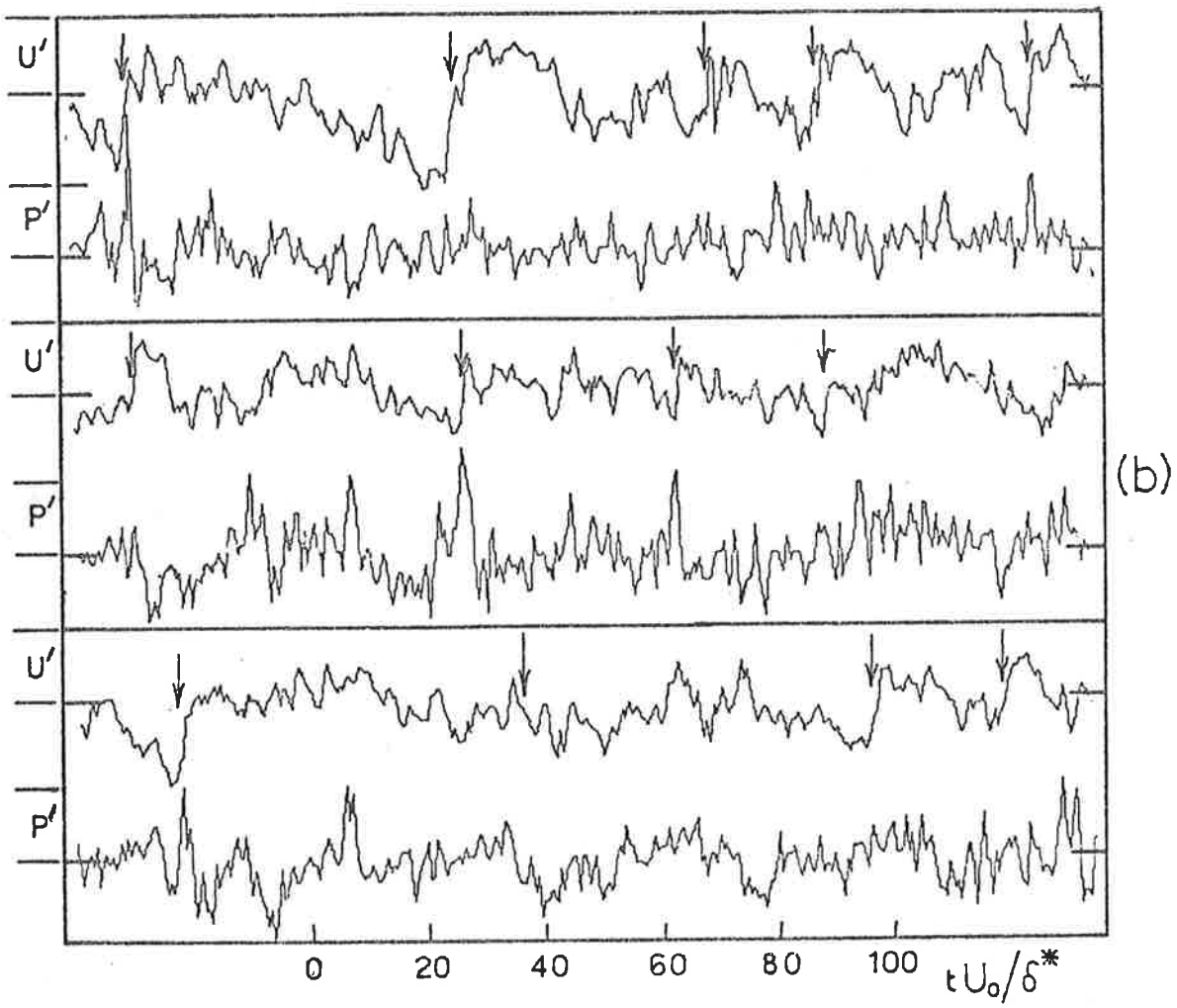

Figure 7.15 (a) Typical velocity time history near the wall and suggested corresponding time history of the wall pressure.

(b) Typical time records of the velocity ($y^+ = 30$) and the wall pressure for the high Reynolds number flow.

of interest moves away from the time of detection, the amplitude of the average becomes small because of the cumulative effect of random variations in the phase and scale of the different realizations used to generate the averaged time history. Therefore an averaged time history does not necessarily reflect the true behaviour of the structural features in the signals. The same effect is present in the velocity averages presented in sections 7.3 and 7.4, but it is far less severe because the velocity signal is considerably more well defined and organized than the pressure signal. Under those circumstances the averaged time histories do represent quite well, the trends that can be visually observed in the signals.

If the inferred pressure signature shown in figure 7.15(a) is correct, then it might be expected that occasions could be recognized in the raw signals that have such a form. Some short time records of the velocity and wall pressure data for the high Reynolds number case, that have been used in these experiments, are presented in figure 7.15(b). Those points where the velocity signal satisfied the high frequency detection criterion have been flagged. Visual examination of the wall pressure signal at the corresponding times shows a few occasions that appear to have the proposed form, but the evidence is by no means overwhelmingly in favour of this form. This would appear to be a result of the fact that at any given instant the wall pressure signal represents a complex summation of the effects of pressure sources across the entire layer. Because of the randomness of the field, these sources are essentially uncorrelated or at best weakly correlated with the velocity signal at $y^+ = 30$. They therefore make a net zero contribution to the average and in this way it can be seen that the averaging process has served to pick out only the component of the

wall pressure signal that is generated by sources in the region around $y^+ = 30$. The presence of other sources and the complete description of the pressure field is lost.

If this is the case, then in principle it becomes possible to compute the component of the wall pressure that is associated with sources in a region above the wall whose typical velocity signatures resemble those given in section 7.4. (These velocity signatures it will be recalled, represent the back or trailing surface of a large structure). Such a computation has been undertaken and is presented in Appendix E. The resulting computed pressure time history (figure E1) is very like the form proposed in figure 7.15(a) and suggests that the averaging process does indeed pick out only the component of the pressure field associated with sources in a region near where the velocity signal (used as a basis for detection) is measured.

The averaged time history of the wall pressure that was determined on a basis of the high frequency activity of the pressure signal itself (figures 7.11(a) and (b)) will presumably not suffer from such effects, and therefore will represent a more general feature of the pressure field. It does, however, suffer from the cumulative effects of the random variations in scale and phase that have been shown to be present. It is, therefore, likely to be a true representation of the wall pressure field only at times quite close to the detection point. The result therefore suggests that when the observed high frequency disturbances occur on the wall pressure, a feature that is more common to all the realizations is a region of falling pressure. A model that accounts for this feature will be presented in section 8 where, on a basis of the work of this section,

the role of the pressure in the turbulent bursting process will be evaluated.

When detection is based upon the velocity at a fixed point, the averaging process apparently gives rise to a bias toward only a component of the pressure field. The same effect will arise if a long time averaged correlation is computed between the wall pressure and the velocity at some point in the layer. Such a correlation is likely to reflect only the correlation between the source terms in the vicinity of the point where the velocity is measured and the component of the pressure that they produce at the wall. This probably explains the significant finding of Willmarth and Wooldridge (1963), that if correlations are computed between the wall pressure and the velocity at different distances from the wall above the pressure transducer, then the region of non-zero correlation occurs at the same time delay no matter how far the hot wire is from the wall. The correlations do not reflect the way structures are inclined to the wall because the local source terms produce a pressure component at the wall that is predominantly directly under the source, and it is this component which dominates the correlations.

7.7. Convection of the Pressure Field

Because of the non-disruptive nature of the wall pressure measurements it becomes possible to follow the passage of discrete pressure disturbances downstream using simultaneous recordings from two pressure transducers, with the second device at various fixed distances downstream from the first. This, it will be appreciated, is difficult to do using hot wires or hot films because the thermal

or aerodynamic wake of the upstream probe will influence the downstream probe.

Several data runs were recorded using two flush mounted transducers; the output of the downstream transducer has been conditionally sampled on the basis of the high frequency detection criterion generated from the signal on the upstream probe. A few typical results are shown for the high Reynolds number case in figure 7.16 (the enhancing technique has, of course, not been used). In each case the nature of the averages is the same as has been found previously for a single probe, except for a time shift which increases as the probe separation increases. At larger separations, the signature becomes progressively less clear, but only at separations exceeding $15\delta^*$ or 2δ can it no longer be identified. This need not be because of a decay of the pressure signature, it is more probably a result of the differences in convection velocity of each realization causing the amplitude of the averages to become small.

If, as previously suggested, the most common feature of the structures represented by these averages is the negative going zero crossing, then a convection velocity may be defined for each separation by finding the times at which this point occurs on each trace. This has been done for the high Reynolds number case, and in addition two other Reynolds numbers which maximize the differences between the values of the scaling parameter U_o/δ^*; the results are displayed in figure 7.17(a) and (b). In all cases the convection velocity obtained is independent of the probe separation and is about 67% of the free stream velocity.

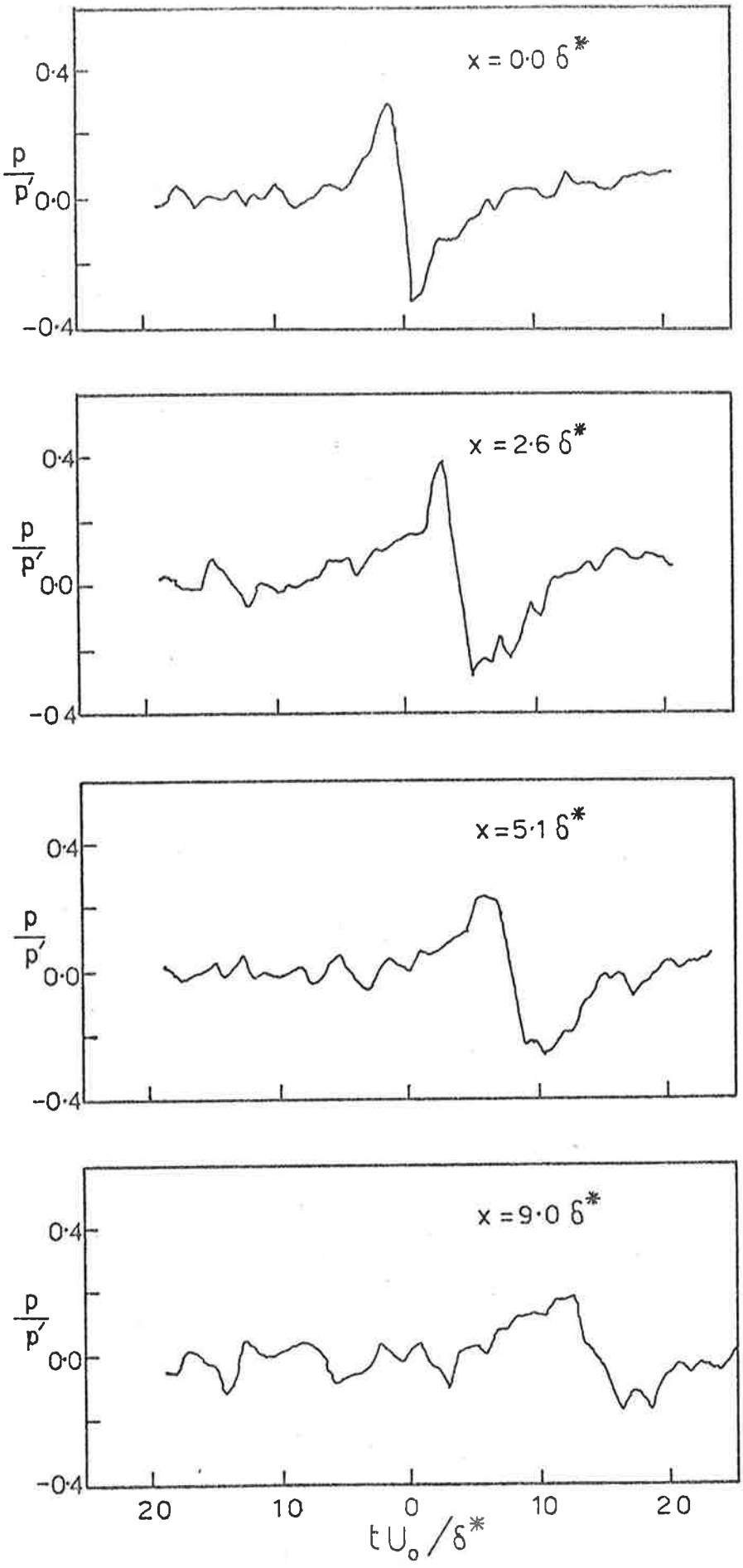

Figure 7.16 Ensemble averaged time histories of the wall pressure with the detection signal being generated on the basis of a pressure transducer placed upstream by the indicated distance.

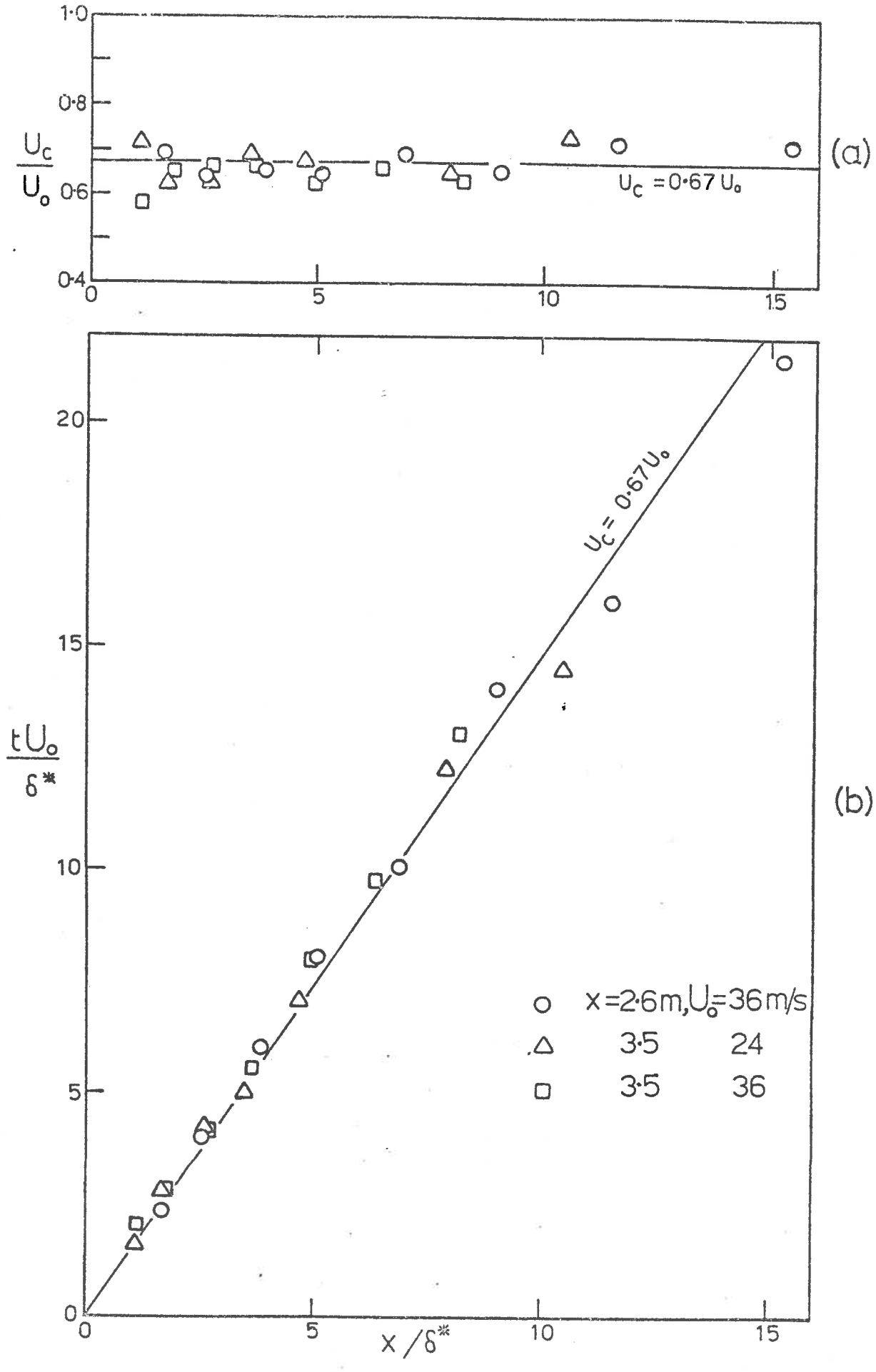

Figure 7.17 (a) Convection velocities determined from the ensemble averaged time histories of the wall pressure.

(b) Corresponding time differences for each of the transducer separations.

Burton (1974) has reported a measurement of the convection of a discrete pressure structure similar to the present structure and he finds a velocity of 0.67 U_o in excellent agreement with the present value. Emmerling's (1973) measurements show discrete small scale phenomena being convected at speeds in the same range, although some are moving rather more slowly. If, following Bull (1967), it is assumed that the dominant source of the pressure disturbances lies at a point where the local mean velocity equals the convection velocity, then the dominant source of these disturbances appears to be at $y/\delta^* = 0.5$ or $y/\delta \approx 0.07$.

The spanwise scale of the disturbances whose convection velocity has been determined, is not large, although it is rather larger than typical wall scales. In the present case the small scale excursions on the wall pressure (which characterize the disturbance) have frequently been simultaneously observed over spanwise separations of the order of 0.25δ. This observation is supported by the fact that the smoothed rectified high frequency component of the pressure is positively, although only weakly correlated over such distances.

8. A MODEL FOR THE LARGE STRUCTURE

The correlation and conditional sampling work that has been reported support the existence of a large organized structure within the boundary layer. In the sections that follow a model for this structure is proposed which consolidates these findings and which is also consistent with many of the previously reported boundary layer studies. It will become apparent that the broad features of this model are similar to those of the turbulent spot that has been observed to occur during transition from laminar flow to turbulent flow and which Coles and Barker (1975) have suggested may be the basic building block of the turbulent boundary layer.

8.1. Results for the Large Structure Streamline Pattern

Before discussing the details of the model of the large structure, an experimentally determined streamline pattern of the large structure will be presented which will show how the conditionally averaged data lead to the model that is proposed. This streamline pattern is shown in figure 8.1 and has been determined from the ensemble averaged time histories of the velocity components from the high Reynolds number flow. Some examples of these were given in figure 7.7 previously and were obtained by applying the high frequency detection criterion to the u component of velocity at various points in the layer. Ensemble averaged time histories of both the u and the v components of velocity were then computed and the enhancing technique was used to improve the averages as described in section 7.4. These averaged time histories have been computed independently of one another; however, it was demonstrated in section 6.2 that the smoothed rectified high frequency detection signal at $y/\delta = 0.25$ is

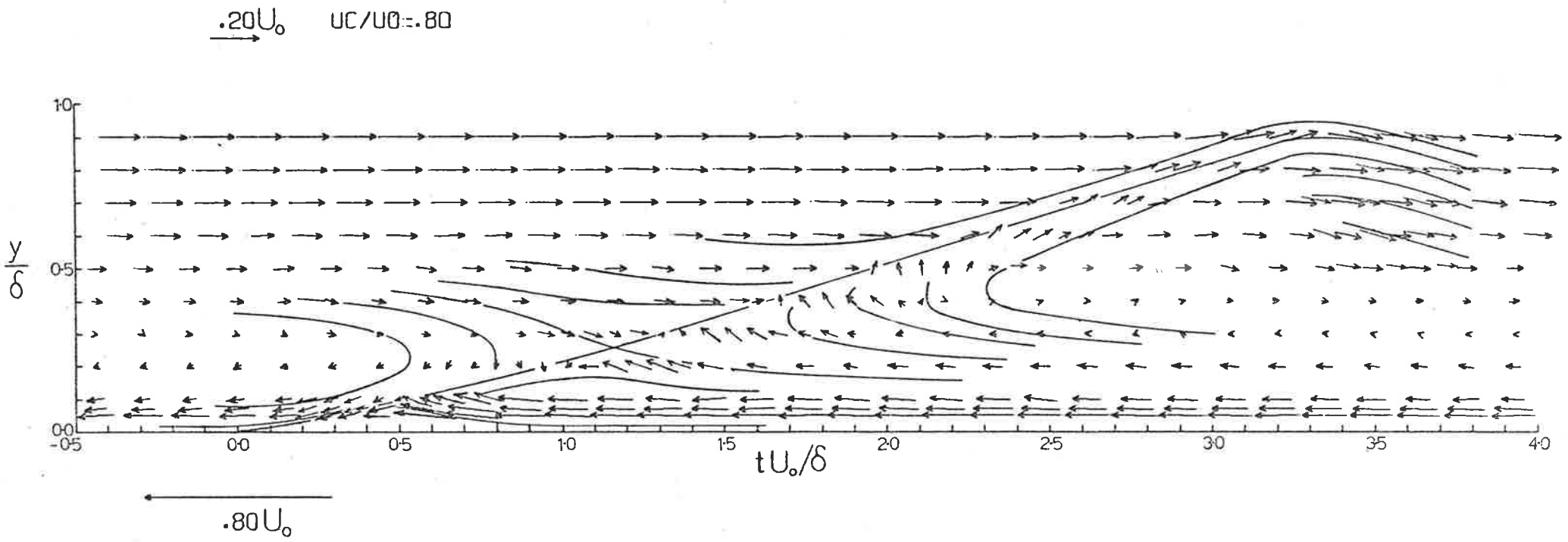

Figure 8.1 Experimentally determined streamline pattern of the large structure.

positively correlated with the corresponding component of the velocity signal at other points in the layer. This suggests that there are times when time histories resembling the averaged time histories occur simultaneously across the layer. The time delays where these correlations peak are a reflection of the way the large structures are inclined to the wall. The line corresponding to this angle of inclination has been shown in figure 5.3(b) and by positioning the independently determined ensemble averaged time histories of u and v along this line, the streamline pattern of figure 8.1 results.

In this figure the direction of each vector has been found from arctan $(v/(U_s + u))$ and the length from $((U_s + u)^2 + v^2)^{\frac{1}{2}}$ where $U_s = U_m - U_c$, U_m is the local mean velocity, u and v are as usual the fluctuating velocity components in the streamwise and normal directions and U_c is the convection velocity of the observer's frame of reference. The centre of each vector corresponds to the point of measurement in each case and the structure has been presented as the view that would be seen by an observer moving with the large structure, that is, an observer moving with a speed, U_c, which is of the order of $0.8\ U_o$. (Changing this convection speed does not change the general features of the streamline pattern greatly). Although the horizontal coordinate on the diagram is time, the pattern has intentionally been presented as an equivalent spatial distribution. Since for a fixed observer the spatial distribution of a velocity field is related to the temporal distribution by a negative relation ($x = -U_c\ t$ for a frozen distribution) it has been necessary to invert in time the ensemble averaged velocity time histories used to generate the diagram.

It is notable that the entire set of independently determined averaged time histories when presented in this way form a picture of

a single coherent and organized large structure. This is indicated by the solid lines in figure 8.1 which are not intended to represent streamlines but are presented as a visual guide only.

At distances from the wall in excess of about 0.4δ the dominant feature of the structure is a flow outward away from the wall which turns back toward the wall at the top and front of the structure. Nearer the wall the flow (in the convected frame of reference) appears to be in the upstream direction and turns toward the wall at the back of the structure. This is a consequence of the way the averaged time histories of v change across the layer. Near the wall, at the rear surface of the structure the streamlines show curvature which is convex with respect to the wall. It can be seen therefore that the large structure gives rise to warped streamlines near the wall and the importance of this finding will become apparent in the discussion of section 8.3 where it will be argued that streamline curvature could give rise to a rotational instability in that region.

The most dominant feature of the entire structure is the back or upstream surface of the structure where the steep velocity gradients exist. In this region there is the possibility for shear instabilities to occur which may give rise to the "typical" eddies that have been observed by Falco (1976). Indeed the entire structure can be seen to be very similar to the large structures photographed by Falco at a much lower Reynolds number.

Willmarth and Wooldridge (1963) have computed a large structure streamline pattern on a basis of pressure-velocity correlations. While the general rotation of that structure is the same as in the present case, it does not indicate the important way

the structure is inclined to the wall. The reason for this is related to the effect of the averaging process associated with the generation of the correlations and was discussed in section 7.6.

8.2. Details of the Large Structure Model

Having established some of the broad features of the large structure from experimentally determined data it is now possible to define the more detailed features of the model. A schematic diagram of the structure is shown in figure 8.2 and also shown are the likely wall shear stress and wall pressure distributions that would be measured near the centre line of the structure. The structure is shown in a coordinate system fixed in the large structure, that is a coordinate system in which the streamlines are changing only slowly. The convection speed of this frame of reference is not precisely known but it is likely to be of the order of 0.8 U_o which is the convection velocity of the low frequency or large scale component of the wall pressure as determined by Willmarth and Wooldridge (1962) and Bull (1967). (The precise value of the convection velocity of the frame of reference is not important as far as the present discussion is concerned.)

In this convected frame of reference this structure appears as a horseshoe vortex which gives rise to the depicted velocity field in the centre plane of the vortex. The structure is also inclined to the wall and the results of section 5.1 suggest the most probable value of this angle is about 18°. From the time scales of the wall shear velocity correlations and the time scales of the conditionally sampled measurements, the structure has a length of the order of 2δ at the wall. Additionally the large structure gives

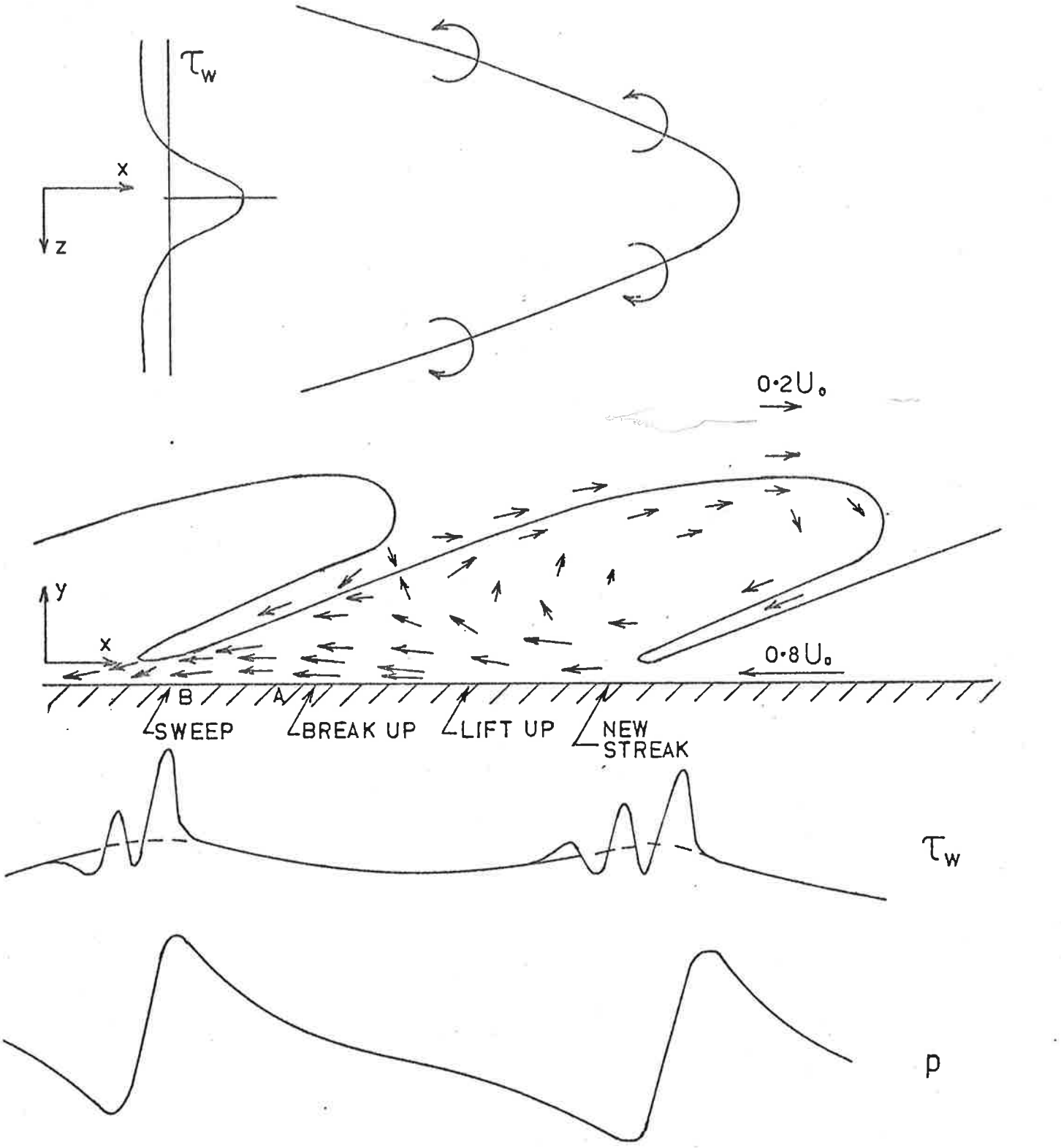

Figure 8.2 Schematic diagram of the large structure and its likely wall shear and wall pressure distributions.

rise to a "slowly" varying part in the wall shear stress and small time scale, large amplitude fluctuations occur just before the maximum in the "slowly" varying part of the signal. An example of this kind of wall shear signal is shown in figure 8.2. Evidently, the large structure gives rise to a characteristic response in the wall region which is observed as high frequency, large amplitude fluctuations. The generation of bursts and sweeps near the wall are probably part of this characteristic response. This slowly varying part of the wall shear is the component that also contributes to the spanwise wall shear correlations presented in section 5.4. A region of positive wall shear occurs along the center line of the large structure but is apparently of rather narrow extent, since the wall shear correlations are negative at larger separations. Such a wall shear distribution would account for the in phase - out of phase behaviour of the spanwise wall shear correlations that was observed in section 5.

The unusual set of spanwise velocity correlations that were reported in section 5 and which showed a characteristic feature of twin maxima, result not only from the shape of the structure but also from the nature of the flow within it. The flow at the rear of the structure is evidently stronger and more highly correlated than that at the front and the structure, therefore, has considerable streamwise asymmetry. Two hot wires at small separations will then record the passage of a side of the structure at different times so that an ensemble of such occasions for both sides will show a feature of twin maxima in the correlation. (This effect would be unlikely to occur if the structure had no streamwise asymmetry.)

A stagnation point exists on the upstream side or rear surface of the large structure where the sharp changes in velocity, discussed previously, occur. These local shear layers are likely to

give rise to the "typical" eddies marked in the smoke picture presented in figure 5.3. Along the rear part of this structure the flow is outward away from the wall and is associated with large positive contributions to the Reynolds stress. Nearer the wall the flow at the rear of the structure is toward the wall and because of the change in the mean velocity profile, this region is also associated with positive contributions to the Reynolds stress.

At the front or downstream part of the structure and at the outer edge of the layer there is another return flow toward the wall. This accounts for the way the conditionally averaged time records of v behave with increasing distance from the wall. Since the large structure is moving with a speed less than the local mean, such a flow implies a negative contribution to the Reynolds stress ($-\rho uv<0$). From the quadrant breakdown of Reynolds stress presented by Lu and Willmarth (1973), however, this quadrant ($u<0$, $v<0$) is associated with rather small values of negative stress. Therefore it is likely that this wallward flow in the outer part of the layer is a more diffuse and weaker flow than the outward migration occurring at the rear of the structure. The early work of Grant (1958) has also shown that outward migrations of fluid tend to be more highly correlated than inward migrations.

Having illustrated the large scale features of the structure, the discussion is now turned toward the organized small scale motions near the wall. In the convected frame of reference the flow near the wall appears as a flow through the base of the structure in the upstream direction. The turbulent bursts near the wall are known to be characterized by a momentum deficiency and are followed by a sweep of high speed fluid towards the wall. Since such velocity signatures have been found at the rear base of the large structure, then it is

likely that the burst-sweep cycle of events occur in this region. These have been indicated in figure 8.2 where the likely positions of "lift up", "break-up" and "sweep" have been shown. In this way the sweeps are perceived as the intense small scale shear stress fluctuations shown in the figure.

Attention is now drawn to the region marked "A" where the streamlines are convex with respect to the wall. Here the mean flow vorticity and circulation are of opposite sign and for a steady flow this is the condition given by Rayleigh (1916) for an inviscid instability. For a viscous fluid it is expected that a characteristic Taylor number will exist for this region above which a cellular structure of Taylor or Görtler vortices will be generated. (That is a secondary flow similar to Taylor vortices between rotating cylinders (Taylor, 1923) or Görtler vortices in a boundary layer on a concave wall (Görtler, 1940)). As suggested by Brown and Thomas (1977) this may be the origin of the longitudinal vortices or streaks in the wall region and at higher Reynolds numbers this basic instability may assist in the "break-up" phase of the burst cycle. (Experimental results will be presented in section 8.4 which support this model). As the longitudinal vorticity is convected into the region marked "B" in figure 8.2, the longitudinal straining motion will intensify the vorticity and return it towards the wall thereby assisting in the formation of a new streak. This behaviour is consistent with the behaviour of wall streaks as reported by Offen and Kline (1973).

The wall pressure distribution shown in figure 8.2 has been suggested on a basis of the work of section 7.6. It has been demonstrated experimentally that the component of the wall pressure generated by a source with a velocity signature characteristic of

those occurring at the rear of the structure, is a short duration region of positive pressure with smaller negative regions to either side (figure 7.15). As the back of the structure passes a measuring point at the wall, the perceived pressure time history will be a result of an ensemble of many such sources which will produce larger and larger contributions to the pressure at the wall as the distance between the source and the wall is decreased. As the base of the structure finally passes the measuring point the effect of these sources will suddenly start to diminish and the time record of the pressure will show a relatively sudden fall. In this way the indicated pressure distribution might be generated and it can be seen to be very similar to the ensemble averaged time history that was determined on a basis of the excursions in the high frequency component of the pressure signal (figure 7.11). In view of the work of section 7.6 the similarity may be a little fortuitous, but there is little doubt that regions of falling pressure can be identified in the signals at the times of significant high frequency activity. These high frequency fluctuations are not shown in figure 8.2, but will be present and are associated with the same motions that give rise to the high frequency shear stress fluctuations. The occurrence of these pressure fluctuations is then associated with the sudden change in pressure which is consistent with the correlation between the high and low frequency content of the pressure signal that was reported in section 6.1.

It can be seen from this that the wall pressure is higher upstream of the region where a burst occurs than downstream. This is in contradiction to Willmarth's (1975a) finding based upon conditionally sampled data. However, as the work of section 7.6 has indicated conditionally sampled measurements of the wall pressure require a subtle interpretation and an ensemble averaged time history need not necessarily reflect the true behaviour of the signals.

Offen and Kline (1973) have suggested that the turbulent bursts are caused by a local adverse pressure gradient at the wall with the pressure being higher downstream of the burst. They argue that the bursts may be viewed in some sense as a convected separation phenomenon. The present results do not support this mechanism and it is for this reason that the alternative mechanism, based upon a rotational instability, has been suggested. (In the convected frame of reference of figure 8.2 the flow at the wall does appear to be in a direction of increasing pressure, however it will be shown in section 8.4 that the pressure gradients are of little significance and will be unlikely to give rise to a perturbed velocity profile).

8.3 Discussion of the Model in Terms of Previous Investigations

Since the features of the model of the large structure of the boundary layer have now been presented, it is possible to compare the model with the observations of some previous investigators.

Kovasznay et al. (1970) have extensively studied the large structure in the outer intermittent part of the layer using both correlation and conditional sampling techniques. Their streamwise velocity correlation contours exhibit the kind of behaviour that might be expected of a large inclined structure that has the form depicted in figure 8.2. The conditional point averages of u and v they present, show that the front of the large structure is characterized by a flow toward the wall. At the back of the structure it is away from the wall for $y > 0.6\delta$ but toward the wall at smaller distances from the wall. Precisely the same kind of behaviour is evident in the schematic diagram given in figure 8.2 although the changeover point for the present data is rather closer to the wall.

The general rotation within the outer part of the large structure is also consistent with the turbulent zone averages of the normal component of velocity presented by Antonia (1972) for both smooth and rough walls. The present model predicts that the broad features of the large scale structure should be independent of the wall roughness, because in this model the events at the wall are simply a response of that region to the passage of the large structure so that changing the nature of the wall will not drastically change the nature of the large structure. The work of Grass (1971) has also shown that the structures responsible for the large contributions to the Reynolds stress have some similar characteristics for different types of surface roughness.

On smooth walls the characteristic response of the wall region to the passage of the large structure is the burst-sweep cycle of events. Offen and Kline (1973) have shown that the initial part of this sequence, namely the lift up of a low speed streak, is preceded by a disturbance which is moving toward the wall from the logarithmic region. In their experiments this is observed as a saw-tooth character being developed in a filament of dye introduced further upstream. The inclined rear surface of the large structure, characterized by steep velocity gradients, could possibly distort a dye filament in this way. Indeed the passage of the rear surface above a burst could also give rise to an instantaneously inflexional velocity profile being observed. The occurrence of such profiles has been reported by Kim et al (1971) and Corino and Brodkey (1969). The same rear surface is probably the interface between regions of acceleration and deceleration that is described by Nychas et al (1973). Along this interface they have observed the frequent

occurrence of a large transverse vortex whose presence is closely associated with the occurrence of bursts or ejections. The rotation of this vortex is usually in the direction of the mean vorticity, although occasionally opposite. This vortex is evidently the result of a shear instability and is likely to be similar to the "typical" eddies of Falco (1976).

The inclined rear surface of the structure can therefore be seen to be an important feature of the flow. It is characterized by large excursions in Reynolds stress and steep velocity gradients. A bandpass filtered velocity signal will be likely to show large excursions at the times when the interface passes the measuring point because of the step response of the filter. It seems probable therefore that the burst rate count data of Rao et al (1971) based on such excursions, was in fact detecting the presence of this large structural feature. This would explain why they find similar results for the burst rate across the entire layer. Likewise the counts of Lu and Willmarth (1973), taken in the outer region of the layer, of the mean period between bursts and the mean period between sweeps (based on excursions in Reynolds stress) are also probably detecting the presence of this feature.

The bursts and sweeps exist near the wall and are of small scale relative to the scale of the layer itself. In this work it has been suggested that they result from a rotational instability occurring near the wall which initially gives rise to the streaks of longitudinal vorticity that have been observed in that region. This will be discussed again in the next section. Since a vortex line cannot end suddenly, it is likely that these streaks take the form of long loops or hairpin geometries. This is consistent with

the work of Offen and Kline (1973), who have suggested that such a flow pattern is fundamental to the occurrence of bursts. As Willmarth (1975a) also suggests and as was suggested in section 8.2, it is the stretching of this vorticity that gives rise to the sequence of events (lift up, oscillation and bursting) near the wall. This kind of distribution of vorticity has also been used by Willmarth and Tu (1967) to explain the generation of their extensive set of pressure-velocity correlations.

Lastly it is interesting to note that the present model of these wall events could account for the sensitivity of the turbulent boundary layer to wall curvature, particularly concave surfaces, although care is required in making the Galilean transformation. It is also interesting to speculate whether the effect of drag reducing polymers is due to the ability of the polymer to resist the formation of the longitudinal vorticity in the unstable region. Small concentrations of the polymer would have little effect upon the large structure but the response of the wall region could be greatly modified.

8.4. Origin of the Turbulent Bursts

One of the significant features of the model that is being proposed is that it can account for the occurrence of wall streaks and their associated lift-up and bursting. The model implies that there should be an intimate relation between these events and the presence of a large structure. Experimental evidence which supports this relation has been presented in section 6 in the form of a correlation between the high and low frequency components of the wall shear stress signal.

It has been suggested that the mechanism behind this relation was in the form of a rotational instability resulting from the streamline curvature near the wall. The experimentally determined streamline pattern of figure 8.1 demonstrates this curvature and further experimental evidence will now be presented to support this feature of the model.

Shown in figure 8.3 is a view of the lower portion of the large structure that would be observed in the convected frame of reference moving at a speed of $U_c = 0.8\ U_o$. In this frame of reference the streamline pattern is steady and the streamlines are curved convex with respect to the wall which, as has already been discussed, could lead to a rotational instability in that region, giving rise to a pattern of cellular vortices in the form of wall streaks. These longitudinal vortices will then become stretched during the liftup phase (see figure 8.3). Willmarth (1975a) has discussed the behaviour of two stretched, contra-rotating vortices near a wall and has indicated that they tend to lift upward away from the wall along hyperbolic trajectories. Therefore, turbulent bursts are modelled as being a consequence of vortex stretching with the initial vorticity resulting from a rotational instability near the wall.

Brown and Thomas (1977) have also presented some computations based on the flow near the wall which allow estimates to be made of the position at which such a rotational instability might be expected to occur. It is assumed that the velocity near the wall depends on the local wall shear so that for a given spatial distribution of shear stress, a stream function at some height above the wall may be determined. The reader is referred to that report for the details of the analysis; the computations show that the wall

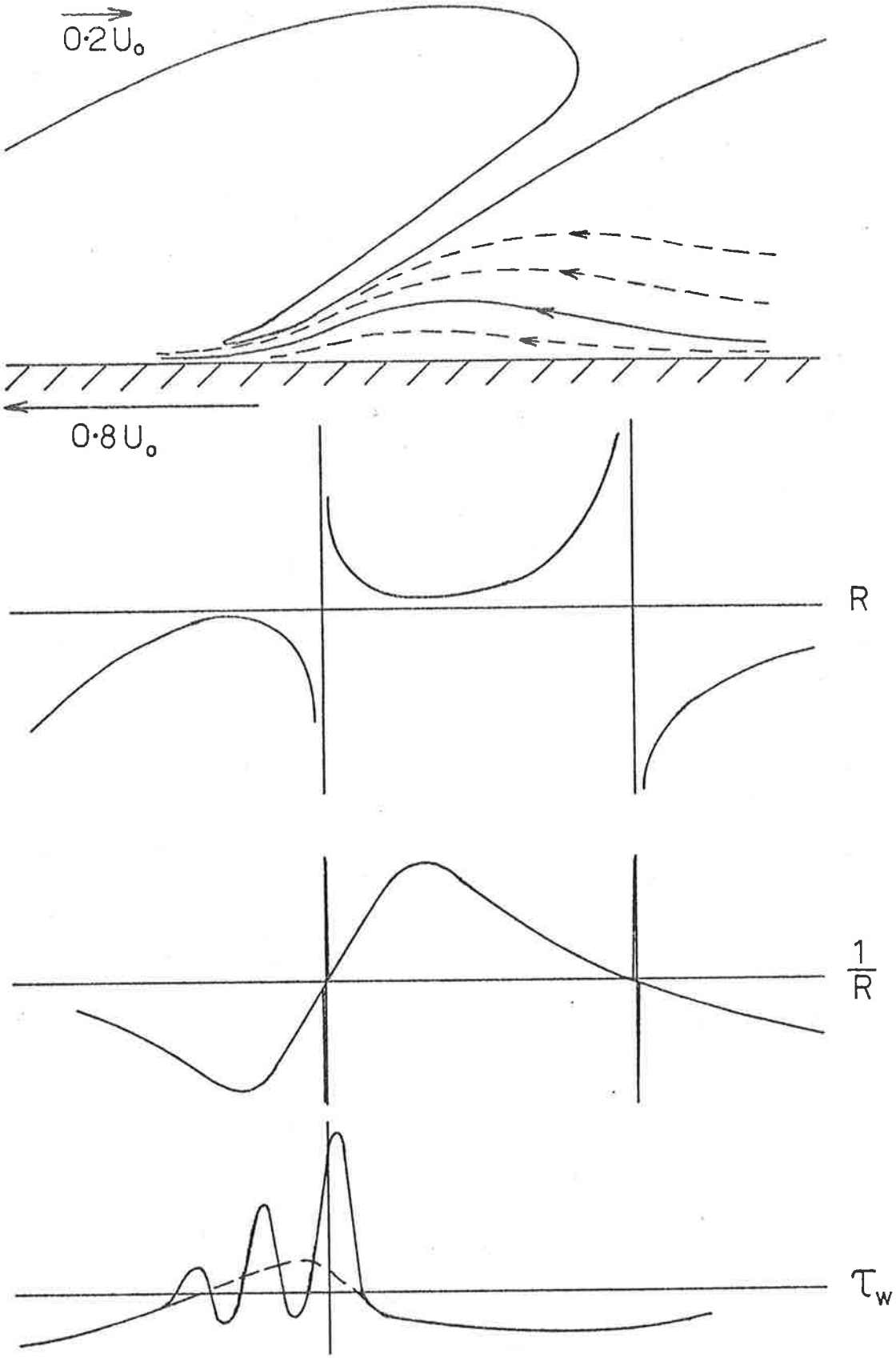

Figure 8.3 Schematic diagram of the flow at the wall beneath the large structure and the associated distributions of wall shear stress, streamline radius of curvature, and reciprocal of radius of curvature.

region is unstable by a Rayleigh criterion and that this instability will occur at about $y^+ = 50$. Thus a mean spacing of 100 wall units between streaks is not inconsistent with the model.

In the present series of experiments it would not have been possible to position a cross wire pair as close to the wall as $y^+ = 50$, however some crossed wire data was recorded at $y^+ = 170$ ($y/\delta = 0.05$) in the high Reynolds number flow and it is of interest to correlate activity at the wall (as recorded by the high frequency activity on a hot film) with the curvature of the flow further from the wall.

For a streamline, the stream function ψ is a constant and the curvature of the streamline is measured by its local radius of curvature R where

$$\frac{1}{R} = - \frac{d^2y}{dx^2} \Bigg|_{\psi = \text{const}} \tag{8.1}$$

The minus sign ensures that positive values of R are associated with convex curvature above the wall. Shown in figure 8.3 is the kind of spatial distribution of R and of 1/R that might be expected for the indicated streamline pattern. It is apparent that R can vary from $-\infty$ to $+\infty$ and it is therefore more useful to characterize curvature instead by 1/R which also has large excursions, but of only very narrow extent.

Estimations of 1/R can now be made on the basis of crossed-wire measurements near the wall. Along a streamline with ψ = constant, there is by definition

$$\frac{dy}{dx} = \frac{v_s}{u_s}, \tag{8.2}$$

where v_s and u_s are the values of the normal and streamwise components

of velocity in the convected frame of reference. Combining 8.1 and 8.2 yields

$$\frac{1}{R} = \frac{-d}{dx}\left[\frac{v_s}{u_s}\right]\Bigg|_{\psi = \text{const.}} \tag{8.3}$$

Now the crossed-wire measurements have been taken at points characterized by y = constant as opposed to ψ = constant. These two variables are related through the von Mises transformation,

$$\psi(y = y') = -\int_0^{y'} u_s dy \tag{8.4}$$

If the mean velocity with respect to the wall is U_m, then in the convected frame of reference $u_s = U_m - U_c + u$ and $v_s = v$. Therefore 8.4 becomes

$$\psi = U_c y' - \int_0^{y'} U_m(y)dy - \int_0^{y'} u(x, y)dy \tag{8.5}$$

In this equation the third term will be small in relation to the first and second terms, and therefore lines of constant ψ can be approximated by lines of constant y. The implication is that the radius of curvature of the streamline pattern is quite large near the wall so that time records of u and v at a fixed height above the wall can be interpreted in terms of changes in the streamline curvature. For this case equation 8.3 becomes

$$\frac{1}{R} = \frac{-d}{dx}\left[\frac{v_s}{u_s}\right]\Bigg|_{\psi = \text{const}}$$

$$= \frac{1}{U_c}\frac{d}{dt}\left[\frac{v_s}{u_s}\right]\Bigg|_{y = \text{const}} \tag{8.6}$$

where the spatial relationship has been converted to a temporal one by use of the convective relation $x = -U_c t$. Temporal records of crossed-wire data may therefore be used to estimate a temporal record of 1/R.

This has been done for the high Reynolds number flow at $y^+ = 170$ where $U_m = 0.62\ U_o$ and as before $U_c = 0.8\ U_o$. Because of the difficulty of accurately differentiating a signal of significant high frequency content, it is useful first to smooth the records of u and v. This has been done by low pass filtering the time records with the same filter cutoff that has been used in most of this work ($\omega_c \delta^* / U_o = 0.43$). Such a process restricts the behaviour of the curvature so that the small scale streamline curvature is lost. It is only the curvature generated by the large scale structures that will remain.

The rms level of 1/R that was obtained was 8.2 m^{-1} which for $\delta = 0.04$ m suggests typical values of R in excess of 3δ. Nearer the wall the values are likely to be much larger and will be infinite at the wall. Although the resulting time record of 1/R was also found to have some large positive and negative excursions (see figure 8.3) it was not found necessary to truncate the signal in any way as they made a negligible contribution to the rms level of the record.

Cross correlations have been computed between the time records of 1/R and both the wall shear stress and the smoothed rectified high frequency component of wall shear. The hot film was positioned directly beneath the cross wire pair and the results are shown in figures 8.4(a) and (b). The correlation with the original wall shear signal is dominated by a negative region at negative

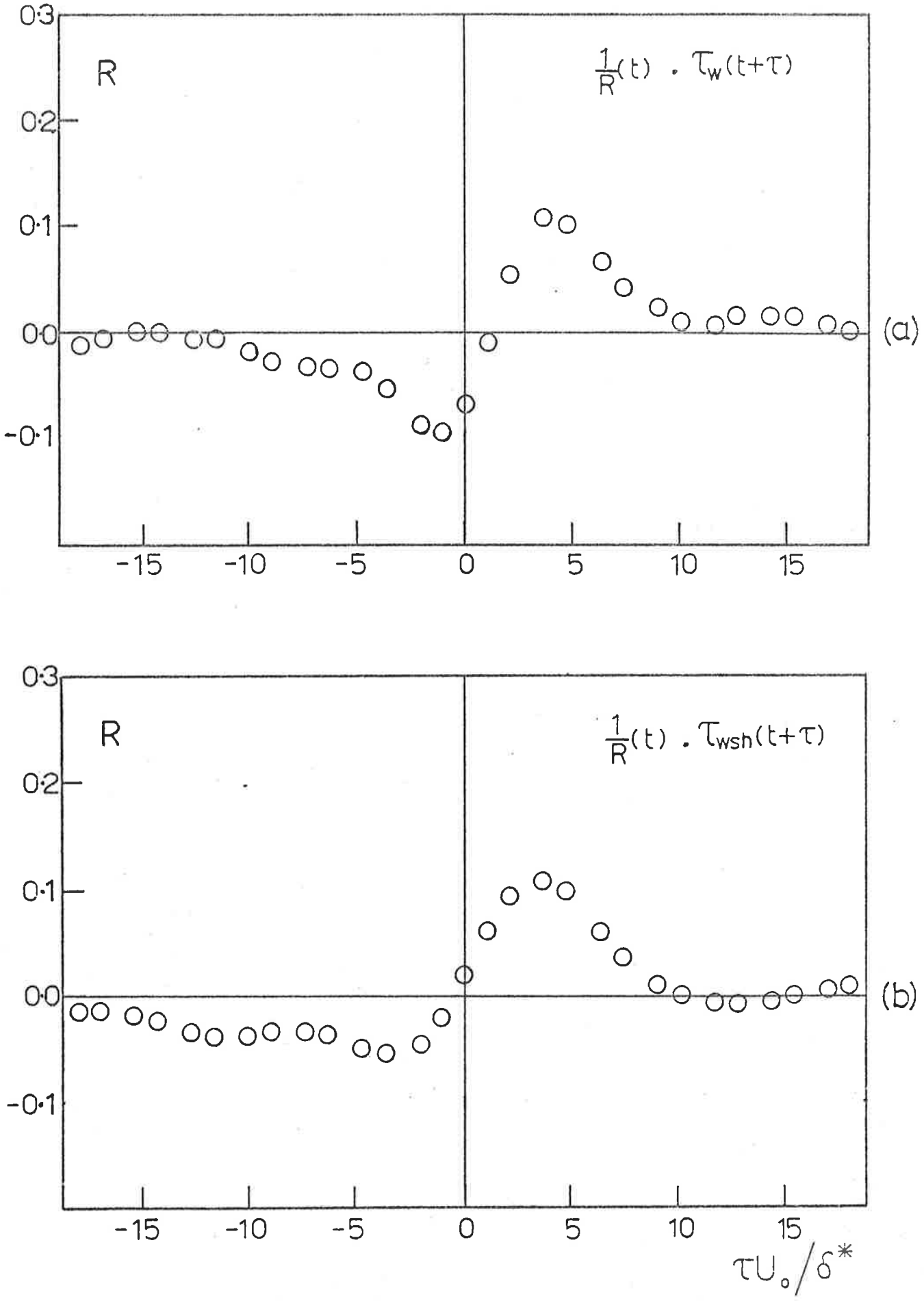

Figure 8.4 (a) Correlation between the wall shear stress and the reciprocal of the radius of curvature of the streamlines at $y^+ = 170$.

(b) Correlation between the smoothed rectified high frequency component of wall shear and the reciprocal of the radius of curvature of the streamlines at $y^+ = 170$.

time delays and conversely a positive region at positive time delays. The distributions of wall shear and reciprocal of radius of curvature shown in figure 8.3 could account for this correlation with positive values of wall shear being associated with positive values of 1/R at a time delay which is a reflection of the way the structures are inclined to the wall.

The correlation with the smoothed rectified high frequency component of wall shear is dominated by a positive peak only. This is important and indicates that small scale wall shear fluctuations occur most often when the streamline curvature is positive, that is, convex with respect to the wall. This curvature is a consequence of the passage of the large structure which warps the streamlines near the wall.

If is of interest to speculate as to the role the streamwise wall pressure gradient due to the large structure might play in this process and in the turbulent bursting process. From figure 8.2 it can be seen that, in the convected view, the wall flow is into a region of increasing pressure which may change the velocity profile and thereby affect the stability of that region. By considering a similar case in Couette flow, however, inflexional velocity profiles will not develop and the flow should, in fact, become more stable. In any case, the pressure forces (characterized in Couette flow by the parameter $P = h/2\overline{\tau_w}$. dp/dx for small pressure gradients) due to the large scale motions, are very small near the wall ($P < 0.01$ at $y^+ = 50$). Therefore, the initial vorticity distribution that becomes stretched giving rise to the turbulent bursts (section 8.3), would not appear to arise from the effects of a streamwise pressure gradient. The pressure field depicted in figure 8.2 could possibly

assist in the generation of the streamline curvature discussed above, but by carrying the Couette flow analogy further, it can be shown that this has an exceedingly weak and negligible effect. The streamline curvature must evidently result from the vertical pressure gradient of the large structure as opposed to the streamwise gradient.

8.5 Origin of the Large Structure

A question of some interest that arises is the origin of the large structure and related to this is the question of the role of the events at the wall in relation to the large structure itself. In view of the earlier findings based on the wall shear velocity correlations and in view of the previous discussion, the model being presented is that bursts near the wall do not lead directly to a new large structure. As has been demonstrated by the work of Kline et al. (1971) and Willmarth and Lu (1971) and others, however, the wall events are associated with large values in Reynolds stress and turbulence production.

Therefore, not surprisingly, the burst-sweep cycle of events must play a role in the dynamics of the process as a whole in order that an energy balance is maintained. Therefore,while they do not appear to directly generate the large structure, they must supply the existing large structure with smaller scale turbulent energy because even a moderate amount of wall suction (to suppress the wall events) leads to the suppression of the entire turbulent field. This still leaves unanswered the question of the origins of the large structure. From the correlations of the streamwise component of velocity at various streamwise positions presented by Kovasznay (1967) it is

clear that the life times of the structures are very large indeed and they can be correlated over distances of 20δ or more. Therefore, local measurements of the kind presented here are unlikely to provide answers to the question of origin.

It is possible to speculate, however, by drawing an analogy with the plane turbulent mixing layer where the large structures observed by Brown and Roshko (1974) can be seen to have their origins near the start of the layer. As the layer grows these structures amalgamate to form larger and larger structures which thereby maintain the linear growth rate. Furthermore, this amalgamation process as described by Brown and Roshko (1974) is quite a sudden and abrupt process in relation to the lifetimes of the structures. If an analogous process occurs in the boundary layer, the large structures may be thought of as originating at the time of transition. As they are convected downstream they grow and start to become crowded together and are likely to amalgamate. If such an amalgamation is also sudden, it is possible that a new large structure may be suddenly perceived at a given point and the sequence of events from that time onwards will probably be as described by Kovasznay et al (1970). The new structure (which it should be remembered is three dimensional) would have a momentum defect and there would be a strong upwelling of fluid from within it because of the induced flow of the vortex line of the structure. The mean flow would accelerate it, so that it extracts energy from the mean flow, and it may become stretched in the mean flow direction. As the layer grows further this process will repeat itself. An evolving process such as this could then give rise to the asymmetrical behaviour of the correlations between intermittency

and normal velocity component that has been reported by Kovasznay et al. (1970).

At points just downstream of the transition region where the Reynolds number is low, the scale of wall events (streaks and bursts) is comparable to the scale of the boundary layer and it is possible that in that region the bursts help to generate the large structures in a direct sense, whereas they may play a more indirect role at higher Reynolds numbers.

It is clear that the same large structure is not the building block of fully developed pipe flow and yet the flow near the wall in a pipe is similar to that in a boundary layer (wall similarity). This is, however, quite likely if a rotational instability is the mechanism behind the events at the wall as this region requires only an impressed streamline curvature due to the passage of a large structure to give rise to the instability described. It is not difficult to imagine such a large scale motion as occurring in a pipe or channel flow.

9. SUMMARY AND CONCLUSIONS

This research has lead to the development of some new experimental and data analysis techniques which have shed considerable light upon an organized large structure that appears to be the basic building block of the turbulent boundary layer. A model of this structure has been developed which is consistent with previously reported findings.

In what follows the techniques that have been used are briefly reviewed and the results that they have yielded are also summarized.

(i) A method for the manufacture of hot film shear stress gauges has been developed which allows a number of films to be produced simultaneously and all of which have very well matched geometrical and electrical properties. As a consequence these films have almost identical responses and sensitivities to wall shear stress fluctuations. The dynamic wall shear signal from these devices has a character very like that of a hot wire signal recorded near the wall and has a power spectrum which appears to display a mixed scaling. The low frequency region ($\omega\delta^*/U_o<0.5$) scales on outer layer variables while the remaining high frequency region scales on inner layer variables. Integration of the spectral data indicate a mean square wall shear value which is 22% of the mean shear at all the Reynolds numbers studied. The spectral region which scales on outer layer variables makes about a 70% contribution to the mean square wall shear, suggesting a strong outer layer influence. Further direct evidence for this influence lies in the finding that the dynamic wall shear can be correlated in the spanwise direction over a distance of about 0.7δ, or more

than 2000 ν/U_τ. This is a scale typical of the outer layer and very much greater than characteristic wall scales.

(ii) The fluctuating wall pressure has been measured with both flush mounted transducers and pinhole orifice microphones. Discrepancies between the results from each transducer type have been demonstrated; these appear to result from the surface discontinuity of the pinhole microphone. From an analysis of the recordings from the flush mounted transducers and comparison with previously reported data, it would appear that the measured rms wall pressure scales on the mean wall shear for a given transducer size expressed as dU_τ/ν. Although the Reynolds number dependency of the rms pressure that would be measured by an infinitely small transducer can not yet be determined, the present data suggest that it too would scale on the mean wall shear. Additionally the spectrum of the wall pressure signal appears to show a scaling similar to that of the wall shear spectrum with the low frequencies scaling on outer layer variables and the high frequencies scaling on wall variables. These statements can not, however, be considered as definite conclusions because of both the severe resolution effects and the limited Reynolds number range of the data.

(iii) Use has been made of the simultaneous recordings taken from an array of hot wires spaced out in both the normal and transverse directions. The use of arrays is not new, although this is possibly the first attempt to find a three-dimensional structure throughout the layer by simultaneous measurements from an array of anemometers spaced in the transverse direction.

The data from the rake of wires in the normal direction have indicated significant correlation between the wall shear

and the outer flow even at a high Reynolds number. By a conditional analysis based upon short time correlation techniques, it appears that this correlation is the result of a large organized structure existing on the scale of the boundary layer thickness, as opposed to smaller scale motions migrating away from the wall. At those times when the correlation across the layer is particularly large, then the wall shear stress has been shown to also have enhanced correlation in the spanwise direction, which further verifies the large structure concept. This large structure is inclined to the wall at an angle of about 18° which is in close agreement with features observed in recent flow visualization experiments.

The data from the spanwise rake of wires have indicated a remarkable degree of structural organization in that direction. The long time correlation between any two recordings of the streamwise component of velocity at points separated only in the spanwise direction, shows, at certain separations, a characteristic feature of twin maxima with symmetry about the axis at zero time delay. This is postulated to arise from a structure which has regions that lie oblique across the flow and a conditional analysis of the data, based once again upon conditionally ensembled averaged short time correlations, has shown this to be so. It appears from this work that the structure has considerable streamwise asymmetry and that the flow at the rear of the structure dominates over and is more correlated than the flow at the front of the structure. Furthermore, this work has shown the structure to have a spanwise scale of the order of δ, and that its sides make an angle with the stream direction of between 20 and 25°. There is some indication that the organized

large scale motion in the turbulent boundary layer may have features not unlike those of the turbulent spot.

(iv) Having established the existence of the large scale organized structure, attention was turned toward the small scale features of the various signals. A novel technique was developed to correlate between the occurrence of small scale, high frequency excursions on a signal and the large scale or low frequency content of the signal. This technique has been based upon the generation of the smoothed, rectified high frequency component of the signal which is then correlated with the low frequency component of the signal. For the shear stress the resulting correlation is very large and peaks at a non-zero time delay. This indicates that high frequency disturbances occur most often when the slowly varying part of the wall shear is high and that there is a definite phase relation between the two scales of motion. Since the slowly varying part of the wall shear is also the part which is correlated with the flow across the entire layer, then it appears that the passage of the large structure gives rise to a characteristic small scale response in the wall region. The turbulent bursts and sweeps are evidently part of this response.

The correlations between the high and low frequency components of the velocity signals at increasing distances from the wall, show a different behavior from that of the wall shear. They reflect a change in the nature of the high frequency content of the signals and indicate the increasing appearance of a steep positive step in velocity (in time) from a negative value to a positive value. This feature can be simultaneously observed across the entire layer and appears to be a signature of the back or upstream side of the large eddy.

The same technique, when applied to the wall pressure signal, indicates that small scale pressure fluctuations occur predominately when the slowly varying part of the pressure is falling, in time, from a positive value to a negative value. On a basis of the conditional sampling and averaging results, it is demonstrated that such a pressure field could arise from the large structure. The small scale pressure excursions associated with this feature are then a signature of the small scale response of the wall region to the passage of this structure.

(v) In order to resolve more of the details of the large structure, crossed wire measurements were undertaken at various points in the layer. Ensemble averaged time histories of various quantities were then generated at those times when the large structure was thought to be present. These times were determined from an unbiased detection criterion based upon the high frequency excursions which were known to be associated with the presence of the large structure. This work has shown that the organized structure makes very large contributions to the Reynolds stress with the conditionally averaged contributions being typically twice the mean value near the wall and nearly sixteen times the mean in the outer part of the layer. The corresponding ensemble averaged time histories of u and v have been used to construct a streamline pattern which shows a large rotating structure characterized by steep velocity changes at its rear or upstream surface. The flow along this interface is outward away from the wall with a more diffuse return flow at the front of the structure.

(vi) Conditional ensemble averaged time histories of the wall pressure have also been generated on a basis of the excursions of a velocity signal recorded just above the point where the pressure is measured. This work was found to require a rather cautious interpretation for two reasons. Firstly, an averaged time history need not necessarily represent the character of the individual realizations used to generate the average. This is because of the cumulative effects of the random variations in the phase and scale of each realization. Secondly, because of the randomness of the field, when detection is based upon the velocity at a given point, evidently only the component of the total pressure field, that is associated with sources in the vicinity of that point, remains after the averaging process. If allowance is made for these effects then some of the averaged pressure time histories have a character that is similar to what might be expected from measured velocity fluctuations if there is dominance of the turbulence-mean shear source term.

On a basis of this work in conjunction with the known streamline pattern of the large structure, the pressure signature of the large structure could be determined as being characterized by a slow rise in time, followed by a sudden fall in pressure. Such features have been observed to occur and have been tracked downstream at a convection velocity of $0.67\ U_o$.

(vii) The small scale distrubances near the wall (i.e. bursts and sweeps) are evidently the result of a vortex stretching process (Willmarth, 1975a) and in view of the strong correlation between the small scale and large scale features of the

signals near the wall, it would appear that the large structure is responsible for the generation of the initial vorticity distribution that becomes stretched. It does not appear, however, that the pressure field of the large structure plays a direct role in this generation process as the pressure field of the large eddy is of neither the correct character nor of sufficient intensity to significantly perturb the velocity profile in the way suggested by other workers.

For this reason an alternative concept based upon a rotational instability has been suggested, in which a Taylor-Görtler mechanism near the wall gives rise to the well documented streaks of longitudinal vorticity in that region. The stretching of this vorticity leads to the small scale turbulent bursts which are in turn followed by sweep motions as the vorticity is swept back toward the wall. This second process gives rise to the positive going, small scale wall shear stress excursions that have been observed. Experimental evidence to support the description of the entire process lies in the finding that, in a frame of reference moving with the large structure, these shear stress fluctuations are associated with a flow near the wall whose streamlines are in opposition to the mean vorticity. This is a necessary (although not sufficient) condition for a rotational instability to occur. This, it is suggested, provides the link between the small scale events at the wall and the large structure in the boundary layer.

In view of the great disparity in scale between these two types of motions, and in view of the nature of the reported wall shear-velocity correlations, it would appear that the

large structure does not arise as a direct consequence of the repeated pairing of the small scale disturbances originating from the wall. These events must play a role in the process as a whole, but although only speculative, the large structure probably has its origins much further upstream, possibly even at the time of transition.

* * * * * * * * * * *

Appendix A

The Time Response of Hot Films

The following presents an analysis of the dynamic behaviour of a small hot film element in a constant temperature feedback operating mode. It was originally derived by G.L. Brown of the University of Adelaide, and the author is grateful for allowing it to be presented here. Only the important points of the analysis will be discussed.

The film is mounted on glass and shown schematically in figure A.1. It is subjected to a step change in convective heat transfer q_a by an amount Q. These give rise to current and resistance perturbations i_f and r_f but since second order terms are small, the perturbation in power dissipation from the film is $2\ I_f\ R_f\ i_f$, so that an energy balance gives

$$q_g = \frac{2\ I_f\ R_f\ i_f\ (t)}{A_f} - Q \qquad (A.1)$$

Now conduction into the substrate of the film may be assumed one dimensional so that the equation for the temperature is

$$\frac{\partial T}{\partial t} = \kappa \frac{\partial^2 T}{\partial y^2} \qquad (\kappa = \text{thermal diffusivity of glass})$$

or in terms of Laplace transforms

$$\frac{s}{\kappa} \cdot \overline{T}(y,s) = \frac{d^2\overline{T}(y,s)}{dy^2}$$

which has a solution $\overline{T} = \overline{T}(y=0,s)\ e^{-(\frac{s}{\kappa})^{\frac{1}{2}}y}$.

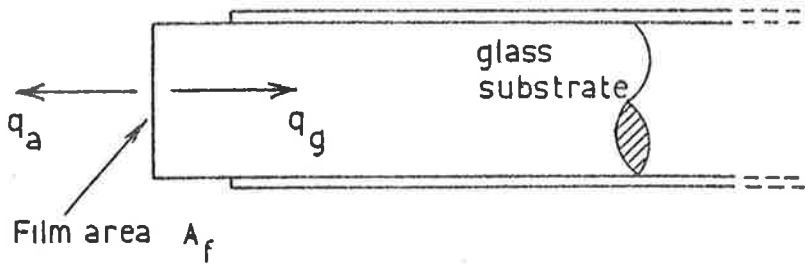

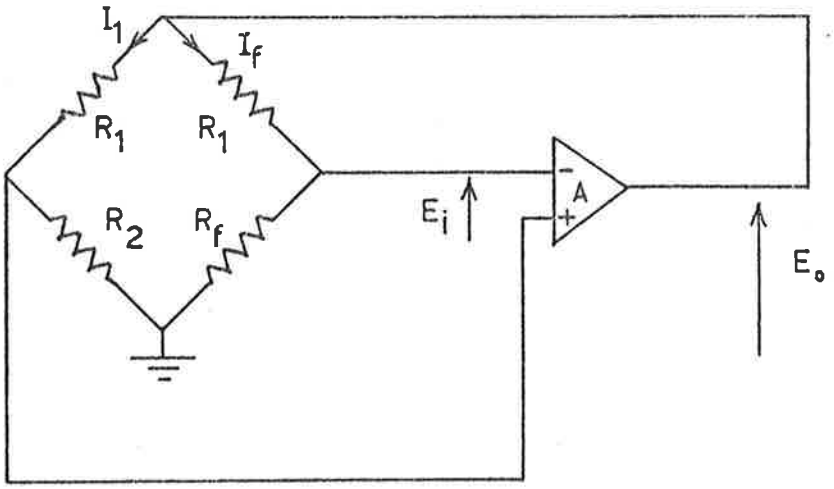

Figure A.1. A thin film subjected to a sudden change in convective heat transfer and the associated feedback bridge.

But the Laplace transform of the heat flux per area $\bar{q}$ (y=0) is

$$\bar{q} = -\lambda \left.\frac{d\bar{T}}{dy}\right|_{y=0}$$

λ = thermal conductivity of glass.

so that $\bar{T}(y=0) = \bar{q}(y=0)\ (\frac{s}{\kappa})^{-\frac{1}{2}} \frac{1}{\lambda}$.

In order to find the inverse transform of this relation, the convolution theorem is used which yields the following relation for T(y=0, t),

$$T(o,t) = \frac{1}{\lambda} \cdot (\frac{K}{\pi})^{\frac{1}{2}} \int_0^t q_g(t-\tau) \cdot \frac{d\tau}{\tau^{\frac{1}{2}}}$$

and substitution from equation A.1 for q yields

$$T(o,t) = \frac{2\ I_f\ R_f}{A_f . \lambda}\ (\frac{K}{\pi})^{\frac{1}{2}} \int_0^t i_f(t-\tau)\ \frac{d\tau}{\tau^{\frac{1}{2}}} - \frac{2Q}{\lambda} \cdot \frac{K}{\pi} \cdot t^{\frac{1}{2}} \quad (A.2)$$

where $R_f = R_o\ (1 + \alpha \Delta T_f)$

and $r_f = R_o . \alpha . T_g(o,t)$

α = temperature coefficient of resistivity of film.

This result is important because it relates temperature variations to current changes within the film. It is however also clear that some account needs to be taken of the way the bridge circuit itself operates.

Under steady d.c. conditions it may easily be shown that

$$\frac{E_i}{E_o} = \frac{R_1}{R_1 + R_2}\ 1 - \left(\frac{R_1 + R_2}{R_1 + R_b}\right) . \quad (A.3)$$

Under transient conditions however, E_i and E_o are perturbed by some small amount ℓ_i and ℓ_o where $\ell_o = -A\ell_i$ and this gives rise to current changes i_1 and i_f and a film resistance change r_f. By simple application of Ohms Law it is possible to write

$$\ell_o = i_1 (R_1 + R_2) = i_f (R_1 + R_f) + I_f r_f$$

$$\ell_1 = R_1 (i_1 - i_f)$$

and since $\ell_o = -A\ell_i$ it is possible to further write

$$i_1 - i_f = - \frac{i_f (R_1 + R_f) - I_f r_f}{AR_1}$$

After some manipulation and making use of the result in equation A.3, i_f is finally obtained as

$$i_f = \frac{-I_f R_1}{(R_1+R_f)(R_1+R_2)} \frac{1}{\frac{E_i}{E_o} + \frac{1}{A}} \left| 1 + \frac{R_1+R_2}{AR_1} \right| r_f$$

Now for $A \gg 1$ and $R_f \approx R_2$

$$\therefore \quad i_f = -Cr_f \text{ where } C = \frac{I_f R_1}{(R_1+R_f)^2} \frac{1}{\left(\frac{E_i}{E_o} + \frac{1}{A}\right)}$$

$$= -C.R_o.\alpha.T_g(o,t)$$

By this means it has been possible to relate the current perturbations in the film to the electrical parameters of the bridge as well as the temperature of the film. By combining this result with equation A.2 we get the following integral equation for the temperature of the film

$$T_g(o,t) = \frac{-2\ I_f\ R_f\ \kappa^{\frac{1}{2}}}{A_f\ \pi^{\frac{1}{2}}}\ .\ C.R_o^{\alpha} \int_0^t T_g(o,\ t-\tau)\ \frac{d\tau}{\tau^{\frac{1}{2}}} \qquad (A.4)$$

$$- \frac{2Q}{\lambda} \left(\frac{\kappa t}{\pi}\right)^{\frac{1}{2}}$$

Clearly any attempt to determine the response time of the film in the feedback loop requires a solution of A.4 and this is a complex problem. Some simplification is possible by introducing a function f(t) where

$$T_g = \Delta T\ (1 + f(t)),$$

where
$$\Delta T = \frac{-Q\ A_f}{2\ I_f^{\ 2} R_f} \left(\frac{E_i}{E_o} + \frac{1}{A}\right) \frac{(R_1+R_f)^2}{R_1 R_o^{\alpha}},$$

and we are now interested in finding the time for f(t) to become small. By choosing ΔT in this way the second term on the right hand side of equation A.4 can be used to cancel out a term generated by taking the integral of $1 + f(t-\tau)$ so that one obtains after some manipulation

$$1 + f(t) = -S \int_0^t f(t-\tau)\ .\ \frac{d\tau}{\tau^{\frac{1}{2}}}\ , \qquad (A.5)$$

where
$$S = \frac{2\ I_f^{\ 2} R_f}{A_f\ \lambda}\ .\ \left(\frac{\kappa}{\pi}\right)^{\frac{1}{2}}\ .\ \frac{1}{\left(\frac{E_i}{E_o} + \frac{1}{A}\right)}\ .\ \frac{R_1 R_o^{\alpha}}{(R_1+R_f)^2}\ .$$

Now in order to write equation A.5 in a form that is more easily soluble three changes in variable should be made.

Firstly rewrite it in terms of $r = \frac{t-\tau}{t}$,

$$f(t) = -1 - St^{\frac{1}{2}} \int_0^1 (1-r)^{-\frac{1}{2}}\ f(r,t)\ dr,$$

and suppose $f(t) - g(St^{\frac{1}{2}}) = g(\zeta)$

$$\therefore \qquad g(\zeta) = -1 - \zeta \int_0^1 (1 - r)^{-\frac{1}{2}} \, g(\zeta r^{\frac{1}{2}}) \, dr.$$

Now if a second change in variable is made by putting $\zeta r^{\frac{1}{2}} = \phi$ one obtains

$$g(\zeta) = -1 - \frac{2}{\zeta} \int_0^\zeta \phi \, (1 - \frac{\phi^2}{\zeta^2})^{-\frac{1}{2}} \, g(\phi) \, d\phi, \qquad (A.6)$$

and if $\eta = 1 - \phi/\zeta$ then

$$1 + g(\zeta) = -2\zeta \, g(\zeta) \int_0^1 (1 - \eta) \, . \, 2^{-\frac{1}{2}} . \, (1 + \frac{\eta}{4}) \, . \, \eta^{-\frac{1}{2}} . \, d\eta.$$

If it is further assumed that the major contribution occurs as ϕ/ζ approaches unity then we get

$$1 + g(\zeta) = -2\zeta \, g(\zeta) \, 2^{-\frac{1}{2}} . \, 2.$$

Since we are interested in the response time, then this is the same as asking at what time does $g(\zeta)$ become small. Since we can write for $g(\zeta)$

$$g(\zeta) = \frac{-1}{1 + 2. \, 2^{\frac{1}{2}}\zeta},$$

then $g(\zeta)$ is down by 90% say, if $\zeta \approx 3.2$ and this occurs if $t^{\frac{1}{2}} = 3.2/S$. Therefore the response time of the film T_F may be approximated as

$$T^{\frac{1}{2}} = \frac{3.2 \, A_f \pi^{\frac{1}{2}} \lambda}{2 \, I_f^{\,2} \, R_f \, \kappa^{\frac{1}{2}}} \cdot \frac{E_{off}}{E_o} \cdot \frac{(R_1 + R_f)^2}{R_1 \, R_o^{\,\alpha}}, \qquad (A.7)$$

where $\frac{E_{off}}{E_o} = \frac{E_i}{E_o} + \frac{1}{A}$ and E_{off} = offset voltage.

This result clearly demonstrates the need for small films operating at high overheat ratios. It is clear also that the material for the substrate should be chosen carefully.

The importance of having the correct offset voltage is apparent and the system will become unstable if this is too low. Perry and Morrison (1971) have similarly demonstrated that offset control is important when using hot wires and behaves in some respects like a damping term.

Appendix B

High frequency wall-pressure fluctuations in turbulent boundary layers

M. K. Bull and A. S. W. Thomas

Department of Mechanical Engineering, University of Adelaide, South Australia
(Received 2 June 1975; final manuscript received 29 December 1975)

Directly comparable spectral measurements with piezoelectric and pinhole-microphone transducers show pinhole measurements to be significantly in error. The increase in measured rms pressure with reduction of transducer size is not nearly as dramatic as previous work has suggested.

The transducer used to measure wall-pressure fluctuations in a turbulent boundary layer should form an integral part of the boundary surface and be smaller than the smallest length scale of the fluctuations. Piezoelectric transducers meet the first criterion, but in most experiments they appear to have suffered limited high-frequency resolution, even for ratios of diameter d to boundary-layer displacement thickness δ^* approaching 0.1. A small capacitor microphone in conjunction with a pinhole allows still smaller d/δ^*, but continuity of the boundary surface is not preserved.

Pinhole microphone measurements by Blake,[1] Emmerling[2] and others have indicated significant high-frequency contributions to the pressure spectrum, not detected by earlier piezoelectric measurements (such as those of Willmarth and Roos,[3] Schloemer,[4] and Bull[5]). In a recent review, Willmarth[6] concludes, on the basis of optical measurements by Emmerling,[2] that these contributions are not produced just by the flow disturbance due to the pinhole. However, this leaves unanswered the question of whether the pinhole measurements contain any or no contribution resulting from flow disturbance caused by the pinhole itself. We have therefore made measurements with piezoelectric and pinhole transducers of the same diameter in the same flow.

The boundary layer was that one flat wall of an open-circuit wind tunnel (see Lim[7]) with a working section nominally 230×230 mm and 5 m long. One wall of the working section is flexible and allows accurate setting of the pressure gradient in the flow. There is a sonic choke downstream of the working section. The tests

reported are for zero-pressure gradient.

Power spectral densities ϕ were measured for two values of δ^* (in the ratio $\approx 1.4:1$) at each of three flow speeds (range 1.5 : 1) with the 0.75 mm diameter transducers detailed in Fig. 1. All transducers were calibrated in a shock tube and the calibration checked in an acoustic coupler (for frequencies up to 12 kHz) before and after each run. The resonance frequency of the pinhole and cavity was about 30 kHz. Measurements covered the range $200 \leq f \leq 12\,500$ Hz.

The results, nondimensionalized by wall variables (Fig. 2), form two distinct sets according to transducer type; the pinhole results agree closely with those of Blake[1] and the piezoelectric results (considering dU_τ/ν differences) are consistent with those of Lim,[7] Bull,[5] and Willmarth and Roos.[3] They indicate that for $\omega\nu/U_\tau^2 > \approx 0.1$ the pinhole does produce a spurious contribution to ϕ. Figure 2 also shows ratios of measured values. In the extreme case the pinhole result is larger by a factor of about 4.

Measurements were then made with the piezoelectric transducer converted to a pinhole transducer by fitting a cap to it (see Fig. 1). The pinhole diameter was exactly the same as that used with the capacitor microphone. The instrument had a resonance frequency the same as that of the pinhole capcacitor microphone (30 kHz). Further measurements were made with a second cap having a pinhole of the same diameter and length but no cavity. Spectral densities from both devices are shown in Fig. 3; they lie precisely on the mean curve of the pinhole capacitor microphone data given in Fig. 2.

The measurements were then repeated with the pinhole and cavity of the first cap filled with silicone grease to again produce a continuous boundary surface. This transducer still showed a normal response to shock and acoustic testing, but with sensitivity considerably below that of the original transducer (by a factor of about 2). The results (Fig. 3) lie on the mean curve of the direct piezoelectric measurements.

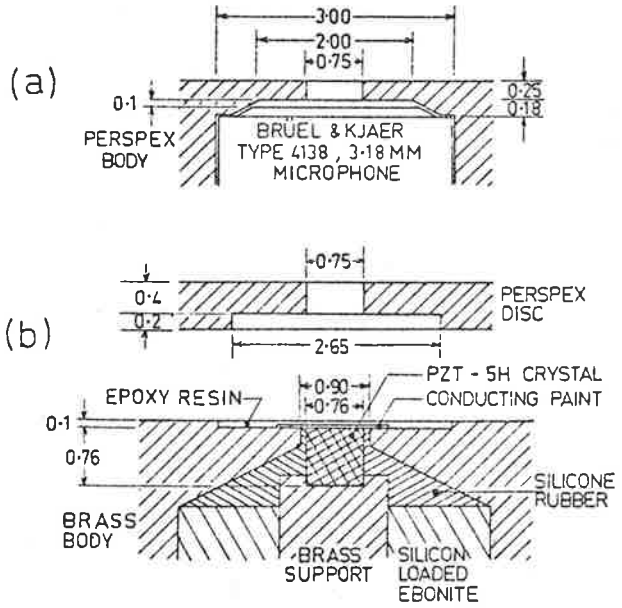

FIG. 1. Details of (a) pinhole microphone, and (b) piezoelectric transducer and modifying cap. Dimensions in mm.

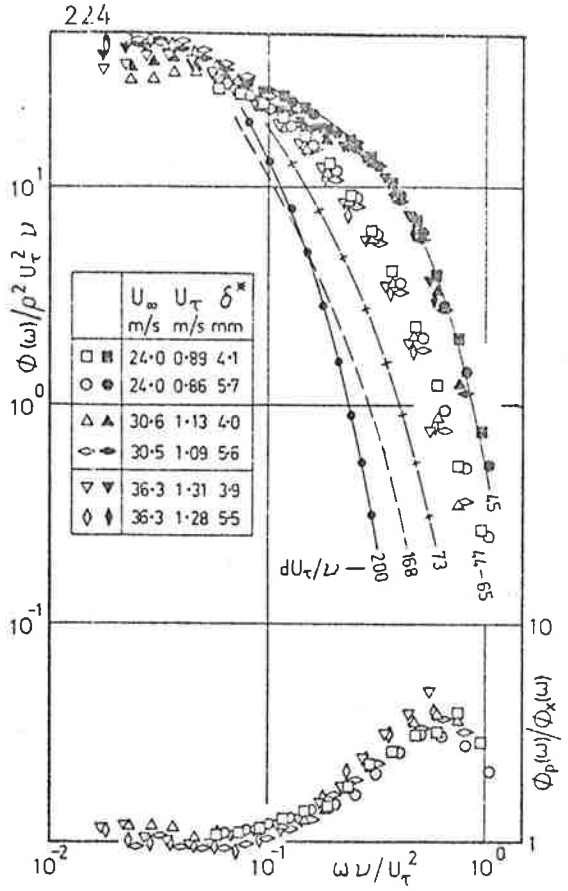

FIG. 2. Power spectrum of wall-pressure fluctuations. Piezoelectric data: filled circles on solid curve, Willmarth & Roos[3]; dashed curve Bull[5]; curve broken by plus signs, Lim[7]; open symbols, present data. Pinhole data: solid curve Blake[1]; solid symbols, present data. ϕ_P and ϕ_X are spectral densities measured by pinhole and piezoelectric transducers, respectively.

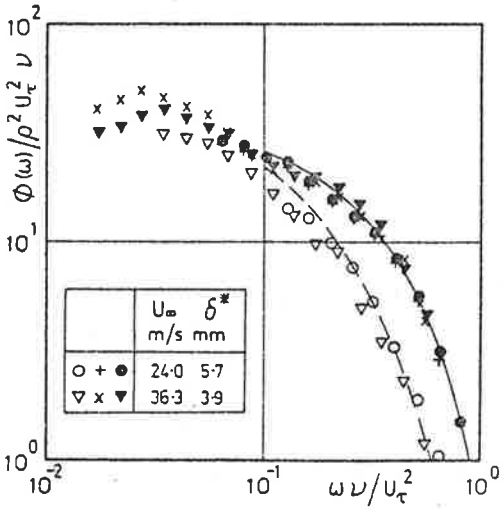

FIG. 3. Spectral data from pinhole microphone (black solid curve); pinhole piezoelectric transducer (● ▾ pinhole with cavity, + × pinhole only); ○ ▽ grease-filled pinhole-piezoelectric transducer; and flush-mounted piezoelectric transducer (dashed curve).

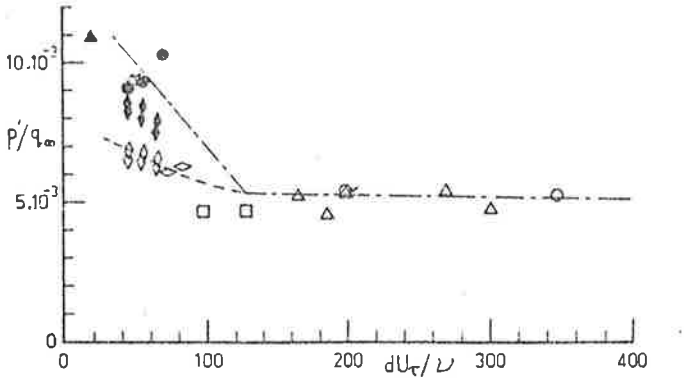

FIG. 4. Variation of measured rms pressure fluctuation with transducer size and type. Pinhole data: ● Blake[1]; ▲ Emmerling[2]; solid diamond, present data. Flush-mounted capacitor microphone data: Δ-Emmerling.[2] Flush-mounted-piezoelectric data: ◇ Lim[7]; ○ Willmarth and Roos[3]; △ Bull[5]; □ Schloemer[4]; ◇ present data.

The experiments described clearly lead to the following conclusions in relation to the power spectral density of wall pressure fluctuations.

(1) When a piezoelectric pressure transducer and a capacitor microphone are used with identical pinhole configurations, they will yield identical results.

(2) Measurements made with a pinhole transducer will be significantly in error for $\omega\nu/U_\tau^2 > \approx 0.1$.

(3) The flow disturbances created by a pinhole are localized so that the incorrect spectra obtained from pinhole measurements and genuine boundary layer spectra both scale with wall variables at high frequencies.

Finally, in Fig. 4, we present measured rms pressures (as p'/q_∞) as a function of transducer size (dU_τ/ν). The plot is as given by Emmerling[2] except that we have recalculated Blake's[1] data (by integrating individual curves of $\phi U_\infty/q_\infty^2\delta^*$ against $\omega\delta^*/U_\infty$) and included additional data. This figure does not alter the conclusion that transducers used in earlier measurements were too large to detect a significant part of the high-frequency fluctuations; but it does show that the increase in measured p'/q_∞ at small dU_τ/ν is not nearly as dramatic as Emmerling's[2] original analysis and Willmarth's[6] discussion of it would suggest.

The conclusions in this note rest on the assumption that for a given diameter uncorrected data obtained by a transducer which does not alter the flow and which has a response kernel fairly uniform over its area are essentially "correct"; deviations from such values are regarded as "errors." As the referee has pointed out, our results could be interpreted in terms of differences in response kernels. The extent of flow modification by the pinhole (fundamentally necessary for its function) is then reflected in the "error" or difference in response kernels, depending on the viewpoint taken.

[1]W. K. Blake, J. Fluid Mech. 44, 637 (1970).
[2]R. Emmerling, Max-Planck-Institut für Strömungsforschung Report No. 9 (1973).
[3]W. W. Willmarth and F. W. Roos, J. Fluid Mech. 22, 81 (1965).
[4]H. Schloemer, J. Acoust. Soc. Am. 42, 93 (1967).
[5]M. K. Bull, J. Fluid Mech. 28, 719 (1967).
[6]W. W. Willmarth, in *Annual Review of Fluid Mechanics*, edited by M. Van Dyke, W. G. Vincenti, and J. V. Wehausen (Annual Reviews, Inc., Palo Alto, Calif., 1975), Vol. 7, p. 13.
[7]K. B. Lim, Ph. D. thesis, University of Adelaide (1971).

Appendix C

Nature of Digital Filters Used.

Much of the data analysis presented in this report has relied upon the use of digital filters with zero phase delay. Many such filters have been reported in the literature and usually represent attempts to synthesize digitally certain well known kinds of analogue filters. The filters described by Genesio et al (1972) represent digital realizations of Butterworth and Chebyshev filters and were used frequently in the earlier stages of this work. Such filters can be made to have steep cutoffs and are very nearly linear in phase response over the pass band. Their greatest shortcoming is that an array of many filter coefficients must be known for each desired cutoff frequency and these coefficients must be specified with a high degree of precision in order to prevent instabilities arising from quantization effects.

The filter type described by Lynn (1972) does not suffer from such shortcomings and is precisely linear in phase response at all frequencies. The roll off of the filter is not as well shaped as for a Butterworth filter but this can be to some extent overcome by successive applications of the filter.

In broad terms the filtering process takes an average of a number of points centred upon each sample and the width of the averaging window determines the filter cutoff.

In more precise terms the filter transfer function can be be expressed as (for the low pass realization),

$$\frac{Y}{X} = H(z) = \left[\frac{1 - z^{k}}{1 - z}\right]^{n}$$

where k = order of the filter

n = number of applications of the filter

$z = e^{j\omega T}$

T = sample period.

ω = circular frequency.

Y = Z transform of the output.

X = Z transform of the input.

Z transform representation has been used which represents the digital equivalent of Laplace transform theory and under those circumstances the imaginary axis on the s-plane maps into a unit radius circle on the Z-plane. This allows for the repetition of the filter characteristics at frequencies which are multiples of 1/2T.

The transfer function therefore consists of k zeroes equally spaced around the unit circle with one of them (at $\omega = 0$) being precisely cancelled by a pole yielding a pass band centred upon that frequency. The difference equation of this filter (which is equivalent to the differential equation of an analogue filter) may be written from the above equation as:

$$y_i - y_{i+1} = x_i - x_{i+k},$$

or by a simple change of subscripts as

$$y_{i+1} = y_i + x_{i+k} - x_i,$$

where x and y are the input and output respectively. Thus the filter is recursive in that the new output represents the sum of the previous output plus the difference of two inputs. In addition the gain of the filter can be seen to be k^n and careful consideration of this equation shows that the transmission delay through the filter

is n(k - 1)/2 samples. By appropriate choice of n and k this is an integer and phase correction may be made by simply time shifting each sample by the correct amount. It is clear also that this time shift is the same at all frequencies so the filter is free from phase distortion and can be made, therefore, to have precisely zero phase shift.

The great usefulness of this filter type is that any desired cutoff frequency can be obtained by the specification of only two integers n and k and because of the simplicity of the difference equation used to implement the filter, processing times are very low.

In all the work presented in this report n was 2 and k was usually of the order of 9 or 10 depending on the cutoff required. A typical frequency response for this kind of filter is shown in figure C1 where the 3dB point corresponds to about 450 Hz for T = 80 μsecs, k = 9 and n = 2. The response of the filter to a step input is also presented.

In order to ensure that the programming of this filter was correct and free from phase uncertainties, a low pass filtered signal was correlated with the original unfiltered version and the resulting correlation was found to be symmetrical in time and peaked at precisely zero time delay.

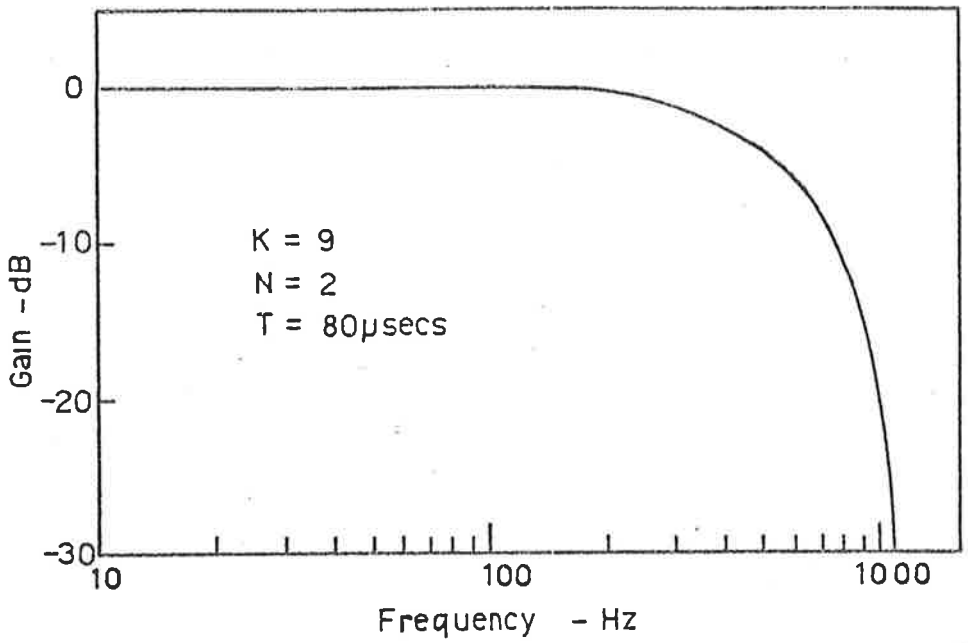

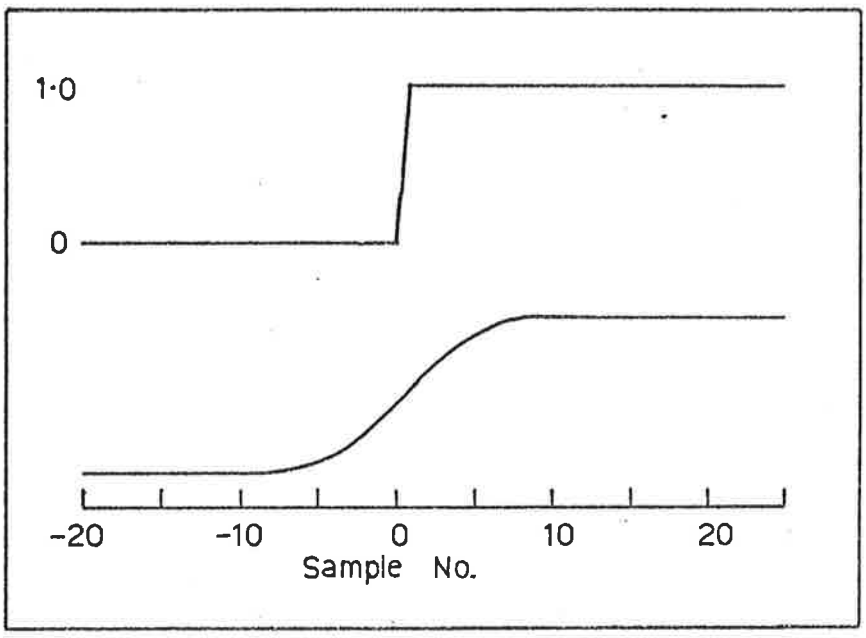

Figure C.1. Frequency response of a typical digital filter and the associated response to a step input.

Appendix D.

Statistical Uncertainty of Correlation Estimates

Since some of the long time averaged correlations presented in this report are of rather small amplitudes, it is worthwhile presenting a brief discussion of the significance of the error bars on the correlations.

Following Bandat and Piersol (1966) if N independent estimations of a mean autocorrelation point $R(\tau)$ are made, then these estimations will be normally distributed about the true mean autocorrelation point determined from an infinite number of independent samples. The standard deviation of this distribution is simply

$$\sigma = \sqrt{\frac{1}{N}} \ ,$$

where the standard deviation has been normalized by the rms value of the signal. Therefore, approximately 95% of the time measured values will be within $\pm 2\sigma$ of the actual value.

However, when an analogue signal is sampled at a sampling frequency which is more than twice the highest frequency of interest (i.e. to prevent Nyquist folding), this relation no longer applies because the successive estimations of the correlation are no longer independent. Under these circumstances one is interested in the equivalent number of independent samples N_e that would constitute the same level of uncertainty in the correlation estimate.

This number is clearly unknown but may be estimated on a basis of the time extent of the autocorrelation function relative to the total record length T. For example, if this correlation decays to 1/e of its initial value at a time delay τ_e then N_e might

be estimated as $N_e = T/\tau_e$.

For the experiments outlined in sections 5 and 6 of this report T = 3.3 seconds and the most severe errors will occur when τ_e is large. This occurs in the outer part of the low Reynolds number boundary layer for which $\tau_e \approx 1$ ms. This yields $N_e \approx 3{,}300$ which may be compared with the actual value of N = 82,000. This suggests that for the present computations, σ lies between one and two percent although this is probably a rather pessimistic estimate.

The characteristic twin maxima reported in section 5.3 for the spanwise veclocity correlations can therefore be seen to be larger than the likely correlation error bars.

Appendix E

Computation of a Wall Pressure Time History on a Basis of a Velocity Time History.

The work of this appendix represents an attempt to compute a typical wall pressure signature that might be associated with the velocity signatures that have been found to be representative of the organized motions. To compute the total pressure field associated with an organized structure would require a great deal of detailed knowledge of the velocity field associated with that structure. In section 7 however it was suggested that the conditional averaging procedure served to pick out only the component of the wall pressure that was generated by sources in the immediate vicinity of the point at which the velocity signature was detected. Under these circumstances it is possible to use the conditionally averaged velocity data to determine this corresponding component of the wall pressure. The resulting pressure signature may then be compared with the averaged time history that was proposed in section 7.

The Poisson equation for the turbulent pressure fluctuations may be found by taking the divergence of the momentum equation (Townsend, 1976) and is

$$\nabla^2 p = -\rho q \ (\underset{\sim}{x}) \qquad \text{E.1}$$

where the source term q is (using conventional tensor notation)

$$q(\underset{\sim}{x}) = 2\frac{\partial U_i}{\partial x_j} \cdot \frac{\partial u_j}{\partial x_i} + \frac{\partial^2}{\partial x_i x_j} (u_i u_j - \overline{u_i u_j}). \qquad \text{E.2}$$

By use of the appropriate Green's function the following equation

is obtained for the instantaneous pressure

$$p(\underset{\sim}{x}) = \frac{\rho}{2\pi} \int_{y>o} q(x_s) \cdot \frac{dV}{\left|\underset{\sim}{x} - \underset{\sim}{x}_s\right|} \qquad E.3$$

where $\underset{\sim}{x}$ is the point of interest on the wall and $\underset{\sim}{x}_s$ is the position of the source term of interest.

The pressure represents, therefore, a volume integral over the entire half space occupied by the boundary layer of all the source terms, with each being weighted by the reciprocal of the distance from the source to the point of measurement. It is clear, however, that the source term as given by equation E.2 would be rather difficult to measure accurately but this problem can be circumvented by taking the first term of equation E.2 only as the dominant contribution. This assumption of the dominance of turbulence-mean shear interaction was first proposed by Kraichnan (1956) and use made of it by Lilley and Hodgson (1960). Willmarth and Wooldridge (1963) have demonstrated that their pressure velocity correlations display the features that might be expected if a large proportion of the wall pressure was produced by this term alone and the detailed computations of Lim (1971) have demonstrated that this term makes about an 80% contribution to the mean square wall pressure. In what follows, therefore, use will be made of this assumption although it should be appreciated that the reports mentioned above demonstrate that the assumption is valid when the discussion is restricted to time averaged quantities. The possibility still exists that the other terms (turbulence - turbulence interactions) do make significant contributions to the instantaneous wall pressure signal at certain times.

Under this assumption equation E.3 becomes

$$p(x) = \frac{\rho}{2\pi} \int_{y_1}^{y_2} 2 \frac{\partial U}{\partial y} \cdot \frac{\partial v}{\partial x} \cdot \frac{dV}{|\underset{\sim}{x} - \underset{\sim}{x}_s|} \qquad 7.4$$

where only the mean gradient in the normal direction is significant. The range of the integration has been restricted since the present discussion is concerned only with the component of pressure generated by sources for which $y_1 < y < y_2$. The computations that follow are based on the ensemble averaged v component of velocity at $y = 0.05\delta$ ($y^+ = 170$) for the high Reynolds number case. This was presented previously in section 7.4 and is shown again in figure E.1 (a). The following assumptions are also necessary:

(i) The local velocity field is convected at the local mean speed ($U_c = 0.64\ U_o$). The precise choice is unknown but different values were found to have little effect on the temporal pressure history that finally results.

(ii) The source term is uniformly distributed over the range $0.025 < y/\delta < 0.075$. Changing this range has no effect on the shape of the computed pressure signature, but merely alters its amplitude.

(iii) The spanwise distribution of the source term is unknown and has therefore been assumed two dimensional. Computations have also been undertaken in which it is assumed two dimensional but weighted by a term such as e^{-Az} which reflects the behaviour of the velocity correlations in this region. This was found to change the amplitude of the computed pressure signature but not its shape. For the present case such assumptions are justifiable since an averaged

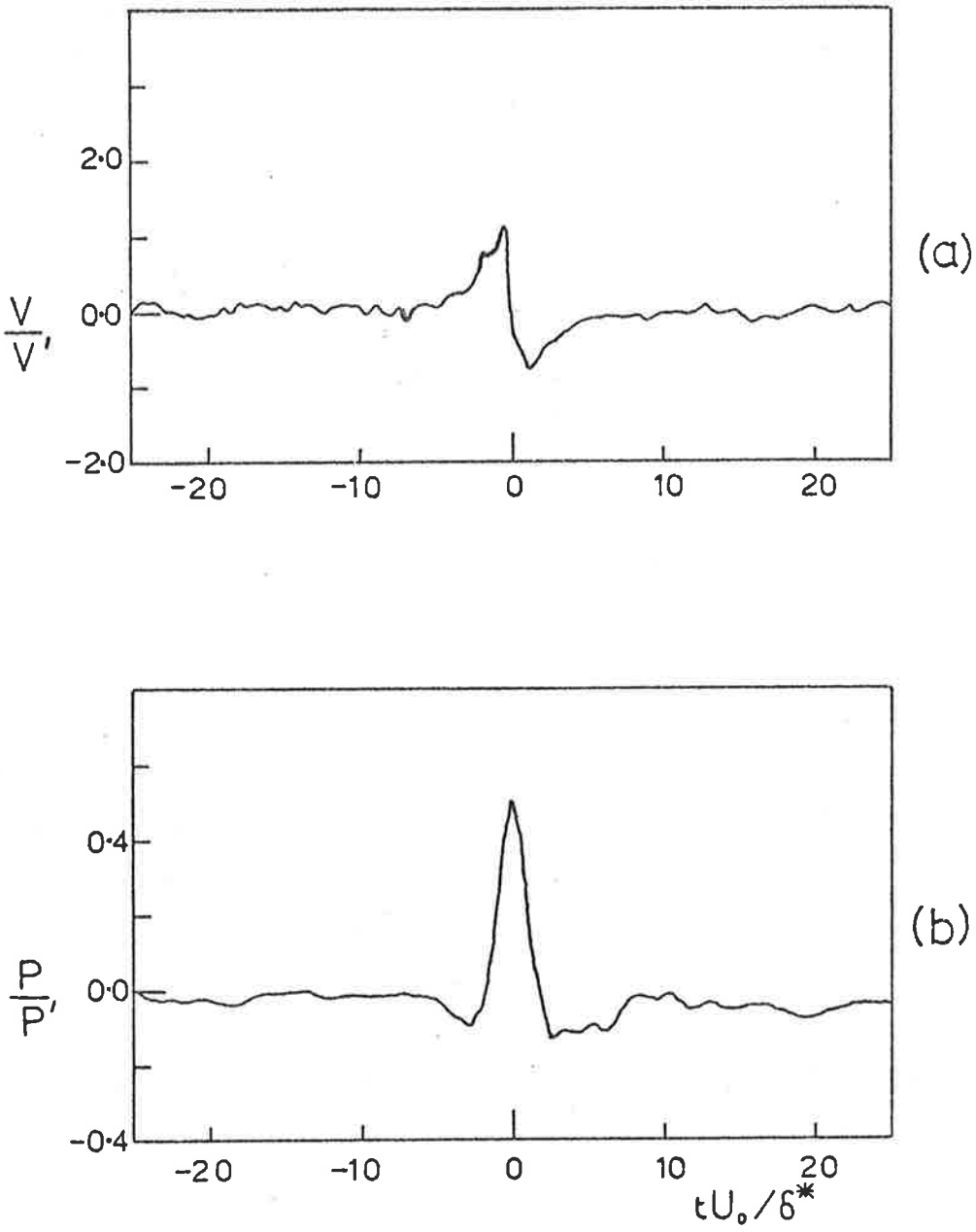

Figure E1(a) Ensemble averaged time history of the normal component of velocity at $y^+ = 170$ for the high Reynolds number case (see section 7.4).

Figure E1(b) Computed time history of wall pressure arising from sources characterized by the velocity distribution in figure E1(a).

velocity field is being used to compute an averaged pressure signature.

Under these circumstances an estimation of a pressure signature that is associated with a velocity signature may be made. The results that were obtained are shown in figure E.1(b) where the velocity signature in figure E.1(a) has been used. The pressure signature shows a large positive region occurring at the time corresponding to the steep fall of velocity, and there are small negative regions to either side of this region. This computed pressure signature can therefore be seen to be very similar to that shown previously in figure 7.15 which was suggested on a basis of the conditional sampling experiments. Evidently the assumption of the dominance of the turbulence - mean shear is acceptable and the conditional averages do appear to represent only a component of the pressure field associated with sources at the point where the detection velocity signal is measured.

BIBLIOGRAPHY

Antonia, R. A. (1972) J. Fluid Mech. 56, 1.

Armistead, R. A., and Keyes, J. J. (1968) Trans, ASME, J. Heat Transfer, 13.

Bakewell, H. P., and Lumley, J. L. (1967) Phys. Fluids 10, 1880.

Bellhouse, B. J., and Schultz, D. L. (1966) J. Fluid Mech. 24, 379.

Bendat, J. S., and Piersol, A. G. (1966) Measurement and Analysis of Random Data, J. Wiley and Sons.

Beranek, L. L. (1971) Noise and Vibration Control, McGraw Hill.

Blackwelder, R. F., and Kaplan, R. E. (1976) J. Fluid Mech., 76, 89.

Blackwelder, R. F., and Kovasznay, L. S. G., (1972) Phys. Fluids, 15, 1545.

Blake, W. K. (1970) J. Fluid Mech. 44, 637.

Brown, G. L. (1967a), D. Phil. Thesis, Oxford University, Department of Engineering Science.

Brown, G. L. (1976b), Proc. 1967 Heat Transfer and Fluid Mech. Institute, (D.B. Olfe and C. W. Van Atta, editors) Stanford University Press, 361.

Brown, G. L., and Davey, R. F. (1971) Rev. Sci., Inst., Notes, 42, 1729.

Brown, G. L., and Roshko, A. (1974) J. Fluid Mech., 64, 775.

Brown, G. L., and Thomas, A. S. W. (1976) IUTAM Symposium on Structure of Turbulence and Drag Reduction, Washington, D. C., June 1976. Proceedings to be published in The Physics of Fluids.

Bradshaw, P. (1967) J. Fluid Mech., 30, 241.

Bradshaw, P. (1971) An Introduction to Turbulence and Its Measurement, Pergamon Press.

Bull, M. K. (1967) J. Fluid Mech., 30, 241.

Bull, M. K., and Thomas, A. S. W. (1976) Phys. Fluids, 19, 597.

Burton, T. E. (1974) Massachusetts Institute of Technology, Acoustics and Vibration Laboratory, Report No. 70208-10.

Clauser, F. H. (1956) J. Aero. Sci., 21, 91.

Coles, D. E. (1968) A Young Person's Guide to the Data, AFOSR-IFP-Stanford Conference on Computation of Turbulent Boundary Layers, Stanford University.

Coles, D. E., and Barker, S. J. (1975) Project Squid Workshop, Turbulent Mixing in Non-reactive and Reactive Flows, S. N. B. Murthy, Editor, Plenum Press, 285.

Corcos, G. M. (1963) J. Acoust. Soc. Amer., 35, 192.

Corino, E. R., and Brodkey, R. S. (1969) J. Fluid Mech., 37, 1.

Eckelmann, H. (1974) J. Fluid Mech., 65, 439.

Elder, J. W. (1960) J. Fluid Mech., 9, 235.

Emmerling, R. (1973) MPI Stromungsforsch. u. Aerodyn. Versuchsaust., Gottingen, No. 56.

Emmons, H. W. (1951) J. Aerosp. Sci., 18, 490.

Fage, A., and Falkner, V. M. (1931) Aero. Res. Counc. Lond., R & M No. 1408.

Falco, R. E. (1976) IUTAM Symposium on Structure of Turbulence and Drag Reduction, Washington, D. C., June 1976. Proceedings to be published in The Physics of Fluids.

Favre, A., Gaviglio, J., and Dumas, R. (1957) J. Fluid Mech., 25, 719.

Fulachier, L., Giovanangeli, J. P., Dumas, R., Kovasznay, L. S. G., and Favre, A. (1974) Comptes Rendus de l'Academie des Sciences, Paris, t. 278, Serie B, 999.

Genesio, R., Laurentini, A., Mauro, V., and Meo, A. R. (1973) Butterworth and Chebyshev Digital Filters, Tables for their Design. Elsevier Scientific Publishing Co.

Görtler, H. (1940) Nachr. Wiss. Ges. Göttingen, Math. Phys. Klasse, New Series, 2, n. 1.

Grant, H. L. (1958) J. Fluid Mech., 4, 149.

Grass, A. J. (1971) J. Fluid Mech., 50, 233.

Gupta, A. K., Laufer, J., and Kaplan, R. E. (1971) J. Fluid Mech., 50, 493.

Holland, L. (1966) The Vacuum Deposition of Thin Films, Chapman and Hall, London.

Kim, H. T., Kline, S. J., and Reynolds, W. C. (1971) J. Fluid Mech., 50, 133.

Klebanoff, P. S. (1954) NACA Tech. Note 3178.

Kline, S. J., Reynolds, W. C., Schraub, F. A., and Rundstadler, P. W. (1967) J. Fluid Mech., 30, 741.

Kovasznay, L. S. G., Kibens, V., and Blackwelder, R. F. (1970) J. Fluid Mech., 41, 283.

Kraichnan, R. H. (1956) J. Acoust. Soc. Amer., 28, 378.

Laufer, J. (1954) Ann. Rev. Fluid Mech., 7, 307.

Liepmann, H., and Skinner, G. (1954) NACA Tech. Note 3268.

Lighthill, M. J. (1954) Proc. Roy. Soc. A., 224, 1.

Lilley, G. M., and Hodgson, T. H. (1960) AGARD Report No. 276.

Lim, K. B. (1971) Ph.D Thesis, Dept. Mech. Eng., Univ. Adelaide

Lu, S. S., and Willmarth, W. W. (1973) J. Fluid Mech., 60, 481.

Ludweig, H. (1950) NACA Tech. Memo, No. 1284.

Lynn, P. A. (1972) Computer Journal, 15, 337.

Meek, R. L. (1972) AIChE Jour., 18, 854.

Mitchell, J. E., and Hanratty, T. J. (1966) J. Fluid Mech., 26, 199.

Badri Narayanan, M. A., Rajagopalan, S. and Narasimha, R. (1974) Indian Institute of Science, Fluid Mech. Rept. No. 74FM15.

Nychas, S. G., Hershey, H. C., and Brodkey, R. S. (1973) J. Fluid Mech., 61, 573.

Offen, G. R. and Kline, S. J. (1973) Rept. No. MD-31, Dept. Mech. Eng., Stanford University.

Rao, K. N., Narasimha, R., and Badri Narayanan, M. A. (1971) J. Fluid Mech., 48, 339.

Reynolds, W. C., (1976) Ann. Rev. Fluid Mech., 8, 183.

Rayleigh (Lord) (1966) Proc. Roy. Soc., A, 93, 148.

Ronneberger, D. (1972) J. Sound Vib., 24, 133.

Schloemer, H. H., (1967) J. Acoust. Soc. Amer., 42, 93.

Schubauer, G. B., and Klebanoff, P. S. (1956) NACA Rept. No. 1289.

Simpson, R. L. (1975) Phys. Fluids, 18, 1068.

Spence, D. A., and Brown, G. L. (1967) J. Fluid Mech., 33, 753.

Strickland, J. H., and Simpson, R. L. (1975) Phys. Fluids, 18, 306.

Taylor, G. I. (1923) Phil. Trans., A223, 289.

Townsend, A. A. (1949) Aust. J. Sci. Res., 2, 451.

Townsend, A. A. (1976) The Structure of Turbulent Shear Flow, Cambridge University Press.

Ueda, H., and Hinze, J. O. (1975) J. Fluid Mech., 67, 125.

Willmarth, W. W. (1975a) Adv. Appl. Mech., 15, 159.

Willmarth, W. W. (1975b) Ann. Rev. Fluid Mech., 7, 13.

Willmarth, W. W., and Lu, S. S. (1971) J. Fluid Mech., 55, 481.

Willmarth, W. W., and Roos, F. W. (1965) J. Fluid Mech., 22, 81.

Willmarth, W. W., and Tu, B. J. (1967) Phys. Fluids. Suppl., 10, S134.

Willmarth, W. W., and Wooldridge, C. E. (1962) J. Fluid Mech., 14, 187.

Willmarth, W. W., and Wooldridge, C. E. (1963) AGARD Rept. 456.

Wills, J. A. B. (1964) J. Fluid Mech., 20, 417

Zilbermann, M., Wygnanski, I., and Kaplan, R. E. IUTAM Symposium on Structure of Turbulence and Drag Reduction, Washington, D. C., June 1976. Proceedings to be published in the Physics of Fluids.